

E-20137

PROGRESS REPORT

LARGE-SCALE TESTS OF A LOW-RISE UNREINFORCED MASONRY BUILDING SYSTEM

by

Tianyi Yi, Franklin L. Moon, Roberto T. Leon, and Lawrence F. Kahn

Georgia Institute of Technology
Department of Civil and Environmental Engineering
Atlanta, GA 30332

March 1, 2002

ABSTRACT

As part of an on-going project sponsored by the Mid-America Earthquake Center (MAE Center) a full-scale two-story URM buildings will be tested at Georgia Tech in the spring of 2002. The primary objectives are to 1) verify current analytical models as well as those developed through component tests under other MAE Center projects and 2) assess the effectiveness of FRP and prestressing retrofit techniques. The test structure will be subjected to slowly applied lateral force reversals based on the results of a parallel project focused on the dynamic testing of a similar half-scale URM structure. A series of tests will be conducted on the test structure prior to rehabilitation to validate analytical models and obtain performance characteristics such as initial stiffness, change in stiffness and damage progression. The next sequence of tests will be aimed at determining the effect of a series of rehabilitation techniques on the overall building performance, eventually leading to an ultimate test of the fully rehabilitated structure.

This progress report presents a literature review conducted as a background for the project along with a detailed description of the experimental program. Furthermore, the results of the extensive preliminary analyses conducted on the test structure are also presented, including predictions of initial stiffness, damage progression, and force-displacement behavior.

ACKNOWLEDGEMENTS

This work was supported primarily by the Earthquake Engineering Research Centers Program of the National Science Foundation under Award Number EEC-9701785. The authors also wish to acknowledge Cherokee Brick & Tile Co., Lafarge North America Inc., and Dur-O-Wal for their generous donations of construction materials.

TABLE OF CONTENTS

ABSTRACT	ii
ACKNOWLEDGEMENTS	iii
TABLE OF CONTENTS	iv
LIST OF TABLES	ix
LIST OF FIGURES	xi
1 INTRODUCTION	1-1
1.1 Motivation	1-2
1.2 Project Objectives	1-4
1.3 Project Overview	1-4
1.4 MAE Center Project Collaboration	1-5
1.5 Outline of Report	1-6
2 LITERATURE REVIEW	2-1
2.1 Unreinforced Masonry	2-1
2.1.1 Unreinforced Masonry Materials	2-1
2.1.1.1 Compressive Strength	2-3
2.1.1.2 Tensile Strength	2-4
2.1.1.3 Shear Strength	2-5
2.1.1.4 Elastic Modulus and Shear Modulus	2-10
2.1.2 URM In-plane Piers	2-11
2.1.2.1 Experiments on Masonry In-plane URM Pier	2-12
2.1.2.2 Failure Mechanism of In-plane URM Pier	2-15
2.1.2.3 Elastic Stiffness and Deformation Capacity of In- plane URM Pier	2-18
2.1.3 URM Spandrels	2-20
2.1.4 URM Out-of-plane Walls	2-21
2.1.4.1 Failure Mechanism of URM Out-of-plane Wall	2-22

2.1.4.2 Experiments on URM out-of-plane wall	2-23
2.1.4.3 Analysis of URM Out-of-plane Walls	2-29
2.1.5 Flexible Wood Diaphragms	2-31
2.1.5.1 Properties of Flexible Wood Diaphragms	2-31
2.1.5.2 Experiments on Flexible Wood Diaphragms	2-33
2.1.5.3 Analysis of Flexible Wood Diaphragms	2-34
2.1.6 URM Structures	2-35
2.1.6.1 Overview of the Structure Characters of URM Structures	2-36
2.1.6.2 Experiments on URM Structures	2-38
2.1.6.2.1 Reduced-scale Dynamic Test on URM Structure	2-39
2.1.6.2.2 Large-scale Static Test on URM Structure	2-54
2.1.6.3 Analysis of URM Structures	2-62
2.1.6.3.1 Analysis of Perforated In-plane Walls	2-62
2.1.6.3.2 Analysis of Entire URM buildings	2-64
2.1.7 Summaries of Research on Unreinforced Masonry	2-66
2.2 Retrofit Methods	2-72
2.2.1 Traditional Retrofit Methods	2-72
2.2.2 FRP Overlays	2-73
2.2.2.1 Out-of-Plane Behavior	2-73
2.2.2.2 In-Plane Behavior	2-82
2.2.2.3 Application	2-91
2.2.2.4 Summary of Research	2-92
2.2.3 Post-tensioning	2-93
2.2.3.1 Out-of-Plane Behavior	2-93
2.2.3.2 In-Plane Behavior	2-101
2.2.3.3 Summary of Research	2-106

3 EXPERIMENTAL PROGRAM	3-1
3.1 Objectives	3-1
3.2 Test Structure	3-5
3.2.1 Reinforced Concrete Foundation Slabs	3-6
3.2.2 Timber Stud Wall	3-9
3.2.3 Masonry Walls	3-14
3.2.4 Retrofit Strategies for URM Walls	3-18
3.2.5 Wood Roof/Floor Diaphragms	3-21
3.2.6 Retrofit Strategies for Diaphragms	3-23
3.2.7 Construction	3-24
3.3 Preliminary Material Tests	3-30
3.3.1 Shear Tests	3-31
3.3.2 Prism Tests	3-35
3.3.3 Brick Compressive Tests	3-36
3.4 Test Sequence	3-37
3.4.1 Diaphragm and Out-of-plane Walls Tests	3-37
3.4.1.1 Test Step 1-1	3-38
3.4.1.2 Test Step 1-2	3-39
3.4.1.3 Test Step 1-3	3-40
3.4.1.4 Test Step 1- 4	3-41
3.4.1.5 Test Step 1-5	3-41
3.4.1.6 Test Step 1- 6	3-42
3.4.2 In-Plane Walls	3-43
3.5 Instrumentation	3-46
3.6 Proposed Schedule	3-46
4 PRELIMINARY ANALYSIS	4-1
4.1 Objectives	4-1
4.2 Analysis of URM Test Structure	4-1
4.2.1 Three Dimensional Elastic Finite Element Model	4-2
4.2.1.1 Selection of Modeling Method	4-3

4.2.1.2 Diaphragm Elastic Stiffness	4-6
4.2.1.3 Gravity stresses	4-8
4.2.1.4 Elastic Out-of-Plane Wall Stiffness	4-8
4.2.1.5 Elastic In-Plane Wall Stiffness and Coupling Effect	4-11
4.2.1.6 Flange Effect	4-13
4.2.1.7 Locations of Highly Stressed Zones	4-14
4.2.2 Conceptual Dynamic Model	4-17
4.2.2.1 Natural Periods and Vibration Mode Shapes of the Test Structure	4-18
4.2.2.2 Dynamical analysis based on the conceptual model	4-24
4.2.3 Nonlinear Pushover Analysis of URM Structures	4-27
4.2.3.1 URM Pier Damage Model	4-29
4.2.3.2 Pier/Spandrel Interaction	4-34
4.2.3.3 Overturning Moment	
4.2.3.4 Loading History	4-44
4.2.3.5 Coding	4-46
4.2.3.6 Comparisons with Past Experiments	4-48
4.2.3.7 Results of the ST-11 Test Structure	4-54
4.2.4 Nonlinear In-Plane Finite Element Model	4-59
4.2.4.1 Modeling of URM Walls with Contact Elements	4-60
4.2.4.2 Comparison of Nonlinear FE Analysis with Past Experiments	4-66
4.2.4.3 Non-linear FE Analysis of the ST-11 Test Structure	4-73
4.2.4.3.1 Nonlinear FE Analysis Results of Wall 1	4-74
4.2.4.3.2 Nonlinear FE Analysis Results of Wall 2	4-80
4.2.4.3.3 Nonlinear FE Analysis Results of Wall AB	4-85
4.3 Analysis of Retrofit Test Structure	4-90
4.3.1 Post-Tensioning	4-90
4.3.2 FRP Retrofit	4-92
4.3.2.1 FRP Retrofitted URM Pier Damage Model	4-92
4.3.2.2 Analysis Results on FRP Retrofitted ST-11 Test	4-99

Structure	
4.4 Conclusion	4-103
5 CONCLUSIONS	5-1
6 REFERENCES	6-1
APPENDIX A: CONSTRUCTION PHOTOS	A-1
APPENDIX B: INSTRUMENTATION	B-1

LIST OF TABLES

Table 2.1 Mortar Compositions by Volumes	2-2
Table 2.2 Masonry Unit Strengths	2-2
Table 2.3 Ultimate drift of URM pier corresponding to different failure modes	2-19
Table 3.1 Objectives for Project ST-11	3-2
Table 3.2 Dimensions and Weights of the RC slabs	3-6
Table 3.3 Pier sizes and aspect ratios	3-14
Table 3.4 Opening ratios of each wall	3-15
Table 3.5 Summary of Diagonal Compression Test Results (Type N)	3-31
Table 3.6 Summary of Diagonal Compression Test Results (Type O)	3-32
Table 3.7 Summary of Direct Shear Tests	3-34
Table 3.8 Summary of prism test results	3-36
Table 3.9 Summary of brick compression results	3-36
Table 3.10 Summary of the diaphragm and out-of-plane wall test steps	3-38
Table 4.1 Summary of assessment of element accuracy	4-5
Table 4.2 Gravity stresses in the piers	4-8
Table 4.3 Out-of-plane stiffness of the masonry walls 4-10	4-10
Table 4.5 In-plane stiffness of the masonry walls with/without flange effect	4-14
Table 4.6 Structural properties used in analysis with Walls A and A in-plane	4-18
Table 4.7 Elastic stiffness' used for sensitivity analysis (Walls A and B in-plane)	4-19
Table 4.8 Natural periods of the conceptual model (Walls A and B in-plane)	4-20
Table 4.9 Structural properties used in analysis with Walls 1 and 2 in-plane	4-21
Table 4.10 Elastic stiffness' used for sensitivity analysis (Walls 1 and 2 in-plane)	4-22
Table 4.11 Natural periods of the conceptual model (Walls 1 and 2 in-plane)	4-22
Table 4.12 Maximum Displacements of the URM structure under seismic loads	4-26

Table 4.13 Maximum Base Shears of the URM structure under seismic loads	4-27
Table 4.14 Seismic analysis methods	4-27
Table 4.15 Strength equations given by FEMA 273 for URM piers	4-30
Table 4.16 Ultimate drift of URM pier corresponding to different failure modes	
Table 4.17 Force-drift relationships for URM pier failure modes.	4-33
Table 4.18 Material properties used for the analysis of Walls D and B	4-49
Table 4.19. Comparison of inflection point location	4-50
Table 4.20. Summary of results of Wall D	4-52
Table 4.21. Summary of results of Wall B (Magenes et al , 1995)	4-53
Table 4.22. Material properties used for the analysis of the ST-11 test structure.	4-55
Table 4.23. Pier failure modes of the ST-11 test structure.	4-58
Table 4.24. Comparison of pushover analysis with approximation of strength.	4-59
Table 4.25 Summary of nonlinear FE results for Walls B and D (Uof Pavia)	4-68
Table 4.26. Calculated ultimate strength of Wall 1	4-75
Table 4.27. Calculated ultimate strength of Wall 2	4-80
Table 4.28. Calculated ultimate strength of Walls AB	4-85
Table 4.29. Failure modes of Wall AB piers with different levels of post-tensioning stress.	4-91
Table 4.30. Force-drift relationships for URM pier retrofitted with FRP overlays	4-99
Table 4.31. Properties of FRP used in analysis 4-100	4-100
Table 4.32. Predicted failure modes for FRP retrofitted piers 4-102	4-102

LIST OF FIGURES

Figure 1.1. St. Louis firehouse #11.	1-3
Figure 1.2. Charleston firehouse.	1-3
Figure 1.3. Completed ST-11 test structure	1-5
Figure 2.1. Test setup for the flexural tension test (adapted from Costley 1996)	2-5
Figure 2.2 Different shear test setups	2-6
Figure 2.3 Test set up for Shove test (adapt from Costley 1996)	2-7
Figure 2.4 Interface cracks between units and mortar (taken in ST11 material test)	2-8
Figure 2.5 A typical perforated in-plane wall	2-11
Figure 2.6 Different crack patterns for the URM piers	2-15
Figure 2.7 Crack patterns in wall B (Magenes et al 1995)	2-21
Figure 2.8 Dynamical test set up used in ABK out-of-plane test (ABK 1981a)	2-24
Figure 2.9 Dynamical test set up used in MAEC project ST-10	2-26
Figure 2.10. Airbag used in the out-of-plane test of URM wall (taken from Velazquez-Dimas 2000)	2-27
Figure 2.11 Typical URM structure under earthquake (modified from Bruneau 1994)	2-36
Figure 2.12 Specimen House 1 in Clough's test (taken from Clough et al 1979)	2-40
Figure 2.13 Specimen House 2 in Clough's test (taken from Clough et al 1979)	2-41
Fig. 2. 14. Specimen Model 2 in Tomazevic (1990)'s test (taken from Tomazevic 1990)	2-45
Fig. 2.15. Layout and dimensions of the test models in Tomazevic (1993)'s test (taken from Tomazevic 1993)	2-47

Figure 2.16. Distribution of displacements along the top floor (2, 4 the in-plane walls, 3 center of the out-of-plane wall) (taken from Tomazevic 1993)	2-48
Figure 2.17. The test specimens Door wall in Costley's test (taken from Costley 1996)	2-51
Figure 2.18. The test specimens Widnow wall in Costley's test (taken from Costley 1996)	2-52
Figure 2.19 Magenes et al(1995) 's test	2-56
Figure 2.20 Final crack pattern in the dynamical tested specimen (taken from Costely et al 1996)	2-59
Figure 2.21 Final crack pattern in static tested specimen (from Magenes et al 1995)	2-60
Figure 2.22 Schematic of test setup (take from Hamuosh et al., 2000)	2-77
Figure 2.23. Schematic of test setup (taken from Dimas et al., 2000a)	2-79
Figure 2.24. Moment Capacity versus Axial load for various normalized FRP area fractions (taken from Triantafillou, 1998)	2-80
Figure 2.25. Schematic of test setup (taken from Triantafillou, 1998)	2-81
Figure 2.26. Schematic of test setup (taken from Kolsch, 1998)	2-82
Figure 2.27. Force-displacement response (taken from Kolsch, 1998)	2-83
Figure 2.28. Schematic of in-plane test specimen showing the location of FRP reinforcement.(taken from Franklin et al, 2001)	2-85
Figure 2.29. Photographs of test setup used to assess in-plane behavior of URM walls retrofit with FRP overlays (taken from Marshall et al, 2000)	2-86
Figure 2.30. In-plane moment capacity versus axial load for various normalized FRP area fractions. (taken from Triantafillou, 1998)	2-88
Figure 2.31. Schematic of in-plane test setup (taken from Triantafillou, 1998)	2-89
Figure 2.32. Schematic of 3-brick test setup (taken from Ehsani et al, 1997)	2-90

Figure 2.33. Force-displacement response of brick assemblages retrofit with 0-90 and +/-45 FRP overlays (taken from Ehsani et al, 1997)	2-91
Figure 2.34. Schematic of in-plane test setup (taken from Laursen et al., 1995)	2-92
Figure 2.35. Damage sustained prior to retrofit with FRP overlays (taken from Ehsani and Saasatmanesh, 1996)	2-93
Figure 2.36. Schematic of test setup and specimen. (taken from Devalapura et al., 1996)	2-96
Figure 2.37. Force-Displacement behavior of each test specimen. (taken from Devalapura et al., 1996)	2-96
Figure 2.38. Load-deflection curves up to ultimate (taken from Al-Manaseer and Neis, 1987)	2-99
Figure 2.39. Schematic of Test setup (taken from Garrity and Phipps, 1987)	2-101
Figure 2.40. Schematic of in-plane post-tensioned URM pier test setup (taken from Laursen and Ingham, 2001a)	2-104
Figure 2.41. Force-displacement response of partial grouted (PG) and ungrouted (UG) post-tensioned URM piers (taken from Laursen and Ingham, 2001a),	2-105
Figure 2.42. In-plane test setup and instrumentation layout (taken from Page and Huizer, 1998)	2-106
Figure 2.43. In-plane force-displacement curves for each wall tested (taken from Page and Huizer, 1998)	2-107
Figure 3.1 Overview of the tested structure with the L strong walls	3-5
Figure. 3.2 Plan view of foundation layout (dimensions are in in.).	3-7
Figure. 3.3 Reinforcement detail of the foundation slabs (dimensions are in in.).	3-8
Figure 3.4 Photo of the stud wall together with the foundation	3-9
Figure 3.5 Plan view of the ST-11 test structure	3-10
Figure 3.6 Elevation view of Walls A and B	3-11

Figure 3.7 Elevation view of Wall 1	3-12
Figure 3.8 Elevation view of Wall 2	3-13
Figure 3.9 Detail of American bond	3-17
Figure 3.10 Detail of arch lintels	3-17
Figure 3.11 Detail of steel lintels	3-18
Figure 3.12 <i>Sure-Stress</i> TM post-tensioning system (taken from www.duro-wal.com)	3-19
Figure 3.13 Common configuration of FRP retrofit	3-20
Figure 3.14 Special configuration of FRP retrofit to enforce bed-joint sliding at the mid height of the pier	3-21
Figure 3.15 ST-11 roof/floor diaphragm	3-22
Figure 3.16 Simpson connections (taken from www.strongtie.com)	3-23
Figure 3.17 Two different bricks	3-25
Figure 3.18 Post-tension RC slabs to the strong floor	3-26
Figure 3.19 PVC tubes used to leave the holes in the wall	3-26
Figure 3.20 Header course pattern for the three wythe walls.	3-27
Figure 3.21 Openings left at the top of Wall 1	3-28
Figure 3.22 Assembly of the floor systems	3-29
Figure 3.23 Construction of the joist pockets in Walls A and B.	3-29
Figure 3.24 Construction of the floor and roof diaphragms.	3-30
Figure 3.25 Photograph of shear failure through brick.	3-33
Figure 3.26 Direct shear test setup.	3-34
Figure 3.27 Testing of half the roof diaphragm parallel to the joists	3-39
Figure 3.28 Testing of the entire diaphragm parallel to the joists	3-40
Figure 3.29 Testing of the entire diaphragm perpendicular to the joists	3-41
Figure 3.30 Testing of the retrofitted diaphragm	3-42
Figure 3.31 Modified stiffness displacement control scheme	3-45
Figure 4.1 Cantilever wall model 4-4	4-4
Figure 4.2 Three-dimensional model of the ST-11 building	4-7
Figure 4.3 Out-of-plane loading of the masonry wall	4-9

Figure 4.4 Different loading cases for calculation of the in-plane stiffness of masonry walls	4-12
Figure 4.5 Maximum von Mises stresses in the Wall 1 under in-plane loading	4-15
Figure 4.6. Maximum von Mises stresses in the Wall 2 under in-plane loading	4-16
Figure 4.7 Maximum von Mises stresses in Wall AB under in-plane loading	4-16
Figure 4.8 Conceptual model of an URM structure	4-17
Figure 4.9 Vibration modes for the test structure (Walls A and B in-plane)	4-20
Figure 4.10 Vibration modes for the test structure (Walls 1 and 2 in-plane)	4-23
Figure 4.11 Artificial Mid-America ground motion (rock site)	4-25
Figure 4.12 Artificial Mid-America ground motion (soil site)	4-25
Figure 4.13 URM perforated wall and pushover model.	4-29
Figure 4.14 Generalized force-drift curve for the analysis of URM piers.	4-32
Figure 4.15 Idealized perforated wall models	4-35
Figure 4.16 Concepts of elastic spandrel-nonlinear pier model	4-37
Figure 4.17 Idealized perforated wall	4-41
Figure 4.18 Distribution of vertical stress under gravity load and lateral force	4-43
Figure 4.19 Lateral force distributions for all runs in Paulson (1990)'s test	4-45
Figure 4.20 Flow chart of program code	4-47
Figure 4.21 Elevation view of Wall D and Wall B (Magenes et al, 1996)	4-48
Figure 4.22 Comparison between analytical and experimental force-displacement curves	4-50
Figure 4.23 Comparison of pushover analysis with Wall D (Magenes et al 1995)	4-52

Figure 4.24 Comparison of pushover analysis with Wall B (Magenes et al 1995)	4-53
Figure 4.25 Force-displacement curve obtained from pushover analysis of Wall AB.	4-56
Figure 4.26 Force-displacement curve obtained from pushover analysis of Wall 1.	4-56
Figure 4.27 Force-displacement curve obtained from pushover analysis of Wall 2.	4-57
Figure 4.28 Forces on a spandrel	4-61
Figure 4.29 Teeth configurations of the head joints	4-62
Figure 4.30 Schematic of a contact element	4-63
Figure 4.31 Normal forces transmitted between the pair of surfaces (taken from ABAQUS 5.8-19 manual 23.18.37-1)	4-63
Figure 4.32 Force-Relative displacement relationship for contact elements.	4-64
Figure 4.33 Modeling of a perforated wall with contact elements and stabilizing truss elements	4-65
Figure 4.34 Time history for the analysis of the full-scale test in Univ. of Pavia	4-67
Figure 4.35 Failure modes of the tested wall at Univ. of Pavia	4-70
Figure 4.36 Stress contours of the tested walls at Univ. of Pavia	4-71
Figure 4.37 Force-displacement behavior of the URM masonry structure tested at Univ. of Pavia (Magenes et al , 1995)	4-72
Figure 4.38 Force-displacement response of Wall 1 with different bed joint shear friction coefficients	4-76
Figure 4.39 Deformed shape of Wall1 (loaded to the left)	4-76
Figure 4.40 Stress contour of Wall1 (loaded to the left)	4-77
Figure 4.41 Deformed shape of Wall1 (loaded to the right)	4-77
Figure 4.42 Stress contour of Wall1 (loaded to the right)	4-78
Figure 4.43 Force-displacement response of Wall 1 with different material properties (beginning with push to the right)	4-78

Figure 4.44 Force–displacement response of Wall 1 with different material properties (beginning with push to the left)	4-79
Figure 4.45 Force–displacement response of Wall 2 with different friction coefficients	4-81
Figure 4.46 Deformed shape of Wall 2 (loaded to the right)	4-82
Figure 4.47 Stress contour of Wall 2 (loaded to the right)	4-82
Figure 4.48 Deformed shape of Wall 2 (loaded to the left)	4-83
Figure 4.49 Stress contour of Wall 2 (loaded to the left)	4-83
Figure 4.50 Force–displacement response of Wall 2 with different masonry properties (beginning with push to the right)	4-84
Figure 4.51 Force–displacement response of Wall 2 with different masonry properties (beginning with push to the left)	4-84
Figure 4.52 Force–displacement response of Wall AB with different friction coefficients	4-86
Figure 4.53 Deformed shape of Wall AB (loaded to the right)	4-87
Figure 4.54 Stress contours of Wall AB (loaded to the right)	4-87
Figure 4.55 Deformed shape of Wall AB (loaded to the left)	4-88
Figure 4.56 Stress contours of Wall AB (loaded to the left)	4-88
Figure 4.57 Force–displacement response of Wall AB with different masonry properties (beginning with push to the right)	4-89
Figure 4.58 Force–displacement response of Wall AB with different masonry properties (beginning with push to the left)	4-89
Figure 4.59 Force-displacement curves for Wall AB retrofit with different levels of post-tensioning stress	4-91
Figure 4.60 URM Retrofit with FRP Strips	4-93
Figure 4.61 Strain and Stress Diagram for FRP Retrofit URM Pier in Flexure	4-94
Figure 4.62 Strain and Stress Diagram used to calculate shear capacity associated with the compressive failure of masonry	4-95
Figure 4.63 Model used to Obtain Diagonal Tension Strength of FRP Retrofit Pier	4-97

Figure 4.64 Generalized force-drift relationships for URM piers retrofit with FRP overlays.	4-98
Figure 4.65 Force-displacement curves for Wall AB in an unreinforced state and after retrofit schemes 1 and 2	4-100
Figure 4.66 Force-displacement curves for Wall 1 in an unreinforced state and after retrofit schemes 1 and 2	4-101
Figure 4.67 Force-displacement curves for Wall 2 in an unreinforced state and after retrofit schemes 1 and 2	4-101

1 INTRODUCTION

In United States, URM structures had been widely used as residential, commercial and essential facilities buildings until the 1933 Long Beach earthquake revealed their seismic vulnerability. Following that event, URM construction was outlawed in all public buildings in California and other West Coast states. Reinforced masonry (RM) structures, a more ductile type of construction, have been widely used in high seismic areas since that time. However, a large number of old URM buildings are still being used in California and other Western states, and URM structures have continued to be constructed in other regions, which were considered as non-seismic areas until very recently. These seismically deficient buildings present a threat to life safety and research to develop effective and economic seismic hazard mitigation methods for these URM buildings is urgently needed. Many experimental and analytical investigators have studied URM structures in the USA, particularly after the 1971 San Fernando earthquake reemphasized the vulnerability of these structures (Jennings, 1997). One mitigation methodology developed specifically for URM structures in early 1980s was the ABK method, the result of a joint venture of three Los Angeles consulting engineering firms (Agbabian & Associates, S.B. Barnes & Associates, and Kariotis & Associates (ABK 1984)). This methodology has been widely used for the mitigation of seismic hazards in existing URM buildings, and has been adapted with minor modification by several standards, such as UCBC (1991), ATC-14 (1987), ATC-22 (1989), and FEMA (1992a).

Numerous experimental and analytical investigations on URM structures have also been conducted in Europe, especially in Yugoslavia and Italy as a consequence of the 1964 Skopje and 1976 Friuli earthquakes. The research results from Europe, together with those obtained in United States, provide reasonable guidelines for the seismic assessment and rehabilitation of URM buildings in areas of frequent high seismicity.

1.1 Motivation

While much has been learned about URM behavior, the URM problem in Mid America has its special aspects. First, construction of most URM structures in Mid America did not consider seismic loads. Most of these URM structures are stiff, massive buildings that are well suited to resist wind loads. Their mass and lack of ductility, however, makes them highly vulnerable to ground motions. Moreover, some unscientific sampling has indicated that rather weak mortar was commonly used in URMs in Mid America as compared to mortars commonly used in West Coast construction. Second, because seismic hazard was not a consideration, numerous critical structures, including fire stations, police offices, and emergency response centers were built as URM structures (Fig. 1.1 and 1.2). These structures present a critical threat to adequate response and recovery efforts after a major earthquake. Third, the tectonic characteristics of Mid America are likely to produce ground motions with significantly different attenuation and frequency content characteristics than those in the Western US. Thus, much of what has been learned through non-linear dynamic analysis of URM structures subjected to Western ground motions (1940 El Centro, for example) needs to be verified for the ground motions expected in Mid-America. Finally, it is not clear whether the methodologies developed and employed in retrofits of URMs in the Western US are

applicable, both from economic and technical points of view, in Mid-America. This is due primarily to the long return periods of strong earthquakes in this region, which make most retrofits unviable except for historic or critical structures. All these aspects point to the need of special research on URM buildings in Mid America.



Figure 1.1. St. Louis firehouse #11.



Figure 1.2. Charleston firehouse.

1.2 Project Objectives

The specific objectives of this project can be separated into two general areas. The first, involves the verification of current URM analytical tools including those developed through component tests under other MAE Center projects. Specific objectives in this area include the identification of damage progression, critical components, shear force distribution, and torsional effects of a typical URM building composed of perforated walls. These objectives are designed to improve current analysis methods to allow seismic deficiencies of existing structures to be identified. The second general area of interest is the assessment of the effect of several retrofit techniques investigated under other MAE Center projects on overall building performance. The specific retrofit techniques of interest included the use of FRP overlays, post-tensioning, and diaphragm-to-wall connections. Once the effectiveness of these techniques is established, recommendations on the retrofit of existing structures can be made based on the level of structural deficiency.

1.3 Project Overview

The main focus of this project is the quasi-static testing of a full-scale two-story URM building with flexible timber diaphragms (see Fig. 1.3). This test structure contains several features common to typical URM building in Mid America. Some of the general characteristics of the structure include: **parallel** walls with large differences in stiffness, weak mortar-strong unit masonry, arch and steel lintels, flexible timber diaphragms, and piers with several different aspect ratios. The test structure is 23 ft 6 in in height and approximately 24 ft by 24ft in plan. Construction of the test structure was completed in early January, 2002. To accomplish the objectives outlined in the previous section, this

test structure will be subjected to slowly applied lateral force reversals designed to approximate seismic forces. The experimental program consists of a series of loading cycles conducted on the test structure in an unreinforced state as well as after different levels of rehabilitation, eventually culminating with an ultimate test of the fully rehabilitated structure.

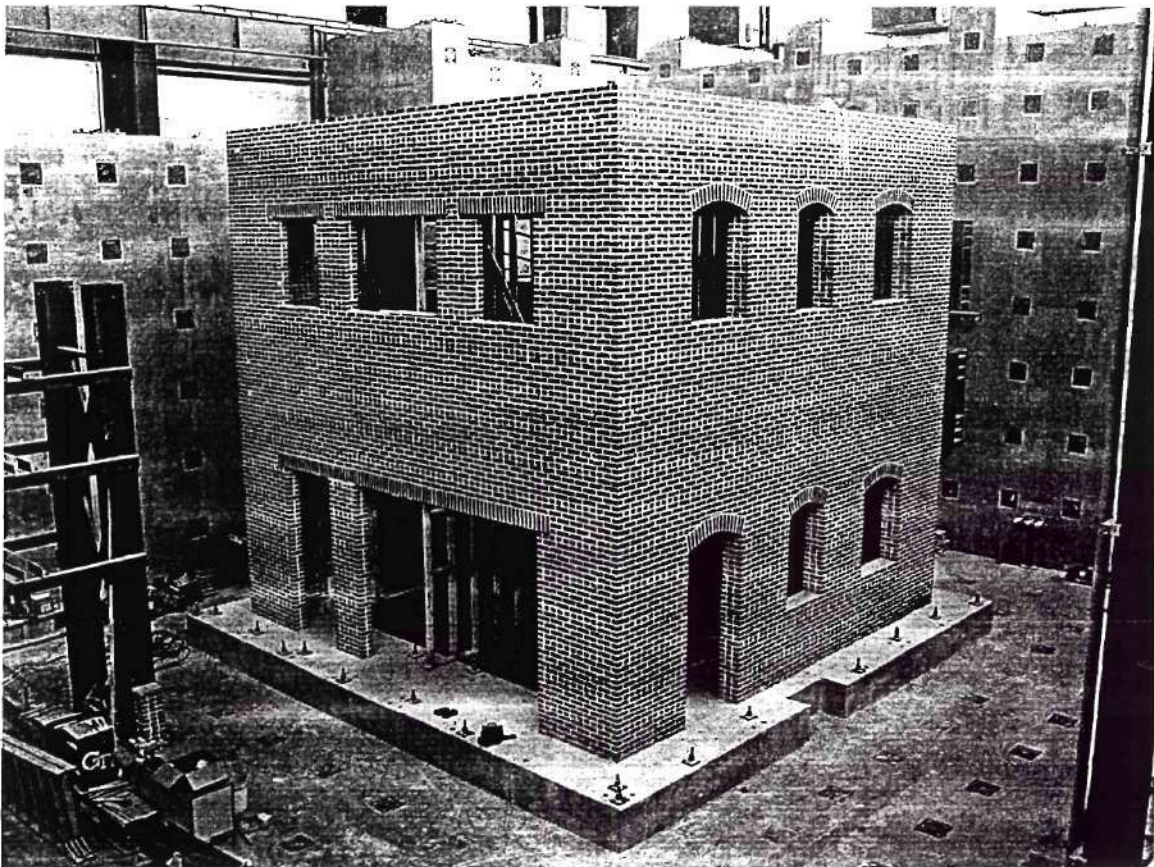


Figure 1.3. Completed ST-11 test structure

1.4 MAE Center Project Collaboration

A group of research projects sponsored by the Mid America Earthquake (MAE) Center are being conducted at several universities. They are aimed at developing strength

evaluation and rehabilitation strategies for URM buildings in the Mid America area. These projects investigate URM structures from many different aspects, including the characterization of the URM building inventory in Mid America (SE-1), in-plane strength and retrofit tests on URM piers (ST6) and analysis (ST-9), URM out-of-plane wall test (ST-10) and analysis (ST-9), and flexible wood diaphragm tests (ST-8) and analysis (ST-5). Project ST-11 along with a parallel project focused on a reduced-scale shaking table test conducted at the US Construction Engineering Research Laboratory (CERL) (ST-22) are designed to act as capstones of these research projects.

1.5 Outline of Report

Chapter 2 of this report presents an extensive literature review of past research conducted on both URM as well as retrofit techniques. Chapter 3 outlines the experimental portion of this project. The results of the comprehensive preliminary analysis of the test structure in both an unreinforced state and after retrofit are presented in Chapter 4. Finally, Chapter 5 summarizes the preliminary conclusions of this project.

2 LITERATURE REVIEW

An extensive literature review on research on URM structures, and the retrofit techniques used for this type of structures has been completed as part of the background of the ST-11 Project. Some of the literature is summarized in this chapter.

2.1 Unreinforced Masonry

The research on unreinforced masonry, including research on URM materials, the behavior of URM in-plane piers and spandrels, the behavior of URM out-of-plane walls, wood floor diaphragms, and entire URM structures will be reviewed in this section.

2.1.1 Unreinforced Masonry Materials

Unreinforced masonry is a composite construction material, consisting of masonry units and mortar. The following intrinsic mechanical properties of unreinforced masonry are important to evaluate the performance of the whole structure:

- The compressive strength, f_c
- The tensile strength, f_t
- The shear strength, f_v
- The elastic modulus, E ; and shear modulus, G

The mechanical properties of unreinforced masonry, as a composite material, are functions primarily of the mechanical properties of the individual masonry units and

mortar and the bond characteristics between units and mortar. The large differences in strength and stiffness between the masonry units and the mortar leads to an uneven distribution of stresses in masonry. This means that failure can occur either through the units or the mortar, or through a combination of the two. In addition to the possible failure of the individual components, the interface between masonry units and mortar provides an additional possible failure location. The large variability in material properties between nominally similar units and mortars is a further complicating factor. Current specifications (ASTM 1992) give large ranges for both the mortar composition (Table 2.1) and the masonry unit strength (Table 2.2).

Table 2.1 Mortar Compositions by Volumes

Mortar Type	Portland Cement	Hydrated Lime	Aggregate Ratio
M	1	¼	2 ¼ - 3 times the sum of the volumes of the cements and the lime used
S	1	¼ - ½	
N	1	½ - 1 ¼	
O	1	1 ¼ - 2 ½	
K*	1	2 ½ - 4	

* No longer used for construction after 1960's

Table 2.2 Masonry Unit Strengths

Designation	Minimum Compressive Strength (brick flatwise), gross area, psi	
	Average of 5 Brick	Individual
Grade SW	3000	2500
Grade MW	2500	2200
Grade NW	1500	1250

Field investigations of URM structures in Mid-America by the Southern Brick Institute (Clemson University, 2000) revealed that representative masonry materials used for old URM buildings in Mid-America area consist typically of strong units and weak mortars. Thus the current research is limited to this combination of unreinforced masonry

materials, in which the failures are expected to occur through the mortar or at the mortar-unit interface.

2.1.1.1 Compressive Strength

The compressive strength of masonry is usually determined by a masonry prism test. Each test prism shall be a single-wythe specimen laid in stack bond, with a height-to-thickness ratio of no less than two nor more than five (ASTM E447). Under vertical loading, the mortar in the masonry prism is in compression in all three principal directions, while the unit is in a tensile-compressive stress state, because the elastic modulus of the unit is typically larger than that of the mortar (Hilsdorf 1969, Lourenco 1996). As a result, vertical tensile cracks will develop in the units, and the compressive strength of masonry is controlled by the strength of units. The European codes (EC6 1995) recommends that the compressive strength of masonry be calculated based on the compressive strength of units and mortar using the following equation (Tomazevic 1999):

$$f_k = K f_b^{0.65} f_m^{0.25} \text{ (in Mpa)} \quad (2.1)$$

where f_k is the characteristic compressive strength of masonry, f_b is the normalized compressive strength of masonry unit, f_m is the compressive strength of mortar, and K is a coefficient depending on the type of units and mortar. The value of K ranges from 0.40 to 0.60. On the other hand, research done by the authors and some other researchers (Hamid 1980, Costley 1996, ST6 2000) shows that, for strong unit -weak mortar (type N or O) masonry, the compressive strength of masonry is roughly 0.25-0.3 of that of the unit.

2.1.1.2 Tensile Strength

The tensile strength of masonry is usually determined from either a bond wrench test or a flexural tension test. The bond wrench test uses a prism made of two or more units in height, and the flexural moment is directly applied to one mortar joint (ASTM C1072). The flexural tension test consists of a simply supported horizontal masonry beam, loaded vertically by a two-point load application system (see Fig. 2.1.) (Costley 1996). For a strong unit-weak mortar masonry, the tensile strength of mortar is lower than that of the unit. The interface between the unit and the mortar also has a weak tensile strength. Therefore, the mortar or the interface characteristics control the tensile strength of masonry. The interface strength is difficult to characterize as it depends on the absorbency of the units, the composition and proportions of the mortar, the surface roughness, and the humidity and temperature conditions during placing. Test results on tensile strength of masonry usually have very large scatter, both because the tensile strength of masonry is rather low and difficult to measure and because of the many factors that influence the bond strength of the interface, which are hard to control from one test batch to another. Costley (1996)'s flexural tension tests, which can be considered typical of older Mid-America construction, gave the average tensile strength normal to the bed joint of masonry with type O mortar as 40.6 psi. Tomazevic (1999) gave the following ratio between the tensile and compressive strength of any type of masonry:

$$0.03f_k \leq f_{tk} \leq 0.09f_k \quad (2.2)$$

where f_{tk} is the characteristic tensile strength of masonry.

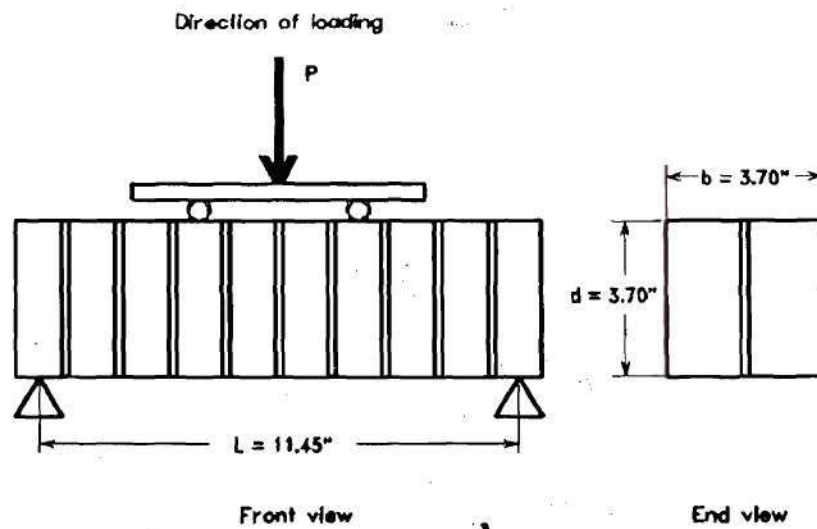
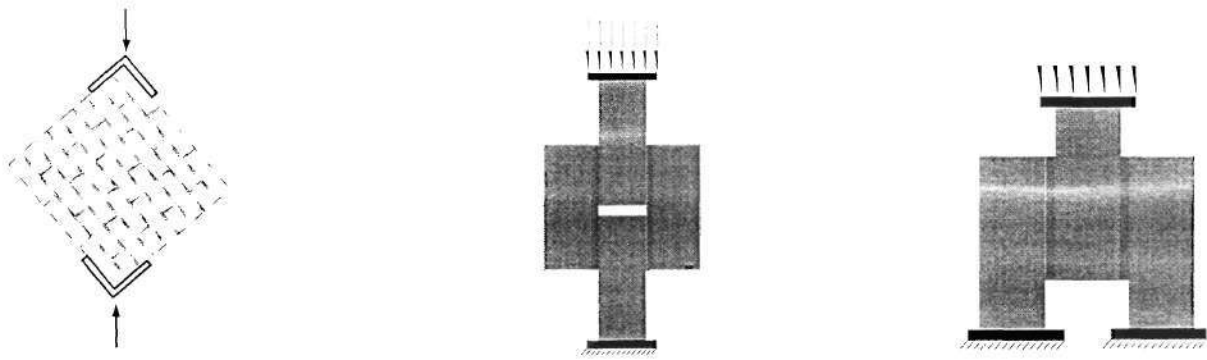


Figure 2.1. Test setup for the flexural tension test (adapted from Costley 1996)

2.1.1.3 Shear Strength

Shear strength is one of the most important mechanical properties of masonry. It is defined as a combination of an initial shear strength under zero compressive stress and an increment in strength due to a compressive stress applied perpendicular to the shear plane. There are two different shear strengths defined for masonry: (a) the shear strength of bed joints, and (b) the shear strength of head joints. The shear strength of bed joints is more important in this research project as the bed joints are parallel to the direction of lateral force induced by an earthquake.



a) Diagonal Compression test b) 4-bricks assemblage direct shear test c) triplet test

Figure 2.2 Different shear test setups

Several different test methods have been used to test the shear strength of masonry in the laboratory. Many investigators (Meli 1973, ABK 1981, Costley 1996) used diagonal compression tests, in which a square masonry panel is loaded in compression between two opposite corners (Fig. 2.2a), to study the diagonal tension and shear strength of masonry. One problem with this type of test configuration is that the concentrated diagonal load creates a complex state of stress in the specimen. FE analyses show that there are not only shear stresses but also normal stresses on the bed joints. As a result, the peak shear strength determined from this type of test includes the contribution of friction on the bed joints. FE analyses also show that the distributions of normal and shear stress on any given bed joint are non-uniform, which makes it difficult to interpret the test results. Meli (1973) used 4-bricks assemblages in a direct shear test (Fig. 2.2b) to investigate bond and friction of bed joints with different unit types. Two central bricks were bonded to two outside bricks by mortar joints. A gap was left between central top brick and bottom brick. Axial load was transferred by shear through the mortar joints. This test setup is similar to the triplet test setup used by Hegemier et al (1978), which is

essentially the top symmetric part of the 4-bricks assemblage test (Fig. 2.2c). Atkinson (1989) used a modified servo-controlled direct shear apparatus to examine the horizontal bed joint shear failure mode and the shear load-displacement behavior of unreinforced brick masonry during static and cyclic loading. Xiao (1995) proposed a zero-moment beam test apparatus to measure the shear strength of bed joint. Both Atkinson (1989) and Xiao(1995)'s test set-ups attempted to obtain a more uniform distribution of shear stresses and normal stresses in the bed joint.

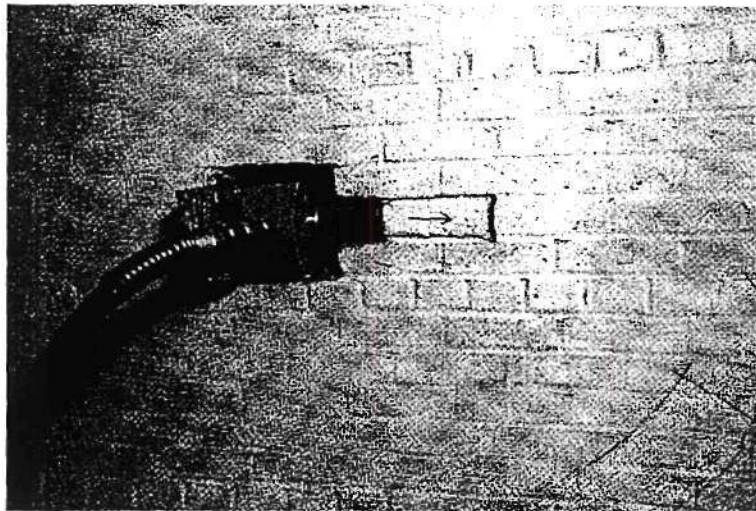


Figure 2.3 Test set up for Shove test (adapt from Costley 1996)

The in-place shear test, or shove test, has been recommended by FEMA 273 (ATC 1997) and is widely used for measuring masonry shear strength in existing masonry buildings. It usually requires the removal of a single brick and a head joint one brick away on the same course. A jack is placed in the cavity and used to laterally push the brick between the cavity and the missing head joint until slip occurs (Fig. 2.3). A total of 19 in-place shear tests conducted in the URM walls of a building being demolished were reported in ABK (1984). The test results showed rather large scatter,

ranging from 15 psi to 105 psi. The shear strength obtained by Costely (1996)'s in-place shear tests exceeded 300 psi, which was much higher than the 46.5 psi shear strength obtained in the corresponding diagonal compression tests. The rather high shear strength obtained in shove test is probably due to local stress concentrations after the removal of bricks in order to put in place the loading jack.

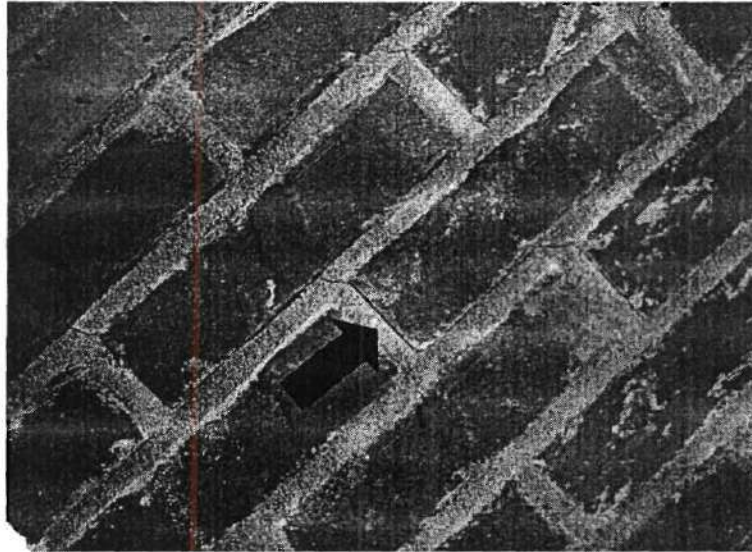


Figure 2.4 Interface cracks between units and mortar (taken in ST11 material test)

As evidenced in the material tests carried out for this research and discussed in Section 3.3, for strong unit-weak mortar type masonry, the shear crack occurs neither in the unit nor in the mortar, but at the interface between units and mortar (Fig. 2.4). The shear strength of this type of masonry depends primarily on the type of mortar, roughness of the surface of the units, water absorption capacity of units, and water volume in units and mortar. All the tests showed that, for a limited range of normal stresses (0 to 50 psi), the linear Mohr-Coulomb envelope is a good model for the shear strength, which expresses the shear strength of a bed joint under normal stress as:

$$\tau = \tau_0 + k\sigma \text{ (psi)} \quad (2.3)$$

where τ_0 is the shear bond strength, σ is the normal compressive stress, k is the effective coefficient of friction.

Hamid (1980) reported the results of bed joint shear tests on 121 four-bricks assemblage direct shear specimens. The mortars investigated were type M, S, and N. The tests showed that the shear bond strength τ_0 was not related to either the strength of mortar or the strength of brick, but quite sensitive to factors such as mortar flow, initial rate of absorption (IRA), and surface roughness of the brick. Either very high (1.94 kg/m²/min) or very low (0.15 kg/m²/min) IRA of bricks led to low shear strengths. The tests also showed that the coefficient of friction k was not related to the strength of mortar or bricks, but decreased substantially (from 1.44 to 0.90) as normal compressive stress increased (from 210 psi to 945 psi). Atkinson (1989) measured the cyclic load-deformation curve of bed joints under shear stress. Based on his test results and the results of some other investigators, he proposed a bed joint friction coefficient of 0.7 as a lower bound estimation for a wide range of masonry units and mortar types. Magenes (1992) used a triplet test to measure the shear strength of masonry with lime mortar (hydraulic lime and sand in volumetric ratio 1:3). His test showed that τ_0 was 30 psi for lime mortar and k was equal to 0.813, which correlated well with Atkinson's (1989) test results.

2.1.1.4 Elastic Modulus and Shear Modulus

Masonry is not an isotropic material. It could be simply considered as an orthotropic material with 5 independent elastic coefficients in 3D space, and 3 independent elastic coefficients in 2D space. Calvi (1996) pointed out that Young's modulus E , shear modulus G , and Poisson's ratio of masonry are unrelated to each other due to the orthotropic nature of masonry. However, empirical formulas, such as $G=0.4E$, are commonly used in masonry research. Deformation measurements in masonry show even larger variation than those for strength. Sinha (1978) used 1/3 scale model brick panels to measure the elastic modulus in two directions under uniform axial compression. He reported the value of E normal to bed joint at about 1230 ksi and the value parallel to the bed joint at about 1701 ksi. Magenes (1992) measured the elastic modulus of masonry normal to bed joint with lime mortar, and reported the elastic modulus at $0.33f_u$ or 434 ksi.

Based on experiment data, the European code (EC6 1995) gives the following formulae for calculating Young's modulus E and shear modulus G of masonry material (Tomazevic 1999):

$$E_1(f_k) = 1000 f_k, \quad G=0.4 E \quad (2.4)$$

where f_k is the characteristic compressive strength of masonry. In fact, the experimental data showed large scatter for E and G , and EC6 (1995) gives out the range as:

$$200f_k < E < 2000f_k, \quad 1000f_{tk} < G < 2700 f_{tk}, \quad 0.03f_k < f_{tk} < 0.09f_k \quad (2.5)$$

where f_{tk} is the characteristic tensile strength of the masonry

2.1.2 URM In-plane Piers

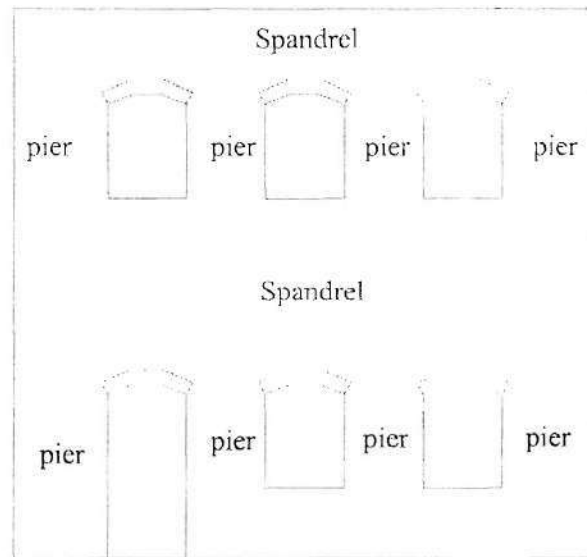


Figure 2.5 A typical perforated in-plane wall

A typical perforated in-plane wall, as shown in Fig. 2.5, is composed of piers between window/door openings and spandrels above and below the openings. Both post-earthquake assessments and shaking table tests on building models have shown that once out-of-plane failures are prevented, the final collapses of URM buildings are associated with the failure of piers in a critical story (usually the first story). Failure or cracking in the spandrels (sometimes called coupling beams) may have important consequences on the degree of coupling of the piers, but the final collapse of URM structure is always due to pier failure (Calvi et al 1995). The piers work like a column restrained by the ground or spandrels at the bottom and the top. If the stiffness of spandrel is much higher than that of the pier, the pier works as a fixed-fixed end column. On the other hand, if the

stiffness of pier is much higher than that of the spandrel, the pier works like a cantilever beam or fixed-free end column that is fixed on the ground. The next sections discuss experimental works on URM piers.

2.1.2.1 Experiments on Masonry In-plane URM Pier

Many experiments have been done to investigate the in-plane properties of URM piers. In-plane tests of masonry piers are typically performed under a given constant axial load, and with the application of a monotonic or cyclic lateral force or displacement. The boundary conditions at the top and bottom of the pier are usually assumed as being either fixed-fixed or fixed-free. In reality, it is almost impossible to achieve these end conditions in an experimental setup. The effect of several parameters, including the aspect ratio and vertical stress of the piers, on the behavior of URM piers has been studied. FEMA 307 (ATC 1999) listed the results of some recent tests on URM piers. These tests provided data on damage progression, ultimate strength, and drift response of the piers under investigation. This resource is a good reference for detailed description of the load-displacement response of URM piers under in-plane forces.

The influence of axial stress, ratio of unit strength/ mortar strength on the crack pattern of URM piers, together with deformability and failure mechanism of URM piers were investigated in the experiments of Konig (1988). A series of URM wall elements with the same height over length ratio of 1.0 were tested on an earthquake simulator. Fixed-fixed boundary conditions were simulated in the test. His main results were as follows:

- In cases where solely or primarily mortar joint cracking occurred, the individual portions of the wall separated by joints cracks would slide on each other, resulting

in large relative deformations. The strength degradation was small, since the strength capacity of pier was governed by the friction resistance, which remained nearly unchanged.

- In cases where unit cracking governed, the individual part separated by cracks were not stable and tended to slide downwards along the straight diagonal crack surface, resulting in a brittle failure model.
- Under low axial load, stepped diagonal cracking developed in the mortar joints along the diagonals. With increasing axial load, more and more straight diagonal cracks were formed passing through the units.

Five walls were extracted from a building constructed in 1917 and tested under monotonic loads at the University of Illinois (Epperson 1989, 1992, Abrams 1993). The height-length ratios of these five walls ranged from 0.5 to 0.8. The test setup used for this experiment utilized a fixed base and a free top. The observed failure modes of the walls are consistent for most specimens. Flexural cracks occurred at the heel of the wall at a moderate level of horizontal load (40 - 60% of the ultimate loads). It was followed by the wall sliding along the bed joints in the vicinity of the center portion of the wall. Next, the diagonal tension cracks opened as the load reached 90% of the ultimate load. Finally, the wall failed due to a rapid extension of diagonal cracks. The following conclusions could be obtained from the experiment:

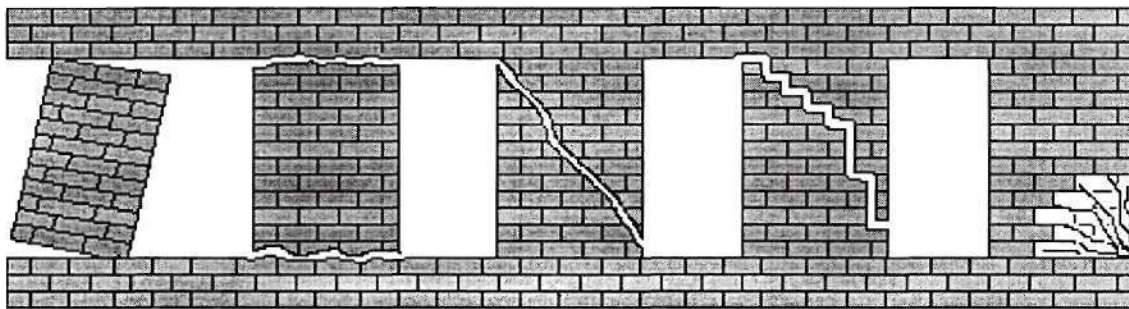
- The ultimate strength for these URM piers was significantly larger than the strength at initial cracking.
- The URM piers have substantial deformation capacity after initial cracking.

- The failure of in-plane masonry piers could be a combination of several different failure modes, such as sliding and diagonal.

MAE Center project ST6 (ST6, 2001) tested a series of URM piers to evaluate the effectiveness of various rehabilitation methods on improving seismic performance of existing URM piers. The test specimens were divided into two series, one was flexural member with large aspect ratio ($h/l=1.77$), and the other was shear member with small aspect ratio ($h/l=0.5$). The mortar used for all the specimens was type O mortar. Therefore the specimens were strong unit-weak mortar type masonry. The piers were tested as a cantilever specimen with various axial stresses ranging from 25 psi to more than 90 psi, in order to investigate the effect of vertical stress. The preliminary test results showed that the ultimate strength of pier increased with increasing vertical stress. Rocking was the dominant failure mode for the flexural members, and base sliding was the dominant failure mode for the shear members. The research of this project is still continuing at the time of writing this report.

2.1.2.2 Failure Mechanism of In-plane URM Pier

The experiments show that URM piers can have considerable deformability and ductility if certain failure mechanisms prevail. This conclusion runs counter to the prevailing wisdom that URM structures are very brittle. From the experiments, it is also found that axial stress, aspect ratio, boundary conditions, and relative strength between mortar joints and units determine the failure mechanisms of masonry wall piers. FEMA 273 (ATC 1997) gives four different crack patterns and failure modes for the URM piers as follows:



(a) Rocking

(b) Sliding

(c) Diagonal tension

(d) Toe crushing

Figure 2.6 Different crack patterns for the URM piers

- A large flexural moment can cause big flexural cracks at the top or the bottom of the pier. Then the pier undergoes rigid body rotation (rocking) along one corner of the pier (Fig. 2.6 a.)

- When the shear force in a pier is larger than the bed joints shear strength of the pier, sliding cracks develop in the bed joint, and the wall has relative sliding movement along the bed joints (Fig. 2.6 b.).
- When the principal tension stress due to external forces exceeds the tensile strength of masonry, diagonal tension cracks develop in the pier (Fig. 2.6c). The cracks are stepped cracks going through the mortar bed joints and head joints in the case of strong unit- weak mortar masonry, and are straight cracks going through the units in the case of similar strengths for the unit and mortar.
- When the principal compressive stress due to external forces exceeds the compressive strength of masonry, Compressive failure develops in the pier (Fig. 2.6d). Since the toe of a pier is usually the zone with high concentrated compressive stress, the compressive failure always develops in that area, and the failure mode is labeled toe crushing.

Rocking and sliding have large deformation capacities. The stepped diagonal tensional cracks going through the bed joints and head joints also have large deformation capacity, since the units slide between each other. On the other hand, the diagonal cracks going through the units make the masonry pier unstable and consequently lead to rapid strength deterioration, which represents a very brittle failure mode. Toe crushing is another brittle failure mode, because the piers lose their strength. It needs to be pointed out that these failure modes are not mutually exclusive. The failure of an in-plane masonry pier is often a combination of these modes. When a pier is subjected to the lateral load and axial load, the stress distribution in the pier is uneven. The shear stress in some parts of the wall is higher than that in some other parts, and so is the vertical stress.

As the result, some cracks develop in some parts of the wall associated with one special type of failure mode. The cracks developed lead to the redistribution of stress throughout the pier, and probably lead to a new high stress zone in another part of the pier. Therefore, as the external force increases, cracks develop in some other parts of the pier, probably associated with another failure mode. The cracking and failure sequence of the pier is determined by the on-going force redistribution in the pier determined by the propagation of cracks. In short, the true failure mode of a pier may be one of the typical failure modes discussed above, or the combination of several failure modes. The failure modes of the test specimen E3 in the test of Epperson (1989), which are the combination of sliding and diagonal cracking, verify the above concept.

Based on the above considerations, FEMA 306 (ATC 1999) gives 8 different failure modes for URM piers:

- URM2A: Wall-pier rocking
- URM2B: Bed-joint sliding
- URM2K: Preemptive diagonal tension
- URM2L: Preemptive toe crushing
- URM1H: Flexural cracking/Toe crushing
- URM1F: Flexural cracking/Toe crushing/ Bed joint sliding
- URM2G: Flexural cracking/diagonal tension

The eight different failure modes are used to describe possible single or combined failure modes of URM piers under different loading conditions. Detailed descriptions of those failure modes can be found in FEMA 306 (ATC 1999). Also, FEMA 273/306/356

(ATC 1997,1999,2000) give equations to calculate the strength of URM piers corresponding to different failure modes.

2.1.2.3 Elastic Stiffness and Deformation Capacity of In-plane URM Pier

The elastic stiffness of masonry piers can be calculated based on classical elastic theory considering flexural and shear deformation as follows (FEMA 274-ATC 1997):

$$K_e = Gt \frac{l}{1.2h \left[1 + \alpha \left(\frac{G}{E} \right) \left(\frac{h}{l} \right)^2 \right]} \quad (2-6)$$

where t is the thickness of pier; h is the height of pier; l is the length of pier, and α is a coefficient determining the position of the inflection point along the height of pier (α is equal to 0.83 in the case of fixed-fixed wall, and 3.33 in the case of a cantilever wall).

The above equation is rather simple and does not correlate well with experimental data. The experimental values are always smaller than the values obtained from this equation, with most tests giving the stiffness values ranging from 0.3 to 0.7 of those given by Equ. (2-6). The likely reasons for this discrepancy include: a) Some undetectable cracking might have developed before the initial stiffness was measured in the test, which would reduce the stiffness of the wall; b) the movement of the specimen foundation, and some other experiment test setup flexibilities increased the measured movement of pier to be larger than that assumed by the equation.

Based on the test data collected by FEMA 307 (ATC 1999), the deformation capacity corresponding to each failure mechanism can be estimated as in Table 2.3.

Table 2.3 Ultimate drift of URM pier corresponding to different failure modes

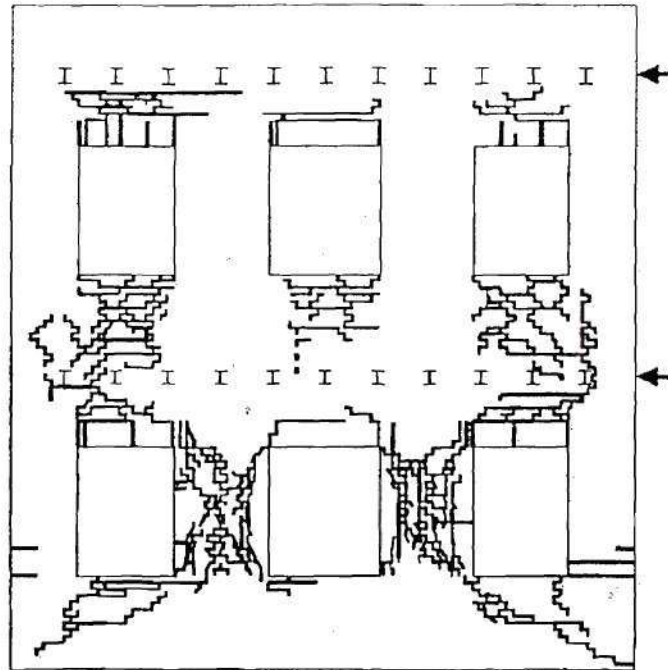
Failure mode	Ultimate drift (%)	References
Rocking	0.6% to 1.3%	Anthoine (1995), Magenes & Calvi (1995), Costley & Abrams (1996)
Bed-joint sliding	0.6% to 2.4%	Magenes & Calvi (1995), Abrams & Shah (1992)
Rocking/Toe Crushing	0.8%	Abrams & Shah (1992)
Flexural Cracking/Toe Crushing/Bed-joint Sliding	0.8% to 1.3%	Manzouri et al (1995)
Flexural Cracking/Diagonal tension	0.5% to 0.8%	Anthoine (1995), Magenes & Calvi (1992), Magenes & Calvi (1995)
Flexural Cracking/Toe crushing	0.2% to 0.4%	Abrams & Shah (1992), Epperson and Abrams (1989)

Based on the experiment data, it is clear that the type of failure mechanism determines the deformation capacity of URM piers. If rocking or sliding occurs before the URM pier fails in diagonal tension or toe crushing, the ultimate drift capacity is rather large, around 1% to 2%. If the pier fails in diagonal tension or toe crushing without rocking or sliding preceding them, the ultimate drift capacity of pier is rather small, around 0.5%.

2.1.3 URM Spandrels

It should be pointed out that most of the experiments on the in-plane behavior of URM walls were focused on the behavior of URM piers. little research has been conducted on the behavior of URM spandrels. The behavior of a spandrel is very different from that of a pier. First, the loading conditions of a spandrel are different from that of a pier. The axial force in the spandrel is very small compared with that of a pier. Second, the strength of the spandrel is determined by the tensile strength and shear strength of the head joints, while the bed joints determine the strength of a pier. Therefore, the strength of a spandrel is different from that of a pier, since the tensile strength and shear strength of the head joints are different from those of the bed joints, as been seen from the material test discussed before.

Field studies and the experimental research show that it is quite easy for cracks to develop in the spandrel (Fig. 2.7). These cracks will influence the behavior of the URM piers, and that of overall URM structure. Thus experiments on the behavior of spandrel elements are needed in the future research.



WALL B

Figure 2.7 Crack patterns in Wall B (Magenes et al 1995)

FEMA 306 (ATC 1999) distinguishes between two different failure mechanisms of the spandrels, which are spandrel joint sliding (URM3D) and spandrel unit cracking (URM3I). Formulas are also provided in the report to calculate the strength of spandrel corresponding to different failure mechanisms. However, those formulas are based on the equations for URM piers. No reference, or justification, or supporting experimental data is provided for the formulas.

2.1.4 URM Out-of-plane Walls

The walls resisting lateral forces normal to their plane are termed “out-of-plane walls” (ATC 1997). The out-of-plane wall works like a thin plate supported on the edges adjacent to the in-plane walls, the connections with the roof and floor systems, and the ground. During an earthquake, the out-of-plane wall vibrates under the seismic force due to its own inertia force and the forces transferred from the roof, the floor and the in-plane walls. The vibration and associated bending deformation may lead to the cracking and out-of-plane collapse of the wall.

2.1.4.1 Failure Mechanism of URM Out-of-plane Wall

Out-of-plane seismic dynamic stability is one of the most important problems for out-of-plane walls (Boussabah, L. 1992). The support conditions of the wall have significant influences on the dynamic stability of the wall in the out-of-plane direction. When not properly connected to the roof/floor and the in-plane walls, the masonry wall can easily become unstable and collapse under out-of-plane vibrations, as has been observed in the case of old masonry buildings during earthquake (Bruneau 1994). On the other hand, if the supports of the out-of-plane wall, especially the connections between the wall and the floor/roof diaphragm have sufficient strength, the supports transform the out-of-plane behavior of the URM wall from an unrestrained cantilever beam to a series of one-story-high panels dynamically excited at each end of floor diaphragms. As a result it can resist more severe earthquakes than the values predicted by traditional static analysis methods (Bruneau 1994, Boussabah 1992). After cracking, each portion of this properly supported wall behaves as a rigid-body member rocking on the wall’s through-cracks. If the gravity forces of the wall are sufficient to prevent overturning of these

individual bodies through the entire earthquake, a condition of dynamic stability of the out-of-plane walls exists.

The out-of-plane damage of a masonry wall usually includes the following cases:

- Parapets behave and fail as cantilevers.
- Out of plane damage of the masonry wall occurs because of inadequate anchors such as “government anchors”, which were not designed to provide earthquake resistance.
- Exterior wythes of multi-wythes walls fail in an out-of-plane manner because of inadequacy of the collar joint (Bruneau 1995).
- Some unstructural components, such as veneers, gables, and unanchored walls, occur out-of-plane failure(Bruneau 1994).

2.1.4.2 Experiments on URM out-of-plane walls

Although the out-of-plane failure of a URM structure can be prevented with appropriate anchors, the out-of-plane behavior of masonry walls needs to be investigated since it will influence the overall behavior of URM structure. Many experiments, including both dynamic and static tests, have been carried out to assess the out-of-plane behavior of masonry walls.

Two methods have been used for applying dynamic load. One method is to use actuators, the other one is to use shaking table facilities. ABK (1981a, out-of-plane) used actuators to apply dynamic out-of-plane excitation of progressively increasing intensity to

masonry wall specimens. The actuators were located at the top and the bottom of the walls, imparting them dynamic displacement time-histories (Fig. 2.8). The specimens were set up as cantilever walls. The top of the wall can rotate and displace vertically. Additional weight was added at the top of the wall to simulate additional wall or parapet masses above the wall section being tested. The purpose of this test was to establish bounds of dynamic stability. It was found that larger compressive loads improved the seismic resistance of out-of-plane walls. The effect of wall slenderness was also found to be significant. The cracks in the wall developed not only at the bottom of the wall, but also at the mid height of the wall, depending on the distribution of acceleration along the height of the wall.

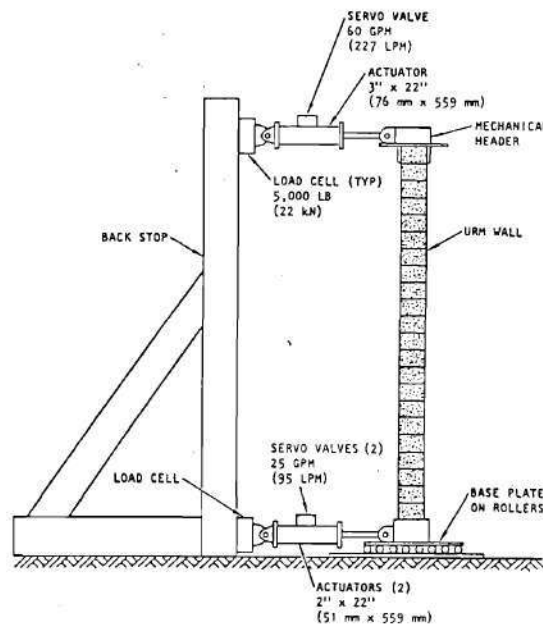


Figure 2.8 Dynamical test set up used in ABK out-of-plane test (ABK 1981a)

Some other researchers have used shaking table tests to investigate the out-of-plane behavior of masonry wall (Prawel and Lee 1990b, Bariola et al 1990, ST10 2000).

- Under external force, the shear cracks and tensile cracks normally go through the mortar or the bondage interface between the units and the mortar instead of going through the unit.

In the component level, lots of research has been done on the URM in-plane piers (see Section 2.1.2). Different failure models (rocking, sliding, diagonal tension and toe crushing) are possible for a pier, and the failure sequence is determined by the masonry materials, the boundary conditions, the aspect ratio and the axial stress of the pier. In the case of the strong unit-weak mortar type masonry that we are interested in, the diagonal tension cracks normally go through the mortar or the interface instead of the masonry unit. The strength and deformation capacity for each failure model has also been investigated in past research. The results can be used to analyze an entire URM structure. However, the inherent uncertainties of the URM material may limit the application of the detailed research. A balance should be sought between the applicability and the accuracy of the analysis methods to be used, especially in view of the scatter of the properties inherent with masonry materials. It should also be pointed out that the boundary conditions of pier in a perforated wall are different from that presented in a single pier test. The boundary restrains provided by the spandrels and the axial stress due to the lateral overturning moment are very important to the behavior of piers. Unfortunately, very little research has been done in this area.

URM spandrels have not attracted much interest from researchers, probably due to the common assumption that the spandrel can be considered as a rigid body in a perforated wall (see Section 2.1.3). Recent research of perforated walls shows that cracks

At the material level, different combinations of units and mortars lead to significantly different properties of masonry materials (see Section 2.1.1). Since the focus of this research is on existing URM buildings in Mid- America, it is important to utilize a material that is representative of “as built” conditions in Mid-America. Based on field investigations, existing URM structures in Mid-America have been classified as strong unit-weak-mortar structure (Clemson University,2000). This type of masonry material has its own special mechanical properties as follows:

- The compressive strength of masonry is controlled by the compressive strength of masonry unit. The compressive strength of masonry is roughly 0.25-0.3 of that of the masonry unit.
- The mortar or the bond at the interface between the units and the mortar control the tensile strength of masonry. The value is typically rather low, and shows large amounts of scatter in different situations.
- The sliding along the interface cracks between the units and the mortar controls the shear strength of masonry. The linear Mohr-Coulomb envelope is a good model for the shear strength. The initial shear bond strength is affected by many factors, such as the water absorption capacity of units. The effective coefficient of friction is more constant, ranging from 0.7 to 1.0.
- The masonry shows an orthotropic behavior. As a simply estimate, the shear modulus can be assumed to be 0.4 of the elastic modulus. The elastic modulus of masonry shows lots of scatter, which is also very sensitive to the stress level.

A discrete, linear-elastic, multi-degree-of-freedom dynamic model was developed by Tena-Colunga (1992) for the dynamic analysis of URM structures with flexible diaphragms. The URM structure was assumed to remain elastic during an earthquake. Masses were lumped at the intersection of the centroidal axes of the walls and the diaphragms and also at the center of each diaphragm. Flexible diaphragms were represented by elastic shear springs, whose stiffness could be roughly estimated by the in-plane shear and bending stiffness of the floor systems. The in-plane walls were represented by equivalent condensed beam with lateral degrees of freedom. A 2D FE model was used for each perforated wall to determine its lateral stiffness. Two generalized springs, one for rotation (rocking) and the other one for direct lateral displacement represented the foundation flexibility. One prototype, the Gilroy firehouse, was analyzed to test the analysis model.

Paquette and Bruneau (1999) used Drain-2Dx to analyze their one-story URM test specimen. Frame elements combined with rotational spring elements were used to model the rocking of the piers. Spring elements with hysteretic behavior were used to model the diaphragm.

2.1.7 Summary of Research on Unreinforced Masonry

A review of the literature available on unreinforced masonry reveals that all aspects of this topic have been studied extensively. However, due to the inherent variability of masonry, it is difficult to draw general conclusions from specific studies. In some cases this variability might lead researchers to draw opposite conclusions about the same phenomenon.

deformations. The building was regarded as consisting of a number of substructures. Each substructure was described by means of equivalent homogeneous materials whose properties were derived from experiments. The out-of-plane walls were considered as additional vertical load capacity components which could resist the overturning moments, but their lateral shear resistances were ignored. The out-of-plane walls were assumed damaged when the interstory displacements evaluated through the FE procedure exceeded the relative displacement limitation of the out-of-plane walls.

Tomazevic (1987) suggested that the storey mechanism model could be most suitable to define the behavior of masonry buildings with rigid diaphragms and subjected to seismic loading. The following assumptions were used:

- The masonry walls were connected together at floor levels by means of tie beams and rigid horizontal floor diaphragms.
- The masonry walls were fixed at both ends.
- The masonry walls with composite cross-sections (such as L, T, and H shaped walls) were considered to be separated along the vertical edge.
- The variation of vertical stress in each pier due to overturning moment was not considered.

Based on those assumptions, the masonry building was mathematically modeled as a multiply-degree-of-freedom shear system, with the masses concentrated at the floor levels. Story hysteresis envelopes were defined for the non-linear behavior of system. The envelopes represented the sum of the idealized hysteresis envelopes of the participating walls in the story considered.

and a dashpot. When the springs were destroyed due to external force, the media became discontinuous.

The smeared-crack model considers the nonlinear effect of the opening and closing of cracks by the variation of the material properties of an equivalent continuous material. It is assumed that the changing of effective elastic modulus and other properties of the element can represent the propagation of cracks inside one element. Chiostri and Vignoli (1991) used it to study the slender unreinforced masonry components. Shing et al (1992) reported that the special interface elements could be used together with the smeared-crack elements to realistically replicate the brittle shear failure of URM walls and the influence of mortar joints.

2.1.6.3.2 Analysis of Entire URM buildings

The detailed nonlinear FE analysis tools used for a single wall are not suitable for the entire structure. The reasons are:

- The structural components of the entire URM building are much more complicated than those of single wall, as they include not only in-plane walls but also out-of-plane walls and diaphragms.
- The analysis for the entire structure will be too time-consuming if the intent is to analyze the response of a single wall.

As a result, some methods based on some simplified assumptions have been used for the analysis of entire URM structures.

Benedetti and Benzoni (1984) used a non-linear 2D FE model to analyze URM structures for which the response mechanism was assumed to be dominated by shear

is strong while the spandrel is weak, another simplified model called “piers-only model” (Bruneau 1994) or “solid-pier/cracked-spandrel model” (Boussabah 1992) can be used. This model assumes that the spandrels in a perforated wall crack under very low lateral loads. It is usually used for reinforced concrete shear walls and has been proven to be excessively conservative in the case of URM perforated walls (Bruneau 1994).

Nonlinear FE methods have also been used to analyze perforated in-plane walls. Bruneau (1994) gave a detailed review of the FE methods used for the URM structures. Two types of nonlinear FE methods are commonly used: the discrete-crack model and the smeared-crack model.

The discrete crack model is a FE model in which a special interface element is introduced to allow the separation of adjacent elements when the tensile strength of masonry is exceeded at this interface. To locate the special interface elements in this FE model, the prior knowledge of the ultimate behavior of the URM walls including the location, direction, and length of the cracks is needed. Chiostrini et al (1989) used it in combination with a micro-element model to analyze a masonry wall monotonically tested in shear. Kirk Martini (1997, 1998) used it to analyze out-of-plane masonry walls.

Another discrete crack model is the modified distinct element method (MDEM) used by Morales (1992) to analyze the failure sequence of an adobe wall. This method was based on Merguro and Hakuno’s (1989) work. The MDEM was a numerical method that can follow the behavior of a media from continuous state to complete fracture. The model was composed of many circular elements (discrete elements). Each element had connections with surrounding elements by a Voight type assembly composed of a spring

2.1.6.3 Analysis of URM Structures

The analysis of URM structure can be divided into two categories: 1) the analysis of the perforated in-plane walls and 2) the analysis of the entire URM structure.

2.1.6.3.1 Analysis of Perforated In-plane Walls

Both simplified and the more complicated FE models and have been used to investigate the behavior of in-plane URM walls. The simplified models for the URM perforated in-plane walls are based mainly on assumptions about the relationship between the piers and the spandrels. As discussed in Section 2.1.2, most of the research has focused on the masonry piers. The spandrel is usually simplified as a rigid body, which leads to a simplify analysis model called “walls model” (Bruneau 1994) or “solid-spandrel /cracked-piers model” (Boussabah 1992). In this model, the spandrels are assumed intact and rigid, and the lateral shear forces are distributed to parallel piers by the spandrels. The overturning moments induced by the lateral forces are usually ignored. The perforated wall fails when several or all piers reach their strength capacities.

Costley and Abrams. (1996) used a nonlinear static pushover method based on the above simplified model to analyze the in-plane perforated URM walls in their thesis. The perforated in-plane wall was modeled with rigid spandrels and flexible piers. The vertical stress in the piers due to the gravity load was considered, while the vertical stress due to the overturning moments was ignored. In this model, the piers were assumed to have perfect elastic-plastic behavior. When an element yielded, the element was simply removed and the incremental loads were applied to the reduced structure.

The “solid-spandrel /cracked-piers model” is suitable only for perforated walls whose spandrels are deep or of short span (Bruneau 1994). On the other hand, if the pier

significant damage developed at a maximum drift of approximately 0.4%. Comparatively, the first level drift for the RD structure corresponding to the maximum lateral force was 0.5%, and the test was terminated with a maximum first floor drift of approximately 1.0%.

The different behavior observed between the RD test and the LS test are possibly due to the following reasons:

- The different materials used in the two structures may lead to different failure modes in the pier.
- The difference between the concentrated lateral forces applied in the LS test and the relatively uniform lateral inertia forces induced in the RD test may lead to different force distributions in the masonry walls, and consentingly lead to different failure modes.
- The LS test provide more time for the cracks to propagate. As a result, the damage of the LS specimen looks more severe than that of the RD specimen.

Fianlly, it should be pointed out that pseudo-dynamic test has been used by some researchers on the URM building. However, the pseudo-dynamic method can't replace the shake table test for URM structure with flexible diaphragms. Most of the mass in this type of URM structure is distributed in the masonry walls, and can not be realistically represented by the concentrated force used in a pseudo-dynamic test. Also, the sensitivity of the URM structure to the loading rate will make the response of a pseudo-dynamic test specimen different from that of a shake table test specimen.

Both the RD test and the LS test showed that the damage of the first floor was more severe than that of the second floor, and that the damage of the in-plane walls was more severe than that of the out-of-plane walls. The two in-plane walls worked as two separate walls, because the flexible floor/roof diaphragm could not provide much coupling between them. However, significant differences existed between the two specimens, which are summarized as follows:

- The damage of the LS specimen is much extensive and more severe than that of the RD specimen.
- The piers at first floor of the LS specimen showed diagonal cracks, which were not observed in the RD specimen.
- The spandrel of LS specimen, especially the area right below the opening, showed extensive damage, which was not observed in the RD specimen.
- The damage to the RD specimen focused exclusively on first floor; on the other hand, some damage was observed in the second floor of LS specimen.
- The out-of-plane wall in the LS specimen worked more like a flange of in-plane wall, since the external force was transmitted to it through in-plane wall, which was *different from the RD case, where the out-of-plane wall had to resist its own inertia force.*

Large difference of the lateral drift between the RD specimen and the LS specimen was also observed. For the RD specimen, the story drift associated with initiation of cracking was approximately 0.1%, which was almost the same as that of the LS specimen. However, the maximum lateral force of the LS structure was initially achieved at a drift of approximately 0.2%, and the static test was terminated when

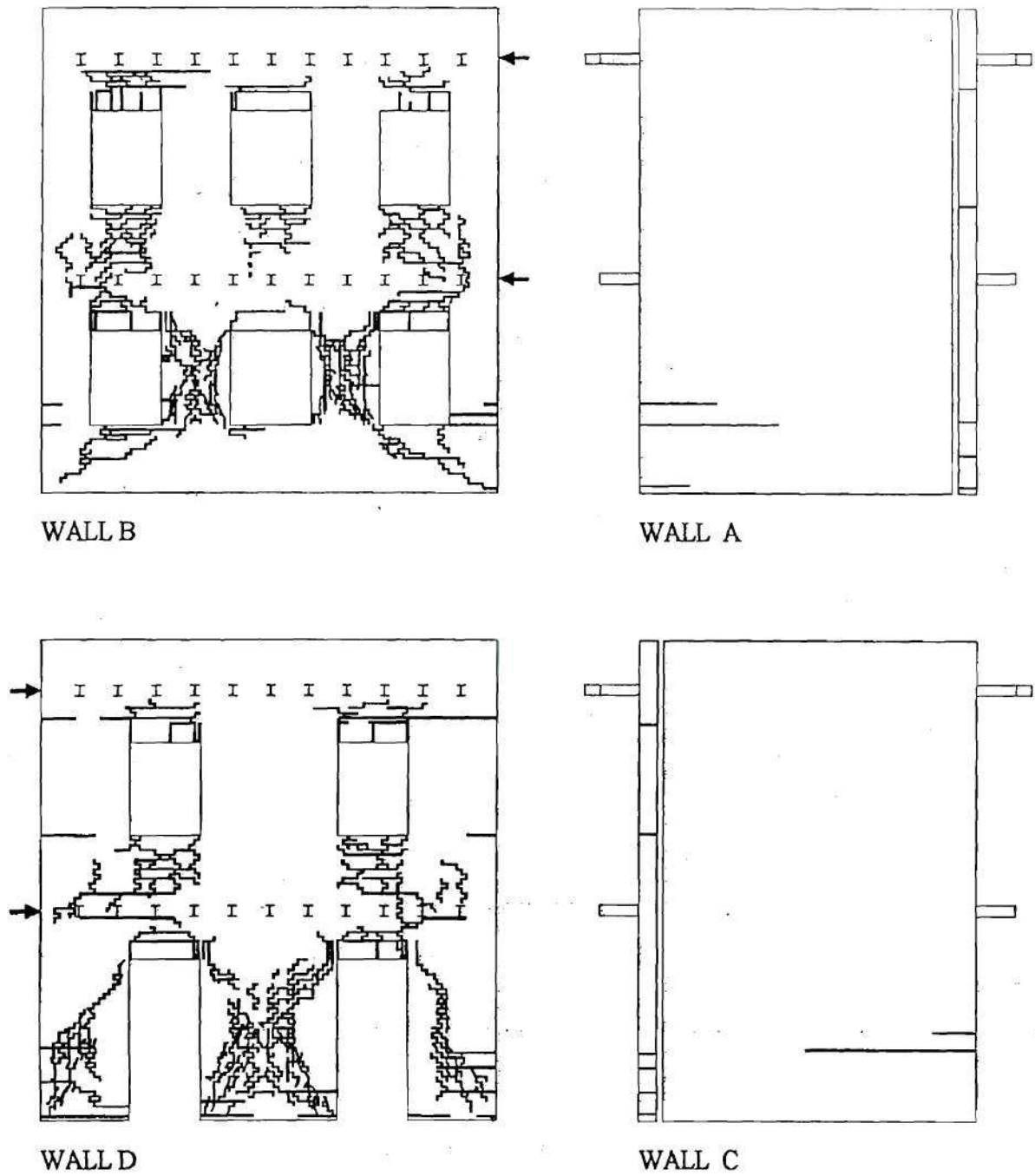
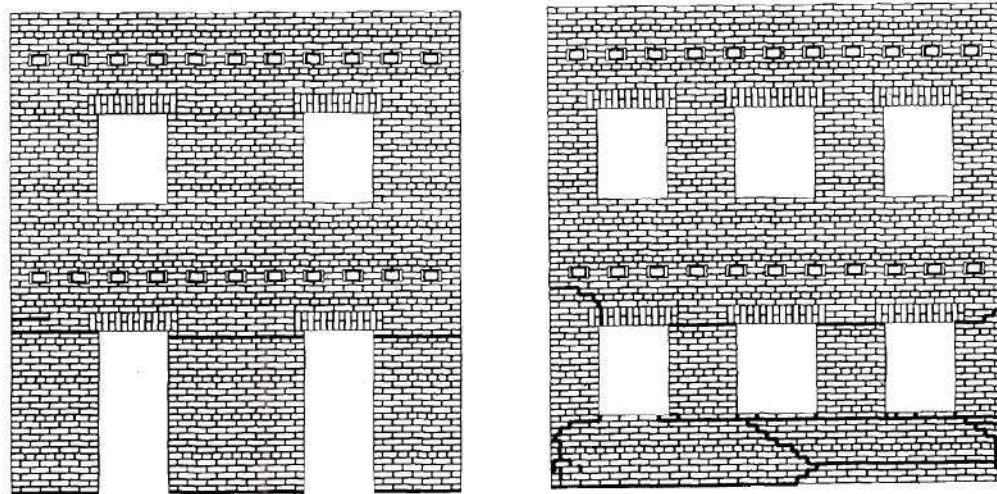
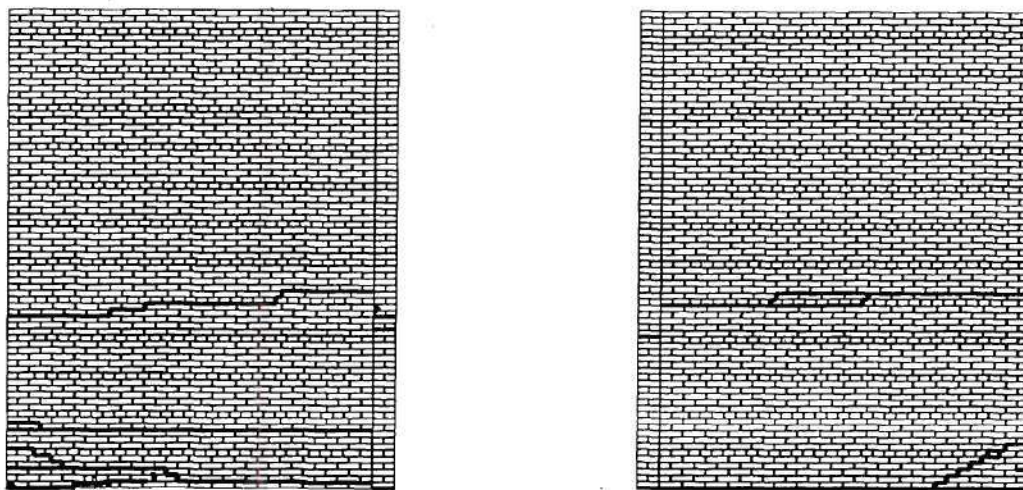


Figure 2.21 Final crack pattern in static tested specimen (from Magenes et al 1995)

the exterior piers in the window wall. However, those piers remained essentially undamaged.



(a) In-plane wall



(b) Out-of-plane wall

**Figure 2.20 Final crack pattern in the dynamical tested specimen
(taken from Costely et al 1996)**

The lateral force was applied to the LS specimen by four screw jacks connected with four steel rods, which distributed the loads to the floor beams. The specimen was tested under displacement control. The top drifts of the two in-plane walls were controlled and were set equal to each other. The displacement at the first floor level of each wall was controlled such that the applied force at the first floor was equal to the applied force at the top floor level. The equal roof/floor forces loading scheme was based on the test results of the RD test.

It is interesting to compare the different failure modes observed in the two tests. The final crack pattern of RD specimen S1 is shown in Fig. 2.20. The out-of-plane wall cracked before the in-plane wall. Cracks in the out-of-plane wall were mainly horizontally, which meant the out-of-plane wall worked more like the flange of the in-plane wall. All the cracks in the in-plane walls focused on the first floor. All piers developed flexural horizontal cracks at bottom and top. However, no diagonal cracks were observed in the piers. Some cracks also developed in the portion below window opening in the window wall. No cracks developed in the spandrel. The final crack pattern of the LS specimen was shown in Fig. 2.21. The crack pattern of the out-of-plane wall was similar to that of the RD specimen. However, the crack pattern of the in-plane wall was different from that of RD specimen. Initially, cracking was limited to the spandrels between the openings in both in-plane walls. As cracks developed in the spandrels, the coupling between masonry piers decreased. Eventually, the cracks in the spandrels ceased to propagate further, and the failure mechanism was dominated by shear cracking in the center piers in the first floor. At the maximum drift level, the exterior piers in the door wall failed in shear. Some flexural horizontal cracks were observed at the bottom of

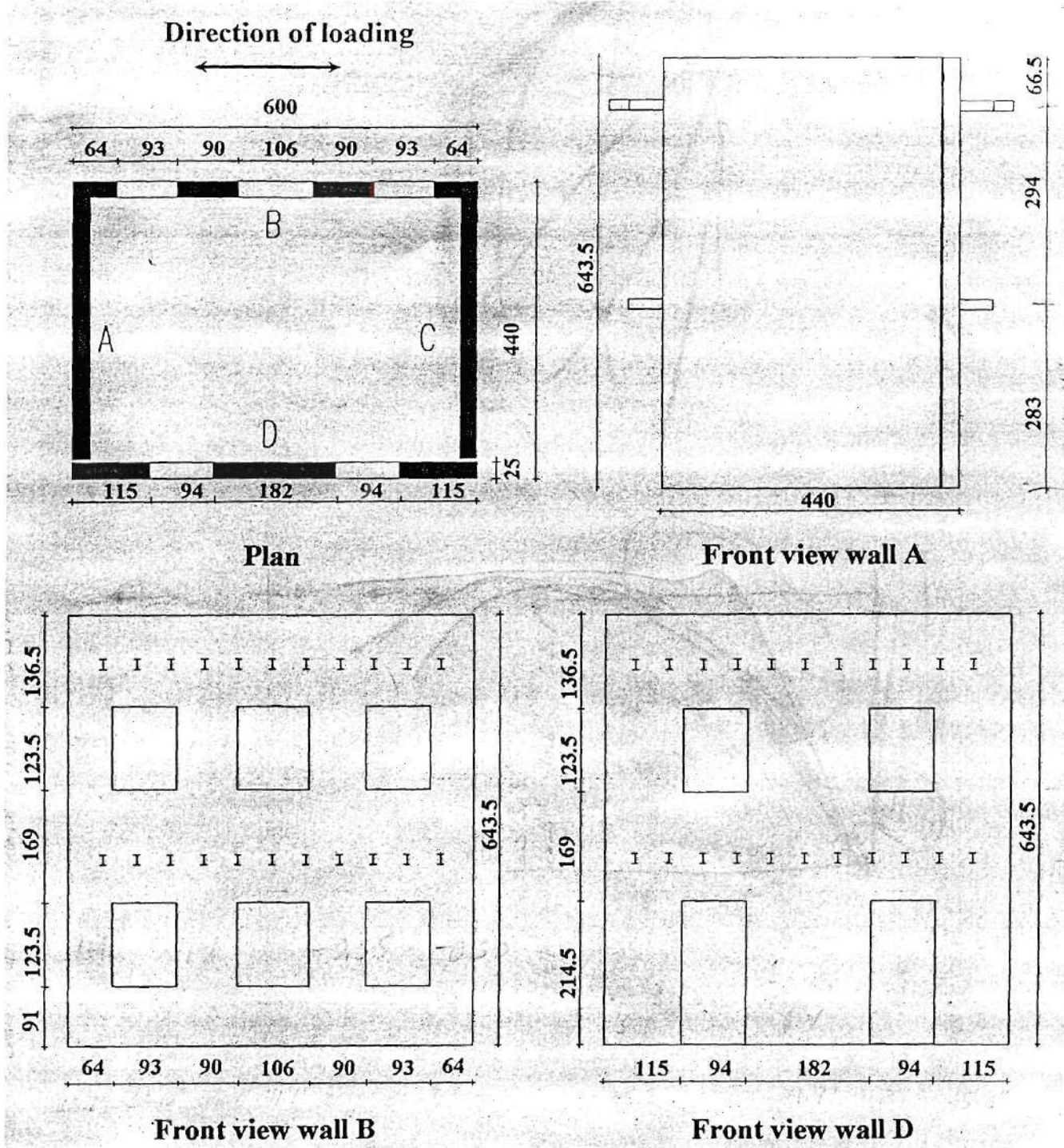


Fig. 2.19 The dimensions of the test structure in Magenes's test (1995)

joists and covered with diagonal boards with a straight board overlay, which was anchored to the wall with through-wall bolts in accordance with UCBC. One actuator applied pseudo-dynamic force at the center of the diaphragm. The analyses of the results are still under development.

Another full-scale test of URM structure was finished by Magenes et al(1995) in Italy. The specimen tested in his experiment was a replica of the reduced-scale dynamic specimen tested by Costley and Abrams(1996). The geometry of the large-scale static (LS) test structure was almost identical to that of the reduced-scale dynamic (RD) specimen (see Fig. 2.19). The floor/roof systems of the LS specimen were the same as those used in the RD specimen, and consisted of 11 isolated steel beams directly embedded into the masonry walls. However, different materials were used in the two tests. Clay brick and Type O mortar were used for the RD structure, and clay brick and lime mortar were used for the LS structure. Furthermore, the gravity stress in the first floor piers of the LS structure were 60-70 psi, which were a little larger than the gravity stress of 33-48 psi in the first floor piers of the RD structure.

for the wall decreased to negligible value. Second, after substantial cracking, the large amplification of either the wall acceleration or the base acceleration by the flexible diaphragm diminished to a point where no amplification existed at all. The amplification reduction occurred even when only one supporting wall experienced major cracking.

The test also showed that the equivalent roof level seismic forces were almost the same as the equivalent floor level seismic forces. For the structure in elastic range, the phenomenon could be explained by the fact that the masonry walls might be very stiff. After cracks developed in the structure, these results might also be expected since the upper portion (including both diaphragms) of the structure remained intact and moved as a rigid body on the top of the first floor.

2.1.6.2.2 Large-scale Static Test on URM Structure

Compared with the reduced-scale dynamic experiments, full-scale tests of URM structures are seldom conducted to the cost and test capacity demands.

Recently, a research program was conducted at the University of Ottawa to investigate the flexible-floor/rigid wall interaction in old URM buildings (Paquette and Bruneau, 2000). The test included a single-story full-scale URM with two wythes solid brick walls and Type O mortar. The structure had two symmetric perforated shear walls and two solid transverse walls. There were gaps left between the shear wall and the perpendicular wall at one ends, and were continuous at the other ends to investigate the plane analysis model, and to observe the impact of in-plane rotation of the diaphragm's ends on wall corners. The flexible diaphragm of this building was constructed with wood

Specimen S1 remained in the elastic range through the test up to a maximum base acceleration of 0.436g. When the maximum base acceleration reached 0.641g, both out-of-plane walls debonded from the concrete foundation. With increasing base acceleration, more and more cracks developed both in the in-plane walls and the out-of-plane walls. During Test run 14, the in-plane wall piers fully cracked, and a second full length crack developed at the west out-of-plane wall right below the first story beam connection, while the east out-of-plane wall fully cracked. During test run 15 with the maximum base acceleration of 1.781g, two full-length cracks developed at the east out-of-plane wall; one was right below the first story beam connection and the other was at 9 courses above the bottom. The cracks in the in-plane walls developed further. In the door wall, the outside piers rocked, and the central pier slid. In the window wall, some cracks were observed initiating from the corner of the window opening, and propagating as diagonal cracks into the piers. The entire top portion of S1 appeared to be fixed in space as the first-story walls moved back and forth below.

As expected for a truly flexible diaphragm system, the test showed that little or no coupling was presented between the parallel shear walls. Individual walls vibrated independently of each other with no torsion induced by the diaphragm. It was observed that the deflection of the door-walls was two times larger than that of the window-walls in some cases. The acceleration ratios for the model structure were also interesting. Prior to cracking, the ratios between the wall acceleration and the base acceleration and the ratios between the diaphragm acceleration and the wall acceleration were appreciable, on the order of 1.2-1.7 and 1.7-2.5, respectively. After cracks developed in the walls, two changes in behavior were observed. First, the amplification ratio of the base acceleration

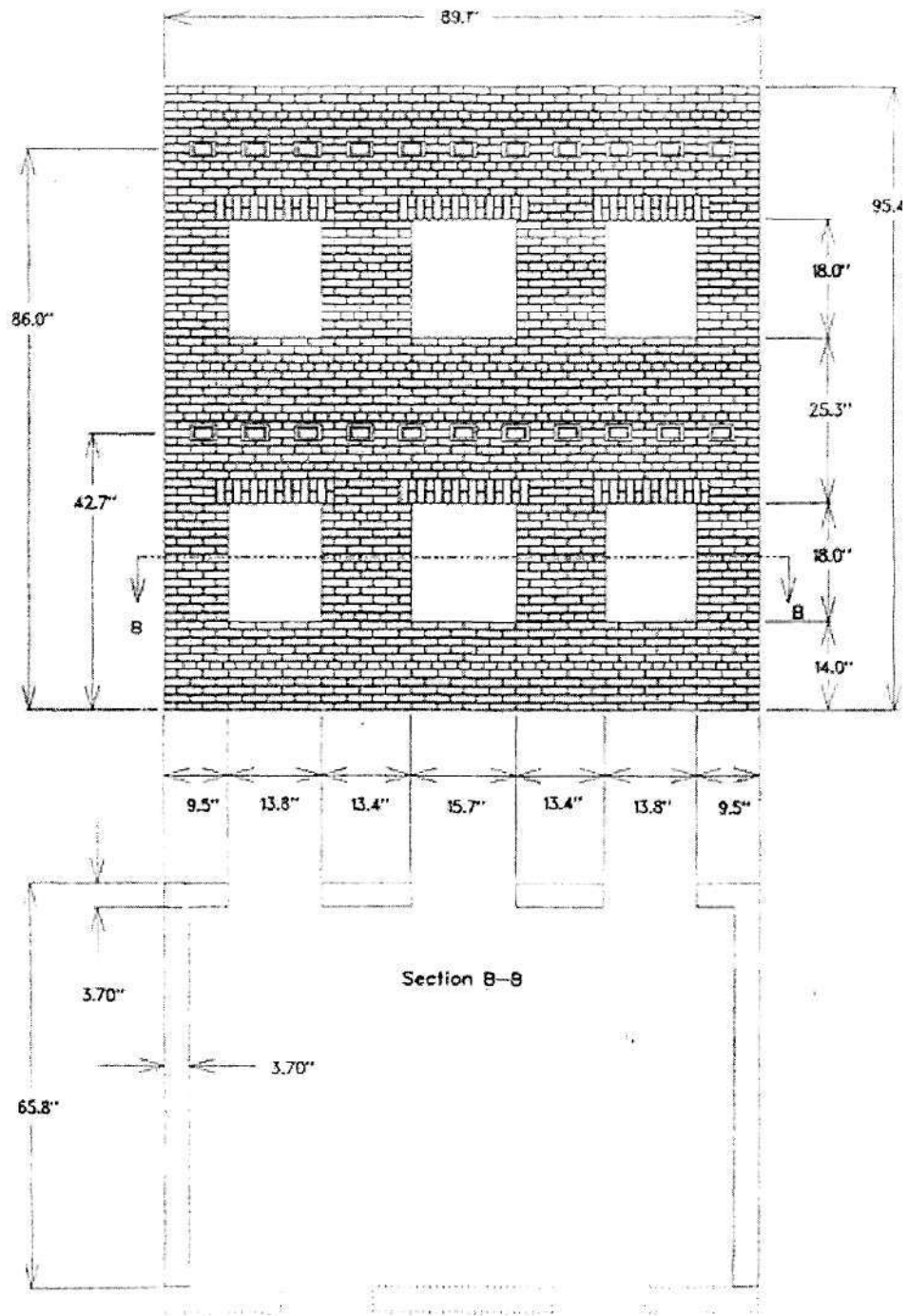


Fig. 2.18. The test specimens Widow wall in Costley's test (taken from Costley 1996)

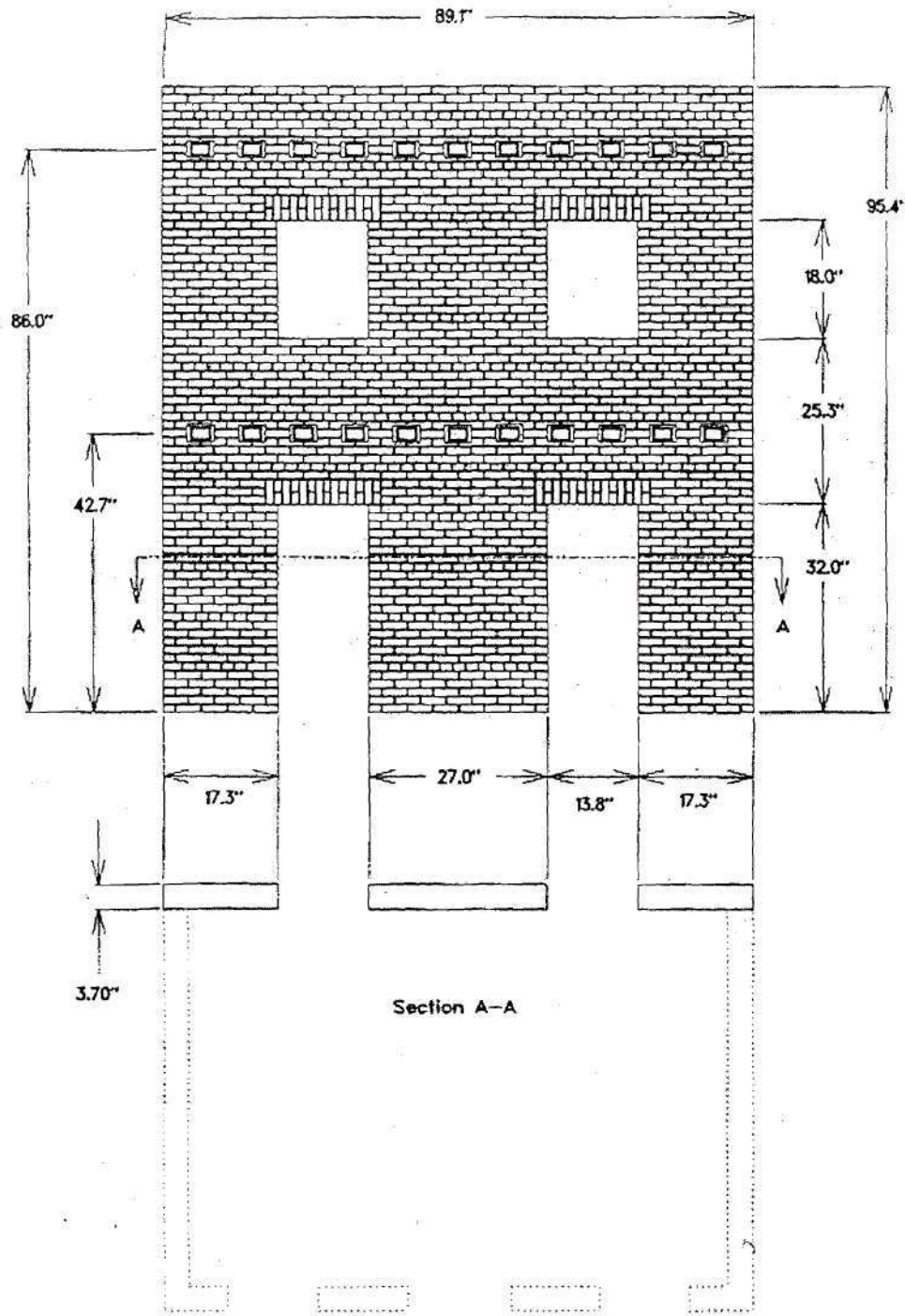


Fig. 2.17. The test specimens Door wall in Costley's test (taken from Costley 1996)

wall was separated by a full-height joint with the width of one mortar joint. A steel diaphragm with additional weight attached to it was used to represent the flexible wood diaphragm. The joints between the diaphragm and the wall were made so that it could transfer the 3D forces but no moments from the diaphragm to the wall. The floor system was also tied to the transverse walls by rods and nuts. Solid brick and Type O mortar was used to build the buildings. Only the first building S1 is discussed here because the second building S2 was constructed by retrofitting the first one, and the cracks developed in the first building might have led to the initial weak portions in the second specimen.

The following conclusions could be obtained from this test (Tomazevic 1993):

- The structural characteristics of the floor/roof diaphragms and the tying of structural walls represented decisive parameters to their seismic resistance.
- For an URM structure without ties to prevent the separation of the walls, the out-of-plane walls cracked easily, as the out-of-plane walls would have excessive deformations because of their small stiffness. As a result, the out-of-plane walls might collapse before severe damage developed in other parts of the structure. Also, the out-of-plane walls in the second floor were much easier to fail than the out-of-plane walls in the first floor.
- If the failure of the out-of-plane walls were prevented by a strong floor system, the damage would concentrate on the first story in-plane walls. When the upper structure rocked and slid on the top of the first floor, the corner of the first floor was failed early in the tests.
- The steel ties or the RC slab with bond beams increases the integrity of the structure and consequently increases the ultimate strength and energy dissipation capacity of the structure.

Recently, two reduced-scale URM buildings were constructed and tested at the University of Illinois by Costley and Abrams (1996). The box-type structures had two perforated shear/bearing in plane walls (window wall and door wall), and two solid out-of-plane walls (Fig. 2.17 and 2.18). For both Test structures S1 and S2, the two out-of-plane walls and the window wall were continuous, forming a C-shape, while the door

developed in the first-story in-plane walls. Also, vertical cracks developed at the corners of the first-story in-plane walls due to the sliding and rocking of the upper second-story box, which led to the separation of the corners in the first floor.

The lateral deformation shapes were also obtained in this experiment. Fig. 2.16. shows the distribution of the displacements along the roof. The displacements of the in-plane walls and the out-of-plane walls were almost the same in the elastic range for the different diaphragms, possibly due to the large thickness of the masonry walls. However, with increasing ground motion, the differences between the lateral displacements of the in-plane walls and that of the out-of-plane wall increased. As observed in the experiment, there was out-of-plane failure in Model A, but not in Model B, C, and D.

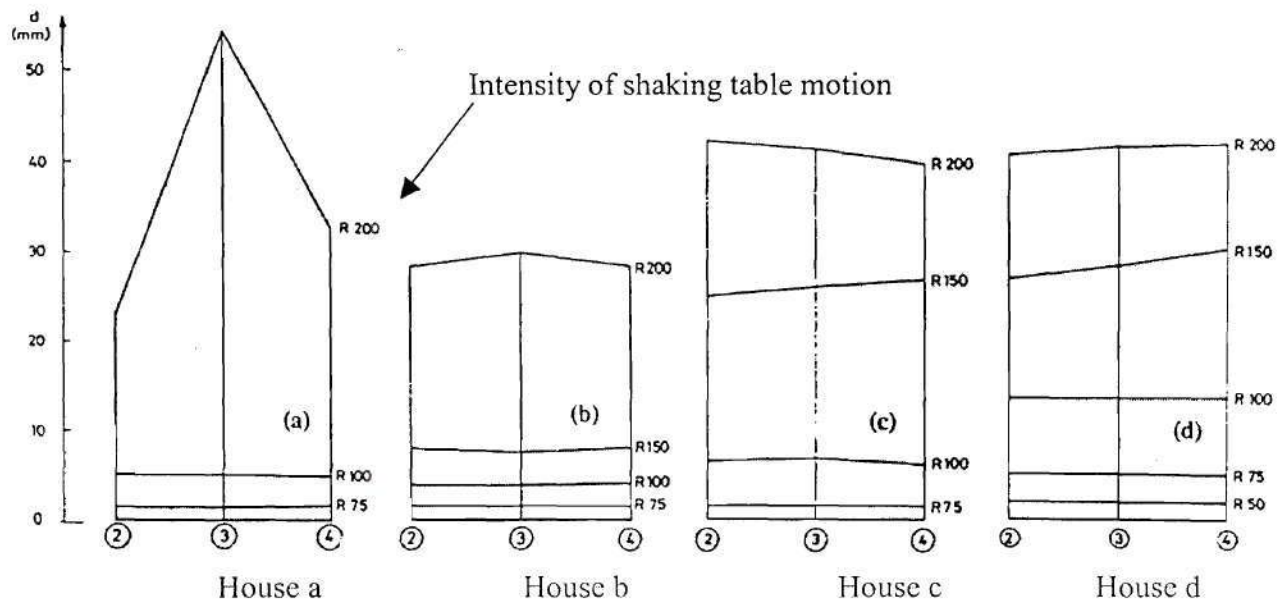


Figure 2.16. Distribution of displacements along the top floor
 (Locations: 2, 4 the in-plane walls, 3 center of the out-of-plane wall)
 (Tomazevic (1993))

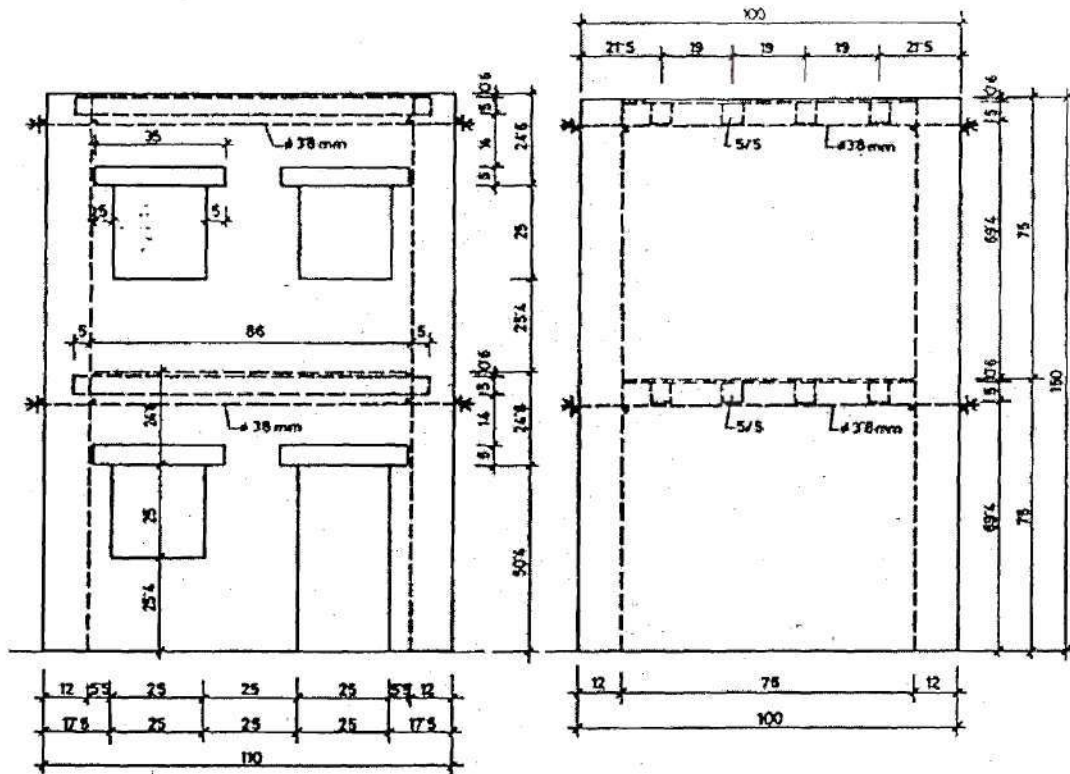
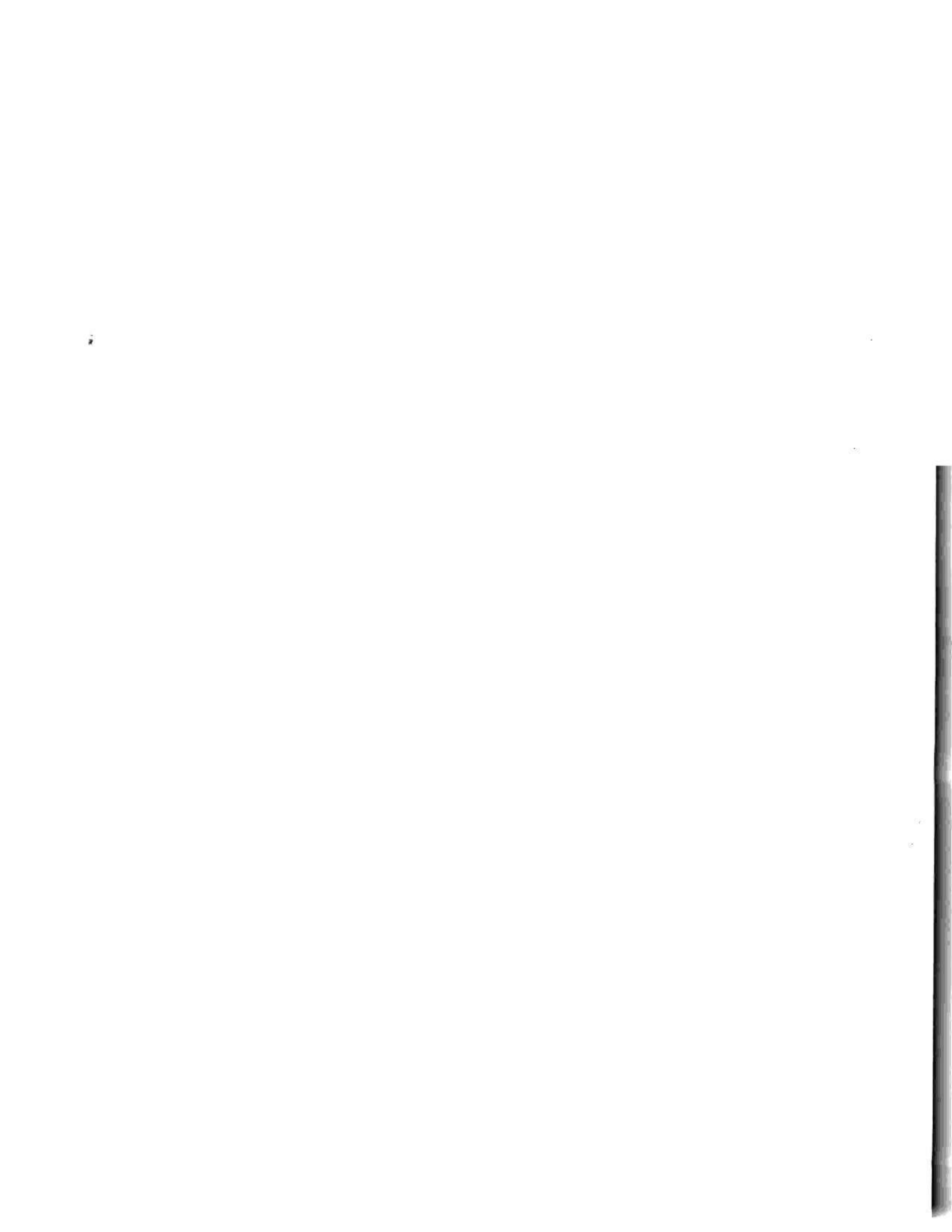


Fig. 2.15. Layout and dimensions of the test models in Tomazevic (1993)'s test (Tomazevic (1993))

The behaviors of Models B, C, and D was similar. All of them collapsed because of the severe damage developed in the walls in the first story, whereas no significant damages to the second story walls were observed. At the beginning of the test, the models were observed rocking and vibrating along the crack at the joints between the walls and the foundation slab. Then horizontal cracks developed all around the models just below the first floor. With the increasing ground motion, the damages kept on cumulating in the first floor walls, while the second story walls vibrated like a monolithic box placed on the top of the first floor walls with little damage. Finally, severe diagonal cracks

Based on the prototypes of old urban brick-masonry residential houses in the earthquake-prone areas of central Europe and Mediterranean, four 1:4 scale simplified two-story URM models were constructed and tested in an one-degree vibration shake table by Tomazevic etc(1993). The URM structures were made from stone and cement mortar (cement: lime: sand in the proportion of 0.5:4:12). The structural configuration of the masonry walls in all the models were identical: the solid loading-bearing walls were oriented in the direction of the shake table motion, whereas the out-of-plane walls were perforated walls with window and door openings (Fig. 2.15.). The diaphragms were different for the four walls. Model A had wooden floors made from freely supported wood joists without steel ties. The diaphragms of Models C and D were identical to Model A, but, their walls were tied with steel ties, placed along the walls on both sides and anchored to steel plates at the ends. The steel ties in Model C were prestressed. The steel ties in Model D were not prestressed, but this model also included additional diagonal steel ties. The diaphragm in Model B consisted of RC slabs with bond-beams along the walls.

The behavior of Model A was as follows. At the beginning of the test, rocking was observed along the cracks at the joints between the walls and the foundation slab. Then more horizontal and diagonal cracks developed in the first floor walls. With the increasing ground motion, the walls in the second story disintegrated, with all the upper corner walls separated. Vertical cracks and horizontal cracks were also observed at the second-story out-of-plane walls. Masonry units began to fall off. Meanwhile, the cracks in the first floor continued to propagate. The test was stopped when one of the corner walls at the second floor collapsed.



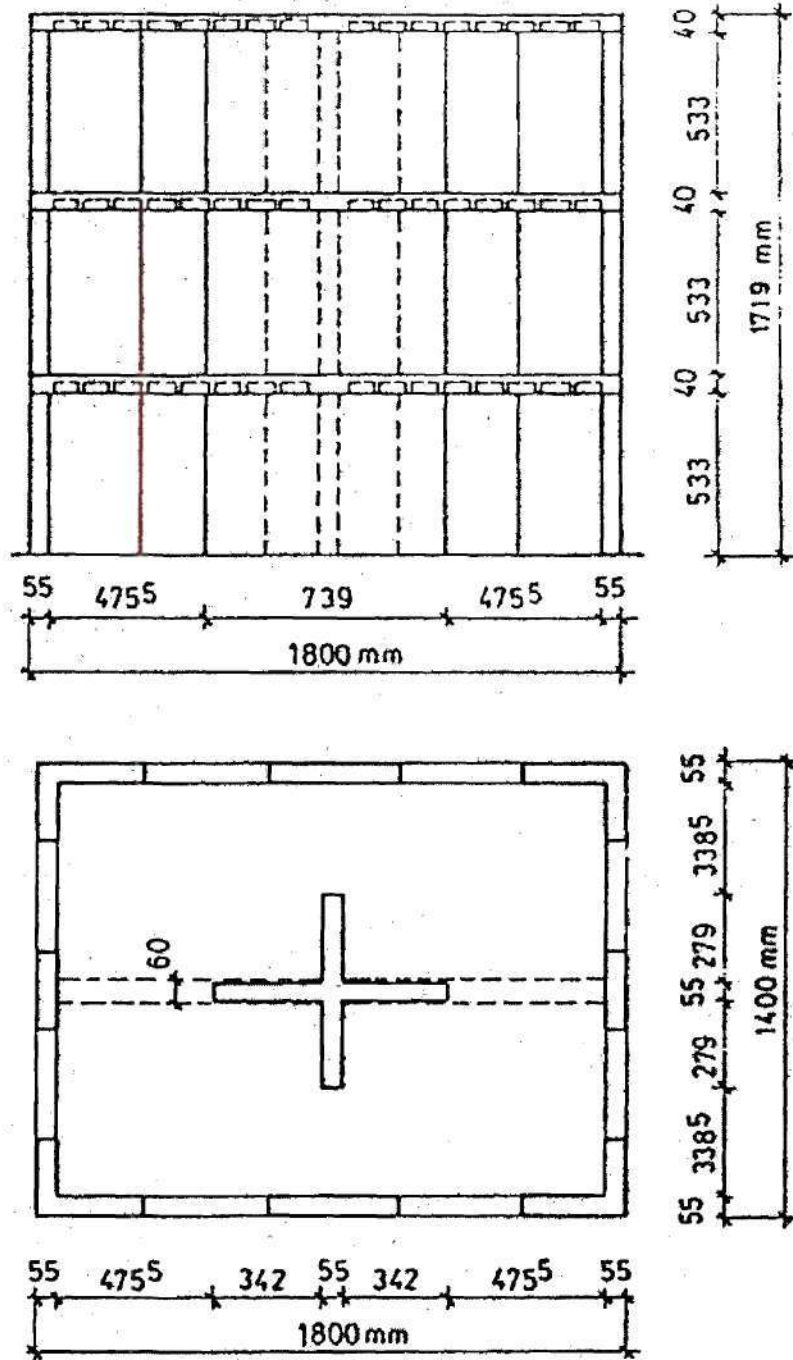


Fig. 2. 14. Specimen Model 2 in Tomazevic (1990)'s test
(taken from Tomazevic 1990)

there were window openings in the out-of-plane walls, the first crack might develop in the pier adjacent to the window opening at the bottom of the window, or at the top level of the window, or at the mid height of the opening. However, all the out-of-plane walls also showed a two-crack mechanism for their failure modes

Four three-story masonry 1:5 reduced scale models have been tested on a simple earthquake simulator in Yugoslavia by Tomazevic(1990) to investigate the seismic behavior of some mixed masonry structure. One of these was a URM structure (Model 4). This model had peripheral masonry walls and a interior cross-shape wall in the center (Fig. 2.14.). The floor slabs were RC slabs, which were supported on the peripheral walls and the RC beams at their mid span. The floor slabs actually made the masonry walls discontinuous at the floor levels.

The damage of the model began with horizontal cracks that developed at the bottom section of one of the peripheral corner walls, followed by the horizontal cracks developed at the bottom of the cross-section wall and the central peripheral in-plane walls. At the ultimate state, horizontal cracks developed at most of the joints between the walls and the floor slabs. The structure collapsed because of the unstable rocking of the first floor, especially due to the collapse of one of the corner walls, while the damage to the upper two stories were insignificantly. In this test, no out-of-plane wall failure was observed, since the RC slabs supported the out-of-plane walls very well.

- Horizontal cracks developed around mid height in the out-of-plane walls. As a result an out-of-plane hinging action developed, which led to the reduced stiffness and the increasing vibration of the walls. However, if partial reinforcements were provided, this type of behavior would not occur.
- All the reinforced walls in the specimens behaved much better than the URM walls during all tests.

Also, the following conclusions can be obtained from the test results:

- The strength of in-plane walls greatly depended on its vertical stress. The type of openings in the walls also influenced the crack patterns and the strength of in-plane walls. In the case of solid in-plane wall (House 1), horizontal cracks developed in the wall and the walls rocked and slide along the cracks. This kind of crack also developed in the door pier. However, in the case of a masonry wall with window openings, it was observed that diagonal cracks developed extending from the corners of the window. This was critical in some cases (House 2 and 3, 4), since the diagonal cracks initiating from the corner became unacceptably large with continued testing.
- The strength of out-of-plane walls also greatly depended on its vertical stress. The openings in the walls also affected the crack patterns. For House 1 where there were no openings in the out-of-plane wall, the first crack developed horizontally near the bottom, and the whole out-of-plane wall worked as if there was a hinge at the bottom. With the increasing seismic excitation, the next crack developed horizontally at about $2/3$ of the height of the wall. For the other houses where

The following phenomena were observed in this experiment (Clough et al 1979):

- Most of the lateral seismic forces to the specimens resulted from the large weight attached to the roof. Since the stiffness of the in-plane wall is much larger than that of the out-of-plane wall, the majority of the seismic forces was resisted by the in-plane walls.
- The masonry structure was so stiff that the motions of the test structures followed the shake table motions very closely, with the deformation of the structure generally being proportional to, and in phase with the base accelerations. Therefore, the peak acceleration, instead of the frequency characteristics, was a major factor to consider when assessing damage. The amplification of the ground motion due to the flexibility of the structure was rather small.
- If one in-plane wall was stiffer than the other, the two in-plane walls might develop different distortion under lateral earthquake excitation, with a resulting tendency to cause rotation of the roof structure. If the roof structure had sufficient membrane rigidity, it would rotate as a rigid unit, and consequently induced out-of-plane deformations in the in-plane walls, and in-plane deformations in the out-of-plane walls. However, if the roof diaphragm was flexible, and the stiffness of masonry walls were larger than that of the roof, the masonry walls would resist this tendency and forced the roof structure to develop shear distortions to accommodate the unequal displacements at the top of the in-plane walls. The test showed relatively little in-plane distortion in the out-of-plane walls.

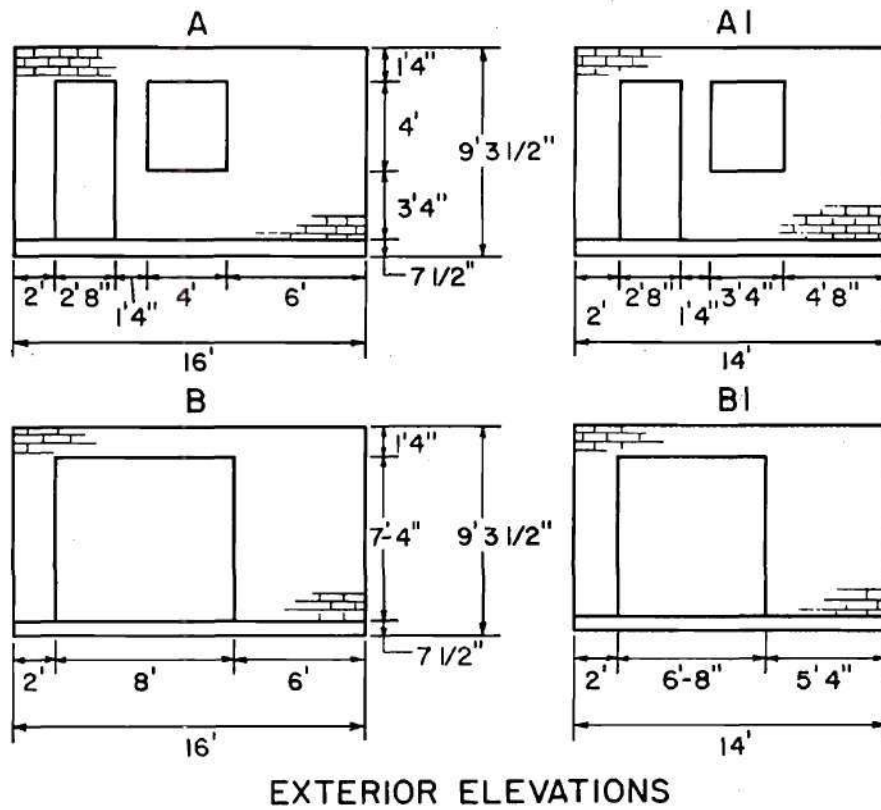
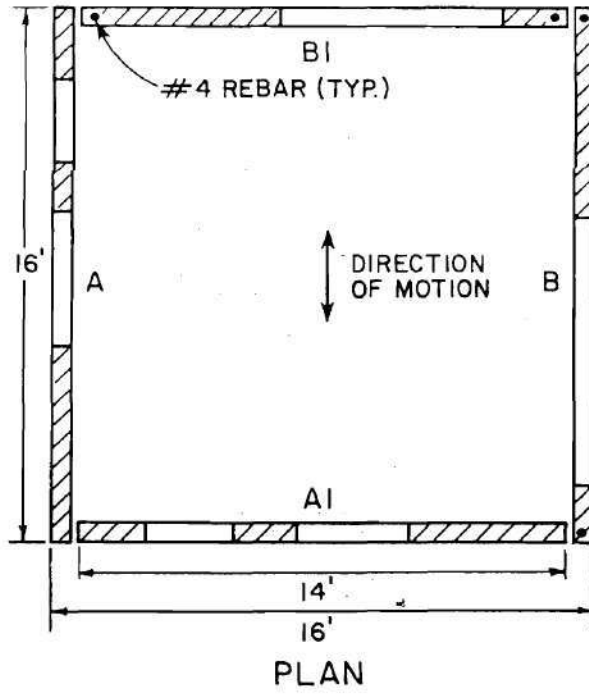


Figure 2.13 Specimen House 2 in Clough's test (taken from Clough et al 1979)

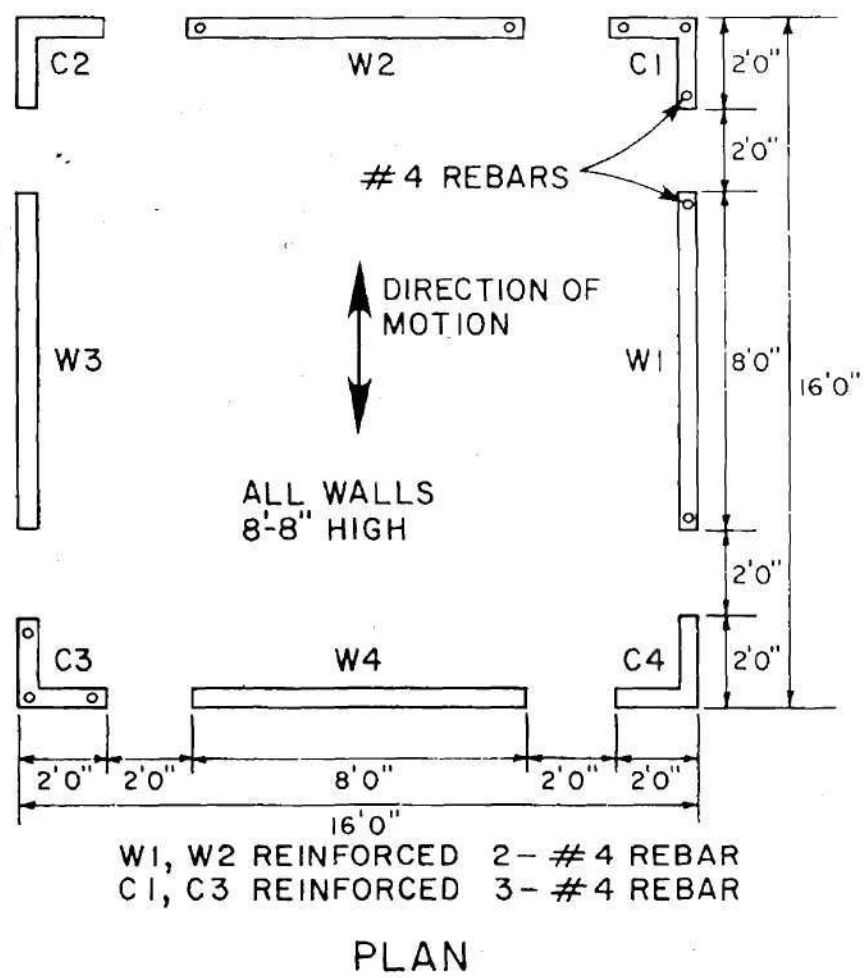


Figure 2.12 Specimen House 1 in Clough's test (taken from Clough et al 1979)

2.1.6.2.1 Reduced-scale Dynamic Tests on URM Structures

The first dynamic experiment on URM structure was conducted by Clough et al (1979). Four masonry one-story houses, with both unreinforced and partially reinforced masonry wall panels, were tested in a shake table. The objective were to determine the maximum earthquake intensity that could be resisted satisfactorily by an URM house, and to evaluate the additional resistance that would be provided to the structure by partial reinforcement.

In this test, the masonry units, the size of the wall components, and the roof-to-wall connections were full-scale to represent the behavior of a real masonry building. On the other hand, the plan areas of the building were one-ninth of a reasonable prototype due to the capacity of the shake table. To represent the realistic gravity stresses in the masonry pier, weights was added at the roof level. The first specimen was designed with a panel in the middle of each of four sides, and with a corner component on each side located at each corner (See Fig. 2.12). It was used to investigate the effect of exterior corners. The other three specimens were designed with four perforated walls with no direct connections between the wall panels (See Fig. 2.13). All four specimens were made from standard two-core hollow concrete block or two-core hollow clay brick and type S mortar. A typical timber truss roof system was used for all the four specimens.

Even if connections are presented between the masonry wall and the diaphragm, the connections are still the possible weak link in a URM building, as observed in the MAE center ST8 experiment (Peralta et al 2000).

- Out-of-plane failures, as have been discussed in Section 2.1.4.
- In-plane failures of URM walls under in plane lateral force, as have been discussed in Section 2.1.2 and will be discussed in detail in the following sections.
- Combined in-plane and out-of-plane failures, including cracks at the corners and the wall intersections (Tomazevic 1999)
- Diaphragm-related failures, which has been discussed in Section 2.1.5.

Of the above different failure modes, the potential out-of-plane failure of URM elements, including out-of-plane structural walls and other non-structural components, constitutes the most serious life-safety hazard for this type of construction. This type of failure mode can be prevented by properly anchoring the masonry walls to the floor/roof system, and is not the focus of current research.

2.1.6.2 Experiments on URM Structures

Reduced-scale dynamic test, pseudo-dynamic test, and large-scale static test have been done on the URM structures. Several important tests will be reviewed in this section.

Some researchers have investigated the reasons for the small amplification often observed in in-plane walls. It has been found that for very stiff structures such as the URM in-plane walls, the seismic response can be reduced to nearly the input acceleration level (Michel Bruneau 1994). Also, the foundation uplift adds up to the effects (Nakaki and Har 1992, ABK 1984).

The post-earthquake investigation and the experimental research show that the typical failure modes of a URM building can be grouped into the following categories (Deppe. K 1988, Boussabah 1992, Bruneau 1994, 1994 ASCE, 1995, Tomazevic, Miha 1999, ST8 2000):

- Lack of anchorage

In many existing URM buildings, the joists of the floor/roof diaphragm are simply supported on the masonry wall without any connections between the wall and the diaphragm. Sometimes, special corbels are constructed for the purpose of supporting the joists. Most commonly the URM walls are constructed around the supported joists, either tightly filling the recessed support with masonry or, less expensively, filling an oversized rectangular pocket housing the supports for the joists with a weak grout. Although the friction forces present at the supports may contribute to preventing sliding and separation between joists and walls at low dynamic excitation levels, “the resistance thus provided was believed small and not considered during seismic hazard assessments” (Bruneau, 1994).

- Anchor failure

different from simply adding up of the performances of each component, since each component will interact with the others, and will, in turn, influence its own behavior.

2.1.6.1 Overview of the Structure Characters of URM Structures

A typical URM building under earthquake excitation is shown in Fig. 2.11. The in-plane walls parallel to the direction of earthquake excitation are excited with little amplification, almost as a rigid body moving together with the ground. The out-of-plane walls perpendicular to the direction of earthquake excitation are excited with rather large amplification, due to their relative lower stiffness. Finally, the floor/roof diaphragms are seismically excited by the URM walls through the connections between the walls and the diaphragms.

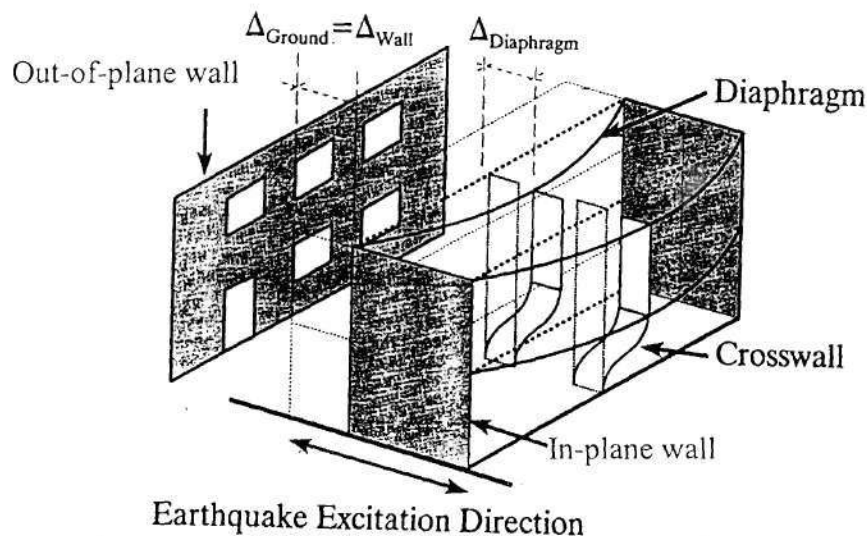


Figure 2.11 Typical URM structure under earthquake
(modified from Bruneau 1994)

The lateral deflection of a straight-sheathed diaphragm with or without plywood panel overlays can be obtained from the following equation provided in FEMA-273 (ATC, 1997):

$$\Delta = \frac{vL^4}{G_d b^3} \quad (2-8)$$

where: Δ is the calculated diaphragm lateral deflection, and v is the maximum shear force per unit diaphragm width, which can be calculated as $V/2b$, where V is the lateral load, and b is the width of the diaphragm. L is the diaphragm span between shear walls or collectors, and G_d is the diaphragm shear stiffness from FEMA-273, which can be obtained from FEMA-273(ATC, 1997).

The effective lateral stiffness of the diaphragm can be calculated as::

$$K = \frac{V}{\Delta} = 2G_d \left(\frac{b}{L} \right)^4 \quad (2-9)$$

FEMA 356 (ATC, 2000) updates the deflection equation (2-8) to the follows:

$$\Delta_y = v_y L / (2G_d) \quad (2-10)$$

It should be noted that the value of G_d in FEMA 356 is different from that has been given in FEMA 273. The results given by the Eq (2-10) is often very different from the old values given by Eq. (2-8). This indicates that it is difficult to calculate the elastic stiffness of the wood diaphragm.

2.1.6 URM Structures

The research on the masonry materials, and each component of a URM structure, i.e., the in-plane pier and spandrel, the out-of-plane wall, and the diaphragm, provide the sound base for the research of an overall URM structural system. The performance of a URM structure is determined by the structural properties of each component, but is also

- The load-displacement curves of the diaphragm showed large areas, indicating that the wood diaphragm had large energy dissipation capacity.
- A small opening in the diaphragm had no significant effect on the behavior of the diaphragm.

2.1.5.3 Analysis of Flexible Wood Diaphragms

Not many analysis models have been developed to analyze the performance of flexible diaphragms. ABK (1984) pointed out that a preliminary hazard mitigation analysis could assume all URM walls were properly anchored to the floor and roof diaphragm. Based on the ABK test results and some other tests results, ABK (1984) gave one table to estimate the yield capacities of diaphragms made for different materials (see Table 9-1 of ABK 1984 report).

ABK (1981) modeled the hysteretic behavior of the wood diaphragm with a series of springs that accounted for the shear stiffness and deformation of the diaphragm. However, it did not consider the axial stiffness of the diaphragm, or the torsion of the diaphragm. Also, this method only considered a one-way lateral force applied on the diaphragm.

FEMA 273 (ATC 1997) gives guidelines for calculating the effective stiffness and in-plane yield shear strength of the wood diaphragm and their retrofits. The guidelines are used for: (1) single straight-sheathed diaphragms, (2) plywood panel overlays on unblocked, unchorded straight sheathed diaphragms, and (3) plywood panel overlays on blocked, unchorded straight sheathed diaphragms.

This has a positive effect on reducing the diaphragms' peak accelerations and velocities (Bruneau 1994).

2.1.5.2 Experiments on Flexible Wood Diaphragms

Some experimental research has been done on the flexible wood diaphragm (APA 1985, 1986, Contryman 1952, 1955, Tissell 1967, Johnson 1956, ABK 1981a, Zagajski 1984, Peralta 2000). The report of MAE Center Project ST8 (Peralta et al 2000) gave a detailed review of those tests conducted on the flexible diaphragms. Only the test results of MAE Center Project ST8 are briefly discussed below.

MAE Center Project ST8 (Peralta et al 2000) tested three full-scale wood diaphragm specimens, which were representative of the wood diaphragms built in pre-1950's URM buildings. The goal of this research was to investigate the behavior of existing and rehabilitated wood diaphragms in URM buildings under lateral in-plane loads. The specimens were tested, retrofitted and retested again under quasi-static reversed cyclic loads. The test results showed that:

- The wood diaphragm behaved very flexibly. For the 24' x 12' diaphragm, the initial lateral stiffness ranged from 1.1 kips/in to 20.6 kips/in, depending on the orientations of the joists and other construction details.
- Measured deformations of the diaphragm-to-wall connections indicated that the connections could contribute to the overall lateral displacements of the diaphragms up to around 13% in some cases.
- The failure modes of the flexible diaphragm included failure of the connections, and pulling out of the nails that connected the sheathing to the joists.

modern structures, the wood diaphragm has some peculiarities characters that have significant effects on the behavior of the entire building.

First, instead of being a hinge support to the out-of-plane wall as in the case of a rigid diaphragm, the flexibility of the wood diaphragm makes its support to the out-of-plane masonry wall a spring support. The interaction between the flexible wood diaphragm and the out-of-plane wall will influence the response of out-of-plane wall. If the diaphragm is not properly connected to the masonry wall, the diaphragm may push or pound the URM out-of-plane wall during an earthquake, and make the wall develop out-of-plane cracks (Bruneau 1994). Also, the in-plane rotation of the diaphragm may induce damage at the wall corners.

Second, the wood diaphragm has large deformation capacity and high strength. The failure of the wood diaphragm itself has rarely been observed during an earthquake. On the other hand, several other failure mechanisms exist for the wood roof/floor diaphragm. For example, the connections between the diaphragm and the masonry wall are usually not strong enough in existing URM buildings. As a result, the connections play a more important role in the nonlinear behavior of diaphragm than the diaphragm itself. Moreover, when the masonry walls vibrate out-of-plane and tend to separate from the roof/floor diaphragm under seismic excitation, the diaphragm may slip off its supports and collapse if the diaphragm is not or inadequately connected to the masonry walls (Bruneau 1994).

Third, while the flexibility of the wood diaphragm produces a large amplification of up to 3 or 4 times the input acceleration in the elastic range, the wood diaphragm may have a highly nonlinear hysteretic behavior when the peak ground acceleration is high.

with that of the in-plane wall. As a result, the stiffness of out-of-plane wall can be neglected in the analytical model for the global URM structure if in-plane walls exist (FEMA 273, 274, ATC 1997). However, it should be pointed out that the stiffness of the out-of-plane wall has to be considered in the dynamical analysis, because some of the seismic forces for the entire structure come from the inertia force of the out-of-plane wall, which is determined by the stiffness together with the mass of the out-of-plane wall.

FEMA 273 (ATC 1997) gives the deformation-acceptance criteria for the out-of-plane wall. The stability of a out-of-plane wall should be checked if the h/t ratio of this wall is higher than some certain value (see Table 7-3 of FEMA 273, ATC 1997).

2.1.5 Flexible Wood Diaphragms

Two different types of floor/roof diaphragms are comma in URM buildings. One is the rigid diaphragm with very large stiffness, such as is the case for a reinforced concrete floor/roof system. The other one is the flexible diaphragm with rather low stiffness, such as is the case for a wood diaphragm or a light steel diaphragm. The flexible wood diaphragm has been found to be the representative roof/floor system for existing URM buildings in Mid America (David et al 2000), and will be researched in this project.

2.1.5.1 Properties of Flexible Wood Diaphragms

A wood diaphragm is an assemblage that typically includes three elements: sheathing, framing and chords. Compared with more commonly used rigid diaphragms in

bodies. Therefore, by assuming that an equivalent plastic moment exists along the cracks, classical yield line theory can be used to determine the ultimate strength of the wall.

The fracture-line model was used by Martini (1998) to investigate the ultimate strength of a URM out-of-plane wall connected with in-plane walls at both sides. In his model, Martini (1998) considered the equivalent plastic moment not only along the bed joints, but also along the head joints. The crack pattern in the URM wall was assumed to be similar to that for RC slabs, as predicted by yield line theory. The method neglects the tensile strength of masonry material, which may underestimate the strength of an out-of-plane wall, especially when the gravity stress is low. Another shortcoming inherent with the fracture-line model is that an equivalent plastic moment is assumed along the cracks, which is not entirely correct since no moment really exists in the fracture line for brittle URM materials.

Nonlinear FE analysis with a special block-interface model were conducted by Martini (1997) to analyze the out-of-plane behavior of a one-way out-of-plane URM wall. In this model, 8-nodes elastic linear brick elements were used to model the masonry material, and 8-nodes surface-contact elements were used to model the mortar joints. This model was developed for the ABAQUS program. The same block-interface model was also used to investigate a two-way out-of-plane URM wall panel, which was simply supported on the side edges, fixed at the bottom, and unsupported at the top (Martini 1998). The analysis could predicate the crack pattern and the ultimate strength of the out-of-plane masonry wall.

The elastic stiffness of out-of-plane wall has not been investigated extensively. It is usually considered that the stiffness of the out-of-plane wall is very small compared

2.1.4.3 Analysis of URM Out-of-plane Walls

Several different analysis methods have been used to describe the out-of-plane behavior of URM walls. FEMA 274 (ATC 1997) gives two equations for calculating the strength of the out-of-plane URM wall. The first equation calculates the lateral strength of the out-of-plane wall based on a rocking mechanism. However, it does not consider the support of adjacent in-plane walls. The equation is as follows:

$$q_{cr} = \frac{6Pt}{h^2} \quad (2.7)$$

where q_{cr} is the uniform pressure on this wall, P is the vertical compressive load, h is the height of the wall, and t is the thickness of the wall. The second equation gives the strength 3 times the value given by Equ. (2.7) considering possible arching action in the wall.

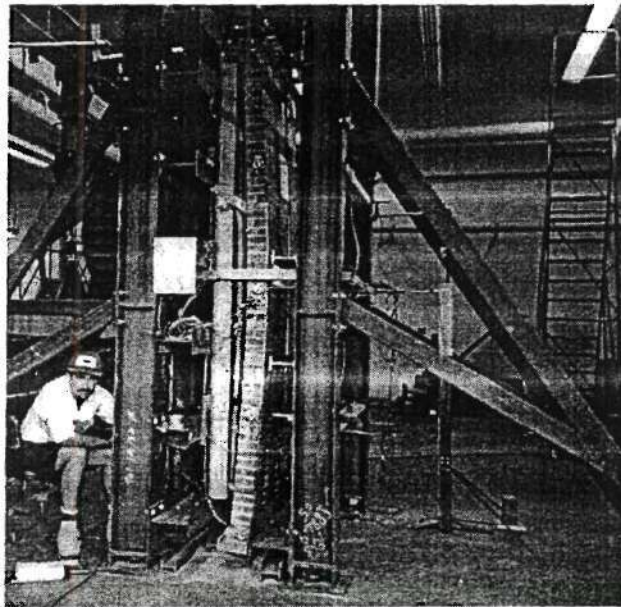
The mechanism for out-of-plane wall after cracking can be illustrated by the dynamic stability concept (Priestley 1985). The walls were modeled as continuous vertical slabs supported at the floor/roof levels and the bases. The supports provided by adjacent in-plane walls were conservatively neglected. After cracking, the wall behaved as a rigid body rocking on the wall's through-cracks (ABK 1981a, 1981b, 1984, Kariotis et al 1985; Adhm 1985b).

The ultimate strength of a URM out-of-plane wall can be calculated by the fracture-line model (Sinha 1978, 1980), which needs to predefine the crack pattern of the wall before the analysis. In this method, all deformations of the wall are assumed to only take place along the fracture lines, and the individual parts of the slab rotate as rigid

Drysdale (1988) tested 21 full-scale concrete block walls subjected to uniform pressure normal to the surfaces of the walls. Different boundary conditions were used for the test walls, which included: 1) simple supported at each edge, 2) simple supported at the bottom and two vertical edges, and 3) simple supported only at the bottom and the top. It was found that different boundary conditions led to different crack patterns. Zhang et al (2001) tested three full-scale reinforced block out-of-plane walls with monotonic and cyclic loads. All walls were C-shaped in plan, i.e., there were in-plane walls at both ends of the out-of-plane wall. One out-of-plane wall specimen was solid, and the other two had door and window openings. Air bags were used to alternately apply pressures on each face of the out-of-plane wall to simulate the out-of-plane seismic forces. Although the nonlinear behavior of a reinforced block wall is different from that of a URM out-of-plane wall due to the effect of rebars in the reinforced block wall, the following results obtained by Zhang's (2001) test are considered applicable to URM out-of-plane walls:

- The deflection of the out-of-plane wall at the central section was linear. Most of the deformation of the out-of-plane wall was due to the opening of the cracks in the mortar joint at the base of the wall.
- The displacements at both ends of the out-of-plane wall were very small compared with that at the central section, due to the support of the in-plane walls.
- The lateral deflection drift of the solid wall at the top of the central section was about 0.8% corresponding to the initiation of diagonal cracks.
- The openings in the out-of-plane wall have significant effect on the ultimate out-of-plane capacity of the wall, especially when the opening is close to the edges of the wall, because it reduces the restraint of the in-plane wall significantly.

the load capacities of the shake tables and dynamic actuators restrict the size of the specimen that can be tested dynamically. Furthermore, most of out-of-plane URM wall specimens used in dynamic tests did not include in-plane walls. More realistic modeling of the connection to the in-plane wall may lead to different crack patterns and failure mechanisms for the out-of-plane wall. Therefore, static tests have also been used to investigate the out-of-plane behavior of masonry wall. The size of the specimens used in the static tests can be rather large. The loading can take the form of a lateral uniform pressure applied to the wall by using airbags (Fig. 2.10), or of only linear or point loads applied at the top of the walls by using actuators. It should be noted that the applied loads in a static test do not represent the realistic distribution of the seismic force for the masonry wall under seismic excitation.



**Figure 2.10. Airbag used in the out-of-plane test of URM wall
(taken from Velazquez-Dimas 2000)**

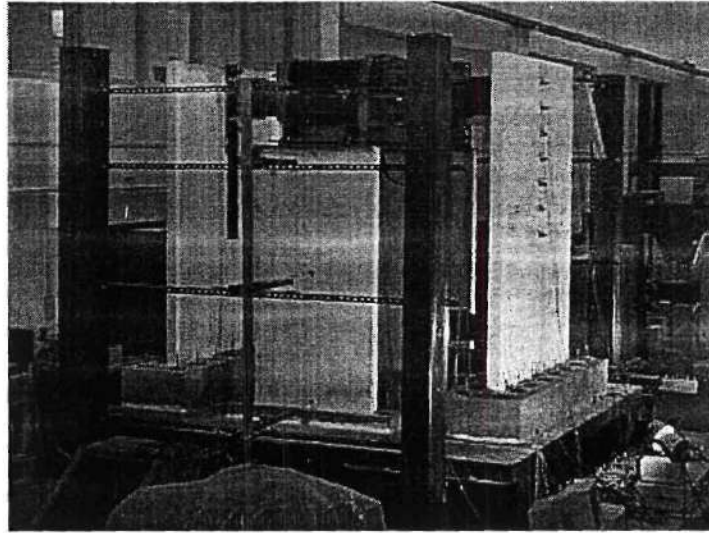


Figure 2.9 Dynamical test set up used in MAEC project ST10

MAE Center project ST10 used a shake table to test one pair of out-of-plane walls with additional masses on the top of the walls to simulate the behavior of URM out-of-plane walls in a real building (Fig. 2.9). The preliminary test results indicated that the URM wall developed horizontal cracks at the bottom of the wall, and rocked about the bottom without collapsing even under an earthquake input of about 1.0g. However, after tripling the mass of the URM wall by adding some weight on the surface of the wall, the URM wall developed horizontal cracks around the mid-height of the wall, became unstable, and eventually collapsed under an acceleration of about 0.2g. The test showed that the distribution of mass between and floor/roof diaphragm has a significant effect on the response of the out-of-plane wall.

The dynamic tests discussed above provide very valuable information about the out-of-plane behavior of URM walls, including data on the dynamic stability of out-of-plane walls, the rocking mechanism of out-of-plane walls after cracking, and the contribution of vertical stress to out-of-plane strength of URM walls. On the other hand,

Prawel and Lee (1990b) applied both static cyclic shear and dynamic shake-table excitation to several unreinforced brick masonry wall specimens in the out-of-plane direction. The walls were fixed and pinned at their base and top respectively, with heavy compressive loads at the top. Prawel and Lee (1990b) reported the following test results:

- Following the onset of the first horizontal full-width crack, additional loading was required to propagate the crack through the thickness and initiate a rocking rigid-body motion about the horizontal cracks. In some cases, 25% reserve capacity existed beyond first cracking, with lateral displacements reaching twice the cracking value at that capacity.
- The general failure mode for the URM walls was flexural combined with some sliding and rocking motion. Although the material itself was brittle, rocking and sliding produced hysteretic behavior with recorded maximum lateral displacements up to five times the crack displacement.

Bariola et al (1990) did shaking-table tests for unreinforced clay-brick walls. The walls were cantilever walls with variable thickness and slenderness. With increasing earthquake severity, the seismic response of the walls evolved from a purely elastic cantilever response to a rigid body rocking movement after cracking occurs at their bases. Ultimately, the walls collapsed by overturning. One interesting result from these experiments is that thicker walls can apparently survive more severe earthquakes, as in the post-cracking range the rocking behavior seems more stable.

the exceptionally high coefficient of variation along with the poor mortar compressive strength was most likely due to the use of a bagged masonry cement.

As a result, the second series of tests used a Type O mortar, which was comprised of a Portland cement to lime to sand ratio of 1:2:9. A total of 10 specimens were tested including 5 constructed of cored brick and 5 constructed of solid brick. The results of this series of tests are shown in Table 3.6.

Table 3.6. Summary of Diagonal Compression Test Results (Type O)

Type of Brick	Mean Shear Strength (psi)	Standard Deviation	Coefficient of Variation
Solid	284	41	0.14
Cored	154	36	0.23

While the coefficient of variation is much lower for this Type O mortar, the shear strength actually increased. More important than the apparent increase in shear strength is the fact that this Type O mortar caused cracks to go through the bricks in some cases (see Fig. 3.25). Based on field studies it seems that this failure mode is not consistent with existing URM structures in Mid-America. That is, if the ST-11 test structure were constructed with this Type O mortar a “strong brick-weak mortar” behavior would not be guaranteed. In addition, the compressive strength of the Type O mortar cubes was found to be 517 psi, which is considerably higher than the expected 350 psi compressive strength for a typical Type O mortar.

determine the compression strength of masonry as well as the compression strength of brick used for the ST-11 test structure.

3.3.1 Shear Tests

The initial shear tests were conducted according to ASTM E519-00 (“Standard Test Method for Diagonal Tension (Shear) in Masonry Assemblages”) with the exception that the specimens tested were 2ft by 2ft as opposed to the specified 4ft by 4ft. This modification was made as a result of the difficulties inherent in testing a 4ft by 4ft masonry panel.

The first series of tests were conducted using a Type N mortar. This mix consisted of a one to three ratio of bagged Type N masonry cement to sand. A total of 16 specimens were tested including 8 constructed of solid bricks and 8 constructed of cored brick. Table 3.5 shows a summary of the results of this series of tests.

Table 3.5. Summary of Diagonal Compression Test Results (Type N)

Type of Brick	Mean Shear Strength (psi)	Standard Deviation	Coefficient of Variation
Solid	123	63	0.51
Cored	88	30	0.35

It should be noted that all of the failures occurred in the mortar and no cracking of the bricks were observed. While a good deal of scatter was expected, the large coefficient of variation associated with this series of tests is troublesome. Furthermore, the Type N mortar cubes tested gave a compressive strength of 360 psi, which is far below the expected 750 psi compressive strength for a typical Type N mortar. It was concluded that



Figure 3.24. Construction of the floor and roof diaphragms.

3.3 Preliminary Material Tests

This section outlines the preliminary material tests conducted. The objectives of this series of tests was to develop a mortar mix that resulted in masonry properties consistent with those found in existing structures in Mid-America as well as supply estimates of material properties for analysis purposes. Analyses conducted at Clemson University of mortar samples taken from existing structures in Mid-America showed low amount of Portland cement. This suggests that masonry with low shear strength is common in existing URM structures in Mid-America. Section 3.3.1 outlines the shear tests conducted in order to determine a mortar that supplied both a low shear strength and low variability. Sections 3.3.2 and 3.3.3 gives the results of tests conducted in order to

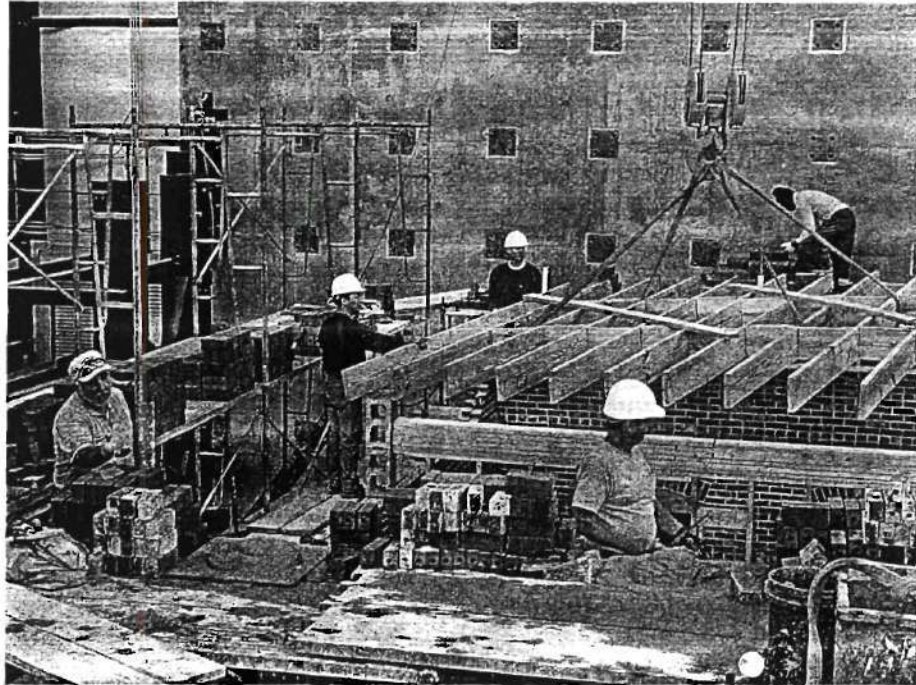


Figure 3.22. Assembly of the floor systems

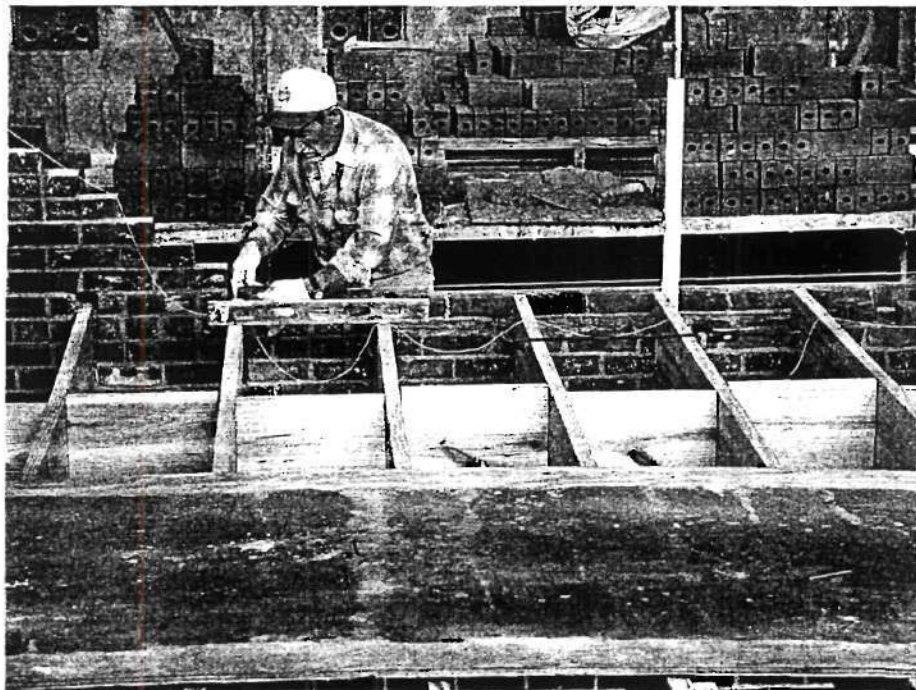


Figure 3.23. Construction of the joist pockets in Walls A and B.

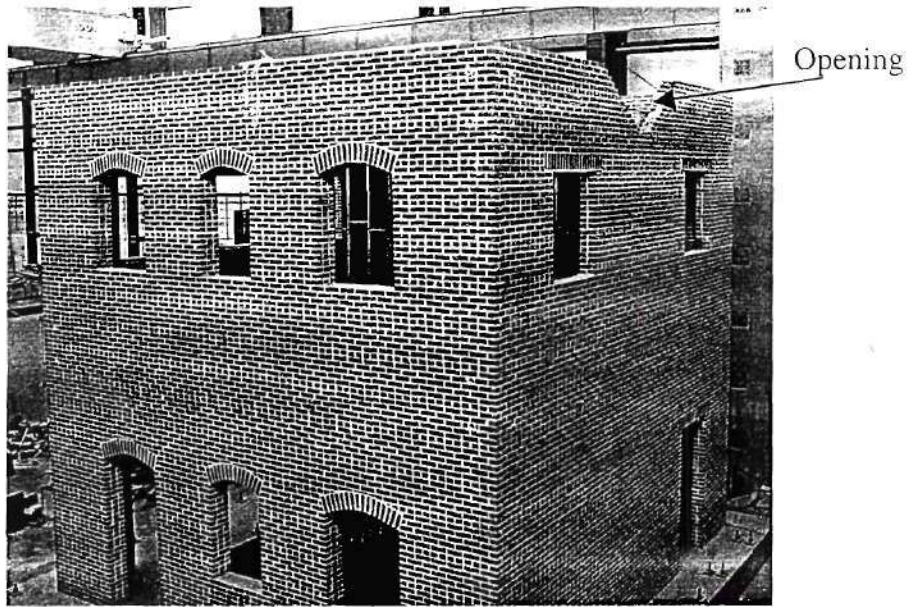


Fig. 3.21 Opening left at the top of Wall 1

Construction of the walls was temporarily halted at the floor and roof levels to allow the floor systems to be placed by the overhead crane (see Fig. 3.22). Once the floor systems were aligned properly on Walls A and B, the pockets were built around the end of the joists to ensure proper fit (see Fig. 3.23). After the floor systems were assembled, 1x6 sheathing was nailed to the top of the joists with 8d common nails (see Fig. 3.24). Additional construction pictures can be found in Appendix A.

Following the preparation outlined in the previous section, construction of the masonry walls began. The masonry walls were built in the standard America bond pattern, with a header course every six courses. This bond pattern continued through the piers and floor levels to the top course. For the three wythe walls, the outside two wythes were tied at the same course as the two wythe walls, while the inside two wythes were tied at the next course (see Fig. 3.20). Four holes were supplied at the corners of the structure at the floor and roof levels to facilitate the post-tensioning tendons used to attach the actuators to the structure. To facilitate the loading of the roof diaphragm, step-back openings were left in the center of Wall A and Wall 1 at the roof level (see Fig. 3.21).

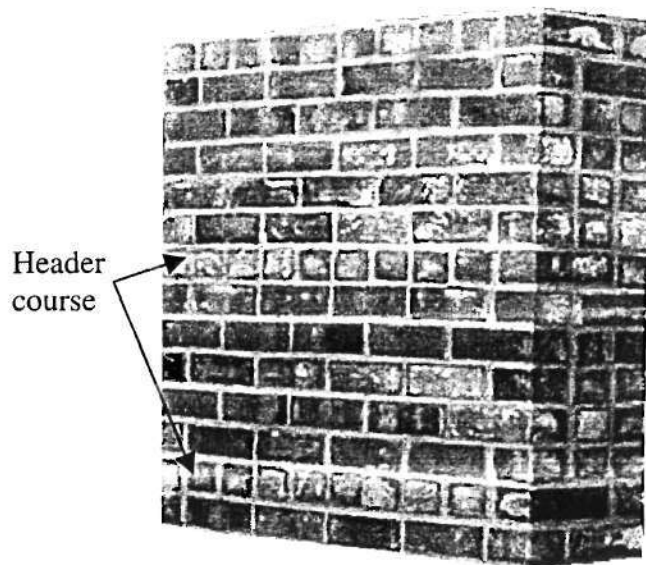


Figure 3.20. Header course pattern for the three wythe walls.

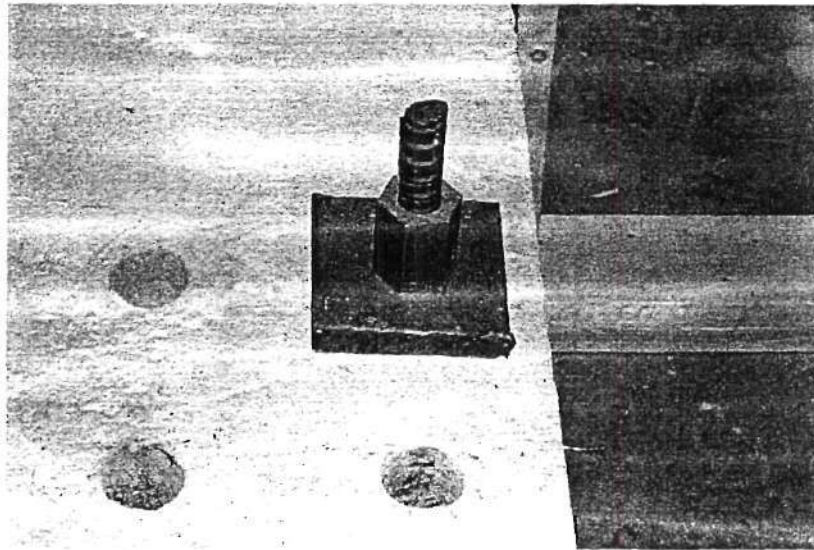


Figure 3.18. Post-tension RC slabs to the strong floor



Figure 3.19. PVC tubes used to leave the holes in the wall

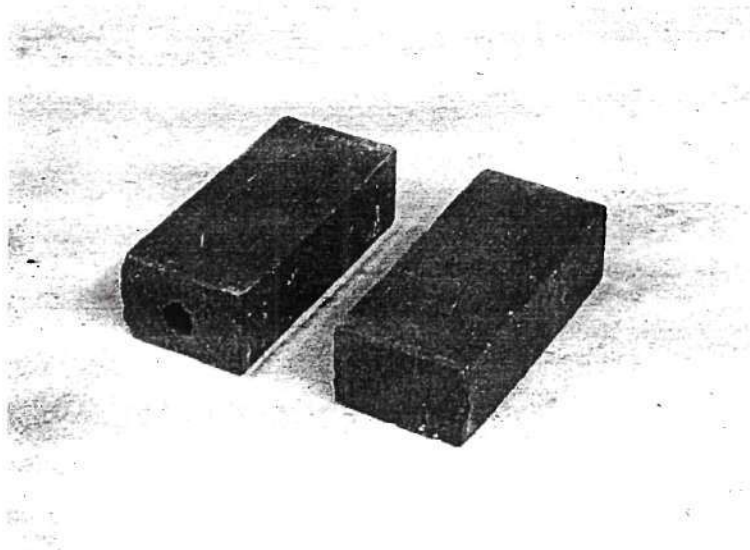


Figure 3.17. Two different bricks

The reinforced concrete foundation slabs were cast and post-tensioned to the strong-floor with high strength Dywidag rods prior to construction (see Fig. 3.18). For ease of construction, the stud walls and joist floor systems were built on the strong-floor and moved into place by the overhead cranes during construction. Next, the formwork for the arch lintels was constructed and the steel Ts used for the lintels in Walls 1 and 2 were cut to the proper size. To facilitate the use of post-tensioning for Wall A, four 14 in deep, 2 in diameter holes were core-drilled into the foundation at the centerline of each of the piers of Wall A. Next the *SureStress*TM anchors shown in Fig. 3.9 were bonded into the foundation with *Sikadur*TM 35 Hi-Mod LV (low viscosity) epoxy. It is important to note that the epoxy recommended by Dur-O-Wal displayed an extremely short pot-life (approx 1min), which made proper alignment of the anchors difficult. As a result the low viscosity *Sikadur*TM system was chosen which had a more reasonable pot-life of approximately 30min. During construction of the walls, PVC tubes were used to leave a void in the URM wall to allow for the insertion of the unbonded post-tensioning tendons (see Fig. 3.19).

stiffness. This type of retrofit will be used to strengthen the roof diaphragm in the ST-11 building. In order to assess the effect of increasing the diaphragm stiffness on overall structural behavior, the proposed ST-11 test sequence requires the structure to be tested with and without a retrofitted diaphragm. Due to the relatively low initial diaphragm stiffness, a retrofit technique that increases the diaphragm stiffness by 200% to 300% is not expected to significantly change the overall structural behavior. This will be verified through the experiment.

3.2.7 Construction

The ST-11 test structure was constructed by experienced masons and is composed of clay bricks and a type K' mortar that was mixed with a 1/2: 2: 9 ratio of Type I Portland cement to lime to sand (discussed in Section 3.3). No attempt was made to control the amount of water in the mortar. The masons were permitted to add water until the desired consistency was achieved. The building employed both solid bricks and core bricks that contained a longitudinal hole through the center (see Fig. 3.17). Nominal dimensions of both types of bricks were 7.75 in length, 3.5 in width, and 2.25 in thickness. The results of preliminary material tests indicated that, while the bed-joint shear strength associated with each type of brick was similar, the masonry compressive strengths had large variations. In an attempt to isolate this anomaly, the solid bricks were used for the lower 54 courses and the cored bricks were used for the remainder of the structure. However, the solid bricks were employed for all header courses.

3.2.6 Retrofit Strategies for Diaphragms

The diaphragm-to-wall connection is likely the most critical component of an URM structure. In order to verify this, the specimen will be subjected to small displacements prior to connecting the diaphragm to the URM walls. These results will provide a base line for which to compare the behavior of the structure after connection retrofit and allow the effectiveness of such a retrofit to be determined. Then the diaphragm will be connected to the masonry walls with different connection elements to investigate the effectiveness of the connection. The commonly used Simpson *Strong-Tie*TM system will be employed in the ST-11 test structure to investigate this type of retrofit (Fig. 3.16). These connections will be used for not only Walls 1 and 2, which are parallel to the joists, but also Walls A and B, which are perpendicular to the joists.

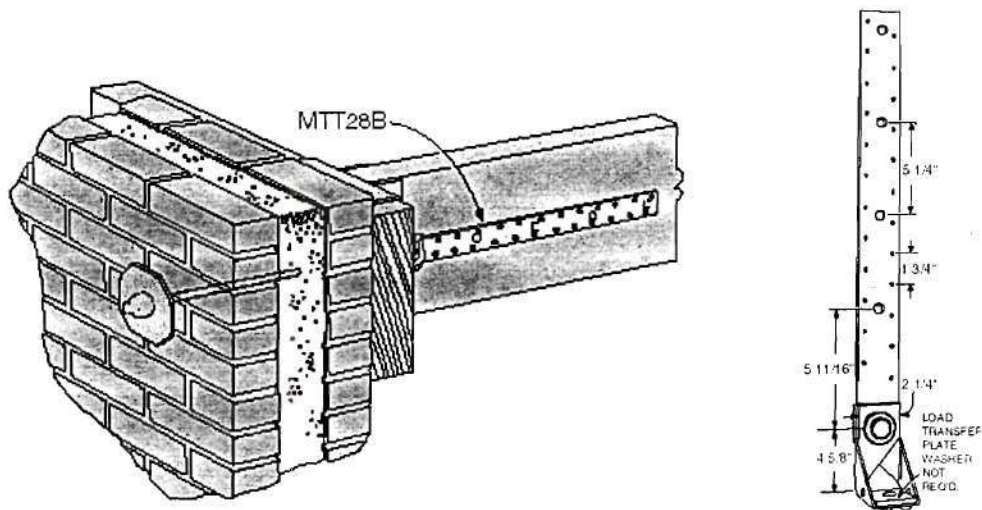


Figure 3.16. Simpson connections (taken from www.strongtie.com)

Project ST-8 investigated several retrofit techniques aimed at increasing the stiffness of the diaphragm. One of the most effective techniques tested in ST-8 was the addition of plywood to the top of the diaphragm in order to increase both strength and

2x10 joists spanning 12ft and spaced 16 inches on center. The joists are simply supported on Walls A and B as well as on the stud wall built through the center of the building. The joists are laterally supported by full depth blocking spaced at approximately 4 ft. on center, and anchored to the periphery masonry walls. Straight Sheathing is provided using 1x6 square edge boards, staggered symmetrically with respect to the diaphragm midspan.

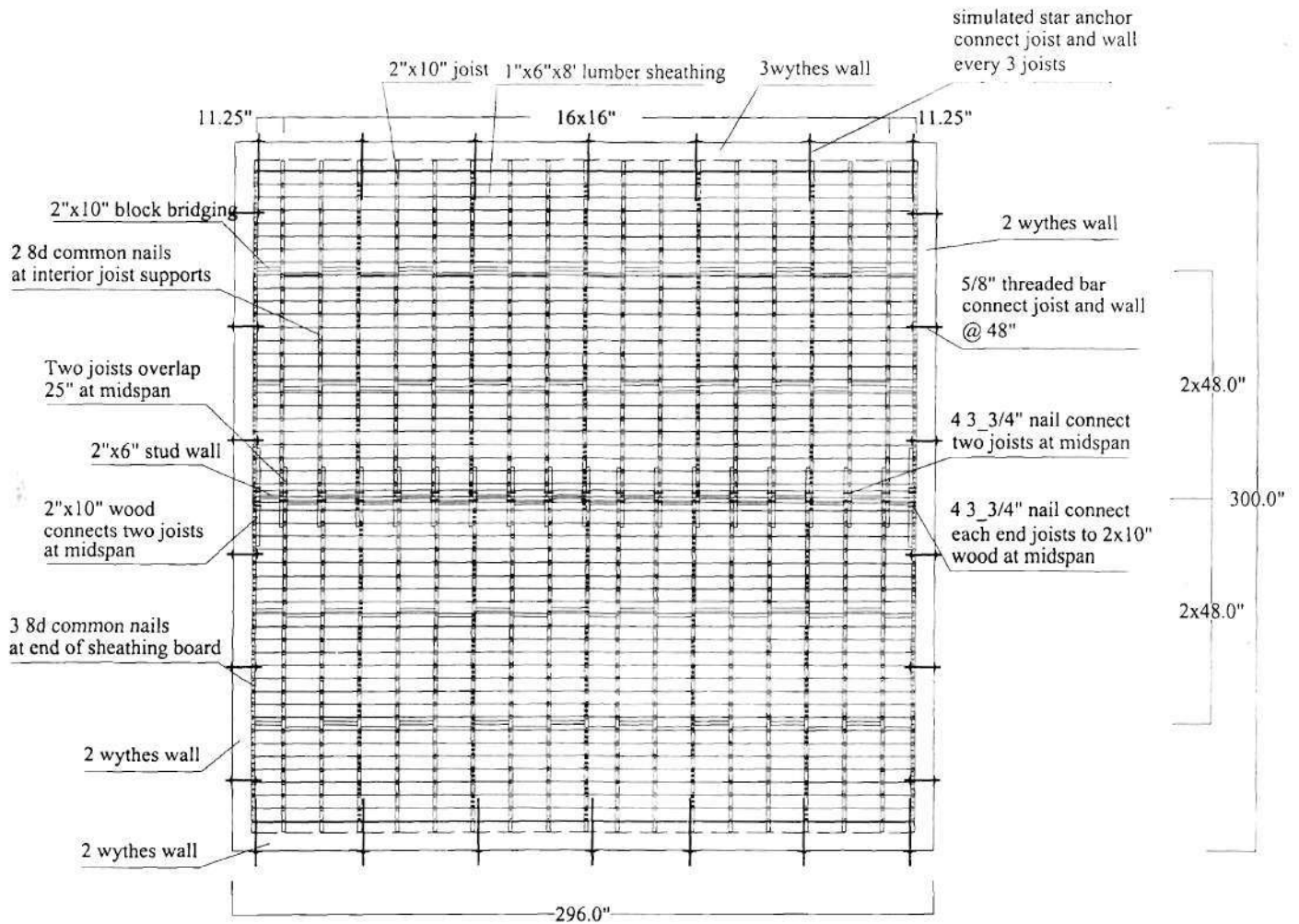


Figure 3.15 ST-11 roof/floor diaphragm

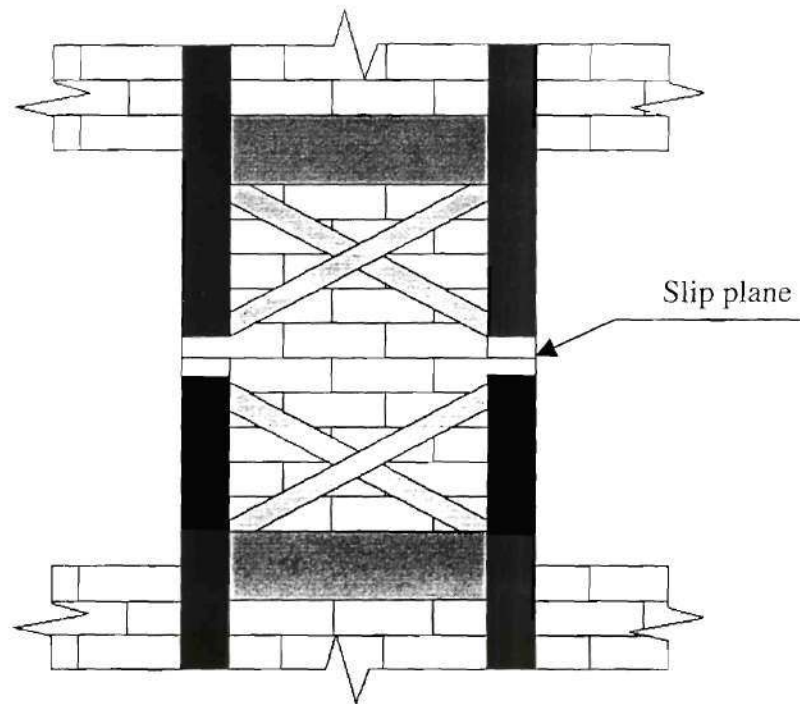


Figure 3.14 Special configuration of FRP retrofit to enforce bed-joint sliding at the mid height of the pier

3.2.5 Wood Roof/Floor Diaphragms

The investigation of pre-1950's URM buildings in Mid-America indicates the widely used timber roof/floor diaphragm and steel roof/floor diaphragm. The timber roof/floor diaphragm was chosen for use in the ST-11 test structure since it represents the lower bound of strength and stiffness of existing diaphragms. The ST-11 test specimen employs a similar diaphragm to the "MAE-2" diaphragm tested in MAE Center project ST-8 (Peralta et al. 2000), as shown in Fig.3.15. The roof diaphragm and the floor diaphragm of the ST-11 building are identical to each other. The framing is composed of

Engineering Research Laboratory (CERL). All experimental results suggest that this glass FRP is a very effective retrofitting material. The overlays will be applied in order to strengthen the piers, as shown in Fig 3.13. It is expected that the location of the FRP overlays will be based upon observed damage. The results of the preliminary analyses outlined in Section 4.2 suggest that the piers will damage in either a rocking or sliding mode. As a result, the initial retrofit will likely employ vertical strips. In addition, if brittle failure modes result, the configuration of the FRP overlays will be altered in order to force a more ductile failure mode. For example, the specific FRP configure shown in Fig. 3.14 (currently being investigated at CERL) is designed to force the ductile bed joint sliding failure mode to develop at the mid height of the pier.

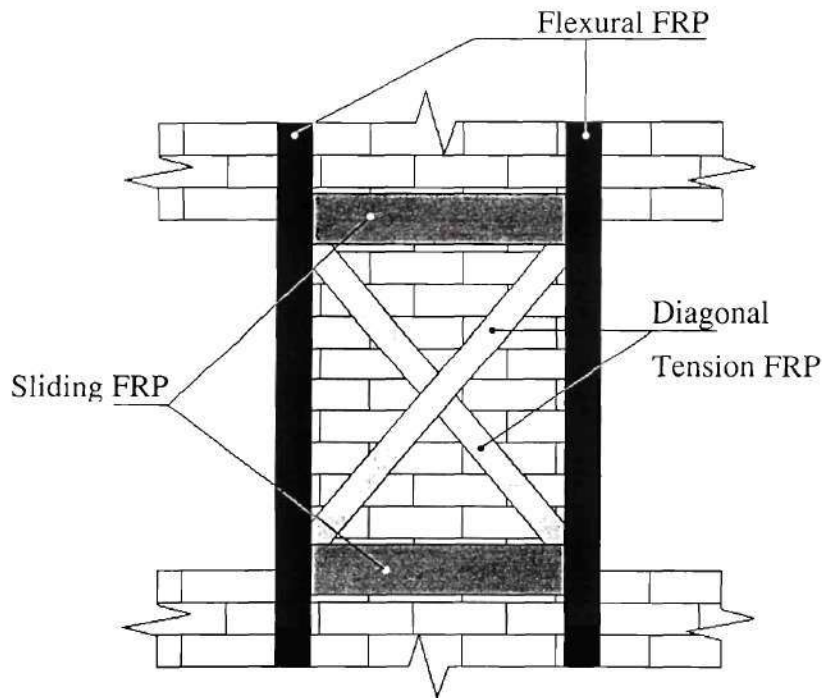


Figure 3.13 Common configuration of FRP retrofit

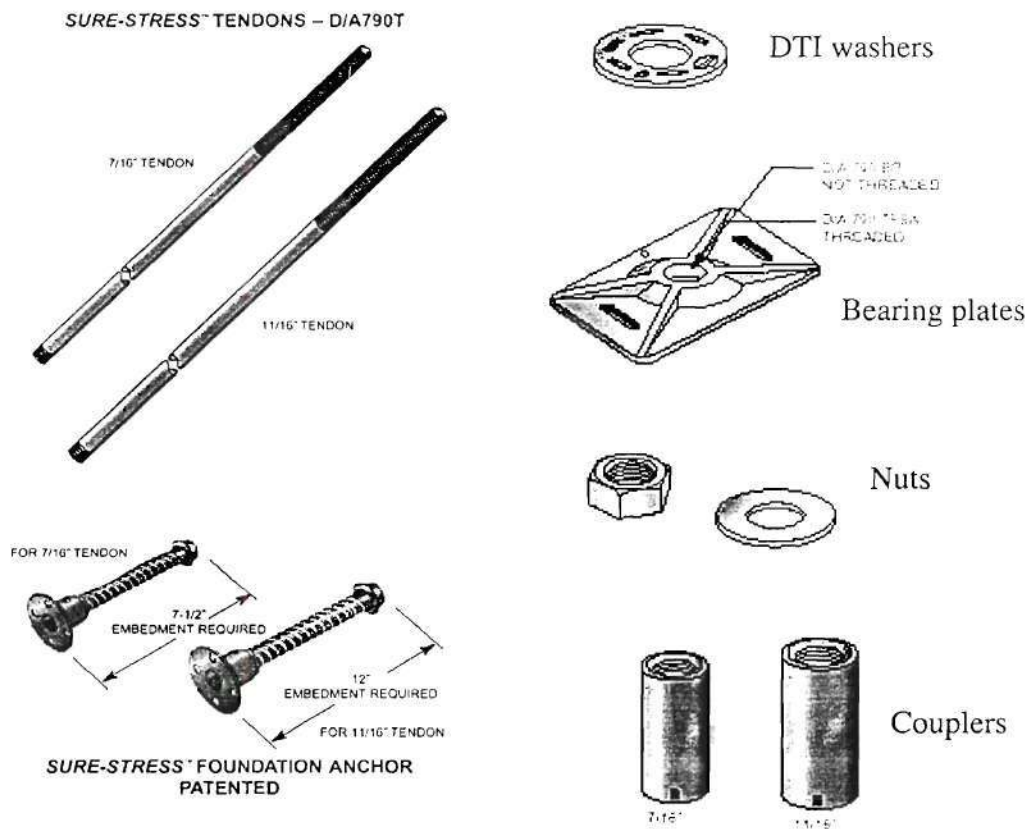


Figure 3.12. *Sure-Stress*TM post-tensioning system

(taken from www.dur-o-wal.com)

Wall A will be retrofitted by this post-tensioning system. In order to gain insight into the effect of different levels of post-tensioning stress, Wall A will be tested with 20psi, 40psi, and 60psi of post-tensioning stress.

To investigate the effectiveness of FRP retrofit of URM, a 27oz unidirectional glass fiber epoxy matrix system was selected. This material was tested in ST-6 and is currently being used for an extensive research program at the US Construction

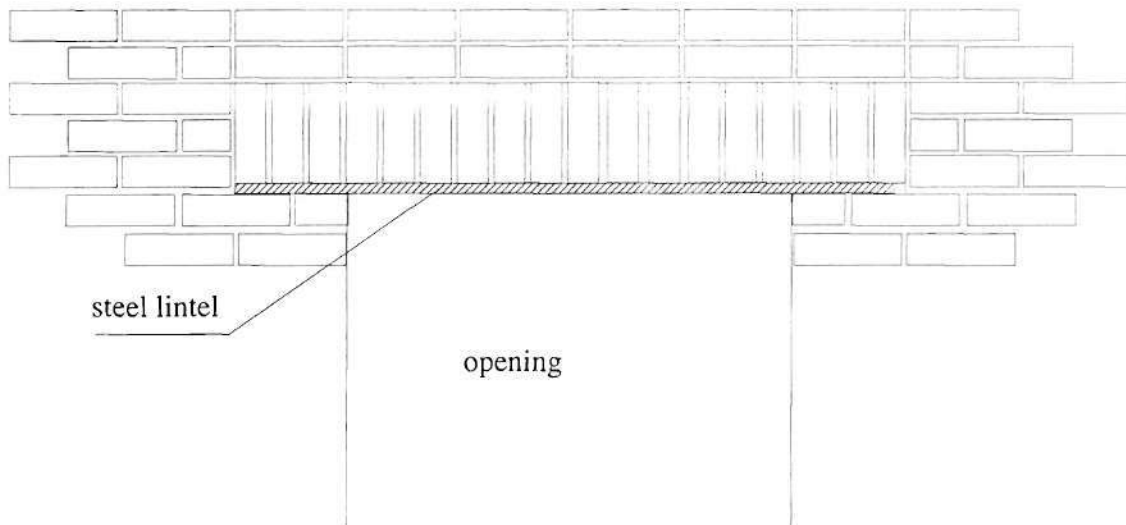


Figure 3.11. Detail of steel lintels

3.2.4 Retrofit Strategies for URM Walls

Two retrofit techniques for masonry walls will be investigated in this test: post-tensioning and the use of FRP overlays.

The *Sure-StressTM* post-tensioning system manufactured by DUR-O-WAL was selected to investigate the effectiveness of a post-tensioning retrofit. This system is composed of 7/16" diameter tendons (100ksi yield strength), foundation anchors, direct tension indicating (DTI) washers, bearing plates, couplers, and nuts, as shown in Fig. 3.12.

The masonry walls are built following construction techniques typical of pre-1950 construction in Mid-America. The walls are composed of clay masonry bricks in a standard American bond (Fig. 3.9). Walls A and B employ URM arch lintels (Fig. 3.10), while Walls 1 and 2 employ steel lintels (Fig. 3.11). Both of the two lintels are representative of typical lintels used for URM structures in Mid-America. All of the lintels are expected to perform well.

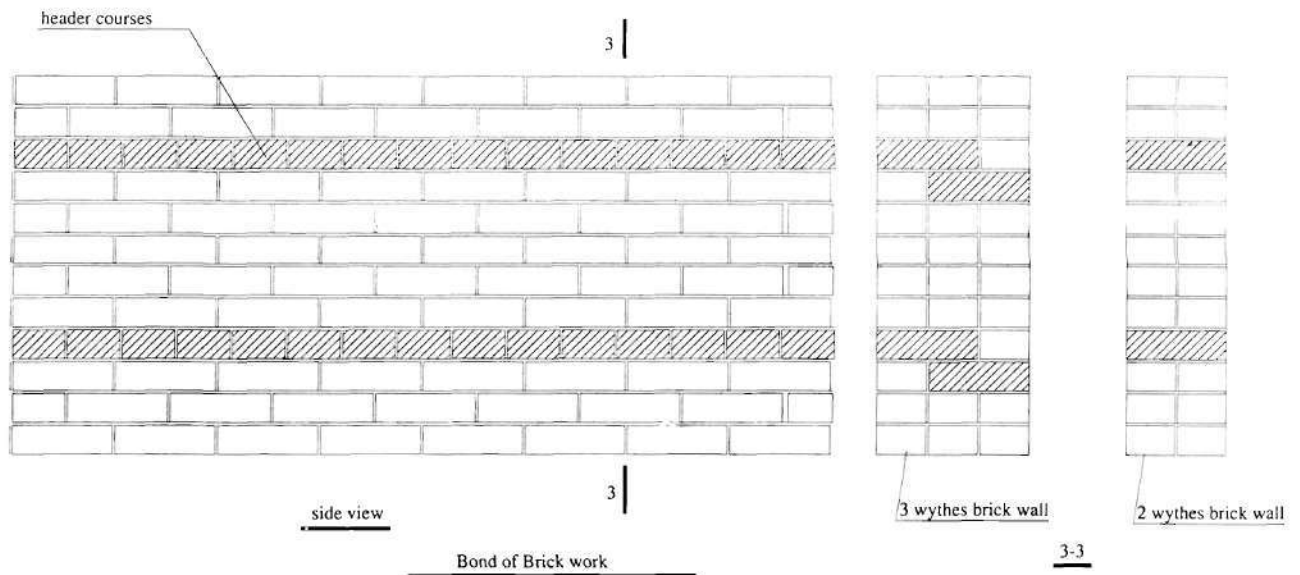


Figure 3.9. Detail of American bond

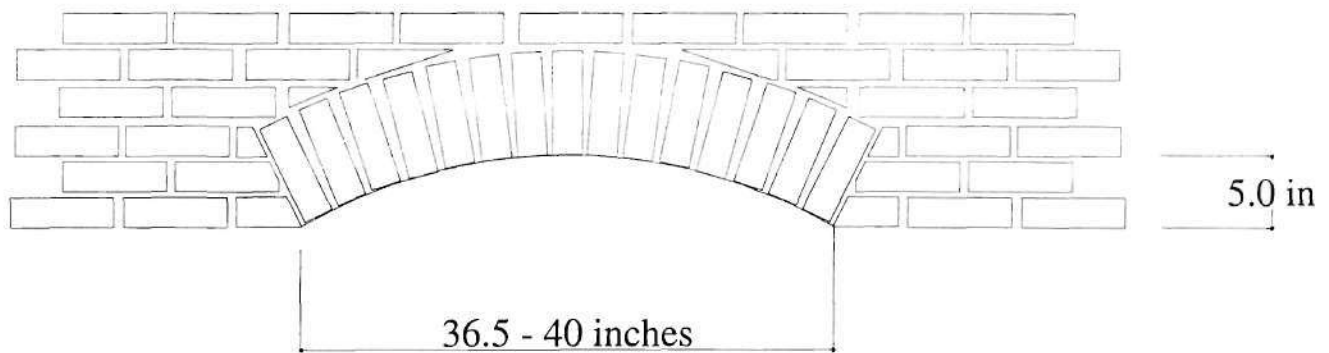


Figure 3.10. Detail of arch lintels

Thus, the behavior of both types of URM piers tested in ST-6 will be investigated in the test of the ST-11 building.

Table 3.4 shows that the opening ratios of Wall 1 and Wall 2 are quite different. Wall 2 contains a large door opening (indicative of the front of a firehouse), and is designed to represent a strong spandrel-weak pier type perforated wall. Wall 1 has relatively small openings, and is designed to represent a strong pier- weak spandrel type perforated wall. Furthermore, Many structures in Mid America contain parallel walls with large differences in stiffness. As a result, the behavior of URM structures with flexible diaphragms subject to torsion is of interest. Walls 1 and 2 allow this type of behavior to be investigated. Due to the relatively small stiffness of the out-of-plane wall and diaphragm, little coupling is expected. This contention is based on the results of the extensive preliminary analysis conducted and outlined in Chapter 4. This will be verified through the large-scale test.

The ST-11 test structure allows the effectiveness of different retrofit techniques to be assessed. Since Walls A and B are identical, two different rehabilitation techniques can be investigated and the results can be directly compared. In addition, the second stories of Walls 1 and 2 are nearly identical. The only difference is that Wall 2 contains an additional opening intended to be infilled. By infilling this opening, a solid pier will be created with an H/L ratio of 0.43, which is identical to the center pier of Wall 1 (i.e. Pier 1-3). This allows the performance of an infilled opening to be compared with that of a solid wall pier. (Note: FEMA 273 states that the performances should be the same). In addition, Walls 1 and 2 contain piers with a variety of aspect ratios. This allows the effectiveness of FRP rehabilitation techniques on several types of piers to be assessed.

Table 3.4 Opening ratios of each wall

No. of wall	Story	Rough area (in ²)	Opening area (in ²)	Opening ratio
A/B	Second	40924	5600	13.7%
	First	43771	7106	16.2%
2	Second	41513	7336	17.7%
	First	44400	16940	38.2%
1	Second	41513	3875	9.3%
	First	44400	3444	7.8%

From Table 3.3, it is apparent that the aspect ratios of piers in the test structure range from 0.4 to 4.0. This range of pier aspect ratios was selected in order to allow both the “shear“ and “flexural” piers tested in MAE Center project ST-6 to be investigated. The focus of ST-6 was on the URM and retrofit behavior of two types of wall piers: (1) cantilever flexural member with an H/L ratio of 1.77 and a vertical stress ranging from 25 psi to 75 psi; and (2) cantilever shear member with an H/L ratio of 0.5 and a vertical stress of 65 psi (ST-6). For design, the piers in the first floor were assumed to act as “fixed-fixed” columns or walls, and all the piers in the second floor were assumed to act as cantilever columns or walls. Following this assumption, the piers with H/L ratios between 3.0 and 4.0 employed in the first floor, and H/L ratio between 1.5 and 2.0 employed in the second floor of the test structure are equivalent to the flexure piers tested in ST-6. Similarly, piers with H/L ratios of 1.0 employed in the first floor, and H/L ratios of 0.5 employed in the second floor are representative of the shear piers tested in ST-6.

3.2.3 Masonry Walls

The plan view of the test structure is shown in Fig. 3.5. The elevation views of each of the walls are shown in Fig. 3.6. – Fig. 3.8. The building is composed of four URM masonry walls constructed in standard American bond with a header course every sixth course. Walls A and B are composed of three wythes of masonry giving a nominal thickness of 12 in., while Walls 1 and 2 are composed of two wythes of masonry giving a nominal thickness of 8 in.. Walls A and B are identical except that four vertical holes were left in Wall A to allow a post-tensioning retrofit to be investigated. Since these walls are identical, direct comparisons can be made on the relative effectiveness of both FRP overlays and post-tensioning as retrofit methods. Walls A and B support the floor system. The pier sizes and H/L ratios are listed in Table 3.3. The opening ratios of each wall are listed in Table 3.4.

Table 3.3 Pier sizes and aspect ratios

Pier	Length (in)	Height (in)	H/L	Pier	Length (in)	Height (in)	H/L
A/B-2	48.375	47.25	1.0	1-4	48.375	47.25	1.0
A/B-3	40.25	47.25	1.2	1-6	48.375	84	1.7
A/B-4	40.25	47.25	1.2	1-7	210.625	84	0.4
A/B-5	48.375	47.25	1.0	2-2	48.375	47.25	1.0
A/B-7	48.375	84	1.7	2-3	24	47.25	2.0
A/B-8	40.25	47.25	1.2	2-4	24	47.25	2.0
A/B-9	40.25	47.25	1.2	2-5	48.375	47.25	1.0
A/B-10	48.375	47.25	1.0	2-7	48.375	94.5	2.0
1-2	48.375	47.25	1.0	2-8	24	94.5	4.0
1-3	121.25	47.25	0.4	2-9	48.375	94.5	2.0

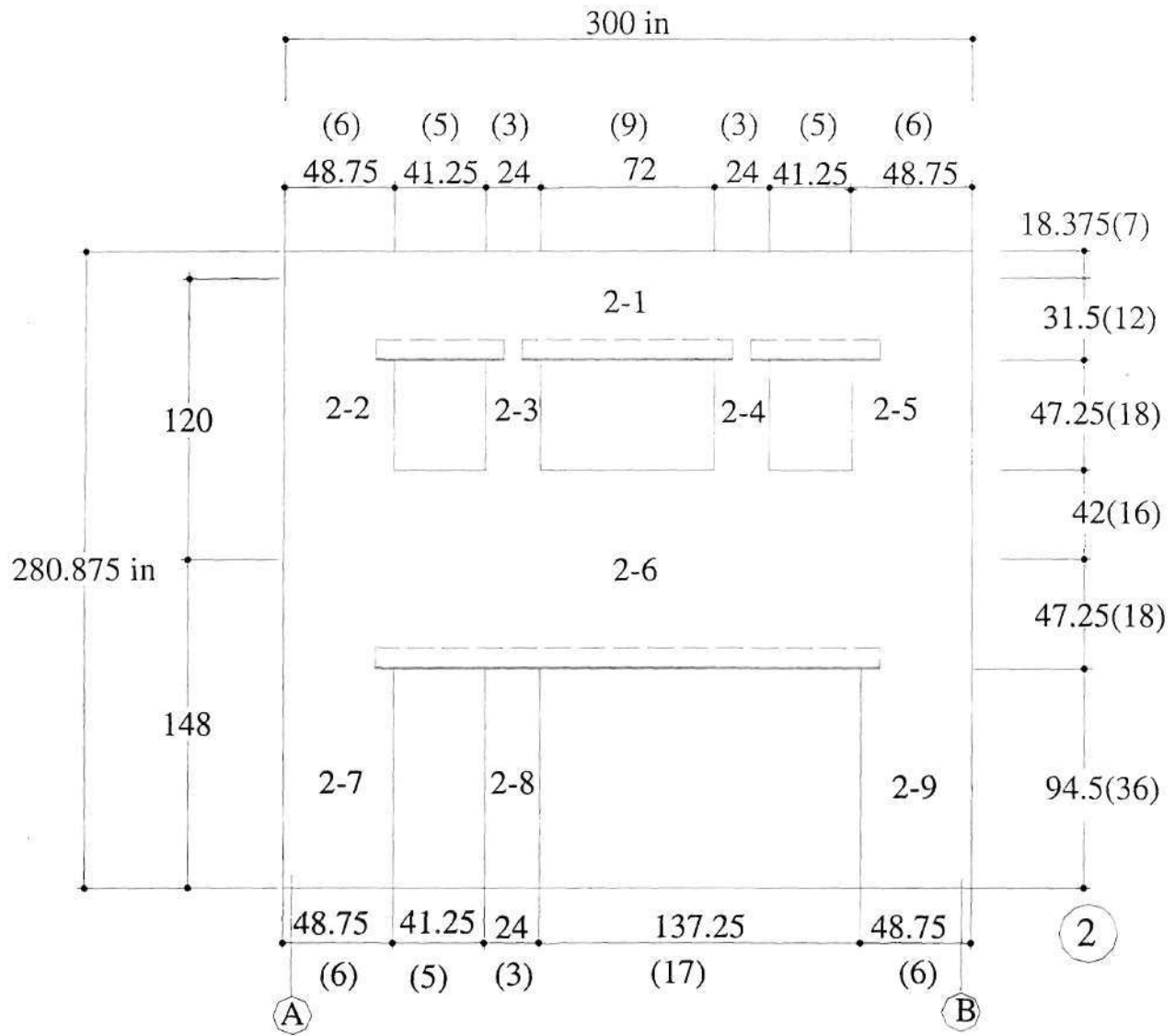


Figure 3.8. Elevation view of Wall 2

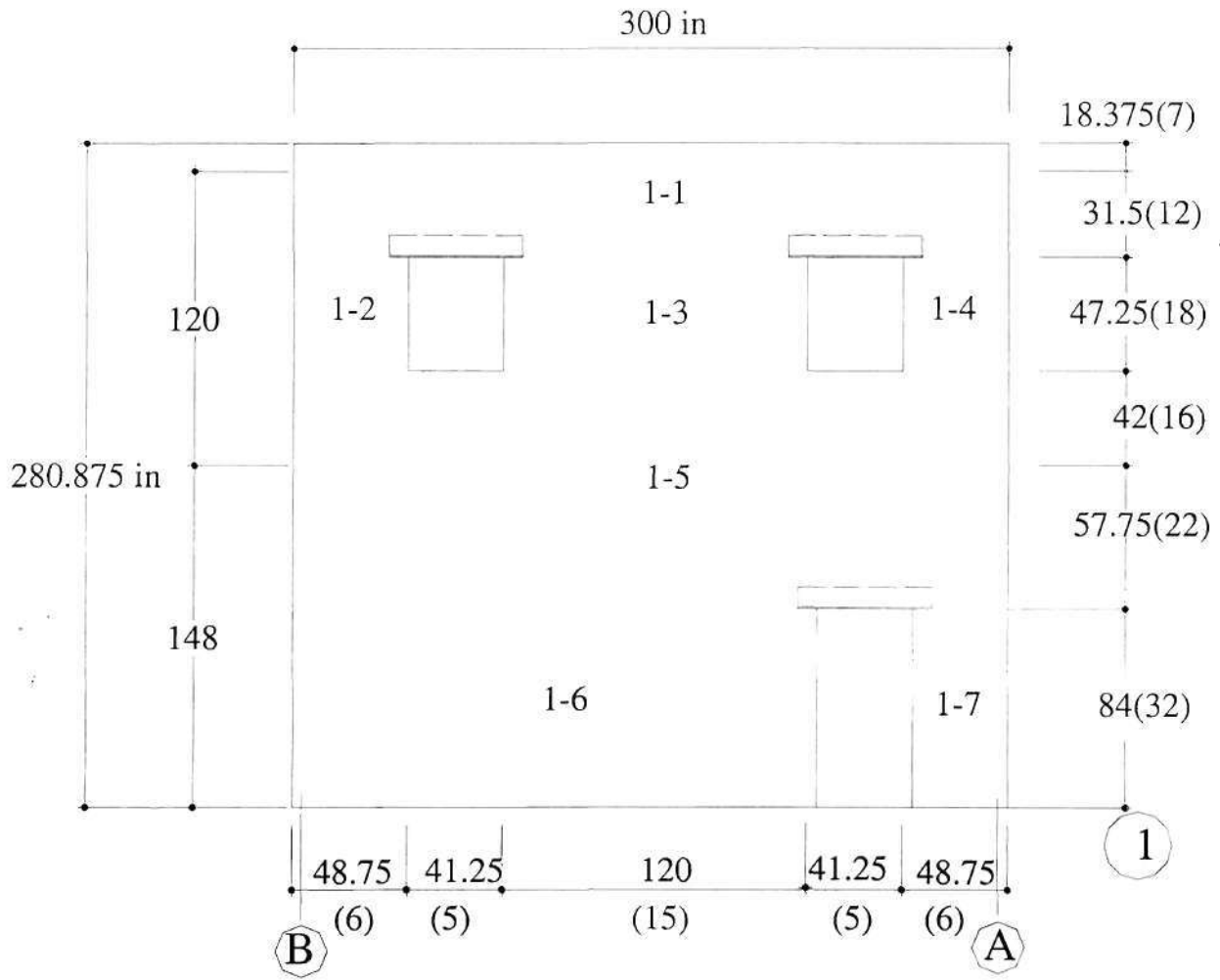


Figure 3.7. Elevation view of Wall 1

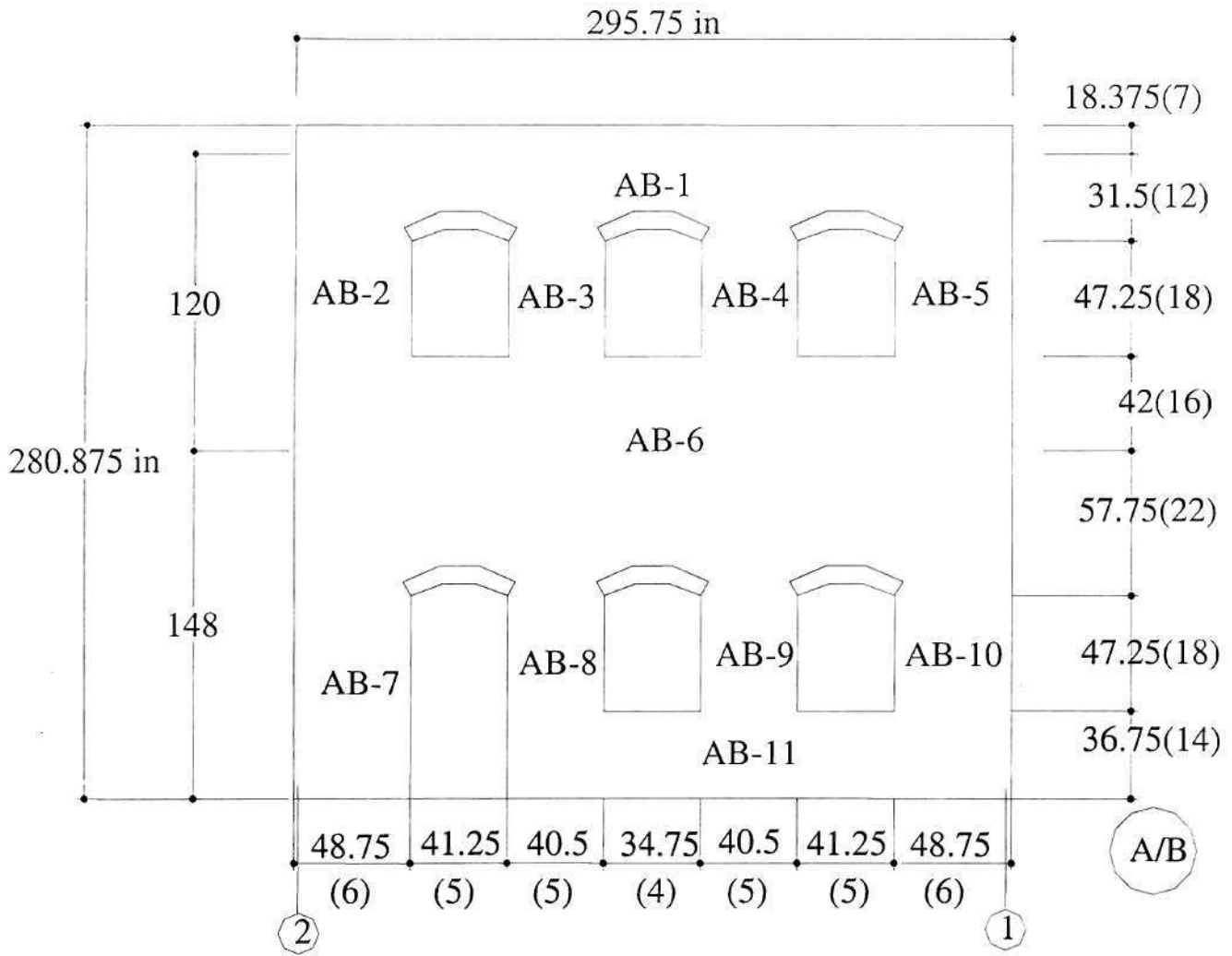


Figure 3.6. Elevation view of Walls A and B

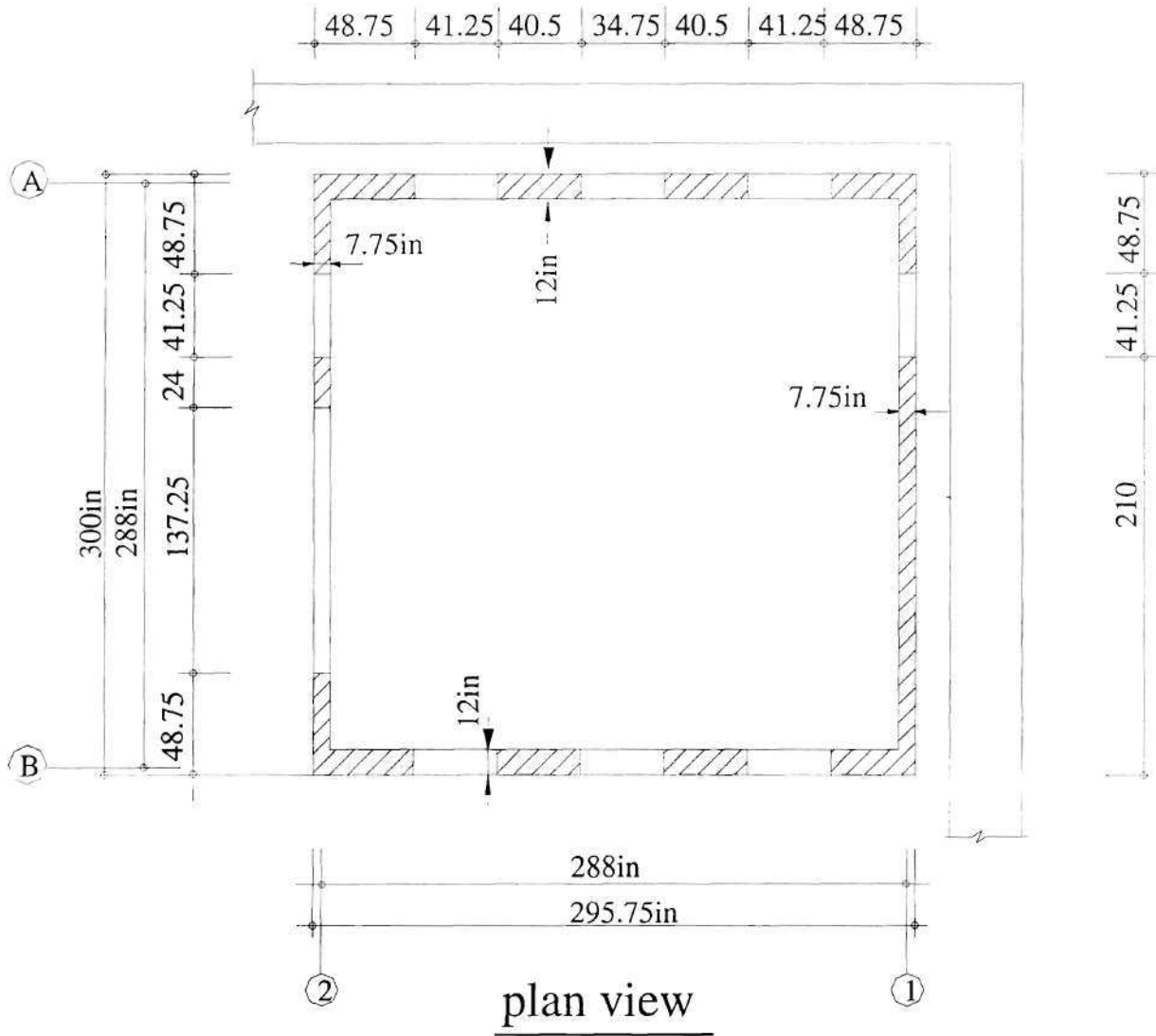


Figure 3.5. Plan view of the ST-11 test structure

3.2.2 Timber Stud Wall

The floor system tested in ST-8 contained 2x10 joists spaced at 16in on center. This type of floor system is only capable of spanning 12 ft.; however, the distance between bearing walls of the ST-11 test structure is 24 ft.. As a result, a timber stud wall was provided in the center of the structure to reduce the required span to 12 ft. and allow the 2x10 joists, as used in ST-8, to be employed. Both the first and second floor stud walls are constructed of 2x6 studs spaced at 16 in. on center with full-depth block supplied at 4 ft. on center (Fig. 3.4). Since these walls are only intended as vertical load carrying members, they contain no sheathing. The stud wall in the first floor is fixed to the strong-floor at the base, and nailed to the floor joists at the top. The stud wall in the second floor is nailed to the floor joists at the bottom and the roof joists at the top.

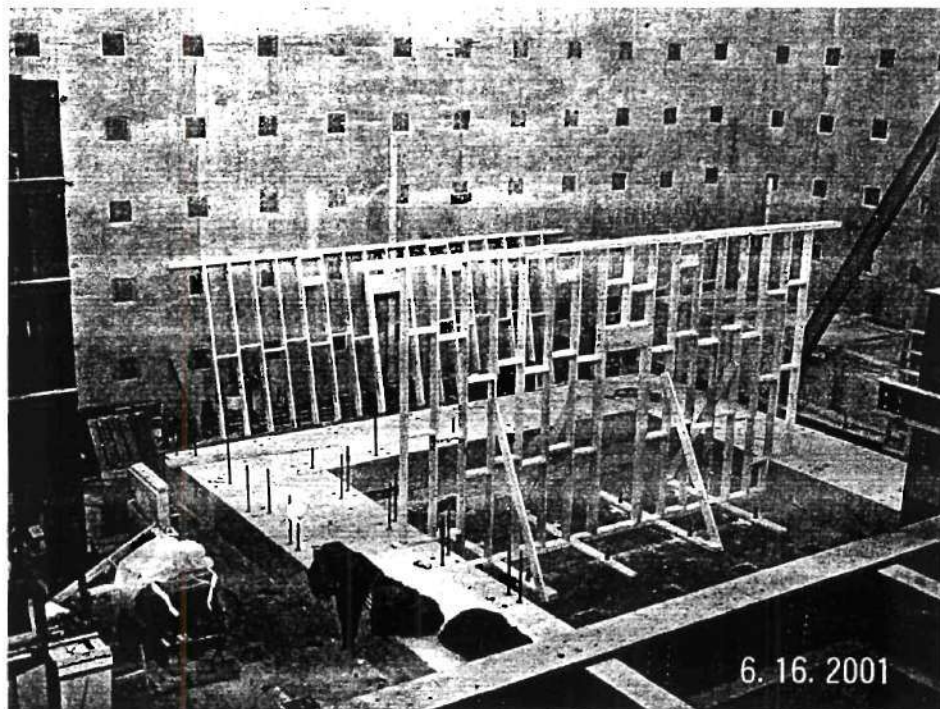
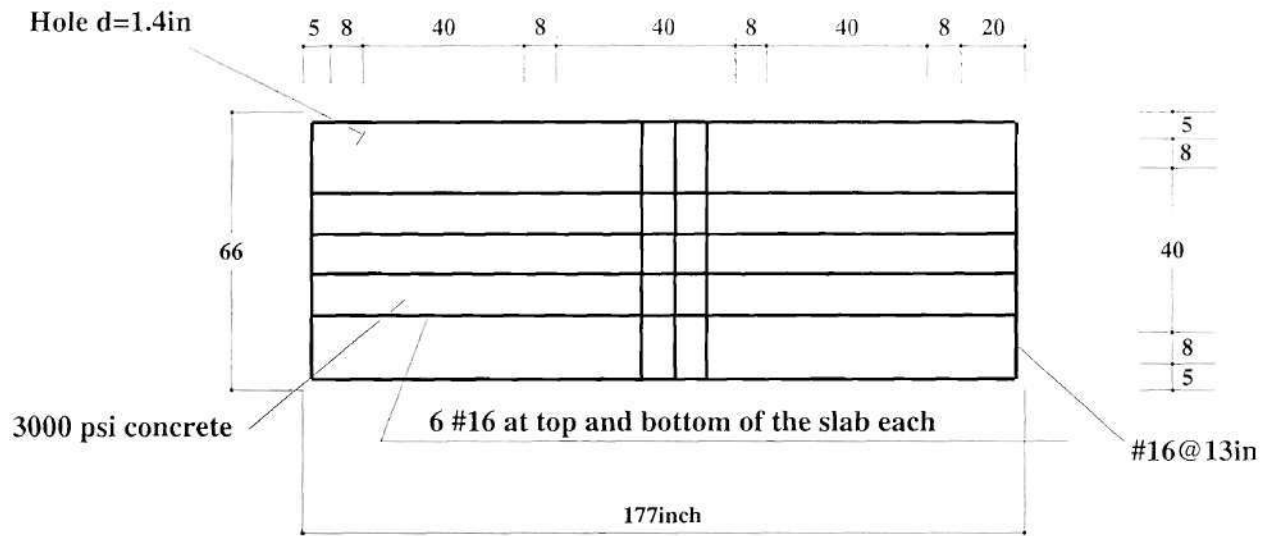
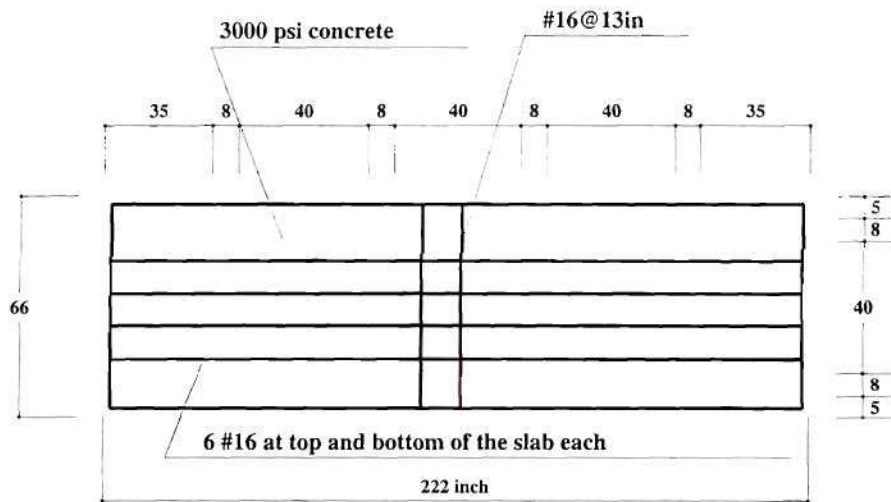


Figure 3.4. Photo of the stud wall together with the foundation



Slab A-1, A-2, B-1, B-2



Slab 1,2

Figure. 3.3. Reinforcement detail of the foundation slabs (dimensions are in in.).

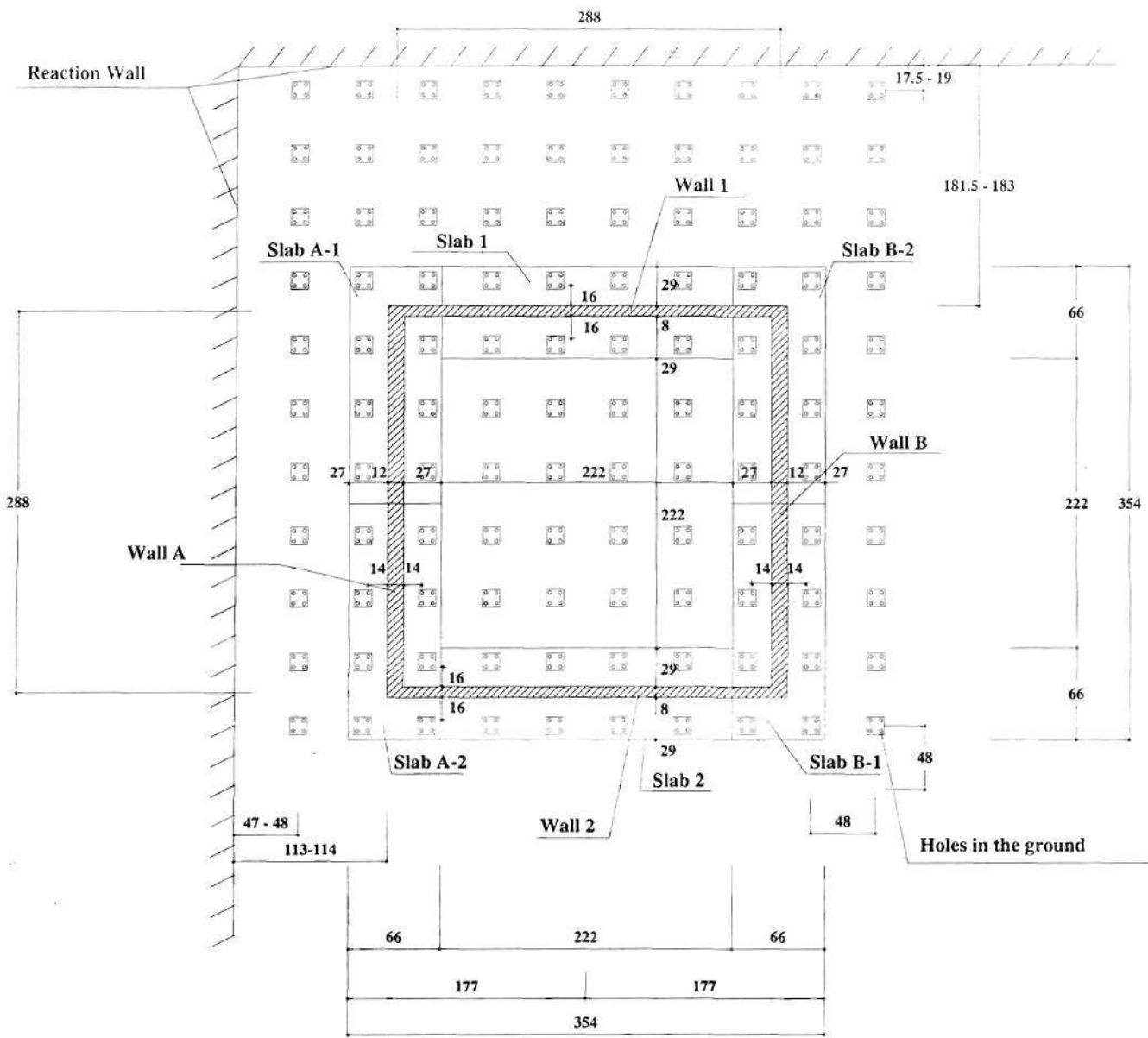


Figure. 3.2 Plan view of foundation layout (dimensions are in in.).

In order to facilitate the use of the same floor system investigated in MAE Center project ST-8, a stud wall was constructed through the center of the structure to support the joists. The design of each component of this building will be discussed in the following sections.

3.2.1 Reinforced Concrete Foundation Slabs

The design of the RC foundation for the URM building is shown in Fig 3.2 and Fig. 3.3. The foundation is composed of six individual RC slabs in order to allow them to be easily moved by the overhead cranes in the laboratory. The dimensions and weights of each RC slab are listed in Table 3.2. The thickness of the foundation slabs is 20 in, which ensures sufficient development length for the post-tensioning anchor bolts to be used for retrofit. The slabs were cast with groups of four holes spaced at 4 ft on center in order to allow the foundation to be post-tensioned to the strong floor, which contains the same pattern of tie downs.

The RC slabs are designed in accordance with the minimum reinforcement requirement of ACI318-95. The governing loading case was due to the self-weight of the concrete when the crane was lifting the slab.

Table 3.2 Dimensions and Weights of the RC slabs

Slab	Dimension (in x in x in)	Volume (in ³)	Weight (lb)
1	222 x 66 x 20	293040	25438 (11.4 ton)
2	222 x 66 x 20	293040	25438 (11.4 ton)
A-1	177 x 66 x 20	233640	20282 (9.06 ton)
A-2	177 x 66 x 20	233640	20282 (9.06 ton)
B-1	177 x 66 x 20	233640	20282 (9.06 ton)
B-2	177 x 66 x 20	233640	20282 (9.06 ton)
Total		1520640	132001 (59.1 ton)

Note: Density of Concrete was assumed to be 150 pound/ft³

3.2 Test Structure

The ST-11 test structure is a two-story URM bearing wall structure with timber floor and roof diaphragms. It is intended to represent a typical existing URM building in Mid-America. The URM building is constructed to fully utilize the L-shaped strong wall in the Structural Engineering Laboratory at Georgia Tech. The dimensions of the building are 24ft by 24ft. in plan with story heights of 12 ft. for the first story and 10 ft. for the second story (see Fig. 3.1). Several openings are provided in the walls in order to allow piers with various aspect ratios to be investigated. Furthermore, these openings simulate typical door and window openings in existing URM buildings. The test structure was constructed on top of a set of reinforced concrete slab foundations, which are post-tensioned to the strong-floor. The foundations are designed to transfer the base shear of the structure to the strong floor and anchor the post-tensioning tendons used for retrofit.



Figure 3.1 Overview of the tested structure with the L strong walls

test method, the design of the ST-11 and ST-22 test specimens is very similar in order to allow the results to be compared. Both the ST-11 and ST-22 test specimens are composed of two parallel walls with large differences in stiffness and two parallel walls with identical configurations.

Objective 5 is to examine the relative effectiveness of different retrofit approaches. The proposed retrofit approaches include:

- Strengthening the connections between the diaphragm and the masonry walls
- Increasing the stiffness of the diaphragm
- Post-tensioning the masonry walls
- Applying FRP overlays to strengthen the masonry walls
- Hybrid retrofit method (i.e. post-tensioning and FRP overlays)

Objective 6 is to assess the effectiveness of selective rehabilitation of individual components. The proposed test sequence consists of several cycles of load to induce moderate damage, the repair of the damaged component, and the reloading of the specimen.

- The contribution of each masonry pier to the strength of the entire perforated wall
- The contribution of the flexible wood roof/floor diaphragm to the overall response of the building system

The second objective is to experimentally identify critical components in order to develop a systematic method to apply rehabilitation approaches. The following critical components or behaviors will be investigated in the ST-11 test:

- The diaphragm-to-wall connections
- The out-of-plane behavior of URM walls
- The torsional behavior of a URM building with unsymmetrical layout
- The progressive damage of piers in a perforated URM wall
- The behavior of secondary elements
- The behavior of different lintels

Objectives 3 and 7 are to experimentally validate available code provisions (FEMA 273), as well as advanced analysis tools for evaluating both unreinforced and retrofitted masonry structures. The proposed ST-11 test specimen represents a realistic configuration for URM structures in Mid America, and thus constitutes a good test for FEMA 273 provisions as well as for advanced analysis tools.

Objectives 4 and 8 are to compare the full-scale quasi-static test with half-scale dynamic test. Several limitations exist for both full-scale quasi-static tests as well as half-scale dynamic tests. For example, half-scale dynamic tests are not suitable to investigate connection behavior and full-scale quasi-static tests will likely miss some critical structural responses due to seismic vibration. Due to the apparent shortcomings of each

Table 3.1. Objectives for Project ST-11

	Objectives
Existing URM	<p>(1) Verify the extrapolation of individual component behavior to the overall response of the building system</p> <p>(2) Experimentally identify the critical components in order to develop a systematic method to apply rehabilitation approaches</p> <p>(3) Experimentally validate standard code (FEMA 273) as well as advanced analysis tools for URM structures</p> <p>(4) Compare the full-scale quasi-static test with the half-scale dynamic test (ST-22)</p>
Rehabilitated URM	<p>(5) Examine the relative effectiveness of different rehabilitation approaches</p> <p>(6) Assess the effectiveness of selective rehabilitation of individual components on overall system performance.</p> <p>(7) Experimentally validate standard code, as well as advanced analysis tools for rehabilitated URM structure</p> <p>(8) Compare the full-scale quasi-static test with half-scale dynamic test</p>
Other	Aid in the development of rehabilitation guidelines

The first objective listed in Table 3.1 is to verify the extrapolation of individual component behavior to the overall response of the building system. This objective is based on the parallel research of other MAE center projects that investigated the behavior of individual components, such as project ST-6 (URM wall piers) and project ST-8 (Flexible wood diaphragms). Specifically, the ST-11 test will investigate the following points:

3 EXPERIMENTAL PROGRAM

The experimental program will be described in this section. First, the objectives of the ST-11 test will be briefly reviewed. Second, the design of the test structure will be presented, including the design of the masonry walls, timber roof/floor system, foundation, and several retrofit techniques. The construction of the building will also be briefly described in this section. Next, the extensive material tests performed in order to select appropriate materials for the construction of the full-scale test structure will be outlined. Finally, the proposed loading sequence, test setup, and the instrumentation will be discussed.

3.1 Objectives

The focus of MAE Center project ST-11 is the quasi-static testing of a full-scale URM structure. The goal of the project is to examine the structural characteristics of existing unreinforced masonry buildings and to explore the effectiveness of several rehabilitation techniques. The categorized research objectives of project ST-11 are listed in Table 3.1.

than equivalent URM walls (Hinkley, 1996). However, diagonal tension failures are common for post-tensioned masonry walls loaded in-plane (Laursen and Ingham, 2001a, and Page and Huizer, 1998). It should be mention that although this type of failure is typically considered brittle, large post-peak displacements have been reported with ultimate drifts greater than 1% in some cases (Page and Huizer, 1998). Similar to out-of-plane behavior, the behavior of grouted versus ungrouted post-tensioned walls is drastically different. Grouted post-tensioned walls display an elastic-plastic behavior while ungrouted walls displayed a nonlinear elastic behavior (Laursen and Ingham, 2001a). Analysis based on the equivalent stress block analogy has shown good correlation with experimental results (Hinkley, 1996).

Further literature on the behavior of post-tensioned masonry walls can be found elsewhere (Al-Hashimi and Curtin 1988; Ambrose et al, 1998; Baqi et al, 1999; Curtin and Howard, 1998; Curtin et al, 1991; Dawe and Aridru, 1992; Devalapura et al, 1999; Fisher et al., 1989; Garrity and Garwood, 1994; Garrity and Garwood, 1990; Graham and Page, 1995; Graham and Page, 1994; Hobbs and Daou, 1988; Huizer and Shrive, 1986; Lacika and Drysdale, 1995; Lissel et al., 1999; Lissel et al, 1998; Montague and Phipps, 1985; Page, 2001; Phipps and Al-Safi, 2001; Rodriguez et al., 1998; Sayed-Ahmed et al., 1999)

with experimental results. It was also noted that pre-cracking deflections were best approximated by the formula for flexure and shear deformation of a cantilever beam.

2.2.3.3 Summary of Research

Several experimental studies have been conducted to assess both the out-of-plane and in-plane behavior of post-tensioned masonry walls. Results of research focused on out-of-plane behavior suggest that the behavior of the wall is strongly dependent on whether the tendons are grouted (i.e. restrained). Walls with ungrouted tendons displayed little reserved capacity after the cracking moment was achieved, while walls with grouted tendons displayed approximately double the strength of the cracking moment (Al-Manaseer and Neis, 1987). Displacement capacity seemed to be independent of whether the tendons were restrained, with both types of walls displaying large drifts of around 2% (Devalapura et al., 1996, Al-Manaseer and Neis, 1987). However, it should be noted that the displacement of the walls with ungrouted tendons was due mainly to one large crack while the walls with grouted tendons displayed a more uniform crack distribution. Experimental results also show that the horizontal flexural strength of masonry is increased by vertical prestressing until the failure mode became vertical cracks through the brick (Garrity and Phipps, 1988). Analysis results based elastic mechanics and the equivalent stress block analogy showed good correlation with experimental data for cracking moment and ultimate strength, respectively. (Devalapura et al., 1996).

Results of research conducted on post-tensioned walls to assess in-plane behavior suggests large increases in strength and displacement capacity are possible. Post-tensioned masonry walls have been reported to display capacities 3.5 to 7 times greater

As noted in Fig. 2.43, Wall A failed prematurely due to localized damage occurring at load introduction. As a result, no conclusions on the effectiveness of horizontal post-tensioning can be made. Both Walls B and C failed due to diagonal cracking; however, diagonal cracking did not occur in the post-tensioned wall until 97% of the capacity was achieved while the reinforced wall showed diagonal cracking at less than 50% of the capacity. This suggests that the presence of vertical stress is effective in delaying the formation of diagonal cracking. Although this failure mode is typically considered brittle, no sudden loss of load carrying capacity was reported at the onset of diagonal cracking in either wall (see Fig. 2.43). Comparing the behavior of Walls B and C shown in Fig. 2.43 it is apparent that a post-tensioned URM displayed approximately 50% more strength than the equivalent reinforced wall.

Hinkley (1966) subjected two URM walls and five prestressed masonry walls to in-plane loads in order to assess behavior. Two wall geometries were examined, square walls with a length and height of 62 in and rectangular walls with a length of 82 in and a height of 54 in. To accomplish prestressing, ungrouted 0.276 in diameter, high-strength steel wires were used. As the prestressed walls were loaded, a flexure crack opened at the base of the wall and grew towards the compression face. Failure was caused by the fracture of the prestressing wire on the tension side of the wall. Capacities of the prestressed wall exceeded those of the URM walls by factors between 3.5 and 7 depending on the level of prestress. The specimens were analyzed using an equivalent stress block analogy as well as an analysis that assumed linear stress variation in the masonry compressive zone in order to calculate the ultimate strength. The equivalent stress block analysis was shown to be superior with an average error of 3% compared

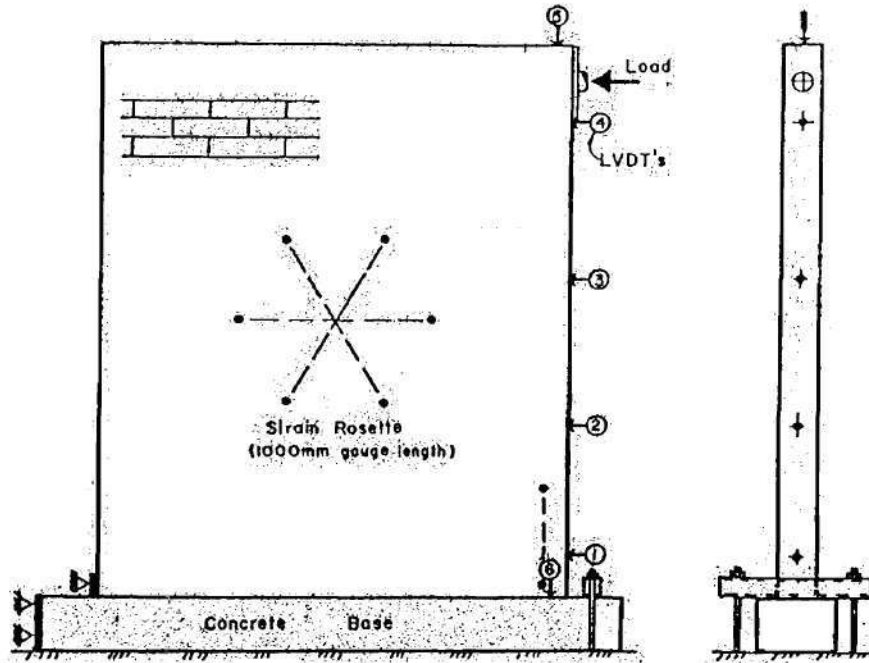


Figure 2.42. In-plane test setup and instrumentation layout (taken from Page and Huizer, 1998)

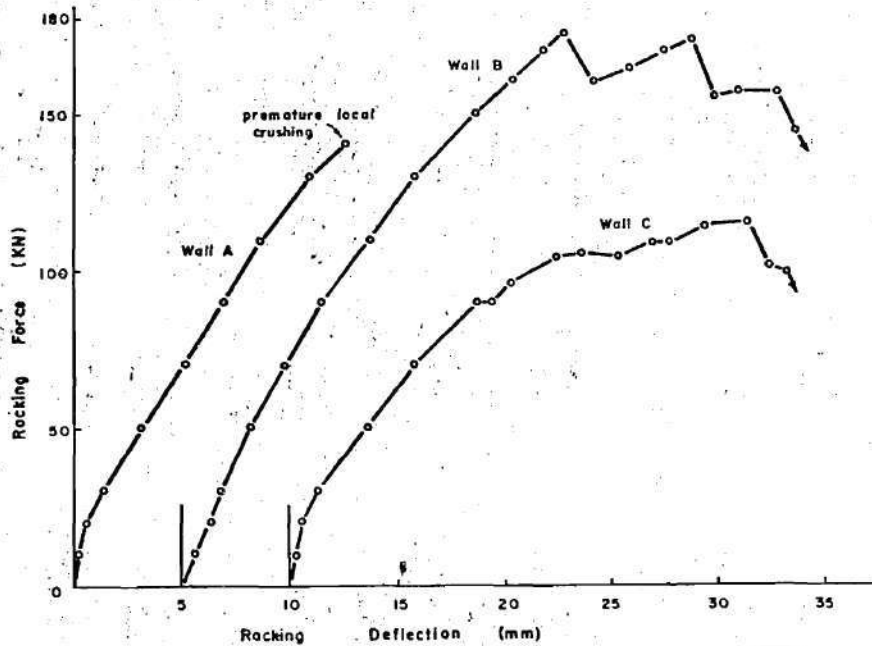


Figure 2.43. In-plane force-displacement curves for each wall tested (taken from Page and Huizer, 1998)

- 7) Select and scale a series of ground motions to the applicable design spectra
- 8) Execute the dynamic analysis and verify compliance with design criteria (if drift demand is excessive damping devices may be required)
- 9) Design wall according to capacity design philosophy

Page and Huizer (1998) report the results of in-plane shear tests conducted on three masonry walls: Wall A, vertically and horizontally post-tensioned, Wall B, vertically post-tensioned, Wall C, vertically reinforced. All walls were constructed with four equally spaced 0.6 in diameter high strength Dywidag rods vertically. For the case of Wall C the rods were left unstressed and grouted, while for Walls A and B the rods were tensioned to provide 290 psi of vertical stress and left ungrouted. Wall A also contained two horizontal rods tensioned to provide 145 psi of horizontal post-tensioning stress. The walls were constructed of "Monach" hollow clay masonry units and were approximately 120 in tall, 100 in wide and 8 in thick. The walls were loaded monotonically until failure. Fig. 2.42 and 2.43 show a schematic of the test specimens and the force-displacement curves for all three walls tested.

nonlinear dynamic analysis is then carried out on an equivalent SDOF system. This equivalent system is obtained by assuming an inverted triangular distribution of seismic forces and essentially is composed of the total structure mass placed at the effective height (approximately $2/3 \cdot H$). In order to illustrate this method and provide insight into the dynamic response of prestressed concrete masonry shear walls, the authors analyzed a 5-story structure constructed of prestressed concrete masonry (bi-linear elastic model) as well as reinforced concrete masonry (elastic-plastic model). The equivalent SDOF systems were subject to 12 ground motions scaled to match the design spectra at the structure's elastic period. As expected, building drift demand and ductility demands for the reinforced concrete masonry structure were far lower (approximately half) than those for the prestressed concrete masonry structure due to the large hysteretic damping of an elastic-plastic model. However, the PCM structure did satisfy the drift limits imposed without the addition of any damping devices. It was also noted that the code-defined approach for ductile seismic design (i.e. the use of 'R' factors) are not applicable to PCM structures as they assume large hysteretic damping. The design procedure presented is summarized as follows (Laursen and Ingham, 2001b):

- 1) Assume wall dimensions and prestressing area (initial estimate could be based on code RCM strength demand)
- 2) Calculate initial tendon stress (based on tendon yield at 2% roof drift)
- 3) Calculate force-displacement characteristics
- 4) Define seismic design criteria (i.e. drift limit)
- 5) Calculate dynamic quantities
- 6) Define equivalent bi-linear elastic SDOF system

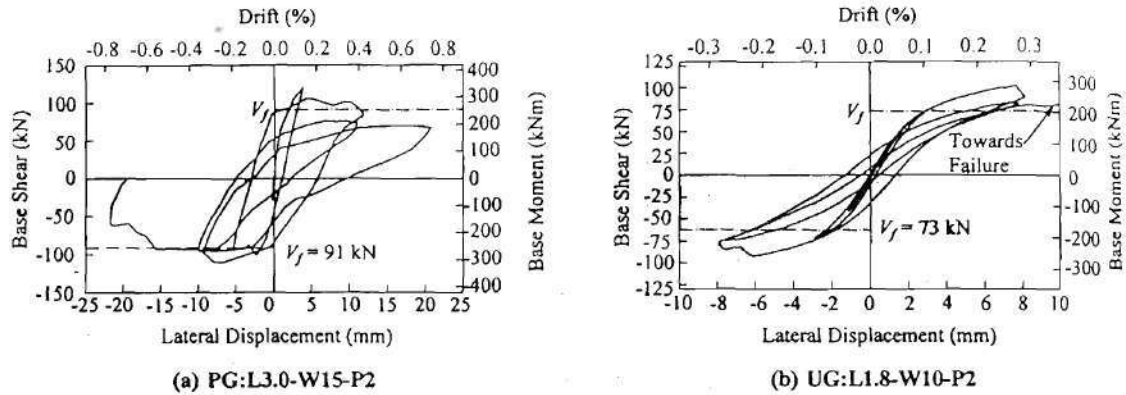


Figure 2.41. Force-displacement response of partial grouted (PG) and ungrouted (UG) post-tensioned URM piers (taken from Laursen and Ingham, 2001a)

In addition, Fig. X shows that the force-displacement response of the partially grouted wall was somewhat elastic-plastic, while the response of the ungrouted wall can be considered nonlinear elastic. In all walls yielding of the tendons was observed which caused a decrease in prestressing force with each cycle. In order to avoid tendon yielding it is recommended that the tendons be stressed between 25% and 50% of the yield stress and that they remain unbonded over two to three stories.

Laursen and Ingham (2001b) outlined a simplified seismic design procedure for unperforated in-plane prestressed concrete masonry shear walls. The method assumes that all walls rock and models the force displacement characteristics as bilinear elastic. The initial stress in the tendons is calculated based on tendon yield at 2% drift assuming rigid body rocking about the lower corner for all piers. Drift limits are taken as either the drift that causes an extreme fiber strain in the masonry of 0.02 (based on an assumed plastic hinge length) or the limits imposed by the governing code which ever is less. A

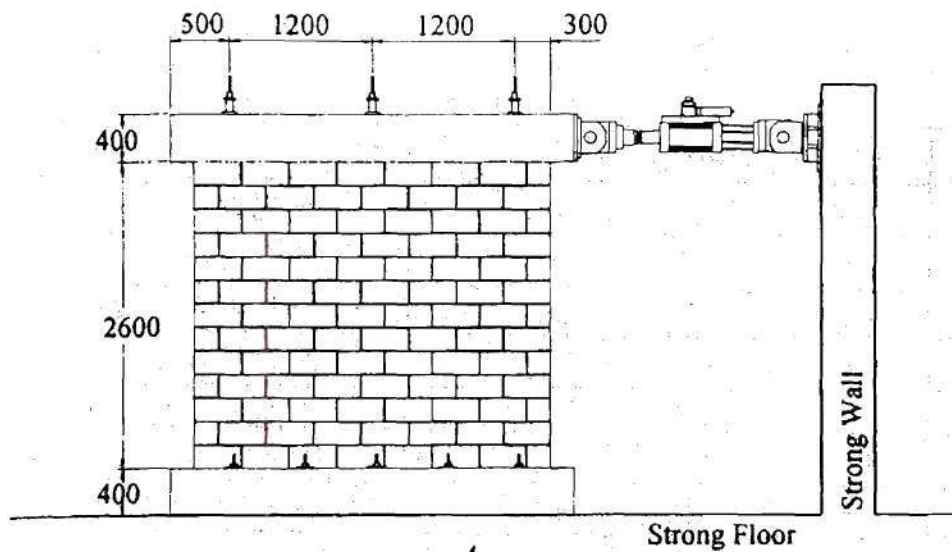


Figure 2.40. Schematic of in-plane post-tensioned URM pier test setup (taken from Laursen and Ingham, 2001a)

The walls were post-tensioned to stresses that range between 158psi and 450psi using either two or three unbonded tendons. It should be noted that these stresses include dead load and live load. In order to investigate the effect of grouting on in-plane behavior, tests were conducted on fully grouted walls, partially grouted walls and ungrouted walls. The fully grouted walls exhibited elastic non-linear behavior. The failure mode was reported as rocking followed by toe-crushing at large drifts. These walls displayed very good ductility with drifts up to 1.4%. It was noted that ultimate drifts had a very strong dependence on wall geometry. Both the partially grouted and ungrouted walls failed in shear. While these failure modes were not ductile, drifts of up to 0.7% were recorded before the resistance of the wall decreased below 60% of the capacity (see Fig. 2.41).

at the front of the abutment was 148psi while the prestress at the heel of the abutment was 542psi. The specimen was loaded by 33 hydraulic rams intended to replicate loads from both earth pressure as well as the longitudinal load from the bridge. Up to the service load the abutment remained crack free with the exception of small vertical cracks at the base of the webs. As the load was increased to the capacity of the rams, the base moment overcame the prestress and tensile strength at the heel of the abutment. This resulted in horizontal cracks at the base and caused a rigid body rotation about the toe of the wall. Upon unloading all cracks closed and the abutment appeared undamaged. Due to the lack of loading capacity a third of the abutment was removed and the remaining portion was tested to failure (Garrity and Garwood, 1993). Failure was ultimately caused by shear cracking of the webs; however after cracks were observed in the web, the abutment was still able to resist a 29% increase in load. Upon unloading the abutment seemed to be stable as a freestanding structure, and while shear cracks remain visible, all other cracks closed. Results indicated that the specimen resisted an average horizontal shear stress of 740psi without sliding deformation. The abutment satisfied the requirements of both service and ultimate conditions.

2.2.3.2 In-Plane Behavior

Laursen and Ingham (2001a) tested eight prestressed concrete masonry walls in order to determine in-plane behavior. All walls tested had a height of 8 ft 6 in and an aspect ratio (i.e. H/L) of either 0.86 or 1.44. A schematic of the test setup is shown in Fig. 2.40, note all walls were tested as cantilevers, that is, rotation at the top of the wall was not restrained.

The prestressed walls failed due to vertical cracks and displayed ductility due to arching action caused by the friction due to the prestressing. Horizontal flexure capacities were directly proportional to vertical prestressing force. The walls prestressed to 200psi and 400psi displayed approximately 3 and 4.5 times the capacity displayed by the URM walls, respectively. No difference in the results of the wallettes tested with all joints filled and those tested without head-joint was observed. It should be noted that frictional restraint introduced into the specimens by prestressing was not accounted for. In order to address this concern Garrity and Phipps (1988) tested similar walls and greatly reduced the frictional restraint by employing slip layers on both sides of the specimens. Results showed that, without arching action, prestressing only increases the horizontal flexural strength of masonry up to the modulus of rupture of the brick. That is, prestressing is effective in increasing the torsional resistance of the bed-joint due to friction and thus altering the failure mode to vertical cracking through the brick. However, once this failure mode is achieved, prestressing offers no further benefit on horizontal flexural strength of masonry.

Garrity and Garwood (1990) and Garrity and Garwood (1991) subjected a prestressed clay brick bridge abutment to out-of-plane loads in order to investigate the potential of such a system. The test specimen was meant to represent a portion of an actual abutment and measured 14ft in height 11ft 1in in width and 5ft 2in in thickness. The abutment consisted of two flanges constructed of two wythes of bricks connected by three web also two wythes in thickness. Post-tensioning was accomplished via six 1.5in diameter high strength steel rods. The rods were placed eccentrically to increase the resistance of the abutment to bending in the dominant direction. The prestress achieved

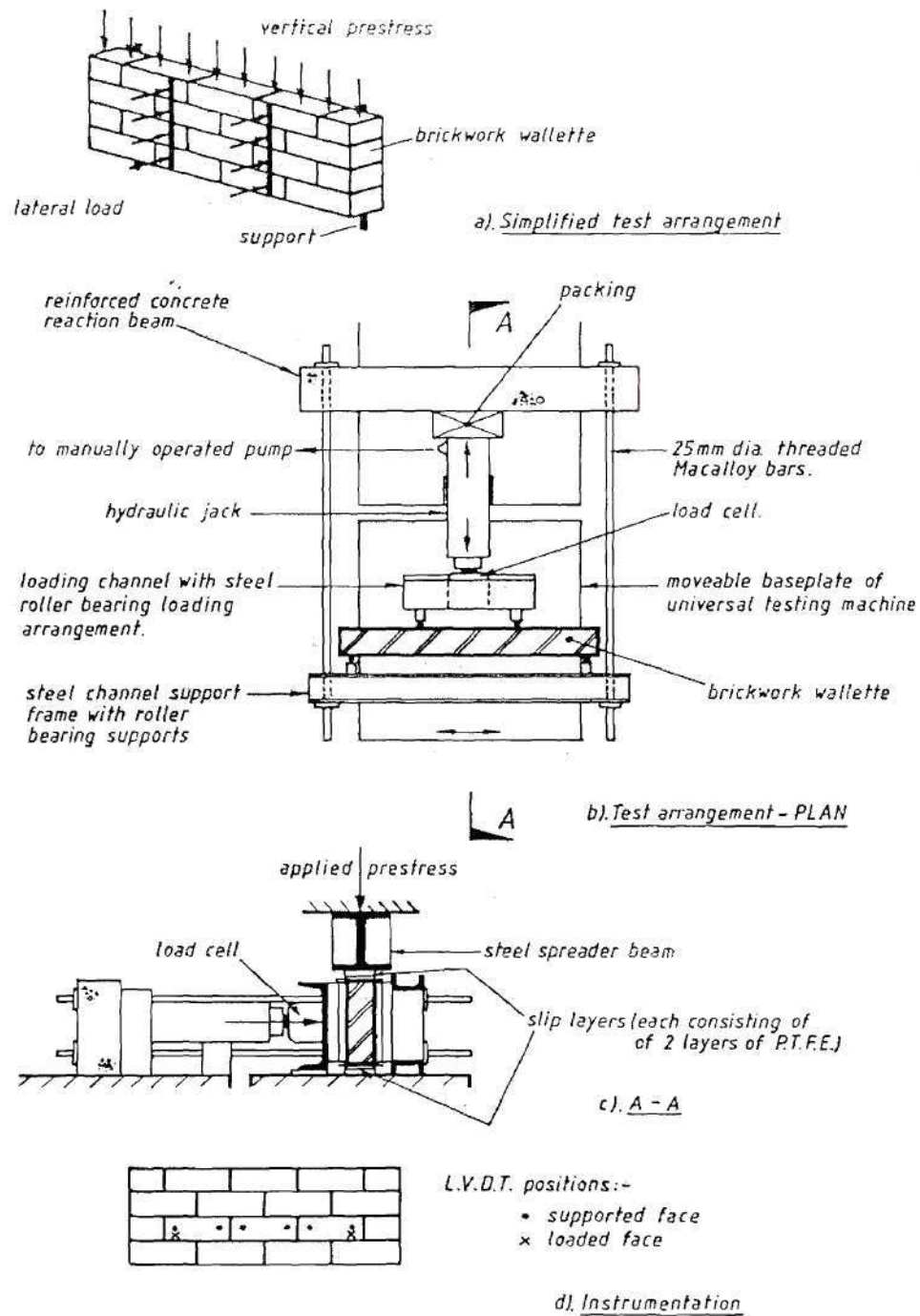


Figure 2.39. Schematic of Test setup (taken from Garrity and Phipps, 1987)

The URM wallettes failed in a brittle manner due to a stepped cracking pattern in which the bricks rotated about a vertical axis (torsional rotation in reference to the bed-joint).

height of the wall. Ultimate capacity seemed to be nearly directly dependent on the level of prestress.

Garrity and Phipps (1987) subject nine prestress masonry wallettes and nine URM wallets to out-of-plane loads in order to assess the effect of prestress on horizontal flexural behavior (i.e. bending between in-plane walls). The wallettes measured approximately 32in in width and 10in in length and were constructed of clay bricks in running bond. The test program examined two levels of prestress, 200psi and 400psi. In order to investigate the effect of the head-joint on horizontal flexural behavior, the head-joints of half of the walls were raked out after construction and half were tested with all joint filled. Fig. 2.39 shows a schematic of the test setup.

load at mid-height. Fig. 2.38 shows the load-deflection curves for each of the walls tested.

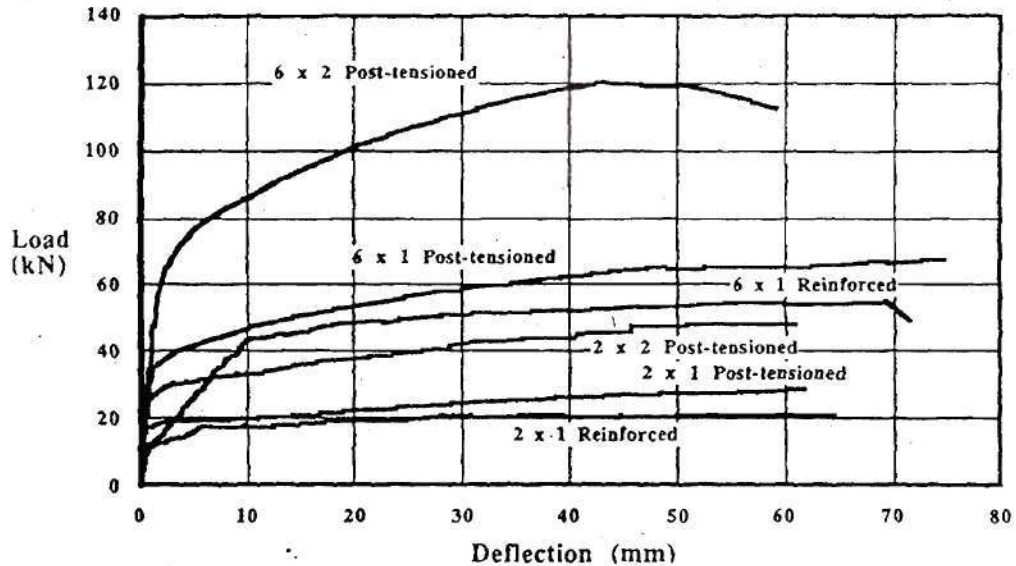


Figure 2.38. Load-deflection curves up to ultimate (taken from Al-Manaseer and Neis, 1987)

The notation in the figure (i.e. 6 x 2) refers to the pattern of prestressing tendons or reinforcing bars in the specimens. From the figure it is apparent that all walls exhibited ductile behavior with drifts up to 1% recorded for post-tensioned walls and 1.15% for reinforced walls. Due to the unbonded tendons, the post-tensioned walls displayed a displaced shape similar to a “V”. That is, all of the displacement was due to a single crack at the center of the wall. It is important to note that upon unloading the cracks in the prestress walls closed almost completely. The reinforced walls, with the steel continuously bonded, displayed a much more distributed cracking pattern throughout the

From the figure it is apparent that while both grouted and ungrouted walls displayed similar ultimate displacements as well as cracking moments, the grouted specimens displayed nearly twice the ultimate strength as the ungrouted specimens. The failure mode for the ungrouted specimens consisted of compression failure and spalling of the clay bricks. Grouted specimens failed due to a vertical splitting of the masonry in the vicinity of the prestressing tendon.

The authors analyzed each wall using linear elastic theory to calculate the cracking moments and obtained the ultimate moment capacity using ultimate strength theory. For the determination of the cracking moment, the modulus of rupture was approximated as 2.5 times the square root of masonry compression strength. Calculated cracking moments predicted experimental results within 3.5%. The ultimate moment capacity for the grouted walls, calculated with an equivalent stress block analysis, gave a value 4% lower than the actual ultimate strength. Less accurate predictions (25% error) were obtained for the case of the ungrouted tendons, which was attributed to the approximation of tendon stress.

Al-Manaseer and Neis (1987) tested two reinforced concrete masonry walls and four post-tensioned concrete masonry walls in order to investigate out-of-plane behavior. All walls were constructed of standard 8in block and measured 8ft tall and 4ft wide. The post-tensioned walls were stressed between 83psi and 500psi in order to examine the effect of different levels of prestressing. All post-tensioning tendons were unbonded. The walls were simply supported at top and bottom and subjected to an out-of-plane line

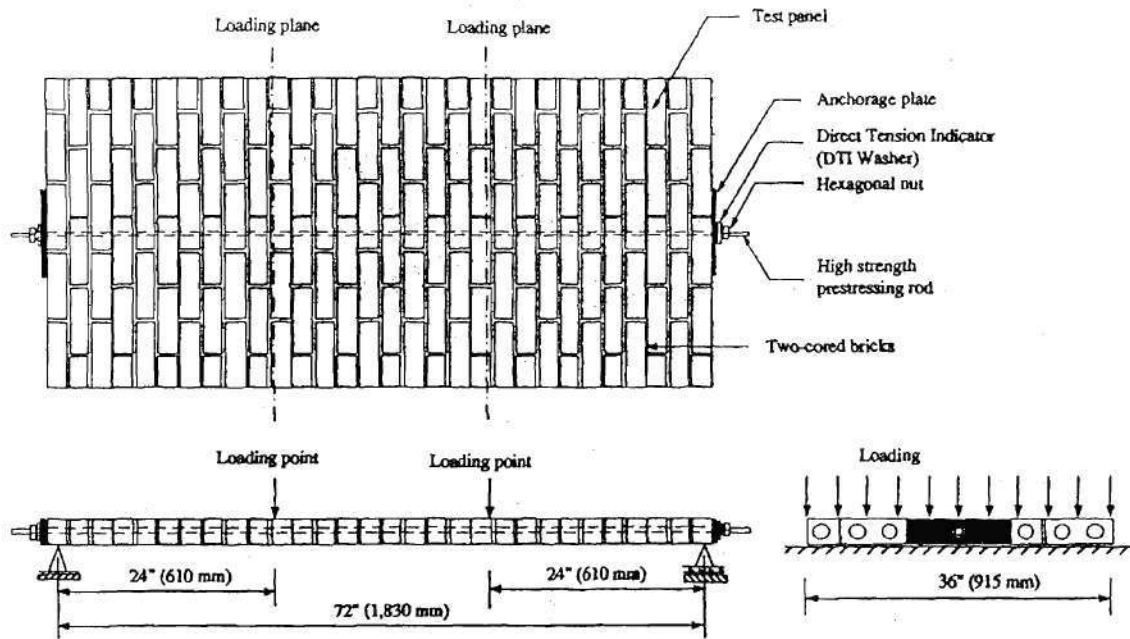


Figure 2.36. Schematic of test setup and specimen. (taken from Devalapura et al., 1996)

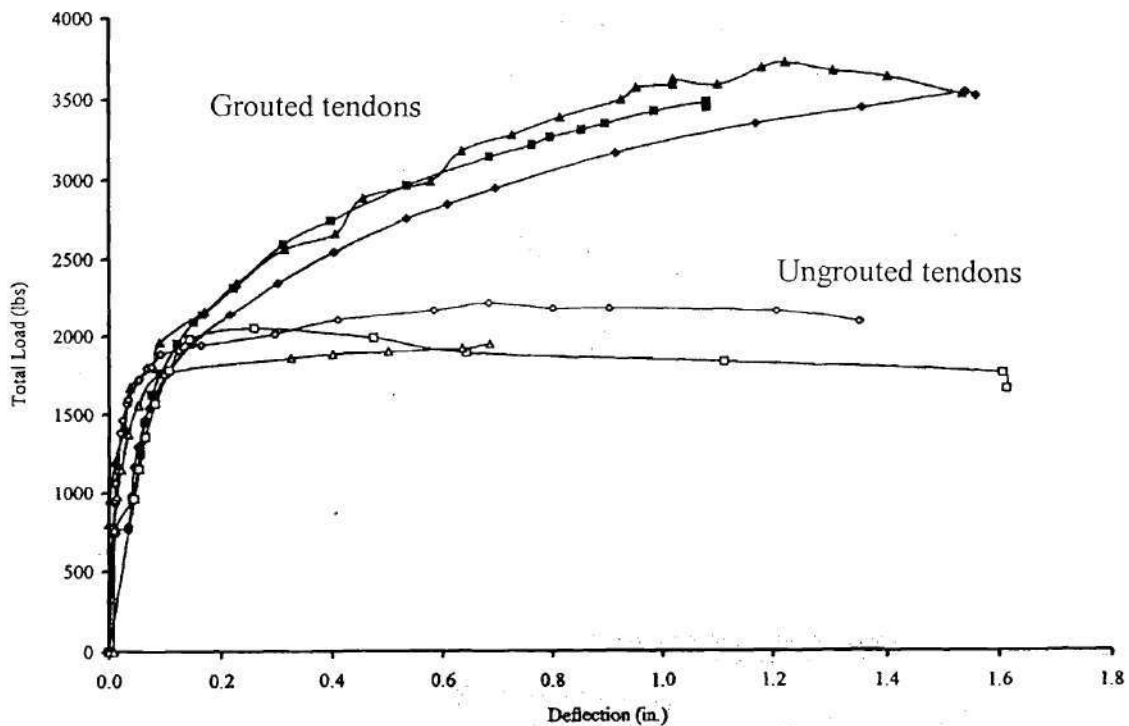


Figure 2.37. Force-Displacement behavior of each test specimen. (taken from Devalapura et al., 1996)

2.2.3 Post-tensioning

Another method that has been proposed to increase the strength of URM walls is the use of post-tensioning. Post-tensioning or prestressing has been used extensively in order to enhance the tensile and flexural capacity of concrete, which is a brittle material with characteristics similar to URM. For retrofit of URM structures this method is applied by core drilling down from the top of the masonry walls and vertically post-tensioning the walls to the foundation. While this method is somewhat costly, it has advantages in that it does not alter the appearance of the structure (especially important for historical structures) and that the occupants of the structure need not be disturbed during the retrofitting process. The following sections outline recent research conducted on in-plane and out-of-plane post-tensioned masonry walls.

2.2.3.1 Out-of-Plane Behavior

Devalapura et al. (1996) tested six post-tensioned clay brick masonry walls in order to determine out-of-plane behavior. Three specimens were tested with the tendons ungrouted and three with the tendons grouted in order to investigate differences. The specimens measured 36 in wide by 72 in high and were composed of a single wythe. To induce the prestressing force a single 5/8in diameter, 100ksi yield, steel tendon was provide in the center of each wall and stressed to 19kips based on a DTI washer. Fig. 2.36 and 2.37 show a schematic of the test setup and the experimentally measured force-displacement curves, respectively.

in bed-joint shear strength of 1000% (Marshall et al, 2000). Laursen et al. (1995) highlights one of the most desirable characteristics of FRP retrofit, the fact that the engineer can force a specific failure mode. In the case of this research, a wall that exhibited a brittle shear failure mode was retrofit with FRP overlays and a much more desirable rocking failure was forced. On the other hand, if a pier is expected to behave in a ductile manner (i.e. rocking or sliding), retrofitting with FRP overlays can alter the behavior resulting in a decreased displacement capacity (Franklin et al., 2001).

Analysis based on the equivalent stress block analogy used in reinforced concrete has been shown to be accurate in predicting the strengths of out-of-plane walls retrofit with FRP overlays when tension failure of FRP is the governing failure mode (Triantafillou, 1998; Hamilton and Dolan, 2001) . It is still unclear if such an analysis provides good results for in-plane wall tests. A method for approximating the bond strength of the FRP has been developed, and while the error associated with the method has been shown to be approximately 30%, the method is conservative (Triantafillou, 1998).

The strengthening of existing structures with FRP has been shown to be economical. Most notably in the case of the building damaged by the Northridge earthquake, in which an FRP retrofit was between 12% and 20% the cost of a shotcrete retrofit (Ehsani and Saadatmanesh, 1996).

Further literature on both in-plane and out-of-plane behavior of URM walls retrofitted with FRP overlays can be found elsewhere (Albert et al., 2001; Ghobarah and Baumer, 1991; Gilstrap and Dolan, 1998; Jai and Springer, 2000a; Jai and Springer, 2000b; Roko et al., 2001; Tumialan et al., 2001).

The FRP overlay retrofit consisted of five parts:

- 1) Existing cracks were filled with mortar,
- 2) The surface was prepared by sand blasting
- 3) A thin layer of epoxy was placed on the wall
- 4) The glass FRP sheets (*QuakeWrapTM*) were pressed into the uncured epoxy,
- 5) A final layer of epoxy was applied to outside of the FRP sheet to ensure complete impregnation.

Cost for the entire retrofit was less than \$4/ft², which is very cost-effective when compared with the shotcreting option that ranges from \$20/ft² to \$30/ft².

Velazquez et al. (2000b), report the use of the *QuakeWrapTM* glass/epoxy FRP system to retrofit existing URM building in Northern California. The retrofit was required due to stability concerns resulting from the excavation of soil directly adjacent to the wall. The retrofit covered the 60 ft long 30 ft high wall with a 0.1 in thick layer of FRP and was complete in less than a week.

2.2.2.4 Summary of Research

Initially, research conducted on FRP strengthening of URM walls had mainly focused on out-of-plane behavior, which is considered the critical direction for a URM wall. Out-of-plane resistance has been reportedly increased by up to 10 times that of equivalent URM walls with large drift capacities up to 4% (Triantafillou, 1998; Dimas et al., 2000a; Dimas et al., 2000b; and Ehsani et al., 1999). Based on the success of out-of-plane strengthening the effects of in-plane strengthening of URM walls has also been investigated. The effects of in-plane FRP retrofit are promising with observed increases

to provided similar results to the double sided retrofit; however the authors concede that this finding needs to be further investigated.

2.2.2.3 Application

Ehsani and Saasatmanesh (1996) and Ehsani (1995) reported the first application of FRP to a masonry structure for retrofit. The structure chosen for retrofit was one-story tall and constructed of concrete block masonry. The structure has been damaged during the Northridge Earthquake in 1994. A few years before the earthquake the structure had been retrofit with a steel frame in the center of the structure and with ties that connected the roof diaphragm with the walls. This retrofit was effective in preventing collapse although severe damage still occurred in part because the shear strength of the masonry was over estimated by a factor of two (Fig. 2.35).



Figure 2.35. Damage sustained prior to retrofit with FRP overlays (taken from

Ehsani and Saasatmanesh, 1996)

perfect bond between the composite and bricks. No nonlinear FEA was performed for the 0° - 90° specimens.

The effectiveness of a unidirectional carbon FRP (CFRP) overlay system on increasing the in-plane behavior of reinforced concrete masonry walls was investigated by Laursen et al. (1995). The two test specimens measured 6ft tall by 6ft wide, and contained 0.14% horizontal reinforcement and 0.54% vertical reinforcement. The specimens were tested in-plane with a vertical stress of 270psi and boundary conditions equivalent to a cantilever (see Fig. 2.34).

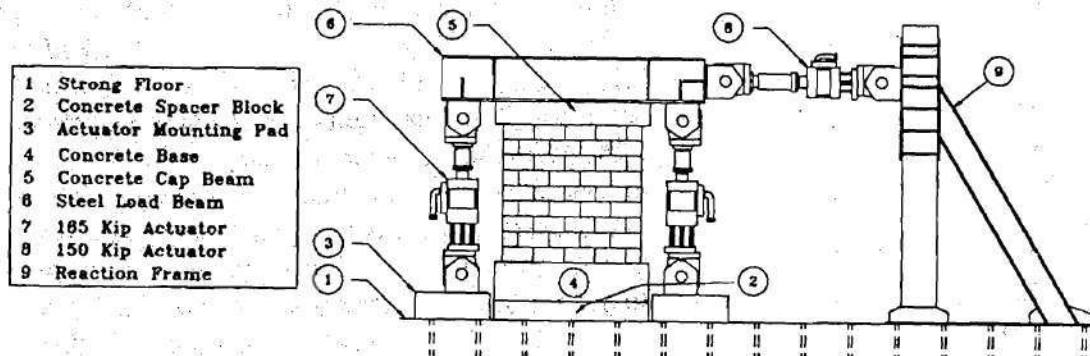


Figure 2.34. Schematic of in-plane test setup (taken from Laursen et al., 1995)

The first wall was tested in an “as built” state as a control specimen and then repaired with CFRP overlays (fibers in the horizontal direction) applied to both faces and retested. The second wall was tested after being retrofit with CFRP overlays on one face only, again with the fibers running in the horizontal direction. As expected the control specimen failed in a brittle shear mode, due to the low horizontal reinforcement. The CFRP employed in both of the walls was effective in suppressing the brittle shear mode of failure and caused the more desirable flexural failure. The single sided retrofit seemed

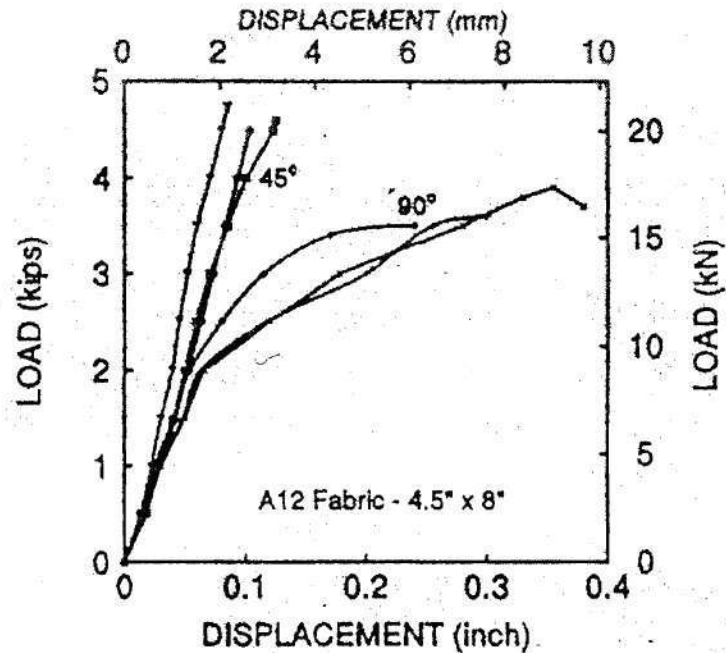


Figure 2.33. Force-displacement response of brick assemblages retrofitted with 0-90 and +/-45 FRP overlays (taken from Ehsani et al, 1997)

From the figure it is apparent that while the ultimate strengths associated with the different fiber orientations did not vary by much, the stiffness of the specimens was greatly affected. That is, the +/-45° fiber orientation resulted in a behavior that can be characterized as linear until failure, while the 0°-90° lay-ups displayed a nonlinear response. This behavior is consistent with the findings of earlier research that reported the stress-strain relation of composites is linear in tension and compression and nonlinear in shear. An elastic finite element analysis was conducted in which the bricks were modeled using eight-node three-dimension solid elements and the composite was modeled using four-node shell elements. Analysis results predicted a stiffness slightly larger than observed for the +/-45° specimens most likely due to the assumption of a

The effectiveness of GFRP in increasing the bed-joint shear strength of clay masonry was examined by Ehsani and Saadatmanesh (1996), Ehsani (1995), and Ehsani et al.(1997). In all, 37 specimens were tested in shear. The design variables considered were bond length (1in, 2.5in), fiber density (10, 12, 18 oz/yd²), and fiber orientation (+45°, 0°-90°). A schematic of the 3-brick test setup is shown in Fig. 2.32.

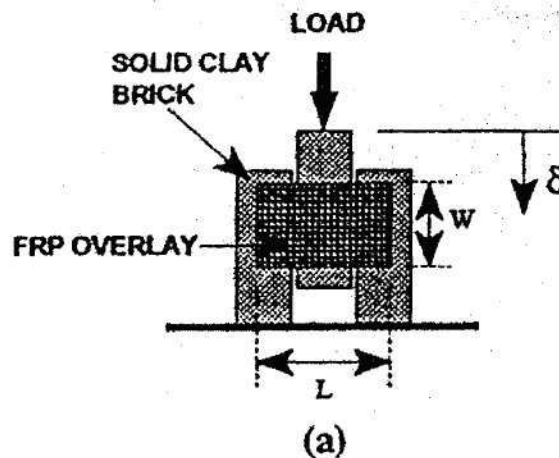


Figure 2.32. Schematic of 3-brick test setup (taken from Ehsani et al, 1997)

The bricks were assembled with lubricated 3/8in plywood between them in order to simulate the effect of a bed-joint, without adding any strength. The assemblages were tested without any vertical stress applied in order to eliminate resistance due to friction. Observed failure modes were dependent on both fiber density and bond length. The lower density GFRP failed in shear regardless of bond length, while the higher density GFRP with the shorter development length failed due to debonding. The force-displacement response of the specimen was highly dependent on the fiber orientation (see Fig. 2.33).

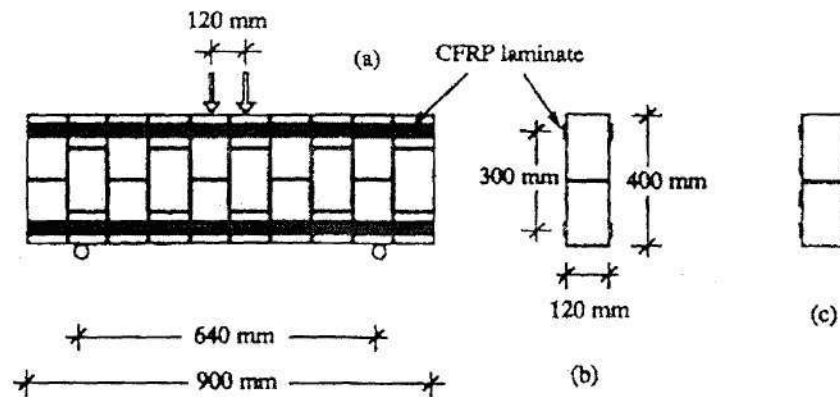


Figure 2.31. Schematic of in-plane test setup (taken from Triantafillou, 1998)

Two of the specimens were retrofit with two CFRP strips, two were retrofit with four CFRP strips, and two were tested in an unreinforced state to assess as built strength. The failure mode of each of the retrofit walls was a debonding of the composite. The analysis results correctly predicted that debonding would govern over FRP fracture and the predicted capacities were between 12% and 30% less than the experimentally determined strength (i.e. the predictions were conservative). It should be noted that no experiments conducted to validate the in-plane shear analysis were reported.

Ehsani and Saadatmanesh (1996) report the results of several shove tests performed on the clay tile masonry of the San Francisco City Hall in order to determine the bed-joint shear strength. To assess the effectiveness of FRP retrofit on bed-joint shear capacity, similar parts of the wall were retrofit with 18oz/yd² FRP on both sides. The FRP contained equal fibers in both the vertical and horizontal directions. Results of shove tests on the retrofit walls showed nearly a 350% increase in shear capacity. In addition, the governing failure mode was crushing of the clay tiles.

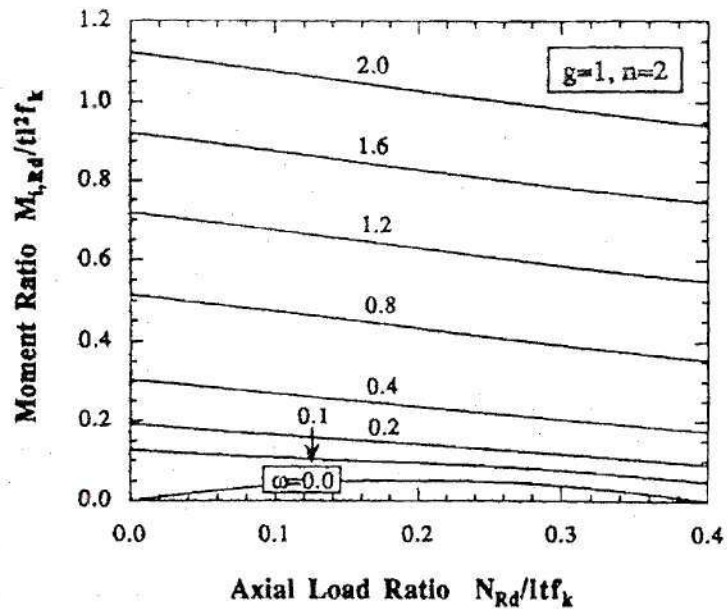


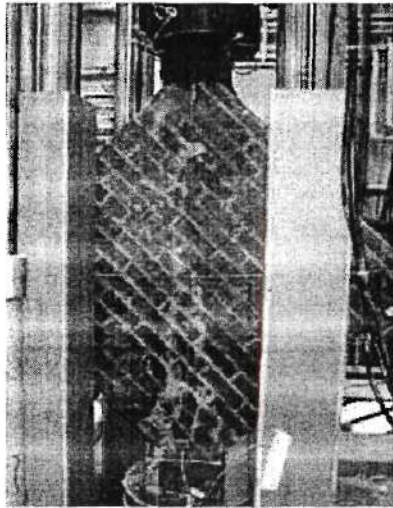
Figure 2.30. In-plane moment capacity versus axial load for various normalized FRP area fractions. (taken from Triantafillou, 1998)

From the figure it is apparent that the in-plane moment capacity is almost directly dependent on the normalized FRP area fraction. That is, if the amount of FRP is doubled, the moment capacity is doubled as well. In addition, an approximate method for determining the peeling strength was presented. For the determination of in-plane shear strength the truss analogy is employed. It should be noted that only the fibers parallel to the bed-joint are considered (i.e the vertical fibers are assumed to provide no dowel action). In order to validate the expressions presented for the calculation of in-plane moment capacity and to investigate the strengthening effect of FRP overlays, six walls were tested in-plane. Fig. 2.31 shows a schematic of the test setup and the test specimens.

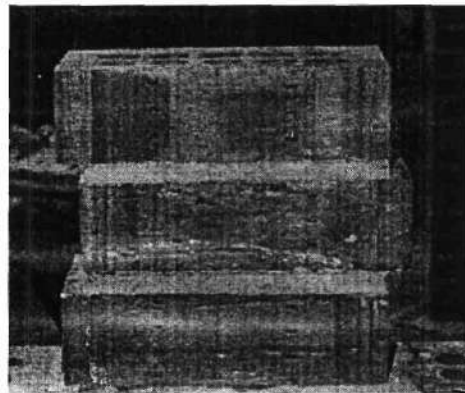
altered. In an unreinforced state, the walls displayed brittle behavior with sharp drops in load carrying capacity after the ultimate strength was reached. In contrast, the walls strengthened with FRP displayed a pseudo-ductile response in that no sharp drops of load carrying capacity were observed. Although this test is standardized, the authors concluded that it does not accurately represent the forces or behavior of URM piers. As a result, an experimental program subjecting retrofitted URM walls to racking loads is currently underway. The three-brick shear specimens displayed up to a 1000% increase in strength over the control specimens. It was noted that the increase in strength was directly proportional to the strength and size of the fabric used. The results of this research suggested that all FRP systems were effective; however, no conclusions on the relative effectiveness of the systems were made.

Triantafillou (1998) presents an analysis method for determining the in-plane flexural and shear strength of URM walls retrofitted with FRP overlays. For the determination of in-plane moment capacity, the equivalent stress block analogy is used. Fig. 2.30 illustrates the relation between in-plane moment capacity and axial load for various normalized FRP area fractions (see Eqn. 2.11).

Marshall et al (2000) studied the effects of four types of composite overlay systems on in-plane behavior of URM walls. All of the systems investigated were composed of fibers oriented in the $0^{\circ}/90^{\circ}$ directions and were classified as: glass/epoxy, carbon/epoxy, glass/vinyl ester, and an adhesively bonded glass epoxy grid. The experimental program consisted of two parts: 1) diagonal compression tests conducted on 40 4 ft by 4ft walls according to ASTM 519-81 and 2) shear tests conducted on 51 non-standard three brick assemblages (see Fig. 2.29). Half of the walls tested were constructed of single wythe CMU and half were constructed of double wythe clay bricks, while all of the three brick shear specimens were composed of clay brick. Specimens were tested after retrofit with each of the four composite systems as well as in an unreinforced state. Results of the wall tests showed that the addition of FRP overlays did not increase the strength significantly; however, the behavior of the walls was drastically



a) Diagonal compression wall test



b) Three-brick shear test specimen

Figure 2.29. Photographs of test setup used to assess in-plane behavior of URM walls retrofit with FRP overlays (taken from Marshall et al, 2000)

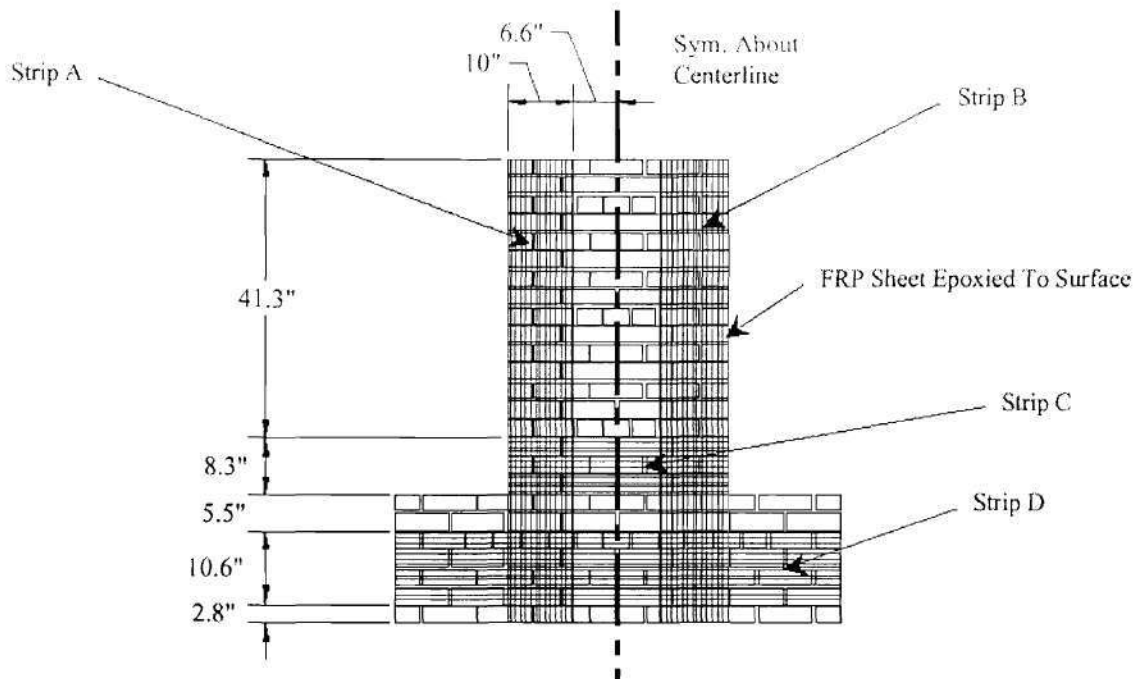


Figure 2.28. Schematic of in-plane test specimen showing the location of FRP reinforcement.(taken from Franklin et al, 2001)

Experimental results showed that the FRP retrofitted pier displayed over twice the strength of the control specimen. However, a decrease in displacement capacity compared with the control specimen was observed (note: the governing failure mode of the control specimen was rocking). It should be mentioned that while the displacement capacity did decrease, a large ultimate drift of 1.9% was reported. The failure mode consisted of gradual debonding of the composite at low displacement levels followed by diagonal cracking through the center of the pier. Finally, the test was concluded when a vertical FRP strip completely delaminated causing a sharp drop in load carrying capacity. Based on the loss of ductility, the authors suggest that this type of retrofit should be avoided if the pier is expected to exhibit ductile type behavior (i.e. rocking or bed-joint sliding).

two stronger composites. No delamination of the GFRP strips was observed. Retrofit beams displayed strengths up to 20 times greater than the expected strength of a corresponding URM beam and deflections up to 1/48 of the span (approx 2%).

Laursen et al. (1995) tested two unreinforced concrete masonry walls out-of-plane retrofit with carbon overlays. The specimens measured 6ft by 6ft and were composed of one with of standard 8in concrete block. The walls were loaded out-of-plane by a single actuator attached to a spreader beam design to apply constant displacement across the width of the wall. The walls were subject to increasing cyclic displacements until failure. The response of both walls can be described as non-linear elastic. The walls displayed flexural cracks spread throughout their height and eventually failed due to a rupture of the composite directly adjacent to bed-joint crack. A maximum drift of 3% was recorded.

2.2.2.2 In-Plane Behavior

Franklin et al. (2001) tested six URM piers in-plane to investigated the effectiveness of several retrofit techniques, including: FRP overlays, shotcrete, ferrocement, and reinforced cores. For brevity only the finding associated with the FRP overlay system will be discussed here. To investigate this retrofit a unidirectional 27oz/yd² glass/epoxy system was used. This system was evaluated on a slender 49.6 in tall URM pier with an aspect ratio (H/L) of 1.77. The pier was subjected to a constant vertical stress of 42 psi and tested as a cantilever (i.e. rotation at the top of the pier was not restrained). In order to obtain hysteretic response, the pier was subjected to increasing cyclic displacements until failure. The test specimen and location of the FRP strips is shown in Fig. 2.28.

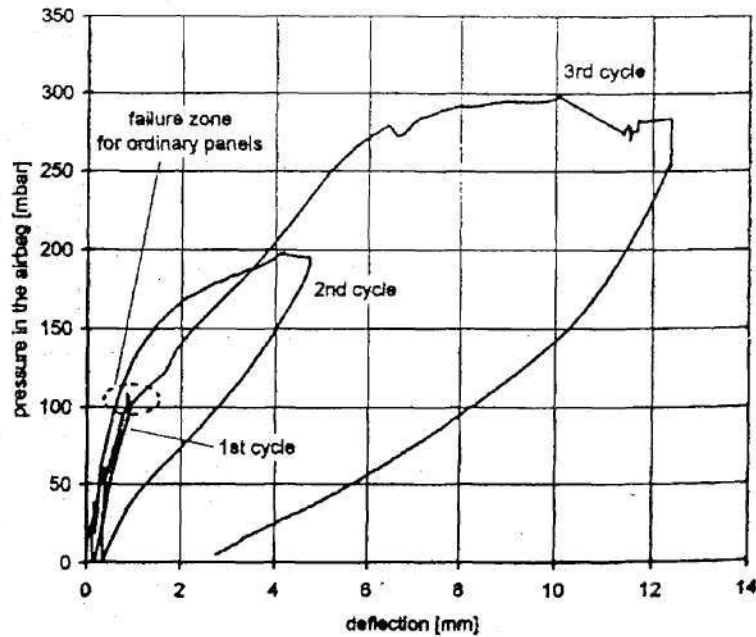


Figure 2.27. Force-displacement response (taken from Kolsch, 1998)

The wall was loaded through a pressurized airbag in order to approximate the distributed inertial forces induced by seismic vibrations. It is noted that the specimen displayed approximately 3 times the strength of a URM wall, and the governing failure mode was an interlaminar shear failure of the composite as well as debonding. Furthermore, the specimen displayed a drift capacity of 0.5%, over ten times that of a typical URM wall.

Ehsani and Saadatmanesh (1995) and Ehsani (1995) studied the out-of-plane flexural response of URM walls retrofitted with FRP overlays by testing small masonry beams. Six beams consisting of 19 solid bricks were tested in four point bending. The beams were 4in deep, 8in wide, spanned 47in, and were loaded statically by two point loads separated by 5in. Three types of GFRP displaying tension strengths of 270lb/in, 855lb/in, and 1422lb/in were investigated. The common failure modes were tensile failure of the GFRP for the weaker composite and compression failure of masonry for the

Kolsch (1998) developed a carbon fiber cement matrix (CFCM) system for the out-of-plane strengthening of brick masonry walls. The strengthening system consists of a unidirectional carbon fabric with a polymer-modified cement matrix to form the reinforcing overlays. Advantages over typical strengthening systems that employ epoxy or polyester resins include compatibility to masonry in terms of bond, moisture permeability, and thermal coefficient. A series of preliminary tests were conducted on unreinforced concrete beams and showed that the CFCM system provided similar strengthening characteristics as glass/cement and glass/epoxy systems. Results of one full scale test on a 10ft by 10ft URM wall strengthened with the CFCM system was reported. Fig 2.26 and 2.27 show a schematic of the test setup and the experimentally measured load-displacement curve, respectively.

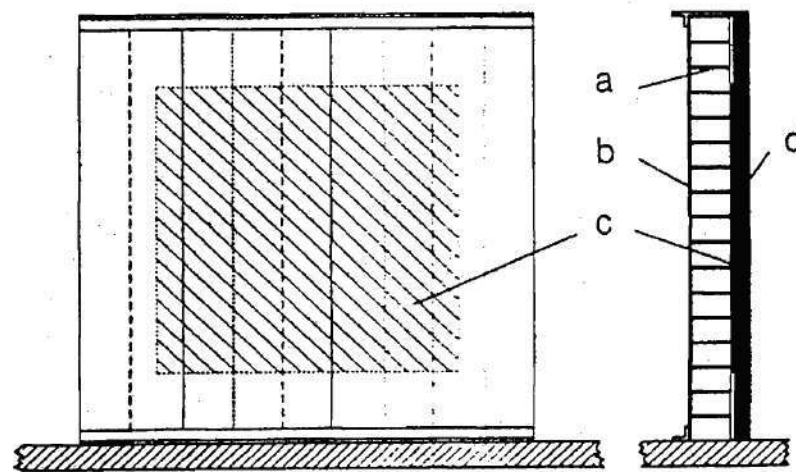


Figure 2.26. Schematic of test setup (taken from Kolsch, 1998); (a) masonry wall; (b) overlay; (c) pressurized airbag; (d) reaction wall

of zero only results in a 0.025 increase in normalized moment capacity. In addition, as the axial force increases the compression strength of masonry begins to govern the capacity, and the moment capacity actually decreases with increasing amounts of FRP.

To validate the analysis method presented and to investigate the effectiveness of FRP overlays to strengthen URM walls out-of-plane, six 5in by 16in by 36 single wythe URM walls were tested (Triantafillou, 1998). Fig. 2.25 shows a schematic of the test setup complete with dimensions.

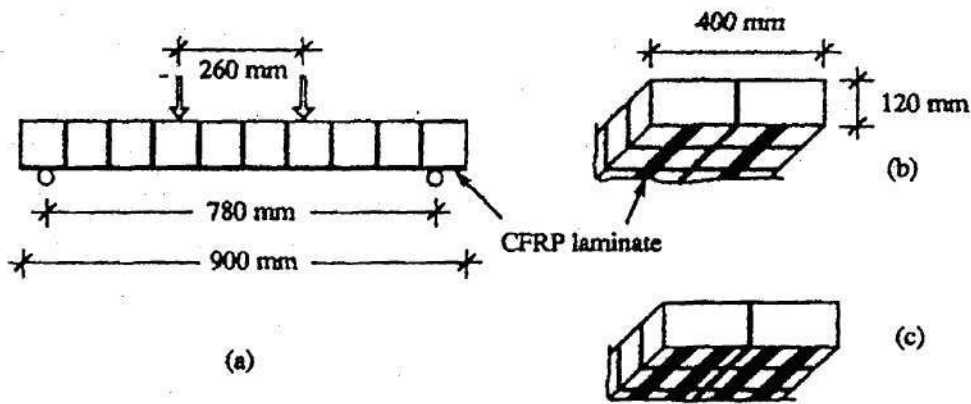


Figure 2.25. Schematic of test setup (taken from Triantafillou, 1998)

Two types of reinforcing was investigated, the use of two CFRP strips (2 specimens) and the use of four CFRP strips (2 specimens) with the remaining two walls tested as control specimens. The failure mode of all of the strengthened walls was tension failure of the composite. The strengthened walls displayed capacities nearly ten times greater than the control specimens. The analysis outlined predicted the experimental results very well with a maximum error of 15%.

beams. The strength equations are formulated with respect to the normalized FRP area fraction (ω) defined as:

$$\omega = \frac{\varepsilon_{M,u} E_{frp}}{f_k} \rho_v \quad (2.11)$$

where, $\varepsilon_{M,u}$ = the ultimate strain of masonry, E_{frp} =the elastic modulus of the FRP, f_k =compressive strength of masonry, and ρ_v = vertical FRP are fraction. Fig. 2.24 shows a plot of moment capacity versus axial load for various normalized FRP area fractions.

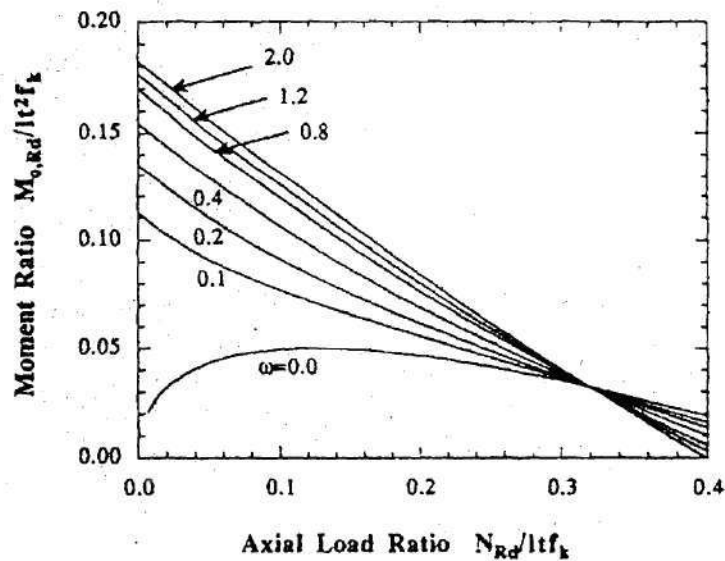


Figure 2.24. Moment Capacity versus Axial load for various normalized FRP area fractions (taken from Triantafillou, 1998).

From the figure it is apparent that for low levels of axial load large increases in moment capacity can be obtained by very small amounts of reinforcement. As the amount of reinforcement increases, the effectiveness of the reinforcement diminishes. That is, an increase from $\omega=0$ to $\omega=0.1$ with an axial load of zero causes a 0.9 increase in normalized moment capacity, while an increase from $\omega=0.1$ to $\omega=0.2$ with an axial load

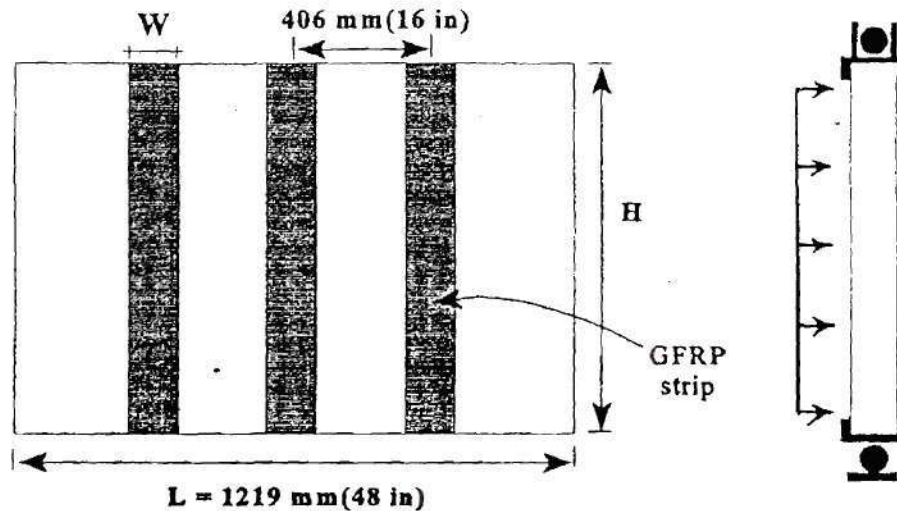


Figure 2.23. Schematic of test setup (taken from Dimas et al., 2000a)

The most commonly observed failure modes were horizontal cracking of the bed joint followed by delamination of the GFRP strips. Tension failure of the composite was observed for the specimens that employed the cross-ply GFRP strips due to the decrease in shear transfer stresses caused by the increase in strip width required to obtain the desired reinforcement ratio. The wall retrofit with three times the balanced reinforcement ratio failed due to the brittle shear failure of the brick (Dimas et al., 2000a). It was recommended that the reinforcement ratio be limited to twice the balanced condition in order to avoid such a failure. Maximum drift seemed to be related to wall geometry and independent of the reinforcement ratio with the short walls failing at a drift of 2% and the slender walls failing at a drift of 4%. Ultimate capacity was shown to be nearly directly dependent on the amount of reinforcement. Capacities ranged from 5 to 30 times the weight of the wall and up to 7.5 times greater than a URM wall.

An analysis method for determining the out-of-plane moment capacity of URM walls strengthened with FRP strips was presented by Triantafillou (1998). The method is based on the equivalent stress block analogy used for the design of reinforced-concrete

of the CMUs were calculated. These calculated strengths ranged from 73 psi to over 145 psi and greatly exceeded the suggested design value of 37 psi. The authors point to dowel action provided by the reinforcement as a possible reason for the apparent over strength. Both the unidirectional and bi-directional retrofits proved to be very effective in increasing strength displaying over 20 times the strength of the control specimens.

Dimas et al. (2000a), Dimas et al. (2000b), and Ehsani et al. (1999) conducted cyclic out-of-plane load tests on seven half-scale URM walls retrofit with E-glass fiber reinforced polymer (GFRP) strips. Two wall geometries were investigated; short walls, with a height of 28in and a width of 48in, and slender walls, with a height of 56in and a width of 48in. The walls were strengthened with vertical GFRP strips, comprised of either a unidirectional or cross-ply lay-up, and corresponded to reinforcement ratios ranging from 20% to 300% of the balanced reinforcement ratio. It should be noted that all specimens were tested without any vertical stress applied. The specimens were simply supported at the top and bottom along the width of the walls and subjected to cyclic loading through an airbag (see Fig. 2.23).

over predicted the strengths observed during testing by up to 30%. One possible reason for this is that equations developed for reinforced concrete strength only consider the tension failure/yielding of the reinforcing and do not address other failure modes such as bond failure that were observed.

Hamoush et al. (2000) loaded fifteen concrete masonry walls with an airbag out-of-plane in order to assess the effectiveness of two types of FRP retrofit systems: a bi-directional glass fabric and unidirectional glass strips in both directions. The specimens measured 6 ft tall, 4 ft wide, and 8 in thick. Fig. 2.22 shows a schematic of the test setup.

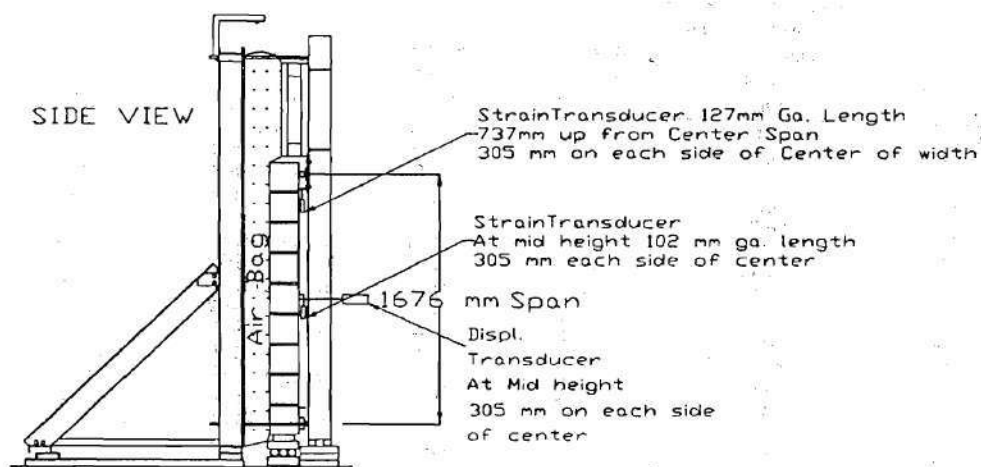


Figure 2.22 Schematic of test setup (take from Hamoush et al., 2000)

Six of the specimens were retrofit with each type of FRP while three walls were tested without reinforcement as control specimens. All of the walls strengthened with GFRP failed by diagonal cracking through the CMU. The crack initiated in the unit and then propagated to the interface between the GFRP and the masonry and eventually continued to the end of the composite strip. It should be noted that no special anchorage was provided at the end of the reinforcement. Based on simple mechanics (i.e. $\tau = VQ/Ib$) and the assumption that the reinforcing did not supply any shear strength, the shear capacities

GFRP retrofitted wall exhibited frequencies much higher than the as built wall; however, as the wall damaged the frequencies became very similar. All walls displayed approximately 5% critical damping throughout testing. The GFRP retrofitted wall experience approximately a 50% larger peak acceleration at collapse over the as built wall. Analysis results for the GFRP retrofitted wall based on a reinforced-concrete stress block analogy were in fairly good agreement (i.e. 10%) with test results.

Hamilton and Dolan (2001) loaded six unreinforced concrete masonry walls strengthened with unidirectional GFRP strips with an airbag to obtain out-of-plane strength. Four of the walls were 6 ft tall by 4 ft wide and two were 15 ft 4 in tall by 4 ft wide, all walls were composed of a single wythe of lightweight or normal weight CMU. The walls were all under-reinforced in order to cause failure of the GFRP to govern the strength. The authors argued that since the strength of the retrofitting material is, in general, more accurately known, a better estimate of strength could be obtained if the FRP reinforcement is designed to govern the strength. To that end, an equation analogous to the expression used in reinforced concrete design was proposed for the determination of the balanced condition. Capacities of the walls ranged from 313 psf to 495 psf for the short walls and 100 psf and 124 psf for the tall walls. Observed failure modes included fracture of the GFRP, delamination of the GFRP, and combinations of both. Strain data suggests the presence of high-localized strains in the GFRP strips in the vicinity of the bed-joints, which is consistent with the visual observation of cracking in the bed-joints. Furthermore, the authors investigated the potential for the equivalent stress-block analogy, developed for reinforced-concrete design, to predict the ultimate capacity of a concrete masonry wall strengthened with FRP. In general, this analysis

techniques have been shown to be effective in improving the behavior of URM walls, they are typically labor intensive and create a great deal of disturbance to the occupants of the structure during retrofit.

2.2.2 FRP Overlays

One of the most promising new methods that has been developed for the strengthening of URM walls involves the use of fiber reinforced polymers (FRP). This technique requires FRP overlays to be bonded to one or both sides of a URM wall and is typically unobtrusive to the building occupants, requires very little surface preparation, and as a result is very economical. The following sections outline recent research conducted on FRP strengthened URM walls for both in-plane and out-of-plane loading as well as several actual applications.

2.2.2.1 Out-of-Plane Behavior

Paquette et al. (2001) report the results of dynamic out-of-plane tests conducted on three URM specimens that were extracted from a building scheduled for demolition in Montreal, Canada. *The building was constructed of URM walls with timber backing composed of 3 in by 10 in rough-cut planks support by posts spaced at 12 ft intervals. The specimens measured 60 in by 48 in by 3.75 in and were removed and tested with the timber backing intact. The walls were tested in various states: the first was tested in the as built condition, the second was tested with through wall ties connecting the timber backing to the masonry, and the third was tested with three strips of Tyfo GFRP bonded to one side. The specimens were supported at the top and bottom and subjected to ground accelerations with increasing magnitudes until failure occurred. Initially, the*

- As a stiff structure, URM structure exhibits small amplification of the earthquake excitation.
- If the out-of-plane failure is prevented, the dominant failure mode of a URM structure is the in-plane failure of the first-story URM walls.

(see Section 2.1.5). Therefore, the wood diaphragm can be assumed elastic in the analysis of the entire building. The elastic stiffness of the flexible diaphragm is important to the behavior of the entire building, and this aspect has not been fully investigated in past research. The formula given by FEMA 273 (ATC 1997) is too coarse to model the realistic elastic stiffness of the diaphragm. More experimental research and analytical research should be done on the elastic stiffness of wood diaphragms with different dimensions and different construction details.

Experimental research and theoretical research of entire URM buildings can provide insight into the interaction between each structural component and how the components work together as an integer structure. This information cannot be obtained from tests of individual components. Several dynamic tests have been conducted on reduced-scale URM building specimens. Full-scale static test is another useful but expensive method to investigate the overall behavior of a URM structure.

Past research on the URM structure revealed the following special characteristics of this type of structure (see Section 2.1.6):

- The overall behavior of a URM structure with flexible diaphragms is determined by the interaction between the in-plane walls, the out-of-plane walls, and the flexible diaphragms.
- The majority of the mass of the structure comes from the masonry walls, not from the floor/roof diaphragm.
- The stiffness of the masonry in-plane wall is much higher than that of the out-of-plane wall and that of the diaphragm. The entire structure is a very stiff assembly.

can also develop in the spandrel, and thus more research is needed on the behavior of URM spandrels.

The out-of-plane behavior of URM wall has been widely investigated not only through experimental research but also by theoretical analysis (see Section 2.1.4). Dynamic stability concepts provide a good explanation for the out-of-plane behavior of URM walls. Fracture line and yield theories have been used by some researchers to calculate the strength of URM out-of-plane walls. However, this method may not give accurate results, since there is no actual plastic moment in the crack line. Alternative analysis methods, such as the nonlinear FE method employing special interface elements which consider the friction mechanism in the interface, should be used to calculate the strength of out-of-plane walls. Insofar as experimental work on the out-of-plane URM walls is concerned, many tests have been conducted to investigate on the failure modes, ultimate strength, and elastic stiffness of the URM out-of-plane wall. However, most of the specimens did not include the in-plane walls adjacent with the out-of-plane walls, which would influence the stiffness and crack patterns of a URM out-of-plane wall. Tests of a full-scale out-of-plane URM wall including also the in-plane walls can provide insight into this problem.

No research has been done on the interaction between the in-plane behavior and the out-of-plane behavior of the URM walls. A simple assumption of uncoupled behavior appears to be a good choice for current research, if the diaphragms are flexible.

Recent research on flexible wood diaphragms show that the deformation capacity and the strength of this type of diaphragm are rather high, although the failure of the anchors connecting the diaphragm with the wall and the failure of the nails are possible

In this section begins by outlining the concept of modeling URM in-plane perforated walls with contact elements. The method is then used to analyze the full-scale URM structure tested at the Univ. of Pavia (Magenes et al , 1995) in order to assess the accuracy of the method. Finally, the results obtained for each of the walls in the ST-11 test structure are presented.

4.2.4.1 Modeling of URM Walls with Contact Elements

As discussed previously, a perforated masonry wall is composed of two types of members, piers and spandrels. In order to develop a method for the analysis of such a system, the loading and possible failure modes of each type of member must be fully understood. The failure modes of masonry piers subjected to horizontal shear forces, vertical axial forces, and moments are well documented. Based on numerous past experiments the following four possible failure modes have been identified: rocking, sliding, toe crushing or diagonal tension. These failure modes were discussed in detail in Section 4.2.3.1. It is important to note that these failure modes are not mutually exclusive, that is, the failure of in-plane masonry piers is often a combination of these modes.

In contrast, the possible failures modes of masonry spandrels have not been well established. The external forces that spandrels in perforated walls are subjected to are different from those of a pier. The flexural moments and shear forces applied to spandrels are perpendicular to the head joints instead of the bed joints (see Fig. 4.28). Moreover, the normal forces applied on the head joints of a spandrel are relatively small compared with the normal forces applied on the bed joints of a pier (i.e. gravity stress). This distinction between the direction of forces in a pier and spandrel is paramount, since

From Table 4.23 it is apparent that rocking dominates initial pier behavior and then degrades into sliding for several piers. These failure modes seem reasonable considering the low vertical stress (i.e. no addition weight was added to the structure) and the aspect ratios of the majority of the piers. In order to assess if the strength estimates provided were realistic, the capacity of the building was approximated by calculating the frictional resistance of the walls (ie. $0.6 \times \text{weight}$). Table 4.24 gives a comparison of pushover results with this simple approximation. Based on the relatively close results, considering the simplified nature of the approximation, it is concluded that the pushover analysis results are reasonable estimates.

Table 4.24. Comparison of pushover analysis with approximation of strength.

	Capacity (pushover) (left to right)	Capacity (pushover) (right to left)	Approximate Capacity
Wall AB	29.6kip	23.8kip	33.4kip
Wall 1	20.2kip	27.0kip	25.62kip
Wall 2	11.4kip	-	19.9kip

4.2.4 Nonlinear In-Plane Finite Element Model

In addition to the simplified pushover analysis, a nonlinear FE analysis, utilizing contact elements, was conducted to assess the in-plane behavior of the walls of the ST-11 test structure. This analysis was employed in order to gain further insight into the ultimate strength, displacement capacity, and failure modes of individual piers in the ST-11 test structure.

Table 4.23. Pier failure modes of the ST-11 test structure.

Pier	Failure Mode (left to right)	Failure Mode (right to left)
AB-2	Rocking	Rocking
AB-3	Rocking	Rocking
AB-4	Rocking	Rocking
AB-5	Rocking	Rocking
AB-7	Rocking => Sliding	Rocking => Sliding
AB-8	Rocking => Sliding	Rocking => Sliding
AB-9	Rocking => Sliding	Rocking => Sliding
AB-10	Rocking	Rocking
1-2	Rocking	Rocking
1-3	Rocking	Rocking
1-4	Rocking	Rocking
1-6	Rocking	Rocking
1-7	Rocking => Sliding	Rocking => Sliding
2-2	Rocking => Sliding	-
2-3	Rocking	-
2-4	Rocking	-
2-5	Rocking => Sliding	-
2-7	Rocking	-
2-8	Rocking => Sliding	-
2-9	Rocking => Sliding	-

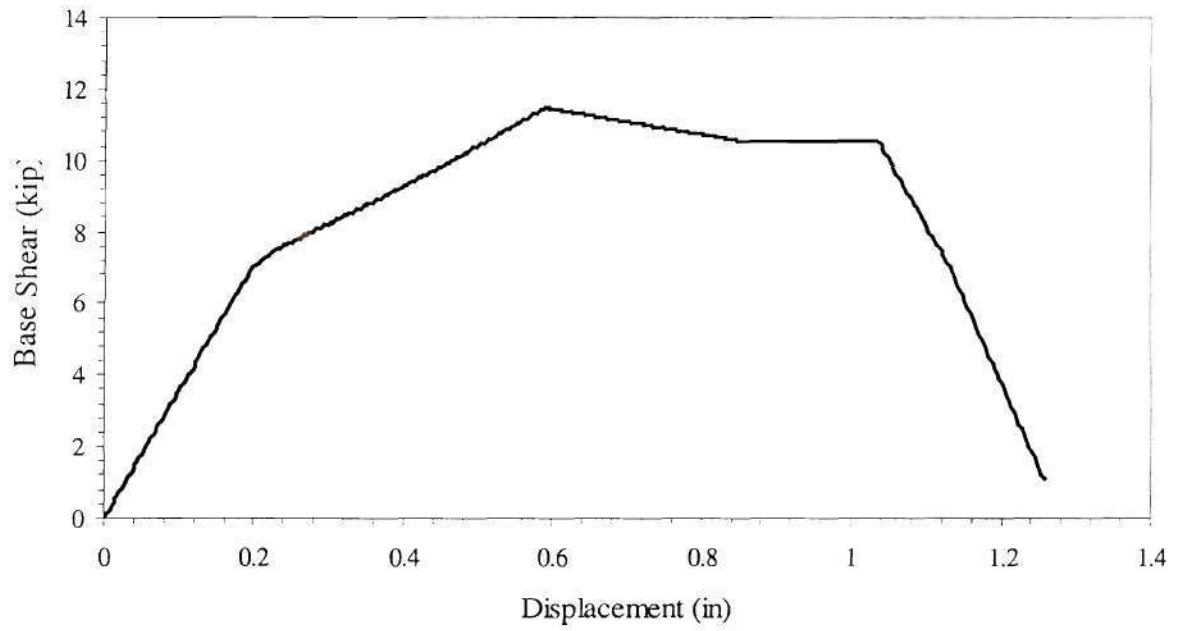


Figure 4.27. Force-displacement curve obtained from pushover analysis of Wall 2.

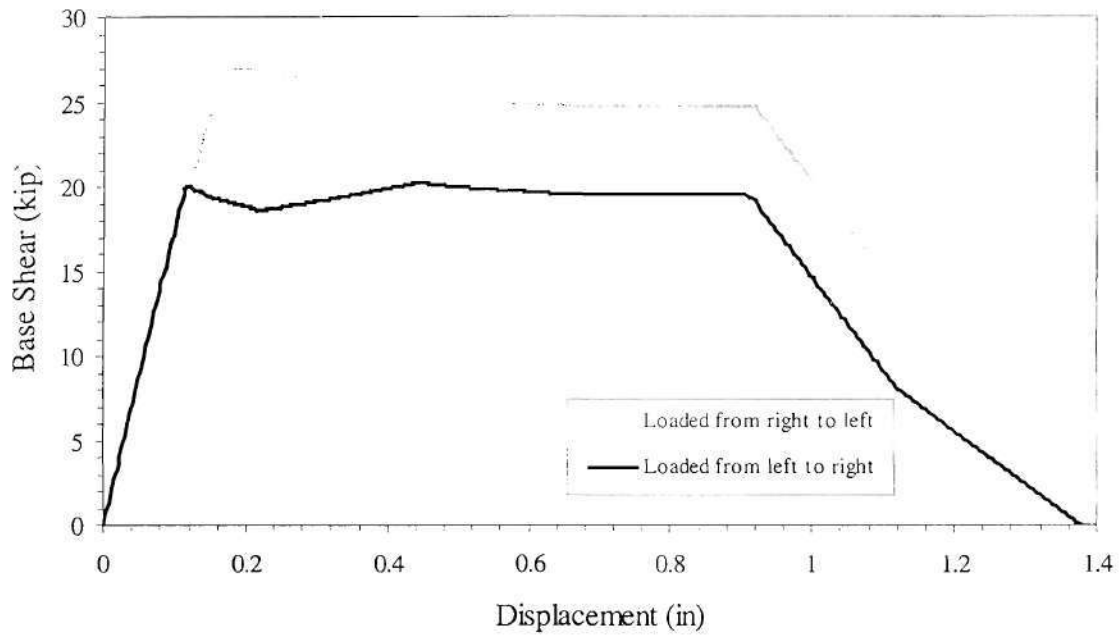


Figure 4.25. Force-displacement curve obtained from pushover analysis of Wall AB.

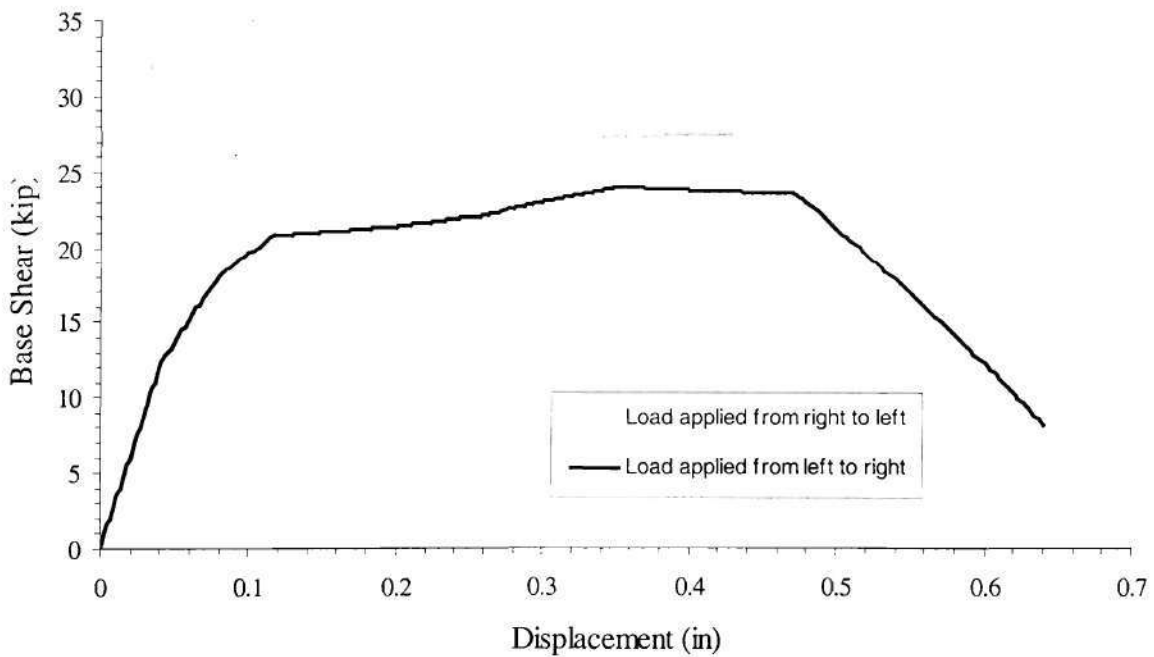


Figure 4.26. Force-displacement curve obtained from pushover analysis of Wall 1.

Table 4.22. Material properties used for the analysis of the ST-11 test structure.

Material Property	Value
Compression strength, f'_m	1800psi
Bed-joint shear strength, v_{te}	60psi
Elastic modulus of masonry, E_m	435ksi
Tension strength of masonry, f_{dt}	30psi

The initial vertical stress in each pier due to weight of masonry was obtained through an elastic FE analysis. The analysis was carried out by imposing a constant ratio of lateral displacements between the second floor and roof levels. This type of pushover was chosen because it is expected that the test structure will be loaded in this manner. In order to approximate the first mode of a damaged structure, 90% of the total roof displacement was imposed on the first story. Fig. 4.25 through 4.27 give the force-displacement curves obtained for each of the walls in the ST-11 test structure. For Walls 1 and AB, the direction of loading refers to the figures of the structure given in the chapter 3. Furthermore, the predicted failure modes determined from each analysis is presented in Table 4.23.

The results of the pushover analysis of Wall D are in very good agreement with the experimental test results. From Table 4.20 it is apparent that failure modes of the first floor piers were all correctly predicted. Furthermore, the predicted ultimate strength was within 14% of the experimentally determined strength and the displacement capacity was fairly well approximated. Results of the pushover analysis on Wall B predicted the ultimate strength fairly well (18% error); however, the displacement capacity was underestimated. This is most likely due to two reasons, 1) the failure mode of pier B4-1 was incorrectly determined to be diagonal tension, which is more brittle than the actual failure mode of rocking, 2) following FEMA 273 the force-drift relationship for diagonal tension (outlined in Section 4.2.3.1) is modeled as brittle which is conservative considering the results of some experiments which report moderate levels of ductility. From Fig. 4.23 it is observed that artificially reducing the elastic modulus (based on the results of Wall D) gave a very good approximation of the displacement corresponding to ultimate strength for Wall B (10% error). The results of the pushover analysis conservatively predicted the experimental results within a reasonable limit, considering the inherent variability of masonry.

4.2.3.7 Results of the ST-11 Test Structure

Each of the three walls in the ST-11 test structure was analyzed using the pushover analysis developed. Due to a lack of symmetry, pushover analyses were performed in both directions of Walls 1 and AB. With the exception of the elastic modulus and the tension strength of masonry, the material properties used in the analysis were determined through material tests and are presented in Table 4.22.

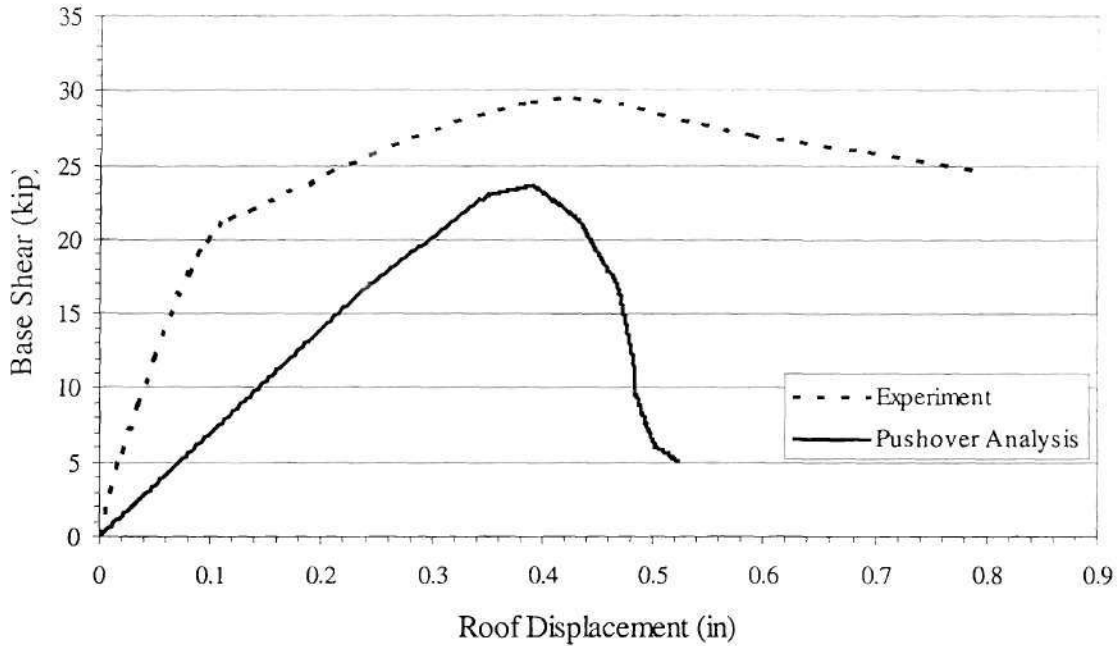


Figure 4.24. Comparison of pushover analysis with Wall B (Magenes et al , 1995)

Table 4.21. Summary of results of Wall B (Magenes et al , 1995)

	Experimental Result	Analytical Result
B1-1 Failure mode	Rocking	Rocking
B1-2 Failure mode	Diagonal cracking	Diagonal cracking
B1-3 Failure mode	Diagonal cracking	Diagonal cracking
B1-4 Failure mode	Rocking	Diagonal cracking
BS1-1	Diagonal cracking	Did not fail
BS1-2	Minor cracking	Did not fail
BS1-3	Diagonal cracking	Did not fail
B2-1 Failure mode	Did not fail	Did not fail
B2-2 Failure mode	Did not fail	Did not fail
B2-3 Failure mode	Did not fail	Did not fail
B2-4 Failure mode	Did not fail	Did not fail
BS2-1	Minor cracking	Did not fail
BS2-2	Minor cracking	Did not fail
BS2-3	Minor cracking	Did not fail
Total base shear	29.2 kip	23.6 kip
Roof displacement at Ult	0.44 in	0.40 in

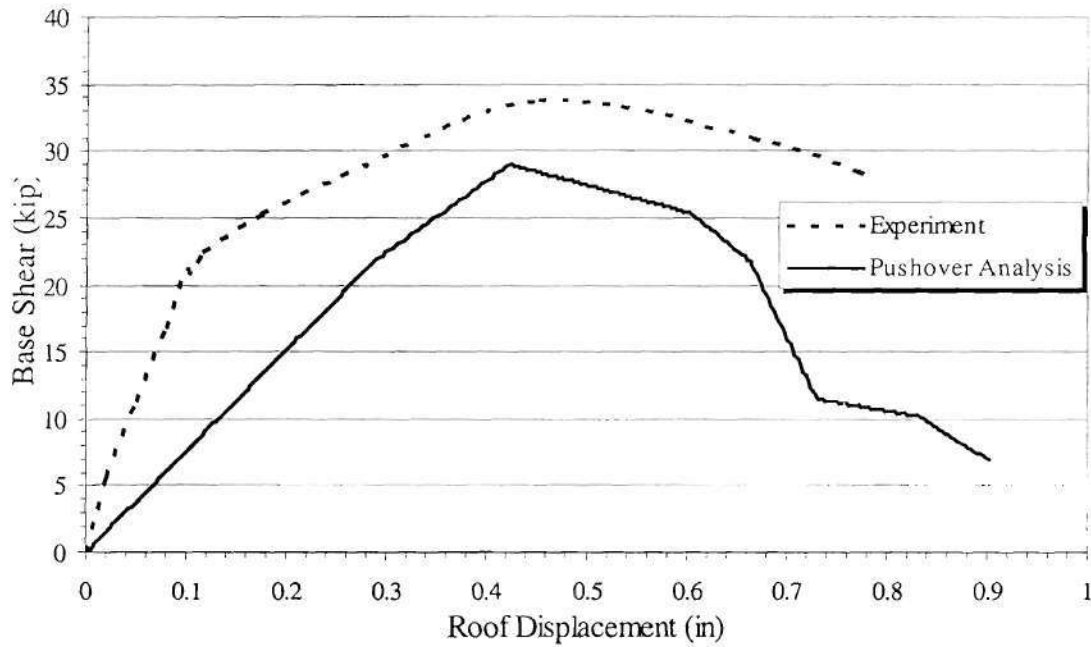


Figure 4.23. Comparison of pushover analysis with Wall D (Magenes et al , 1995)

Table 4.20. Summary of results of Wall D (Magenes et al , 1995)

	Experimental Result	Analytical Result
P1-1 Failure Mode	Rocking	Rocking
P1-2 Failure Mode	Diagonal Cracking	Diagonal Cracking
P1-3 Failure Mode	Diagonal Cracking	Diagonal Cracking
S1-1	Diagonal Cracking	Diagonal Cracking
S1-2	Diagonal Cracking	Diagonal Cracking
P2-1 Failure mode	Rocking	Did Not Fail
P2-2 Failure mode	Did Not Fail	Did Not Fail
P2-3 Failure mode	Rocking	Did Not Fail
S2-1	Minor Cracking	Did Not Fail
S2-2	Minor Cracking	Did Not Fail
Total Base Shear	33.7 kip	29.0 kip
Roof Displacement at Ult	0.48 in	0.415 in

Figure 4.22 shows both the experimentally determined force-displacement curve and the force-displacement curve obtained using the pushover analysis. From the figure it is apparent that while the predicted strength is very accurate (approximately 2% error), the prediction of the displacement capacity is poor. The over estimation of stiffness is most likely due to the fact that the pushover model assumes elastic behavior of the piers until they reach their capacity. In reality, minor damage occurs even at low levels of load, which results in a softening of the structure. This is observed in the continuously changing stiffness of the force-displacement response of the test structure. For simplicity, *this softening of the structure* was modeled by altering the elastic modulus until the peak points of the two curves coincided. The resulting elastic modulus was 12.5% that determined through testing.

The results of the “calibrated” pushover analysis conducted on Wall D as well as the experimental results (Magenes et al , 1995), are given in Fig. 4.23 and Table 4.20. Fig. 4.24 and Table 4.21 give the results of the pushover analysis of Wall B along with the experimental results.

Table 4.19. Comparison of inflection point location

Pier	Elastic finite element analysis, β	Equation X, β
D1-1	0.684	0.67
D1-2	0.722	0.753
D1-3	0.678	0.67
D2-1	0.490	0.535
D2-2	0.547	0.578
D2-3	0.479	0.535

From the table it is apparent that the results obtained from Eqn 4.13 are very similar to those provided by the elastic finite element analysis. Furthermore, the relative values are very close suggesting that both methods follow similar trends.

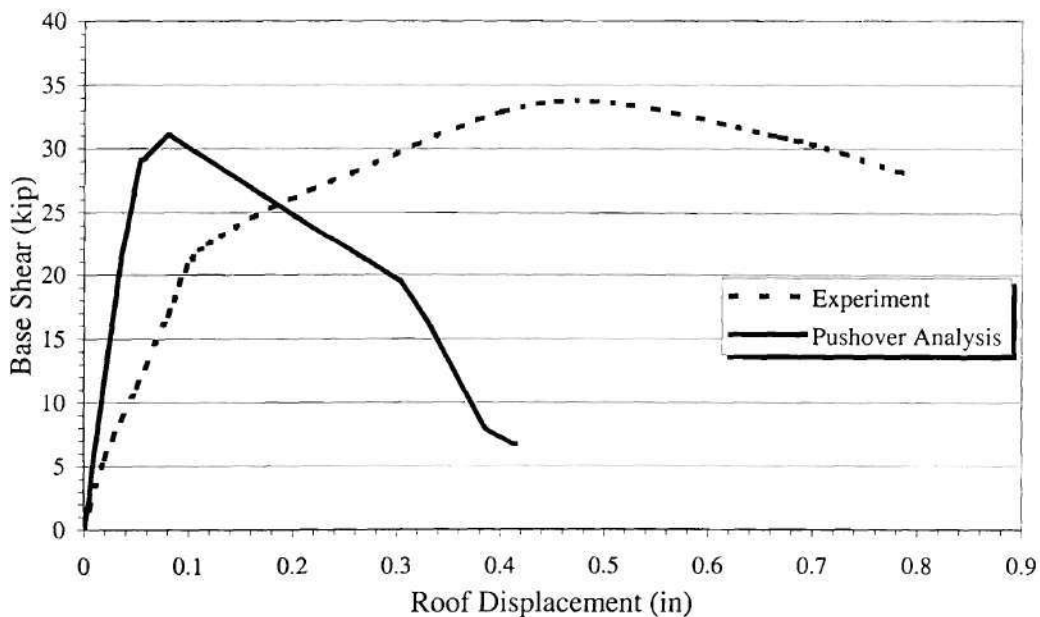


Figure 4.22. Comparison between analytical and experimental force-displacement curves

Table 4.18. Material properties used for the analysis of Walls D and B
(Magenes et al , 1995)

Material Property	Value
Compression strength, f'_m	1200psi
Bed-joint shear strength, v_{te}	30psi
Elastic modulus of masonry, E_m	435ksi
Tension strength of masonry, f_{dt}	15psi

With the exception of the tensile strength of masonry, all of the properties were determined through testing (Magenes et al , 1995). The selected masonry tension strength of 15psi is reasonable considering the relatively weak sand-lime mortar used for the construction.

In order to assess the capability of Eqn 4.13 to determine the location of the inflection point, an elastic finite element model of Wall D was developed. The model was subjected to equal forces at the roof and second floor levels to determine the locations of the inflection points. Using Eqn 4.13 and the method outlined in Section 4.2.3.2 the inflection points were also calculated. Table 4.19 shows the results of both analyses.

4.2.3.6 Comparisons with Past Experiments

In order to assess the accuracy of the pushover analysis developed, the full scale URM building tested at the University of Pavia in 1995 (Calvi, 1992, Magenes et al, 1995) was chosen as the benchmark. Fig. 4.21 shows an elevation of the two perforated URM walls tested. The structure was tested by applying equal forces at the second floor and roof levels. Since the structure was subjected to force reversals, an envelope of the force-displacement behavior of all of the cycles was taken for comparison with the results of the pushover analysis. The material properties used in the analysis are shown in Table 4.18.

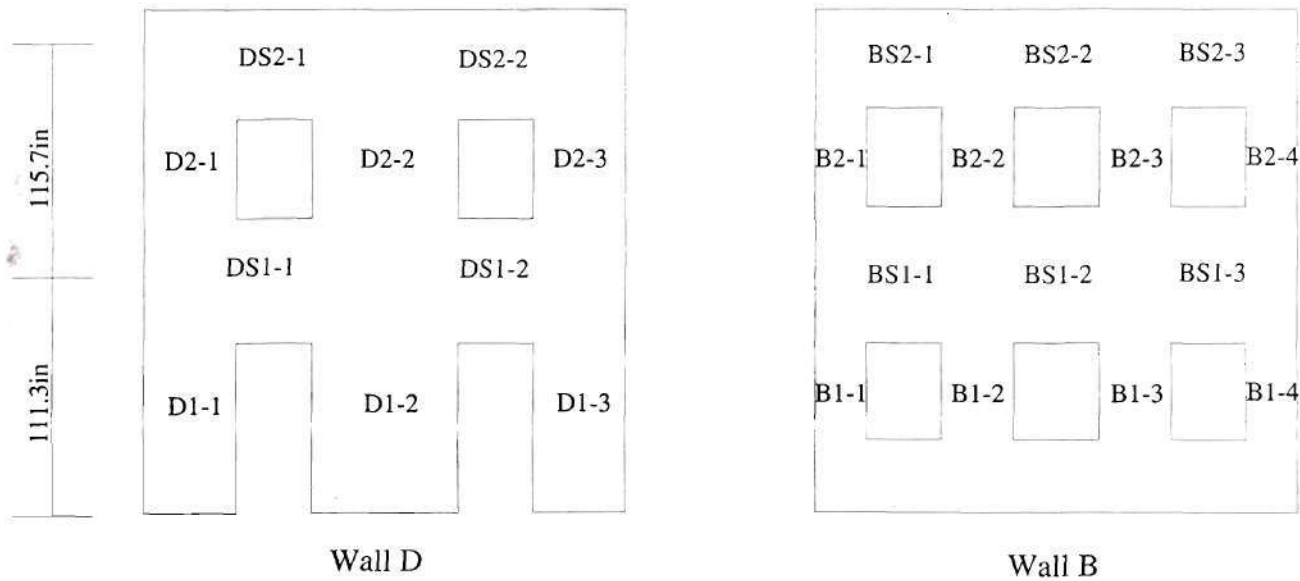


Figure 4.21. Elevation view of Wall D and Wall B (Magenes et al, 1995)

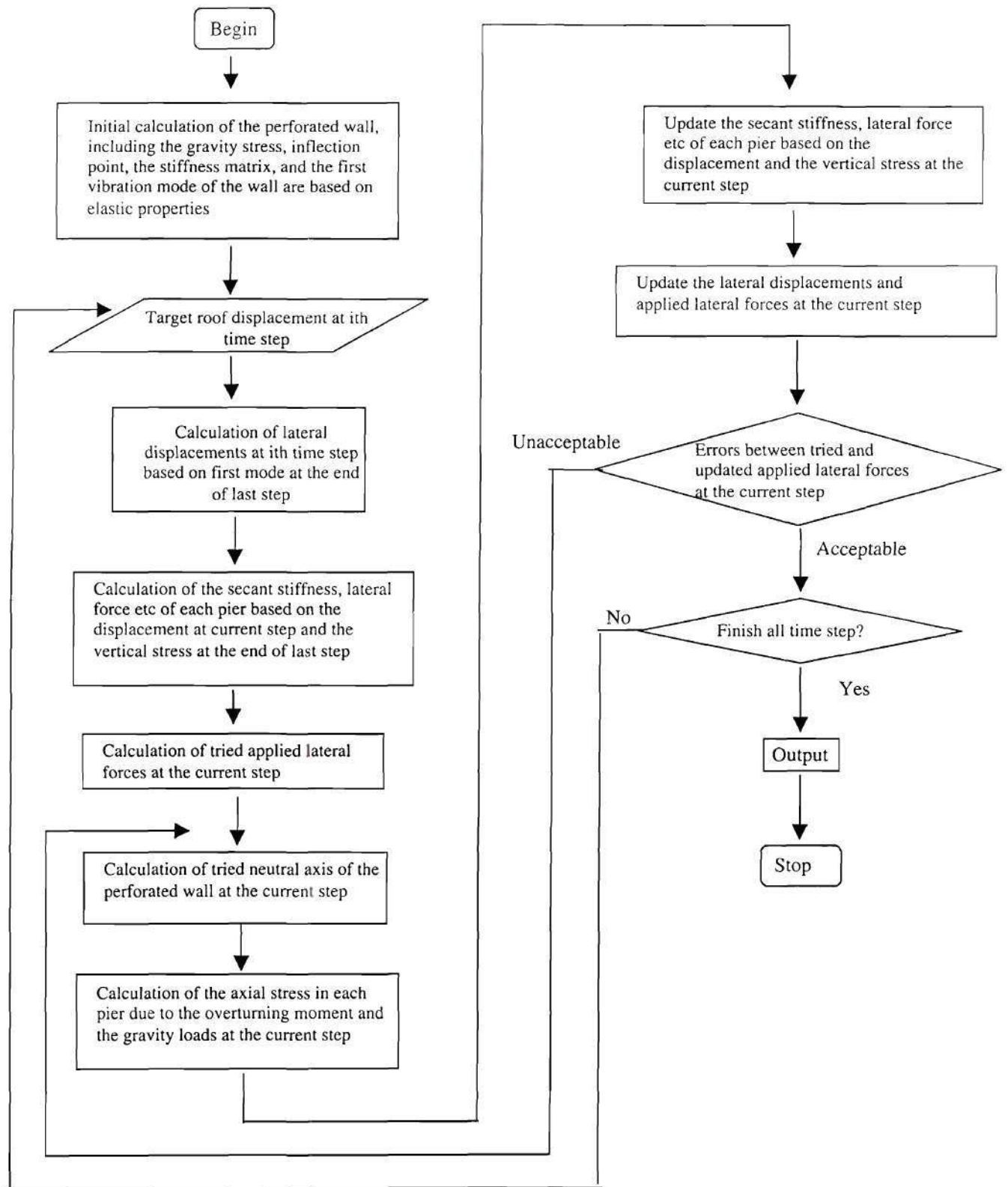


Figure 4.20. Flow chart of program code

4.2.3.5 Coding

Based on the structure model, in-plane URM lateral force-drift relations, and the applied lateral displacement patterns discussed above, a Matlab program was developed to conduct the nonlinear pushover analysis of URM perforated walls. A flow chart of the program is shown in Fig. 4.20.

At each step, the subsequent applied lateral displacement is calculated based the selected type of pushover (i.e. constant displacement ratio, constant force ratio, or current first mode) and the properties of the wall calculated at the end of the previous step. Then the secant stiffness and corresponding lateral shear force of each pier is calculated based on the nonlinear force-drift relationships defined in Section 4.2.3.1. The applied forces are then obtained by summing up of the shear forces of all the piers in each story. Next, the current neutral axis of the perforated wall is calculated based on beam theory. Based on the applied forces the overturning moment and corresponding vertical stress in each pier is then determined. Since the level of vertical stress in each pier can have substantial effects on the force-drift behavior and consequently the secant stiffness of the pier, this portion of the analysis is iterative. The program is designed to output force–displacement curves for perforated URM walls to provide insight into seismic behavior. In addition, the program is capable of outputting failure sequence, individual pier failure modes, and variation of vertical stress in each pier.

throughout loading due to damage accumulation. This is illustrated by Fig. 4.19, which shows the measured lateral force distribution during a dynamic test of a 1/4-scale URM structure (Paulson 1990).

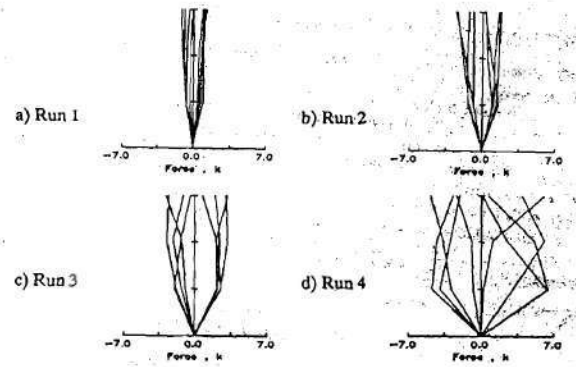


Figure 4.19. Lateral force distributions for all runs in Paulson (1990)'s test

The initial runs show essentially the elastic force distribution of an inverted triangle, which suggests little damage was occurring. However, as the ground accelerations increased more damage occurred and the force distribution became fairly uniform, as seen in the results of Run 3. Finally, at large ground accelerations, after the structure had experienced substantial damage, force distributions became irregular (Paulson 1990). This variation of lateral force distributions was also reported by Costley et al (1996) for the dynamic test of two two-story URM buildings. This shift in lateral force distribution causes changes of shear force distribution as well as overturning moment, which can be important for the analysis of URM buildings.

4.2.3.4 Loading History

Two different types of nonlinear pushover analysis are available: force-control *analysis and displacement-control analysis*. In the first case, the externally applied forces are increased during each analysis step, while in the second case the externally applied displacements are increased. Due to the inability of the force-controlled analysis to provide any results beyond the peak point, the displacement-controlled pushover analysis was chosen in order to gain insight into strength degradation.

The pushover model utilizes three types of displacement-controlled pushover analysis. The first imposes a predetermined ratio of displacement for the first and second story as defined by the user. Typically this type of pushover analysis uses the elastic first mode as the profile of the increasing displacements. Previous research has revealed that for structures with rather low natural periods, such as low-rise URM buildings, the first vibration mode dominates its lateral displacement under seismic excitation.

The second type of displacement-controlled pushover analysis imposes displacements based on the relative story stiffness' in order to maintain a constant force ratio between the floors. FEMA recommends the use of either an inverted triangular lateral load pattern or equal force distributions on all stories, which are indicative of the elastic first mode.

The third and most realistic method imposes displacements based on the current first mode. That is, at each analysis step the stiffness of the floors is updated and the first mode is recalculated. The proceeding displacement is imposed based on the profile of the new first mode. This type of pushover recognizes the fact that, while the response of a URM low-rise building is dominated by the first mode, the mode shape changes

It should be noted that for spandrels not located on the top floor, the vertical stress of the pier above the spandrel must be subtracted from the vertical force in the pier below the spandrel in order to obtain the correct shear force.

Figure 4.18a illustrates the resulting vertical stress distributions obtained. It is important to mention that this distribution is dependent on elastic spandrel properties. However, the damage to the piers is considered by using the secant stiffness to determine k_i and by limiting the maximum net tension of a pier to the tensile strength of masonry. Once this strength is exceeded the pier is assumed to have cracked across its entire length. As a result, the vertical stress in the pier is assumed to be zero and the only resistance offered to overturning moment is the initial gravity stress. Fig. 4.18b illustrates the vertical stress distribution throughout the wall after the tensile strength of a pier has been exceeded.

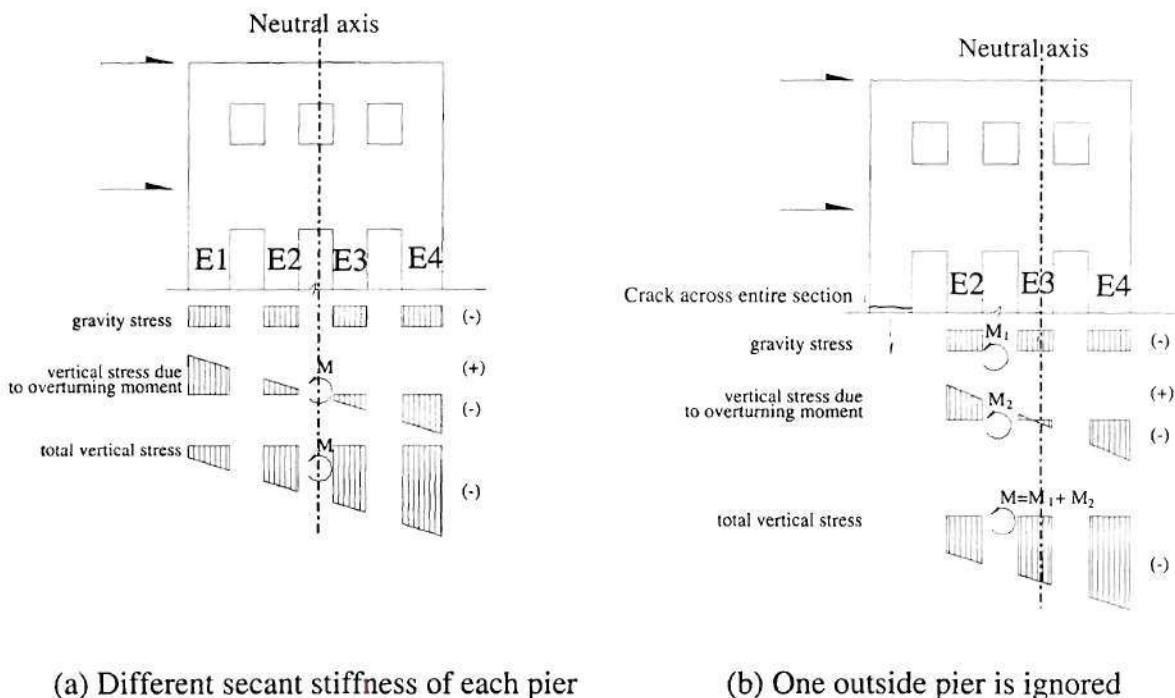


Figure 4.18. Distribution of vertical stress under gravity load and lateral force

The wall is subjected to a lateral force P acting at a distance h above the base. The shear force in each spandrel v_i is assumed to be equal to $k_i P$, where k_i is a factor dependent on the secant stiffness of the pier. Therefore, the portion of the overturning moment that is resisted through the change in vertical stress of the piers can be calculated by subtracting the base moment of each pier from the total overturning moment as:

$$M = \left(1 - \sum_{j=1}^n k_j \beta_j \right) Ph \quad (4.18)$$

where h is the height of the wall and β_j is determined by Eqn 4.13. Following the assumptions of beam theory and assuming a linear-elastic material model for masonry, the curvature at the base of the wall can be calculated as:

$$\phi = M / \sum_{j=1}^n A_j d_j^2 \quad (4.19)$$

where, A_i is the area of the i th pier and d_i is the distance from the centroid of the i th pier to the neutral axis of the wall. The vertical force in the i th pier induced by the overturning moment is then given by:

$$F_i = A_i d_i \phi = \frac{A_i d_i}{\sum_{j=1}^n A_j d_j^2} M \quad (4.20)$$

Considering Eq. (4.18) and (4.20), F_i can be written as:

$$F_i = \frac{A_i d_i}{\sum_{j=1}^n A_j d_j^2} \left(1 - \sum_{j=1}^n k_j \beta_j \right) Ph \quad (4.21)$$

The shear force in each spandrel can then be calculated by:

$$Vs_i = \sum_1^i F_i \quad (4.22)$$

observance of diagonal cracks in the spandrels of URM buildings after earthquakes and during dynamic tests (Calvi, 1995). The details associated with the model's consideration of the effects of overturning moment are presented next.

To illustrate how the pushover model addresses overturning moment consider the idealized wall with n piers shown in Fig. 4.17.

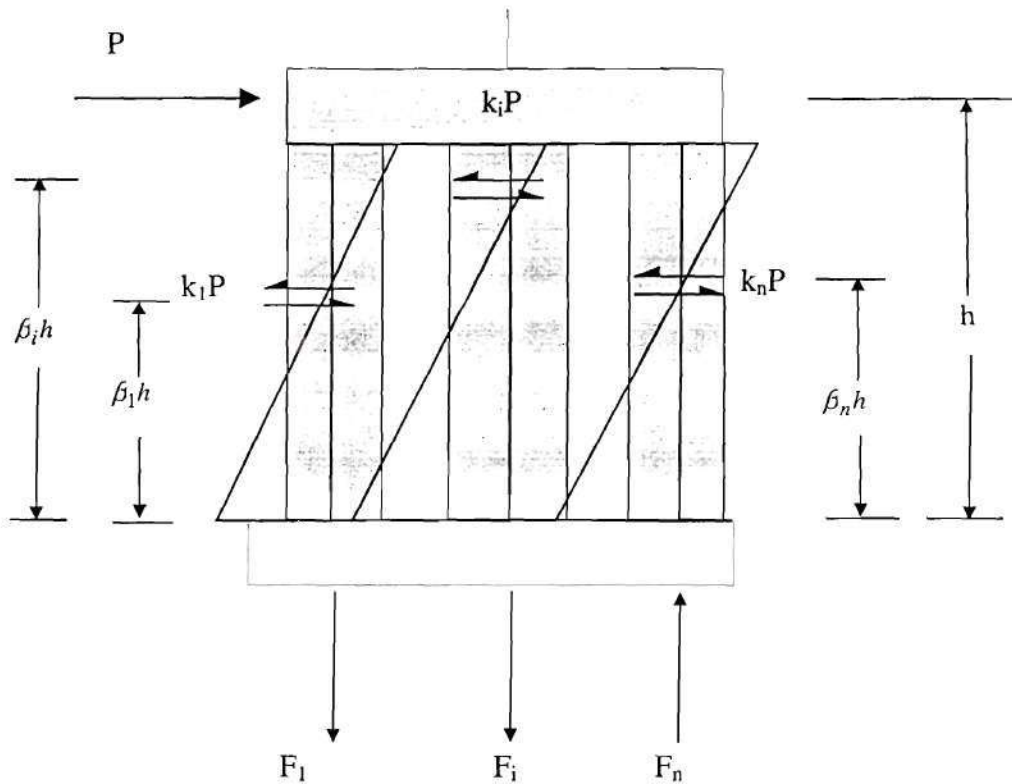


Figure 4.17. Idealized perforated wall

$$K = \frac{1}{k_3 + k_4 \frac{M}{P}} \quad (4.15)$$

where

$$k_3 = \left(\frac{11H_p^3}{12EI_p} + \frac{1.2H_p}{GA_p} \right) - \frac{H_p^4 L_s^2}{E^2 I_c^2} \{1.5 \quad 1\} \begin{bmatrix} r_{11} & r_{12} \\ r_{12} & r_{22} \end{bmatrix}^{-1} \begin{Bmatrix} 2 \\ 1.5 \end{Bmatrix} \quad (4.16)$$

$$k_4 = -\frac{3H_p^2}{4EI_p} + \frac{H_p^3 L_s^2}{E^2 I_c^2} \{1.5 \quad 1\} \begin{bmatrix} r_{11} & r_{12} \\ r_{12} & r_{22} \end{bmatrix}^{-1} \begin{Bmatrix} 2 \\ 1 \end{Bmatrix} \quad (4.17)$$

4.2.3.3 Overturning Moment

Due to the dependence of masonry strength on vertical stress, the effects of overturning moment must be considered in cases where sizable changes in the vertical stress distribution of a URM wall can be expected. These cases include structures where the height of the building is similar to the length. That is, where the overturning moment is relatively large compared with the moment of inertia of the structure, as in the case of several low-rise URM structures including the ST-11 test structure.

As mentioned in the previous section, spandrels of a perforated wall supply the coupling effect, which allows a portion of the overturning moment to be resisted by a change in vertical stress of the piers. In doing this, the spandrels are subjected to vertical shear forces, which can cause damage to the spandrels and consequently limit the amount of coupling between the piers. For simplicity, the model does not consider the effects of spandrel damage; however, the demand/capacity ratio is calculated for each spandrel in order to provide insight into the potential for spandrel damage. The capacity of the spandrel is based on the diagonal tension capacity for a URM pier given by FEMA 273. The diagonal tension model was chosen to represent the spandrel strength due to the

$$r_{22} = \frac{L_s^3}{3EI_{bot}} + \frac{2L_s^2H_p}{EI_p} + \frac{1.2L_s}{GA_{bot}} + \frac{2H_p}{EA_p} \quad (4.11)$$

$$r_{12} = \frac{2L_s^2H_p}{EI_p} + \frac{2H_p}{EA_p} \quad (4.12)$$

where, H_p is the height of the pier; I_p is the moment of inertia of the pier; A_p is the area of the pier; L_s is the length of half the spandrel; I_{top} and I_{bot} are the combined moments of inertia of the spandrels above and below the pier, respectively; A_{top} and A_{bot} are the combined areas of the spandrels above and below the pier, respectively; E is the elastic modulus of masonry; and G is the shear modulus of masonry.

The location of the inflection point of the pier is then written as:

$$\beta = \frac{M_{bot}}{M_{bot} + M_{top}} \quad (4.13)$$

From the Eqn. (4.7) to (4.13), it is clear that β is dependent on the relative stiffness of the spandrels and the piers as well as the external forces, and can be written in general form as Eq. (4.14).

$$\beta = \beta(M/PH_p, I_p, A_p, H_p, I_{top}, A_{top}, I_{bot}, A_{bot}, L_s) \quad (4.14)$$

In order to employ this method of determining β , the ratio of M/P must be known. To do this, it is assumed that the applied moment, M , at the top of second floor piers is equal to zero. This allows the inflection point of the second floor piers to be determined. For the calculation of the first floor piers, the applied moment, M , is estimated from the shear forces and the locations of the inflection points of the second floor piers.

In addition, the elastic lateral stiffness of the piers can also be determined by the model shown in Fig. 4.16(b) as:

of inflection point. It is important to note that these characteristics are also dependent on external forces (i.e. lateral shear force 'P' and moment 'M') as well as the flexibility of the spandrels (see Fig. 4.16b).

Fig. 4.16(b) illustrates the simple model used to calculate the location of the pier inflection point. The spandrels connected with the pier are modeled as simply supported at their inflection points, which is assumed to be located at the mid-span of the spandrels. The effect of the pier below the pier being considered is accounted for; however, for simplicity the moment of inertia and area are assumed to be equal to the pier being considered. The pier above the pier being considered is replaced by the assumed base shear force (P) and base moment (M) it transfers to the pier being considered.

Based on elastic analysis of this model, the moment on the top and the bottom of the pier can be written as:

$$\begin{Bmatrix} M_{top} \\ M_{bot} \end{Bmatrix} = \{K_1\}P + \{K_2\}M \quad (4.7)$$

where M_{top} and M_{bot} are the moments at the top and the bottom of the pier, respectively.

The factors K_1 and K_2 can be written as

$$\{K_1\} = \begin{Bmatrix} 0 \\ H_p \end{Bmatrix} + \frac{H_p^2 L_s^2}{EI_p} \begin{bmatrix} 1 & 0 \\ -1 & 0 \end{bmatrix} \cdot \begin{bmatrix} r_{11} & r_{12} \\ r_{12} & r_{22} \end{bmatrix}^{-1} \begin{Bmatrix} 4 \\ 3 \end{Bmatrix} \quad (4.8)$$

$$\{K_2\} = \begin{Bmatrix} -1 \\ 1 \end{Bmatrix} + \frac{H_p L_s^2}{EI_p} \begin{bmatrix} 1 & 0 \\ -1 & 0 \end{bmatrix} \cdot \begin{bmatrix} r_{11} & r_{12} \\ r_{12} & r_{22} \end{bmatrix}^{-1} \begin{Bmatrix} 4 \\ 2 \end{Bmatrix} \quad (4.9)$$

with,

$$r_{11} = \frac{L_s^3}{3EI_{top}} + \frac{4L_s^2 H_p}{EI_p} + \frac{1.2L_s}{GA_{top}} + \frac{4H_p}{EA_p} \quad (4.10)$$

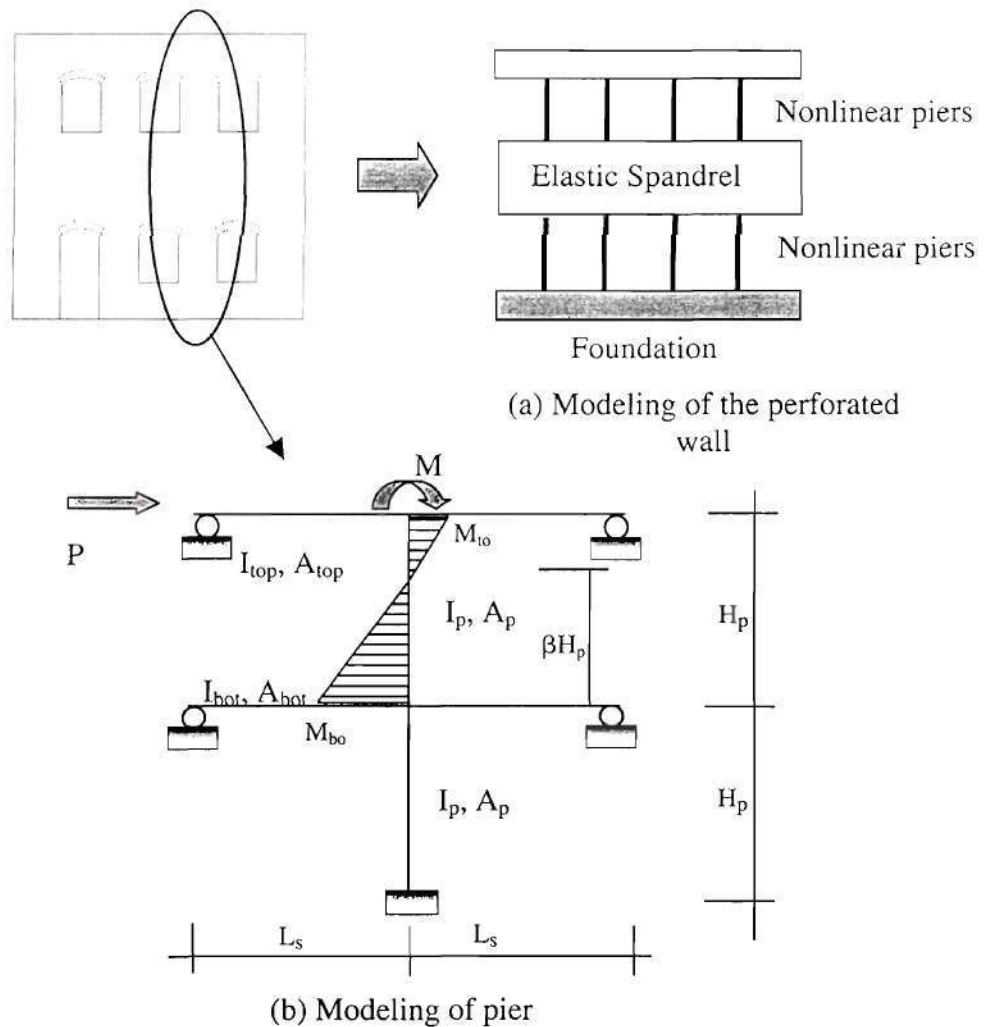


Figure 4.16. Concepts of elastic spandrel-nonlinear pier model

As illustrated in Fig. 4.16, the spandrels are modeled as elastic bodies and the piers are modeled as nonlinear springs to account for possible damage. The finite element analyses, outlined in Section 4.2.1, indicated that most of the in-plane wall displacement is due to the deformation of the piers. As the results, it is assumed that the elastic spandrels do not deform laterally. However, the flexibility of the spandrels is considered in determining pier characteristics such as elastic lateral stiffness and location

The assumption of rigid spandrels, as adopted by FEMA-356, oversimplifies the effect of spandrels on the performance of the entire perforated wall. Ignoring the flexibilities of the spandrels, especially in cases where the spandrels are relatively slender compared with the piers, can result in errors associated with the elastic stiffness as well as unconservative estimates of pier strength. The other extreme is the model depicted in Fig. 4.15b in which the stiffness of the spandrels is ignored. While this model will produce a conservative strength estimate, large errors can be expected in cases where spandrel stiffness is high. As an alternative, an elastic spandrel-nonlinear pier model, as shown in Fig. 4.16, is chosen due to its potential to accurately model a large range of perforated wall geometries.

Essentially the spandrels serve two purposes, 1) they supply coupling between piers to resist overturning moment and 2) they provide a certain degree of fixity to the ends of the piers, which affects pier behavior. In short, the spandrels affect the efficiency of the perforated wall to resist lateral loads, but do not directly transfer the forces to the foundation. The piers, on the other hand, are directly responsible for transferring the lateral loads to the foundations. As a result, the integrity of the in-plane wall depends on the integrity of the piers and not the spandrels. Post-earthquake assessments as well as shaking table tests on building models support this contention, observing that once out-of-plane failures are prevented, the final collapse of an URM building is associated with the shear failure of piers in a critical story (usually the first story) (Calvi 1996).

The spandrel model used in relation to the coupling effect will be discussed in the following section; this section will focus on the effect of the spandrels on pier boundary conditions. Consider the idealized perforated walls shown in Fig. 4.15. The flexible pier-rigid spandrel model is illustrated in Fig. 4.15a.

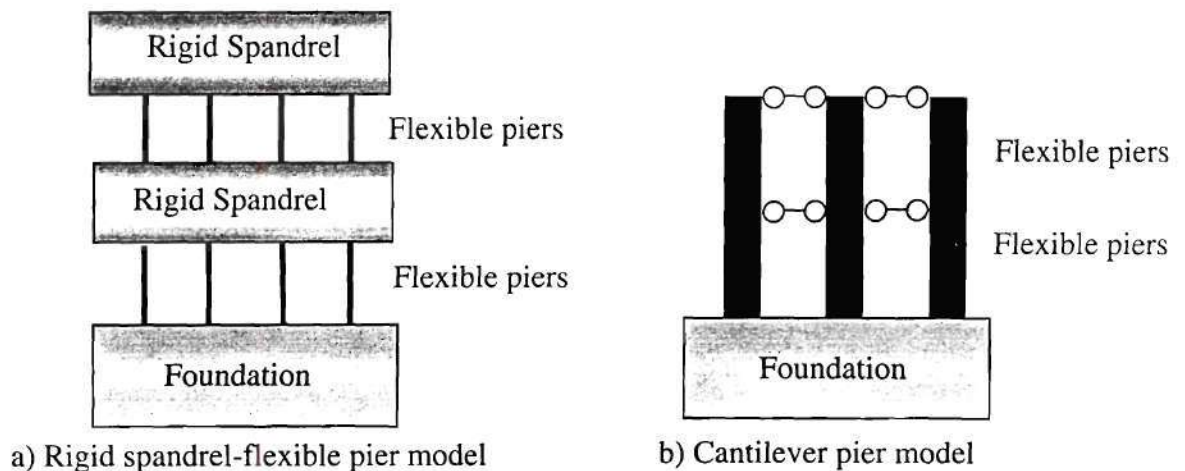


Figure 4.15. Idealized perforated wall models

defined as displacement controlled failure modes due to their ductile nature. Based on these assumptions the failure modes of the URM piers are updated throughout the analysis. After the initial capacity of a pier is exceeded, the pier begins to follow the force-drift curve given for the governing failure mode. If this failure mode is force-controlled the pier is required to continue along the curve until the pier has completely failed. That is, once a force-controlled failure mode initiates, the pier failure mode is no longer updated. However, if the failure mode is displacement controlled, the pier follows the governing force-drift curve until either 1) the strength capacity of a force-controlled failure mode is exceeded or 2) the capacity associated with a different displacement-controlled failure mode (calculated at the current drift) is exceeded. In either case, the force-drift behavior is switched to the curve corresponding to the new failure mode and the analysis continues. Furthermore, the drift capacity defined in Table 4.17 for the force-controlled failure modes is defined as the additional drift upon initiation of failure. For example, if rocking governs until a drift of 3%, at which point diagonal tension failure occurs, the a pier is allowed to displace an additional 0.3% (see Table 4.17) until complete failure for a total drift of 3.3%. This is done due to the large displacement capacities observed in tests where displacement-controlled failure modes degraded into force-controlled failure modes (ATC 1999).

4.2.3.2 Pier/Spandrel Interaction

An important issue in the modeling of a perforated URM wall is how to describe the interaction between the piers and spandrels. In a perforated wall, piers act together with the spandrels to resist the lateral shear forces due to seismic or wind loads. However, there is a distinct difference in the importance of the two members.

Table 4.17 Force-drift relationships for URM pier failure modes.

Failure modes	Drift d (%)	Drift e (%)	Drift x (%)	Residual Capacity C
Rocking	0.4(H/L)	0.8(H/L)	1.2(H/L)	$0.9V_r$
Sliding	0.4	0.8	1.2	$V_{bjs2} = \mu f_a L_{tm}$ (friction)
Toe-Crushing	0.3	-	0.4	$0.5V_{tc}$
Diagonal Tension	0.3	-	0.4	$0.5V_{dt}$

The values for drifts d and e for both the rocking and sliding failure modes were taken directly from FEMA 273. However, due to the lack of rocking strength degradation observed during pier tests (FEMA 306) it is felt that the residual strength value of $0.6V_r$ given by FEMA 273 is overly conservative, as a result a value of $0.9V_r$ was chosen. Furthermore, the residual strength associated with the sliding failure mode is taken as the frictional resistance of the bed joint, V_{bjs2} ($\mu=0.6$), instead of the value of $0.6V_{bjs1}$ suggested by FEMA 273. Additional modifications were made in reference to the displacement capacities of the toe-crushing and diagonal tension failure modes. While the pushover model does recognize the brittle nature of these failure modes, the test results suggest that a small amount of drift capacity is provided and, as a result ultimate drift values of 0.4% were chosen.

In order to address the possibility of several failure modes occurring (as observed during experiments, see Table 4.16) the failure modes are allowed to change throughout the analysis. The FEMA classification of force-controlled or displacement-controlled failure modes is adopted. Due to their brittle-type failures, diagonal tension and toe crushing are classified as force-controlled failure modes, while rocking and sliding are

From the table it is clear that the deformation capacity of a URM pier is strongly dependant on the governing failure mechanism. Piers in which rocking or sliding governs the response have displayed large drift capacities between 1% and 2%. In contrast, piers that fail due to diagonal tension and toe crushing (not preceded by rocking or sliding) exhibit relatively small ultimate drifts of around 0.3%.

Based on experimental and analytical results, lateral force-drift curves can be estimated for each different failure mode. Fig. 4.14 shows a generalized force-drift curve for a URM pier.

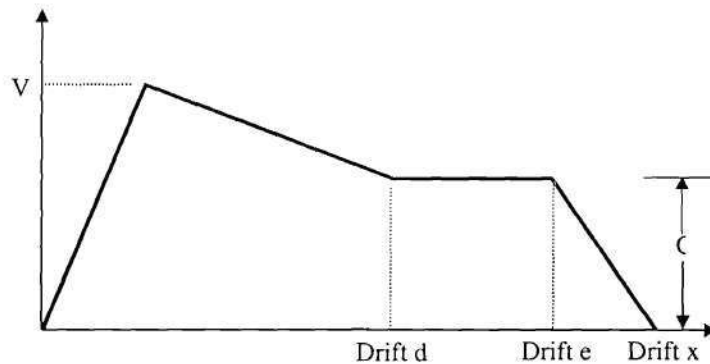


Figure 4.14. Generalized force-drift curve for the analysis of URM piers.

This initial stiffness is taken as the elastic stiffness of the pier and is discussed in more detail in Section 4.2.3.2. It should be mentioned that this curve differs from the one given in FEMA 273 in that it does not contain any sharp drops. This variation was made in order to better estimate test data as well as to avoid any convergence problems during analysis. Table 4.17 gives the values used for each of the four failure modes in order to specialize the generalized force-drift relations given by Fig. 4.14.

where, α is 0.5 for cantilever piers and 1.0 for fixed-fixed piers, f_u is the vertical stress in the pier, t_m is the thickness of the pier, L is the length of the pier, H is the effective height of the pier, v_{te} is the shear strength of the bed-joint, f'_{dt} is the tension strength of masonry, and f'_m is the compression strength of masonry. The strength and failure mode of a URM pier is then determined by the lowest principle capacity.

In addition to strength, large differences in deformation capacity were observed for different failure mechanisms. Table 4.16 gives a list of the deformation capacity and failure modes observed during the in-plane testing of several URM piers (ATC 1999).

Table 4.16. Ultimate drift of URM pier corresponding to different failure modes

Failure mode	Ultimate drift (%)	Reference
Rocking	0.6% to 1.3%	Anthoine (1995), Magenes & Calvi (1995), Costley & Abrams (1996)
Bed-joint sliding	0.6% to 2.4%	Magenes & Calvi (1995), Abrams & Shah (1992)
Rocking/Toe Crushing	0.8%	Abrams & Shah (1992)
Flexural Cracking/Toe Crushing/Bed-joint Sliding	0.8% to 1.3%	Manzouri et al (1995)
Flexural Cracking/Diagonal tension	0.5% to 0.8%	Anthoine (1995), Magenes & Calvi (1992), Magenes & Calvi (1995)
Flexural Cracking/Toe crushing	0.2% to 0.4%	Abrams & Shah (1992), Epperson and Abrams (1989)

- Bed-joint sliding – failure initiates by the formation of horizontal shear cracks in the bed-joint. The pier deforms by sliding along the bed-joint with resistance offered by friction alone.
- Diagonal tension – failure is identified by diagonal shear cracking caused by the maximum principle tension stress exceeding the tension strength of masonry. The cracks may propagate in a stair-stepped manner through the bed-joints and head-joints of the masonry or may pass directly through the bricks, depending on the relative strength of the mortar joints, brick-mortar interface, and bricks.
- Toe crushing – is defined as a compressive failure of masonry occurring at the toe of the pier.

Corresponding to these four potential failure modes, FEMA 273 and FEMA 306 give the principal capacities of a URM pier shown in Table 4.15.

Table 4.15. Strength equations given by FEMA 273 for URM piers

Failure mode	Strength (FEMA 273)
Rocking	$V_r = 0.9\alpha f_a t_m L \left(\frac{L}{H} \right)$
Bed joint sliding	$V_{bjsl} = \frac{0.75(0.75v_{te} + f_a)}{1.5} (Lt_m)$
Diagonal tension	$V_{dt} = f_{dt} Lt_m \left(\frac{L}{H} \right) \sqrt{1 + \frac{f_a}{f_{dt}'}}$
Toe Crushing	$V_{tc} = \alpha f_a Lt_m \left(\frac{L}{H} \right) \left(1 - \frac{f_a}{0.7 f_m'} \right)$

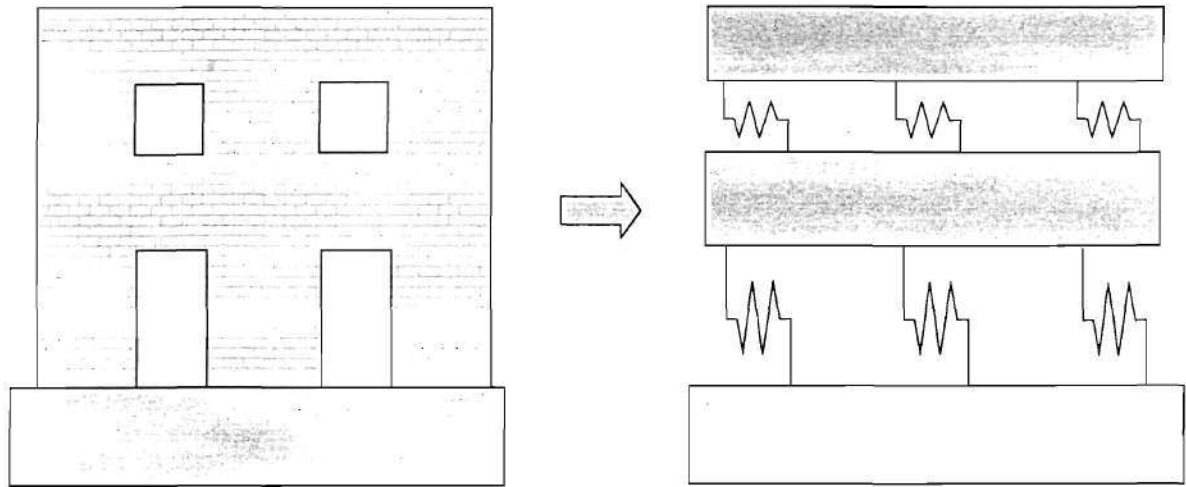


Figure 4.13. URM perforated wall and pushover model.

4.2.3.1 URM Pier Damage Model

Numerous experiments have been conducted on URM piers in order to investigate in-plane behavior. (Konig 1988, Epperson 1989, 1992, Abrams 1993, Erbay et al. 2001). FEMA 307 (ATC 1999) presents a fairly comprehensive summary of the experimental studies including force-displacement responses and failure modes. The experimental results suggest that aspect ratio and vertical stress are the most important factors in determine the failure mechanisms of URM piers. The following four basic failure modes were observed and identified in FEMA 273 and FEMA 356.

- Rocking - failure initiates with large flexural cracks developing at the bottom and the top of the pier. As the displacement increases the pier deforms as a rigid body rotating about the compressive toe.

matched by the quality of the results. On the other hand, the linear models were considered too simplified, as they are not capable of identifying the failure modes of critical members. The failure modes of members in a URM structure directly affect the displacement capacity of the structure, which is paramount when assessing the seismic response. As a result, the nonlinear-static method of analysis was chosen. The pushover analysis represents the simplest form of seismic analysis capable of supplying insight into the failure modes of critical members as well as strength and displacement capacities. Based on the pushover curve obtained from the analysis along with the applicable design spectrum, FEMA 273 provides a method that defines a target displacement. This target displacement is an estimate of the maximum displacement the structure would undergo during an actual earthquake. Therefore, comparing the target displacement with the structures displacement capacity allows the seismic performance of the structure to be assessed. The remainder of this section will focus on the determination of the pushover curve for a URM structure.

The pushover model developed recognizes two types of members in perforated URM walls, piers and spandrels. The piers are considered to be the most critical members and as a result are modeled using nonlinear springs, which can account for potential pier damage. The failure modes and associated displacement capacities considered for the piers are based on experimental test results and are discussed in the following section. The spandrels of the perforated walls are modeled as elastic bodies; however, the demand/capacity of the spandrels are calculated in order to predict expected damaged. This is discussed in detail in Section 4.2.3.3. Fig. 4.13 illustrates how a perforated URM wall is modeled by this pushover analysis.

Table 4.13 Maximum Base Shears of the URM structure under seismic loads

Ground motions	Structure samples	Maximum base shear of the in-plane wall (g)	Maximum base shear of the out-of-plane wall (g)	Maximum base shear of the entire structure (g)
Rock site	AB-flexible	0.413	0.378	0.201
	AB-basic	0.319	0.596	0.261
	AB-stiff	0.439	0.583	0.307
	12-flexible	0.333	0.380	0.261
	12-basic	0.410	0.456	0.296
	12-stiff	0.382	0.543	0.376
Soil site	AB-flexible	0.791	1.125	0.606
	AB-basic	0.460	1.30	0.532
	AB-stiff	0.637	1.062	0.568
	12-flexible	0.620	0.936	0.606
	12-basic	0.477	1.330	0.760
	12-stiff	0.763	0.840	0.631

4.2.3 Nonlinear Pushover Analysis of URM Structures

Four analysis methods, presented in FEMA 273, were considered with the goal of creating a simplified program capable of performing seismic analysis on URM structures. Table 4.14 outlines the material models as well as the types of loading employed in each of the methods considered.

Table 4.14. Seismic analysis methods

	Linear-Elastic Material	Nonlinear Material
Static Loading	Linear-Static	Nonlinear-Static (Pushover)
Dynamic Loading	Linear-Dynamic	Nonlinear-Dynamic

Due to the inherent variability in the behavior of masonry, the nonlinear-dynamic procedure, which is the most refined, was considered to be an inefficient method of analysis. That is, the sophisticated nature of the analysis could not be expected to be

plane walls are very small. This is expected due to the large stiffness' of the in-plane walls.

Table 4.12 Maximum Displacements of the URM structure under seismic loads

Ground motions	Structure samples	Maximum displacement of the in-plane wall relative to the ground (in)	Maximum displacement of the out-of-plane wall relative to the ground (in)	Maximum displacement of the diaphragm relative to the in-plane wall (in)
Rock site	AB-flexible	0.035	0.329	0.337
	AB-basic	0.009	0.173	0.179
	AB-stiff	0.006	0.085	0.084
	12-flexible	0.021	0.345	0.347
	12-basic	0.009	0.138	0.150
	12-stiff	0.004	0.082	0.081
Soil site	AB-flexible	0.067	0.979	0.973
	AB-basic	0.013	0.377	0.387
	AB-stiff	0.009	0.154	0.153
	12-flexible	0.039	0.849	0.874
	12-basic	0.010	0.402	0.418
	12-stiff	0.008	0.127	0.125

* Note: all the displacements relative to ground displacements.

The calculated maximum base shears for the in-plane walls, the out-of-plane walls, and the entire structure are listed in Table 4.13 for the six different structures analyzed. The maximum base shears are presented in terms of percentages of the components weight. The analysis results show that the maximum base shears for the structure are about 0.3 of the total structural weight in the rock site, and about 0.6 of the total structural weight in the soil site. Compared with the maximum ground acceleration of 0.26g in the case of the rock site, and 0.50g in the case of the soil site, it suggests that the amplification of ground acceleration to URM structures is small. However, the table also shows that the maximum base shears for the out-of-plane walls are rather high (about 0.5g in the case of the rock site, and about 1.1g in the case of the soil site), which indicates potential damage to the out-of-plane walls of the URM structure.

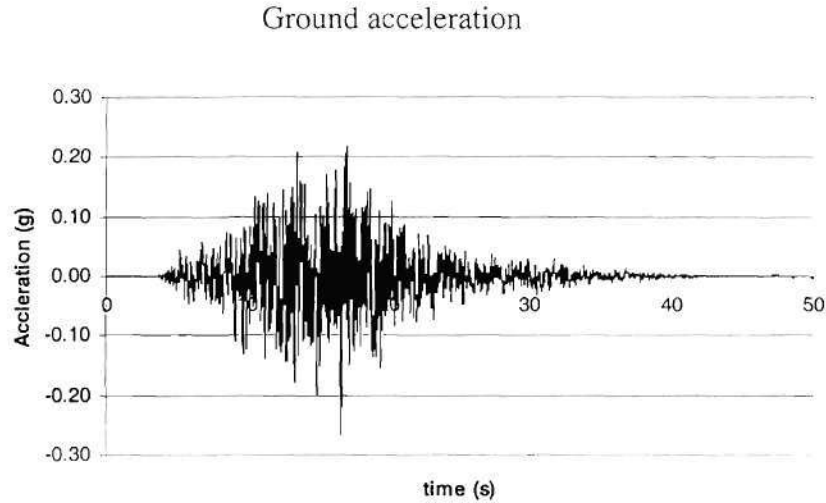


Figure 4.11. Artificial Mid-America ground motion (rock site)

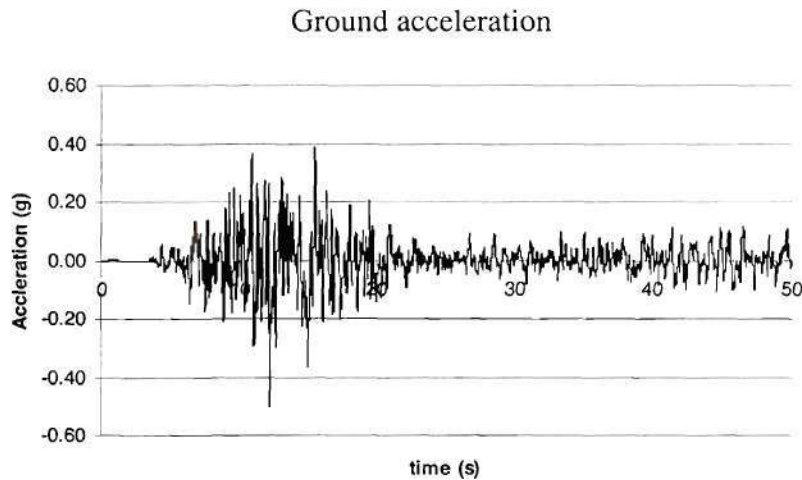


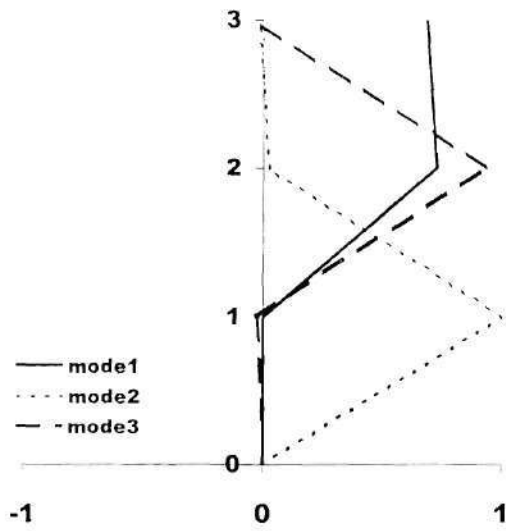
Figure 4.12. Artificial Mid-America ground motion (soil site)

The calculated maximum displacements of each component for the six different structures discussed before are listed in Table 4.12. From the table it is apparent that the displacements of the out-of-plane walls are much larger than those of the in-plane walls. This supports the early contention that the out-of-plane walls are the weak component of the URM structure. Furthermore, the results indicate that the displacements of the in-

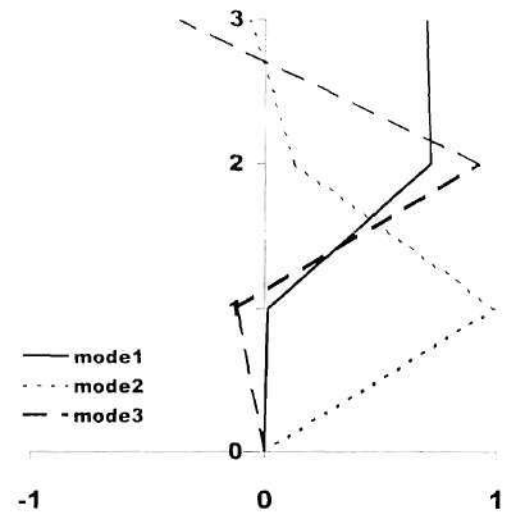
are less than 0.1 seconds, and fall into the decreasing range of the hazard response spectra for Mid-America (ATC 1997, Wen 2001). The low values for the second and third natural periods suggest that the first vibration mode will dominate the response of the test structure under seismic excitation. The analysis results also show that the possible variations in the stiffness of the structure have little effect on the overall mode shapes. In the first vibration mode, the in-plane wall does not move much, while the out-of-plane wall and the floor/roof diaphragm vibrate in phase. Since the first mode dominates the response of the structure this suggests that the out-of-plane is most vulnerable to seismic vibrations. This is consistent with observed failures of URM structures after earthquakes.

4.2.2.2 Dynamical analysis based on the conceptual model

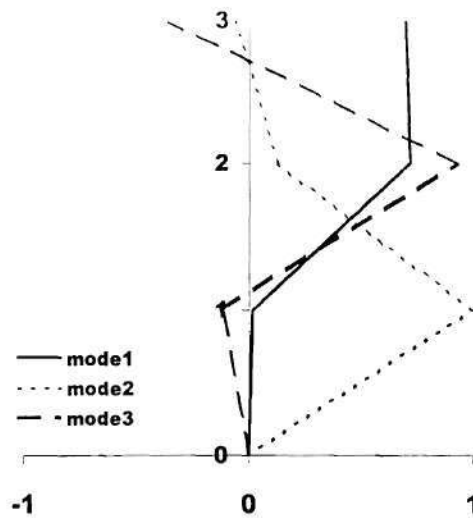
Dynamic analyses were also conducted using the conceptual model and two artificial Mid-America ground motions. The first ground motion is indicative of a rock site, with a peak ground acceleration of 0.26g and a predominant period of about 0.1 seconds (Wen 2001). The second ground motion is representative of a soil site, with a peak ground acceleration of 0.50g and a predominant period of about 0.15 seconds. The time histories of the two earthquake motions are shown in Fig. 4.11 and 4.12.



8 Basic case



9 Flexible



7 Stiff

Figure 4.10. Vibration modes for the test structure (Walls 1 and 2 in-plane)
(Y axis, 1: in-plane wall; 2: diaphragm; 3: out-of-plane wall)

The calculated fundamental natural periods range from 0.14 to 0.36 seconds, which is reasonable when one considers the relatively high stiffness and low mass associated with the test structure. The second and third natural periods of the structure

stiffness values represented a very flexible structure while the other represented a very stiff structure. The stiffness values used in each case are listed in Table 4.10.

Table 4.10 Elastic stiffness' used for sensitivity analysis (Walls 1 and 2 in-plane)

	12-Flexible	12-Basic	12-Stiff
K_i (kip/in)	1079	3237	6474
K_o (kip/in)	127	381	762
K_{di} (kip/in)	14	14	140
K_{do} (kip/in)	580	1740	3480

The calculated natural periods of the structure are given in Table 4.11. The mode shapes corresponding to each natural period are shown in Fig. 4.10. Again, the y-axis represents each component of the structure with 0 = ground, 1 = in-plane wall, 2 = diaphragm, and 3 = out-of-plane wall, and the x-axis represent displacement in each mode.

Table 4.11 Natural periods of the conceptual model (Walls 1 and 2 in-plane)

Natural period (s)	12-Flexible	12-Basic	12-Stiff
Mode 1	0.343	0.205	0.1355
Mode 2	0.08	0.046	0.0326
Mode 3	0.074	0.043	0.0301

The second analysis conducted assumed that Walls 1 and 2 were in-plane walls and Walls A and B were out-of-plane walls. The properties used in this analysis are shown in Table 4.9 and were determined from the elastic FE analysis.

Table 4.9 Structural properties used in analysis with Walls 1 and 2 in-plane

Stiffness of in-plane wall K_i (kps/in)	3237 ⁽¹⁾
Stiffness of out-of-plane wall K_o (kps/in)	381 ⁽²⁾
Axial stiffness of the floor/roof diaphragm K_{do} (kps/in)	1740 ⁽³⁾
Shear stiffness of the floor/roof diaphragm K_{di} (kps/in)	14 ⁽⁴⁾
Weight of the in-plane wall M_i (kps)	69 ⁽⁵⁾
Weight of the out-of-plane wall M_o (kps)	116 ⁽⁶⁾
Weight of the diaphragm M_d (kps)	45 ⁽⁷⁾
<p>Note:</p> <ol style="list-style-type: none"> 1. The stiffness of the in-plane wall was taken as combined in-plane stiffness of Walls 1 and 2 assuming equal forces were applied at the roof level and the floor level. 2. The stiffness of the out-of-plane wall was taken as the combined out-of-plane stiffness of Walls A and B assuming a uniformly applied lateral pressure. 3. The axial stiffness of the floor/roof diaphragm was based on the axial stiffness of the sheathing. 4. The shear stiffness of the diaphragm was the combined shear stiffness of the floor and roof diaphragms, which were both assumed to be 7kps/in based on the test results of ST-8. 5. The weight of the in-plane wall was taken as the total weight of Walls 1 and 2. 6. The weight of the out-of-plane wall was taken as the total weights Walls A and B. 7. The weight of the diaphragm was taken as the total weight of the floor and roof diaphragms, including 15psf of dead load and 50psf of live load. 	

Again, to assess the effect of the inherent variability of masonry materials, two additional sets of stiffness values were used for a sensitivity analysis. One set of the

Table 4.8. Natural periods of the conceptual model (Walls A and B in-plane)

Natural period (s)	AB-Flexible	AB-Basic	AB-Stiff
Mode 1	0.356	0.218	0.1385
Mode 2	0.093	0.054	0.0378
Mode 3	0.068	0.039	0.0277

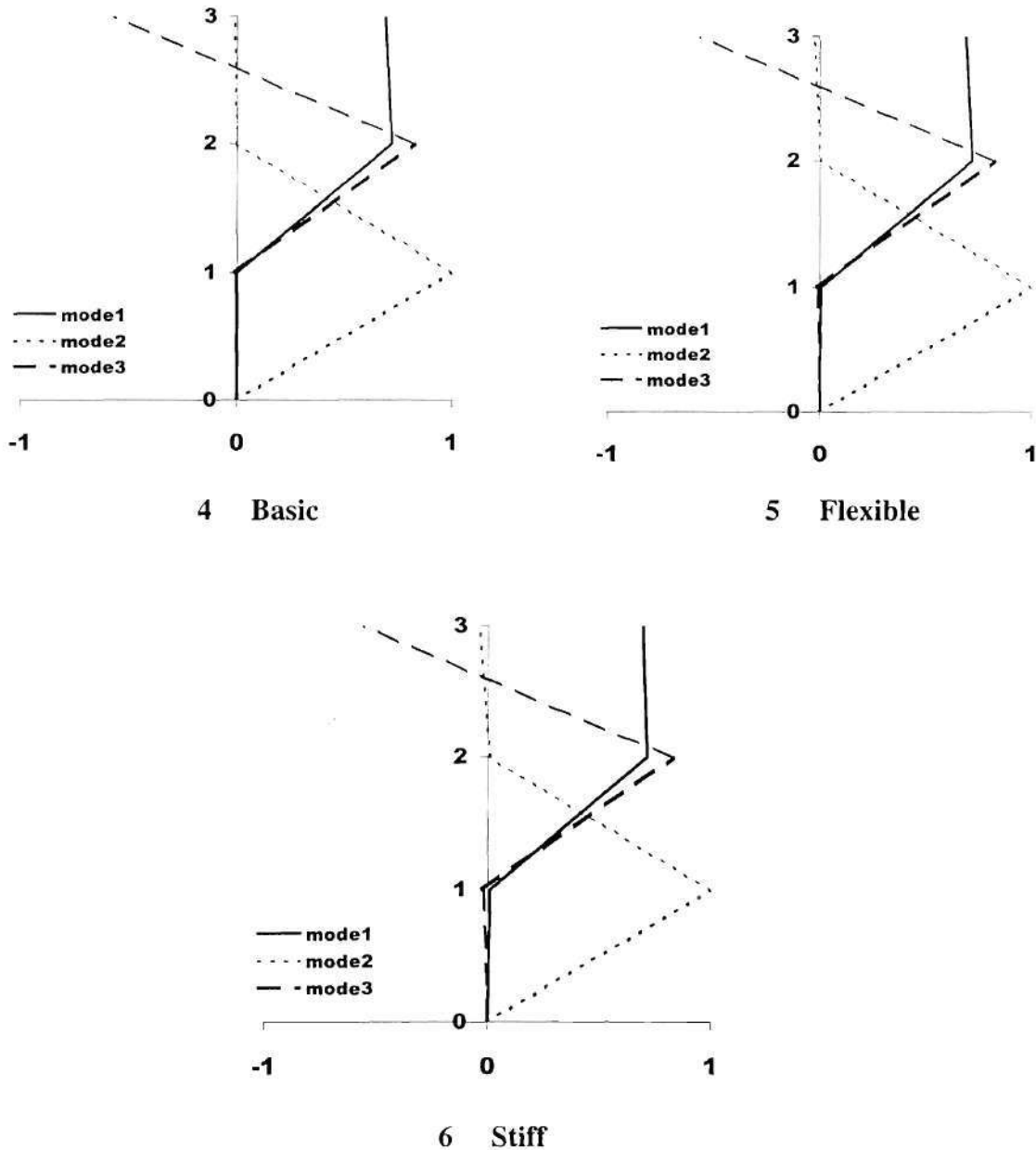


Figure 4.9 Vibration modes for the test structure (Walls A and B in-plane)

(Y axis, 1: in-plane wall; 2: diaphragm; 3: out-of-plane wall)

To assess the possible effects of the inherent variability of the mechanical properties of masonry, two additional sets of stiffness values were used in a sensitivity analysis. One set of the stiffness values represented a lower bound on stiffness (i.e. flexible case) while the other represented an upper bound on stiffness (i.e. stiff case). The stiffness values used in each case are listed in Table 4.7.

Table 4.7. Elastic stiffness' used for sensitivity analysis (Walls A and B in-plane)

	AB-Flexible	AB-Basic	AB-Stiff
K_i (kip/in)	1360	4079	8158
K_o (kip/in)	78	234	468
K_{di} (kip/in)	14	14	140
K_{do} (kip/in)	580	1740	3480

The stiffness and mass matrices of the conceptual model are shown in Eqs. (4.4) and (4.5). The natural periods of the structure obtained through the solution of the Eigen problem are shown in Table 4.8. The vibration mode shapes of each structure were scaled so that the largest displacement is equal to one and presented in graphical form in Fig. 4.9 (note: the y-axis represents each component of the structure with 0 = ground, 1 = in-plane wall, 2 = diaphragm, and 3 = out-of-plane wall, and the x-axis represent displacement in each mode).

$$\begin{bmatrix} K_i + K_{di} & -K_{di} & 0 \\ -K_{di} & K_{di} + K_{do} & -K_{do} \\ 0 & -K_{do} & K_{do} + K_o \end{bmatrix} \quad (4.5)$$

$$\begin{bmatrix} M_i \\ M_d \\ M_o \end{bmatrix} \quad (4.6)$$

4.2.2.1 Natural Periods and Vibration Mode Shapes of the Test Structure

The first analysis was conducted assuming that Walls A and B were in-plane and Walls 1 and 2 were out-of-plane. Based on the results of the 3D elastic FE analysis and past experiment data, the properties shown in Table 4.6 were used in the analysis of the ST-11 test structure.

Table 4.6 Structural properties used in analysis with Walls A and B in-plane

Stiffness of in-plane wall: K_i (kips/in)	4079 ⁽¹⁾
Stiffness of out-of-plane wall: K_o (kips/in)	234 ⁽²⁾
Axial stiffness of the floor/roof diaphragm: K_{do} (kips/in)	1740 ⁽³⁾
Shear stiffness of the floor/roof diaphragm: K_{di} (kips/in)	14 ⁽⁴⁾
Weight of the in-plane wall: M_i (kips)	116 ⁽⁵⁾
Weight of the out-of-plane wall: M_o (kips)	69 ⁽⁶⁾
Weight of the diaphragm: M_d (kips)	45 ⁽⁷⁾
<p>Note:</p> <ol style="list-style-type: none"> 1. The stiffness of the in-plane wall was taken as combined in-plane stiffness of Walls A and B assuming equal forces were applied at the roof level and the floor level. 2. The stiffness of the out-of-plane wall was taken as the combined out-of-plane stiffness of Walls 1 and 2 assuming a uniformly applied lateral pressure. 3. The axial stiffness of the floor/roof diaphragm was based on the axial stiffness of the sheathing. 4. The shear stiffness of the diaphragm was the combined shear stiffness of the floor and roof diaphragms, which were both assumed to be 7kps/in based on the test results of ST-8. 5. The weight of the in-plane wall was taken as the total weight of Walls A and B. 6. The weight of the out-of-plane wall was taken as the total weights Walls 1 and 2. 7. The weight of the diaphragm was taken as the total weight of the floor and roof diaphragms, including 15psf of dead load and 50psf of live load. 	

4.2.2 Conceptual Dynamic Model

Due to the large number of elements required for the elastic FE model, the investigation of the test structure's dynamic properties is nearly impossible. As a result, a simplified conceptual model was developed. Essentially, the dynamic performance of the test structure as a whole is dominated by the interaction between the in-plane walls, the out-of-plane walls, and the flexible diaphragms. Considering this, a conceptual model containing three lumped masses and four elastic springs can be used to represent the basic components of an URM building (i.e. in-plane wall, out-of-plane wall and floor/roof diaphragm). The configuration of this model is shown in Fig. 4.8.

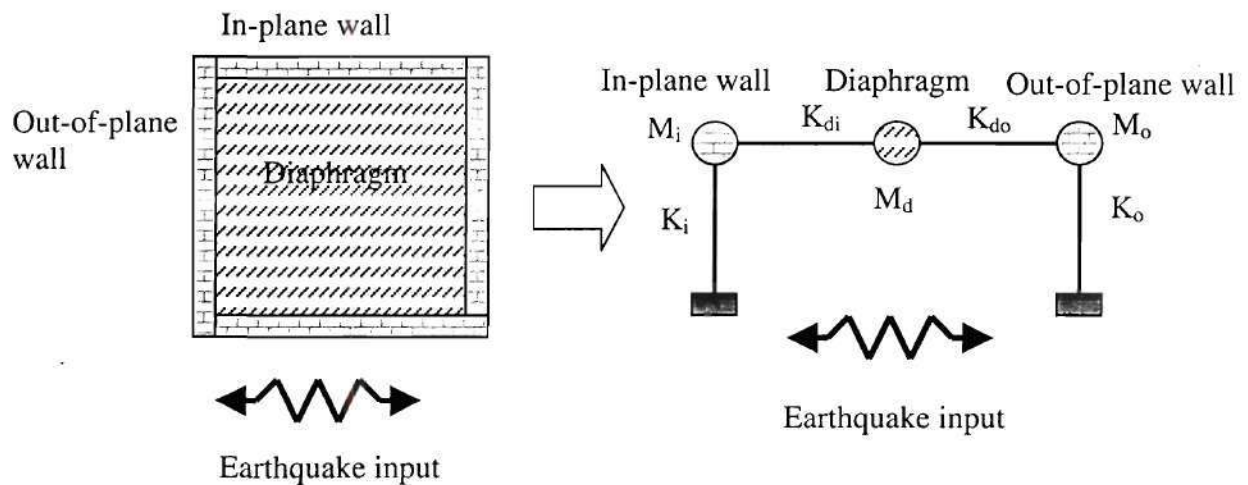


Figure 4.8. Conceptual model of an URM structure

where, K_i and K_o are the stiffness' of the in-plane wall and the out-of-plane wall, respectively, K_{do} is the axial stiffness of the floor/roof diaphragm parallel to the earthquake input, K_{di} is the shear stiffness of the floor/roof diaphragm, and M_i , M_o , and M_d are the lumped masses of the in-plane wall, out-of-plane wall, and floor/roof diaphragm, respectively.

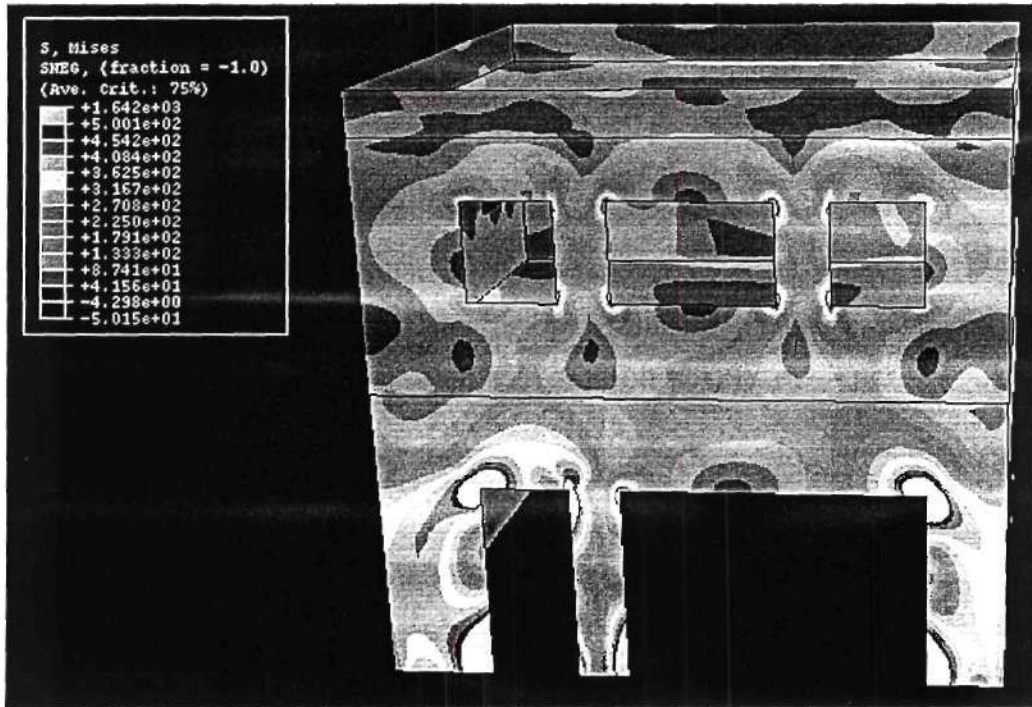


Figure 4.6. Maximum von Mises stresses in the Wall 2 under in-plane loading

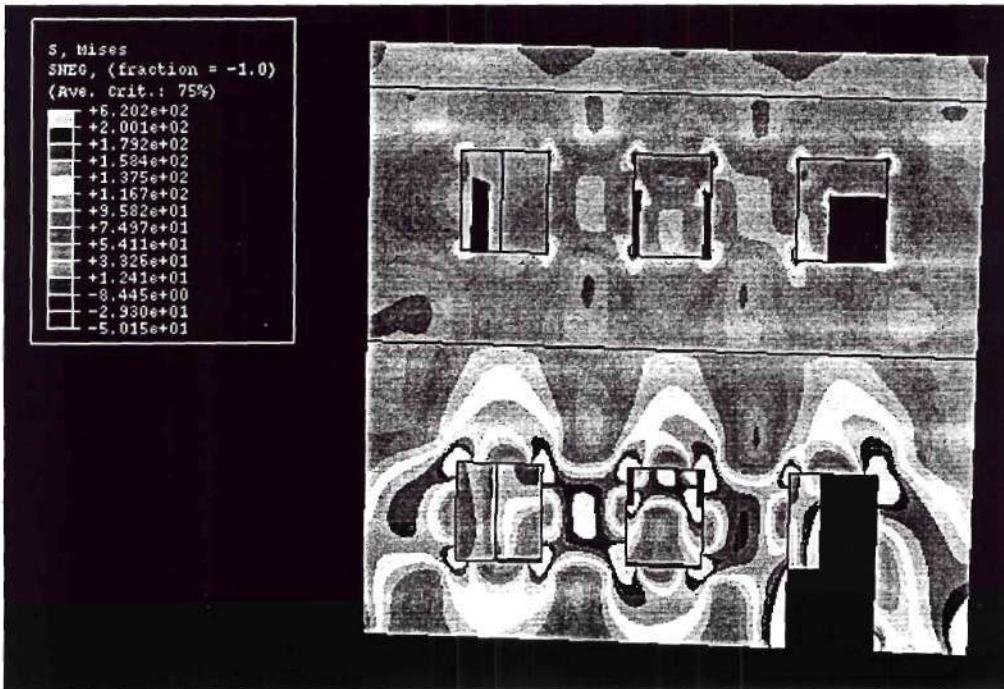


Figure 4.7. Maximum von Mises stresses in Wall AB under in-plane loading

1996). The maximum calculated von Mises stresses for each of the walls of the ST-11 test structure in Fig 4.5 through 4.7. The analysis results show that, for the selected loading case, the highly stressed zones for each of the walls are located in the first floor piers. This is expected as these piers are subjected to the largest shear force.

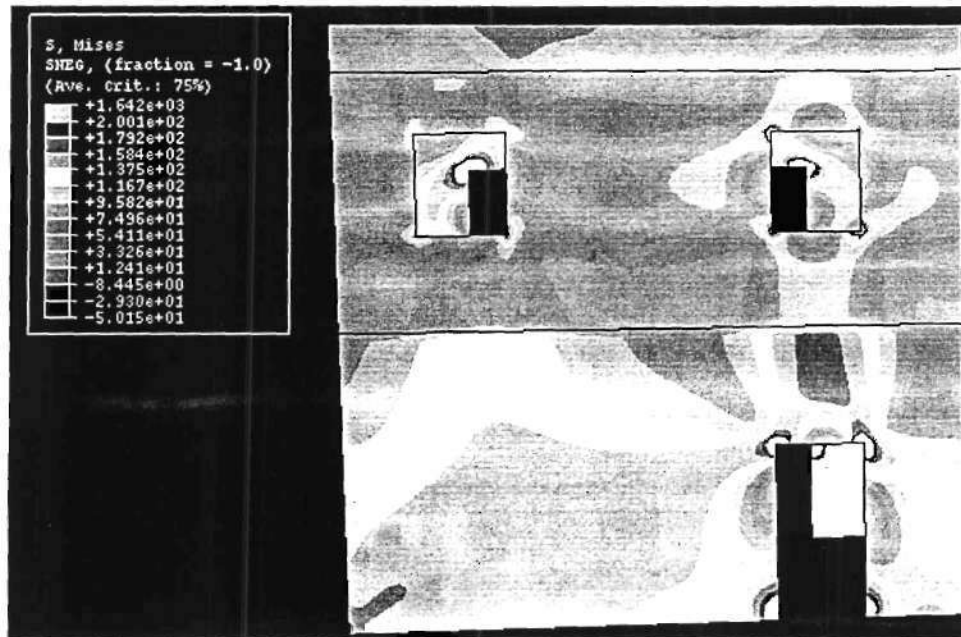


Figure 4.5. Maximum von Mises stresses in the Wall 1 under in-plane loading

element size were used in the analysis. The calculated in-plane stiffness' of the four walls obtained from both analysis methods are shown in Table 4.5.

Table 4.5 In-plane stiffness of the masonry walls with/without flange effect

Stiffness (kps/in)		3D analysis	2D analysis	Ratio between 3D analysis and 2D analysis
Wall A	Equal forces on the roof and the floor	2031	1515	1.34
	Forces applied on the roof	1507	1100	1.37
Wall B	Equal forces on the roof and the floor	2048	1515	1.35
	Forces applied on the roof	1523	1100	1.39
Wall 1	Equal forces on the roof and the floor	2506	1606	1.56
	Forces applied on the roof	1817	1157	1.57
Wall 2	Equal forces on the roof and the floor	731	464	1.58
	Forces applied on the roof	588	379	1.55

The analysis results show that the flange effect considerably increases the elastic in-plane stiffness of the masonry walls. The increase ranges from 0.34 to 0.58.

4.2.1.7 Locations of Highly Stressed Zones

While the 3D FE elastic analysis cannot model damage, such an analysis can provide information on locations of highly stressed zones in which cracks can be expected to form. This information will be used to select the locations of the contact elements employed in the nonlinear FE analysis described in Section 4.2.4. For the purpose of locating these highly stressed zones, equal forces were applied at both the roof and floor levels of each in-plane wall as this is fairly indicative of seismic loading (Calvi,

Table 4.4 In-plane stiffness of the masonry walls

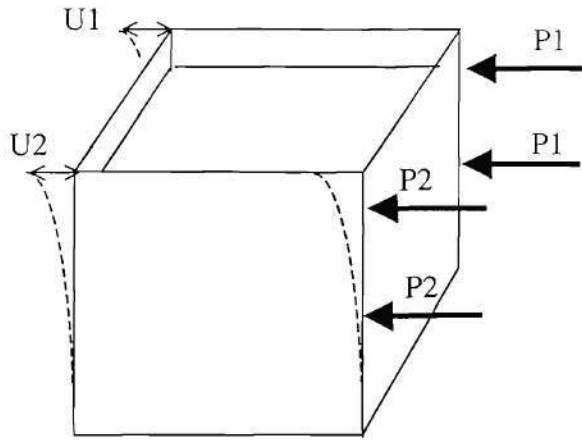
Stiffness (kps/in)		Equal forces at the roof and the floor	Forces applied at the roof
Walls A, B	In-plane stiffness of Wall A	2031	1507
	In-plane stiffness of Wall B	2048	1523
	Coupling effect stiffness	45	46
Walls 1, 2	In-plane stiffness of the wall 1	2506	1817
	In-plane stiffness of the wall 2	731	588
	Coupling effect stiffness	2.5	6

The table shows that Wall 1 displayed the highest stiffness while Wall 2 displayed the lowest stiffness. This is expected due to the large differences in the opening ratios for these two walls. Comparing Table 4.3 and Table 4.4, it can be seen that the in-plane stiffness of the masonry walls was much higher than their out-of-plane stiffness. The ratios range from 13.4 for Wall 2 to 50.5 for Wall 1. Furthermore, the table also shows that coupling stiffness is negligible compared to the in-plane stiffness. As a result, the coupling effect between two in-plane walls is ignored in further analysis.

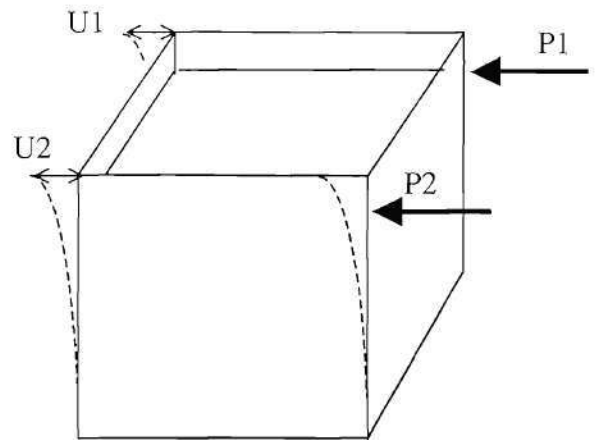
4.2.1.6 Flange Effect

In order to facilitate the use of two-dimensional analysis of in-plane masonry walls, the effect of the out-of-plane wall on in-plane behavior (i.e. the so-called flange effect) must be assessed. The in-plane stiffness' of the walls determined through the 3D analysis in the previous section include this flange effect. For comparison the elastic stiffness of each masonry wall was calculated again as a plane-stress problem without considering the effect of the out-of-plane walls. The same shell element and the same

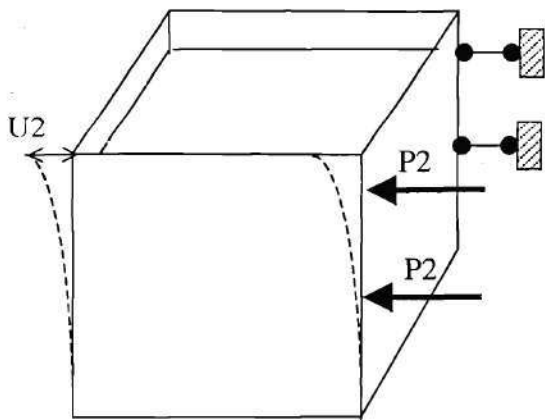
where, u_1 and u_2 are the in-plane lateral roof displacements of the in-plane walls; P_1 and P_2 are the lateral in-plane forces applied on the walls, k_{11} and k_{22} are the in-plane stiffness' of the masonry walls, and k_{12} is the coupling stiffness. The calculated results are listed in Table 4.4.



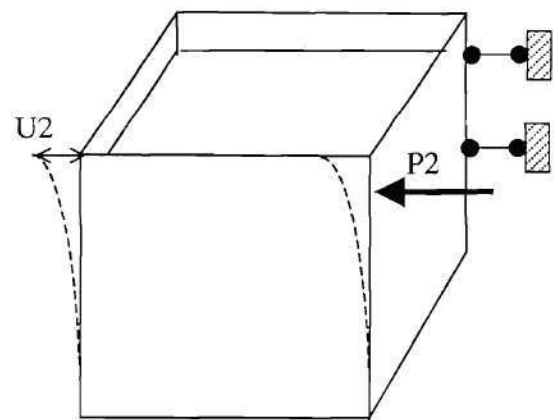
(a) Loading case 1



(b) Loading case 2



(c) Loading case 3



(c) Loading case 4

Figure 4.4. Different loading cases for calculation of the in-plane stiffness of masonry walls

However, the effect is minor because the stiffness of the diaphragms is small compared with that of the masonry walls. In the case of the ST-11 building, the out-of-plane stiffness of the masonry walls are between 4 to 30 times of the stiffness of the diaphragms.

4.2.1.5 Elastic In-Plane Wall Stiffness and Coupling Effect

The 3D elastic FE model was used to obtain estimates of the in-plane wall stiffness as well as the coupling effect. The coupling effect refers to the coupling supplied between in-plane walls by either the diaphragm or the out-of-plane walls. This coupling is important because it can cause torsional action in an unsymmetric structure during seismic excitation, leading to severe damage. Furthermore, this coupling, along with distribution of external forces, affects the in-plane stiffness of the walls. In order to investigate the in-plane stiffness and coupling effect of the walls in the ST-11 test structure, four loading cases were employed. The loading cases were: 1) equal lateral force applied at both the roof and floor levels of the two parallel in-plane walls (see Fig. 4.4a); 2) equal lateral force applied at the roof level of the two parallel in-plane walls (see Fig. 4.4b); 3) equal lateral force applied at both the roof and floor level of one in-plane wall, with the displacement of the other in-plane constrained (see Fig. 4.4c); 4) lateral force applied at the roof level of one in-plane wall, with the displacement of the other in-plane constrained (see Fig. 4.4d).

The in-plane behavior of the masonry walls can be described by the following equation:

$$\begin{bmatrix} k_{11} & k_{12} \\ k_{12} & k_{22} \end{bmatrix} \begin{Bmatrix} u_1 \\ u_2 \end{Bmatrix} = \begin{Bmatrix} P_1 \\ P_2 \end{Bmatrix} \quad (4.3)$$

contribution of the roof/floor diaphragms to the out-of-plane stiffness of the masonry walls, the out-of-plane deformations of the masonry walls were calculated both with and without roof/floor diaphragm connections. The results are listed in Table 4.3.

Table 4.3 Out-of-plane stiffness of the masonry walls

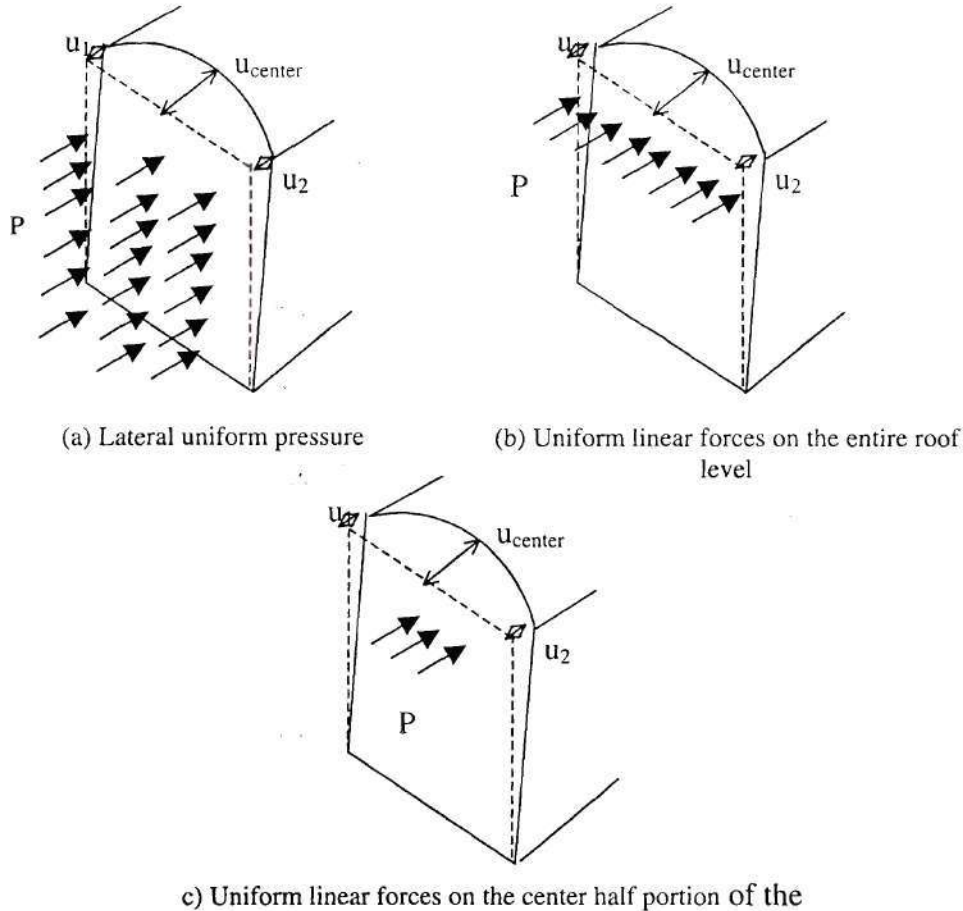
Out-of-plane stiffness (Kps/in)		Without roof/floor diaphragms	With roof/floor diaphragms	Contributions of roof/floor diaphragms
Wall A	Uniform pressure	-	190.5	-
	Full roof force	75.8	81.2	5.4
	Half roof force	51.5	55.0	3.5
Wall 1	Uniform pressure	-	130.0	-
	Full roof force	44.7	49.6	4.9
	Half roof force	28.5	31.5	3.0
Wall 2	Uniform pressure	-	104.4	-
	Full roof force	39.1	43.8	4.7
	Half roof force	25.0	27.9	2.9

The table shows that the estimated out-of-plane stiffness for Walls A and B is larger than for Walls 1 and 2. This is expected since Walls A and B are three wythes in thickness, while Walls 1 and 2 are two-wythes in thickness. Furthermore, the out-of-plane stiffness of Wall 1 is larger than that of Wall 2. This is due to the relatively small opening ratio of Wall 1 compared to that of Wall 2. However, since Walls 1 and 2 display similar stiffness, the effect of the opening ratio on the out-of-plane stiffness appears to be small. The opening ratio of Wall 2 is 3.3 times of that of Wall 1 (see Fig. 3.7 and 3.8); however, the out-of-plane stiffness of Wall 1 is only 14% higher than that of Wall 2.

The table also shows that the out-of-plane stiffness of the walls depend on the distribution of the external force. Uniformly applied pressure leads to a higher stiffness estimate than an applied linear force. Furthermore, the presence of the floor/roof diaphragms does have an effect on the out-of-plane stiffness of the masonry walls.

$$K_{out} = \frac{P}{u_{center} - 0.5(u_1 + u_2)} \quad (4.2)$$

where, P is the total out-of-plane force, u_{center} is the out-of-plane displacement at the center point of the roof level, and u_1, u_2 are the displacements of each in-plane wall at the roof level, respectively (see Fig. 4.3).



(a) Lateral uniform pressure
 (b) Uniform linear forces on the entire roof level
 (c) Uniform linear forces on the center half portion of the

Figure 4.3. Out-of-plane loading of the masonry wall

Three different loading cases were employed to obtain estimates of the out-of-plane wall stiffness: 1) uniform lateral pressure (see Fig. 4.3a); 2) uniform linear force applied along the entire roof level (see Fig. 4.3b); 2) uniform linear force applied along the center half of the roof level (see Fig. 4.3c). In addition, to gain insight into the

4.2.1.3 Gravity stresses

Estimates of the vertical stress in each pier due to gravity loads were obtained using the 3D elastic FE model. The calculated gravity stresses in each pier are listed in Table 4.2. The designation of each pier was given in Fig 3.6 – Fig. 3.8.

Table 4.2 Gravity stresses in the piers

Pier	Gravity stress (psi)	Pier	Gravity stress (psi)
A-2	8	B-2	8
A-3	9	B-3	9
A-4	9	B-4	9
A-5	7	B-5	6
A-7	23	B-7	28
A-8	25	B-8	23
A-9	26	B-9	25
A-10	22	B-10	19
1-2	8	2-2	7
1-3	8	2-3	12
1-4	7	2-4	9
1-6	20	2-5	8
1-7	23	2-7	26
		2-8	37
		2-9	30

From the table it is apparent that the vertical stresses due to gravity loads in each pier are rather low, with a maximum value of 37psi. These relatively low vertical stresses are expected, as the gravity load is caused only by the structure's self-weight (i.e. there is no added weight). Based on these low vertical stresses, it is expected that compressive failures of masonry will not be observed.

4.2.1.4 Elastic Out-of-Plane Wall Stiffness

An estimate of the elastic out-of-plane stiffness of each wall of the ST-11 test structure was obtained by utilizing the 3D FE model. The out-of-plane stiffness was defined as the follows:

experimentally measured stiffness was altered to calibrate the model. Based on analysis results obtained through ST-8, the lateral stiffness was assumed to be 7.0 kips/in. In the ST-11 ABAQUS 3d model, S4R shell elements (discussed previously) were used to model the diaphragm. The thickness of the shell element was assumed to be 1 inch. Through trial and error it was determined that an elastic modulus of 2.8 ksi along with a Poisson's ratio of 0.25 provided a lateral diaphragm stiffness of approximately 7.0 kips/in. As a result, these values were used in the analysis. The density of the equivalent diaphragm shell element was assumed to be 0.062 lb/in^3 .

The 3D model of the ST-11 building is shown in Fig 4.2. The total number of the nodes used in this model was 27344, the total number of the elements was 26909, and the total number of DOF was 164064.

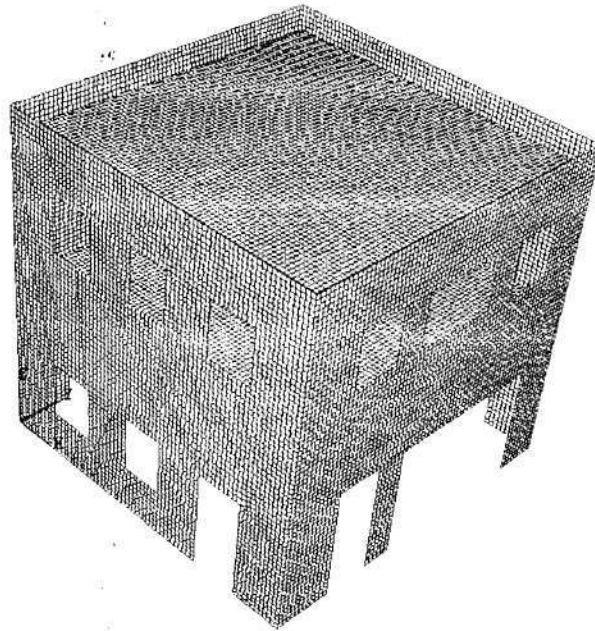


Figure 4.2. Three-dimensional model of the ST-11 building

model the ST-11 test structure. Additional models were analyzed to investigate smaller mesh sizes and it was observed that decreasing the mesh size had a negligible effect on the accuracy of the results. Therefore, the mesh size was held at 4 in. In the analysis, the density of masonry was taken as 0.06944 lb/in^3 , the elastic modulus was taken as 1000 ksi, and the Poisson's ratio was taken as 0.25.

4.2.1.2 Diaphragm Elastic Stiffness

Due to the configuration of the sheathing and joists, the determination of the elastic stiffness of the wood roof/floor diaphragm used in the ST-11 building is not straightforward. Theoretically, this type of diaphragm displays orthotropic behavior since the joists and sheathing run in perpendicular directions. However, no experimental data describing this orthotropic behavior of this type of wood diaphragm is available. As a result, an isotropic material model was employed for the diaphragm model. In order to obtain a reasonable diaphragm model, the elastic modulus of the diaphragm was selected to provide an elastic stiffness consistent with the results of past experimental research.

MAE center project ST-8 (Peralta et al 2000) tested several different wood diaphragm systems. Based on these test results, the MAE-2 diaphragm was chosen for the ST-11 structure due to the low stiffness and strength it displayed (i.e. the diaphragm represents a worst-case scenario). It should be mentioned that the size of the MAEC-2 diaphragm tested in ST-8 (i.e. 24ft x 12ft) was approximately half the size of the diaphragms employed in the ST-11 test structure (i.e. 24 ft. x 24 ft.). Results from the ST-8 testing program showed that the lateral secant stiffness of this diaphragm gradually degraded from 20.6 kips/in to 4.0 kips/in with increasing lateral displacement. Since the diaphragms of the ST-11 structure are twice the size of the diaphragms tested in ST-8, the

The second structure used to assess the accuracy of the elements was the same as the first except the wall was pin supported along the vertical edges and loaded out-of-plane by a constant pressure. This structure was meant to provide insight into the accuracy of the elements to predict out-of-plane behavior. To assess the results a uniform out-of-plane pressure q equal to 14.4 psf was applied to the wall. Based on classical elastic theory, the maximum out-of-plane deformation of the wall is 0.207 in (Timoshenko 1959). Again, for the FE elastic analysis a 4 in. mesh size was used for each element type.

Table 4.1 shows a comparison between the displacements predicted by the two elements as well as a percent error compared to the classical elastic solution.

Table 4.1. Summary of assessment of element accuracy

Element	In-plane displacement (in)	% error	Out-of-plane displacement (in)	% error
3D solid	0.0715	5.4	0.15	27.5
Shell	0.0725	4	0.1835	11

From the table it is apparent that both the 3D solid element and shell element gave reasonable results for the in-plane behavior of the given masonry wall. However, the use of the 3D solid element led to large errors (27.5%) for the out-of-plane deformation of the sample wall. In contrast, the calculation error observed for the prediction of out-of-plane displacement associated with the shell element was much smaller (11%). Furthermore, if shell elements are used to model the ST-11 test structure instead of the 3D solid elements, far fewer elements are needed because the shell elements do not require the walls to be meshed in the thickness direction. As the result, the shell element (S4R) was chosen to

load, P , was taken as 100kips, and Poisson's ratio was taken as 0.25. This structure was analyzed using each of the elements discussed previously with mesh size of 4in. The three-dimensional solid element model consisted of 10500 elements and 48564 DOFs, while the shell element model consisted of 5250 elements and 32376 DOFs. Based on classical elastic theory, the lateral displacement at the top of the wall is given by:

$$u = \frac{P}{K} = \frac{Pl}{Gt} \left[1.2h \left(1 + \alpha \left(\frac{G}{E} \right) \left(\frac{h}{l} \right)^2 \right) \right] \quad (4.1)$$

where, K is the elastic stiffness of the wall; G is the shear modulus of masonry, which can be calculated as $E/2(1+\nu)$. The factor α is 3.33 for the cantilever wall. Therefore, the classical elastic solution for the lateral top displacement of the calculated wall is 0.0756in.

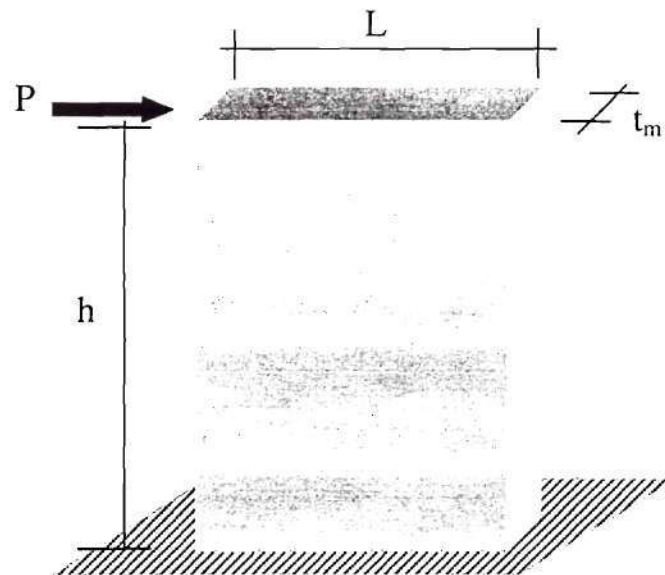


Figure 4.1. Cantilever wall model

- Locations of highly stressed zones in the masonry walls under lateral forces

4.2.1.1 Selection of Modeling Method

The FE model developed includes both the perforated masonry walls and the wood floor/roof diaphragms of the ST-11 test structure. Since the stud wall in the test structure only supports vertical loads and provides negligible lateral stiffness, the FE model omits the stud wall. The three-dimensional geometry of this model was developed using ABAQUS-CAE, a graphical interface program, while the external forces were entered manually into the input file. The commercially available ABAQUS finite element code was used to analyze the model, and ABAQUS-CAE was used as a to view the analysis results.

Both shell elements and three-dimensional solid elements were investigated for the analysis of the 3D test structure. The three-dimensional solid element used was the C3D8R element, which is an 8-node linear brick element with reduced integration. The shell element used was the S4R element, which is a 4-node doubly curved element with reduced integration. To assess the accuracy of these two elements, two simple structures were analyzed using each of these elements and the results were compared to classical solutions.

The first structure used to investigate the accuracy of the different elements was a simple cantilever wall with a concentrated load at the free end (see Figure 4.1). This structure was used to assess the ability of the elements to predict in-plane behavior. For the analysis the height, h , was taken as 280in, the length, L , was taken as 300in, the thickness, t , was taken as 8in, the elastic modulus, E , was taken as 1000ksi, the applied

The 3D FE elastic model was employed to obtain estimates of the elastic properties such as stiffness, and to provide insight into three-dimensional effects such as coupling between parallel walls and flange effects in the elastic range. The simplified dynamic conceptual model was developed to analyze the dynamic parameters of the test structure, such as natural frequencies and vibration mode shapes. The response of the test structure to seismic vibrations was also examined with this simple model. Based on the elastic properties from the above analyses and results from previous experimental research, a simplified nonlinear pushover model specially designed for the analysis of URM structures was developed. This model was generated to allow the strength, displacement capacity and damage progression of the in-plane walls to be investigated. Finally, a nonlinear FE analysis utilizing contact elements was employed to further study the failure modes and ultimate strength of the test structure. This method also serves as a benchmark for the other analysis tools.

4.2.1 Three Dimensional Elastic Finite Element Model

As briefly mentioned previously, a three-dimensional FE elastic analysis was utilized to provide insight into the test structures performance in the elastic range. Specifically, the objectives of this portion of the analysis were to obtain estimates of the following quantities:

- Gravity stresses in each pier
- Out-of-plane elastic stiffness of the masonry walls
- In-plane elastic stiffness of the masonry walls
- Coupling effect of the masonry walls
- Flange effect of the masonry walls

4 PRELIMINARY ANALYSIS

4.1 Objectives

Preliminary analyses have been conducted on the ST-11 unreinforced masonry building both before and after retrofit. The analyses were aimed at predicting the elastic and inelastic properties of this test building, such as the elastic stiffness, ultimate strength, displacement capacity, and the failure modes. The analyses also investigated the effect of several different retrofit methods, including the strengthening of the wood floor/roof system, and the use of FRP overlays and post-tensioning to improve the in-plane behavior of the masonry walls. The analysis results will be used as a guide prior to testing the ST-11 test structure, and be compared with the experiment results.

4.2 Analysis of URM Test Structure

This section outlines the extensive analytical study that was conducted in order to gain insight into the behavior of the test structure in the unreinforced state. The following four analysis methods were utilized to provide estimates of specific properties of the test structure.

- 3D finite element (FE) elastic model
- Simplified dynamic conceptual model
- Simplified nonlinear pushover model
- Nonlinear FE analysis employing contact elements

3.5 Instrumentation

Linear variable displacement transducers (LVDTs), strain gauges, and load cells will be used to measure the response of the test structure during loading. Specifically, the measured responses include:

- Global deformations of the structure, including lateral and vertical deformations of the diaphragms, in-plane deformations of the masonry walls, and out-of-plane deformations of the masonry walls
- Flexural, shear and axial deformations of selected individual piers
- Possible in-plane rocking and sliding deformations of individual piers
- Flexural, shear and axial deformations of selected spandrels
- Axial strain of FRP overlays on retrofitted piers
- Post-tensioning force in each tendon

All test data will be collected through a MEGADAC data acquisition system and stored for future analysis. Detailed drawings containing the location and types of gages for each loading case can be found in Appendix B.

3.6 Proposed Schedule

The construction of the test specimen was completed in early January 2002. The first series of tests is expected to be completed by mid-March 2002. The entire testing program will be concluded by early summer 2002.

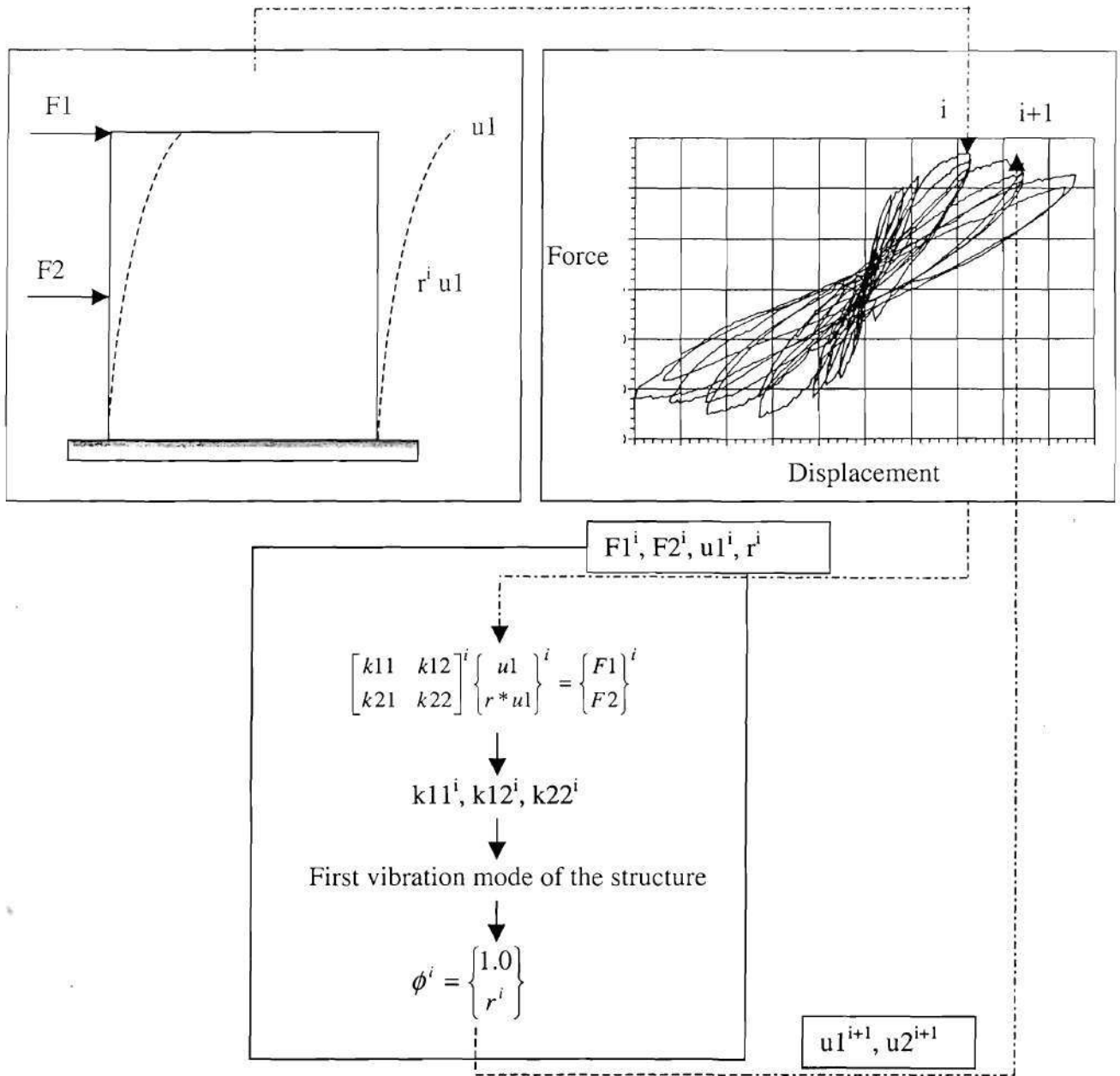


Figure 3.31. Modified stiffness displacement control scheme

4.2.2). However, it is important to note that the first vibration mode changes throughout loading due to damage accumulation, which results in a decrease in stiffness. Therefore, in order to apply realistic loads to the structure this evolution of the first mode must be addressed. To do this, the proposed loading sequence for each of the walls begins by imposing an inverted triangular displacement profile (i.e. assumed elastic mode shape, $r = 0.5$). The structure will be cyclically displaced in this profile to obtain the current desired maximum roof displacement, u_1^i . Based on these displacements and the applied forces F_1^i and F_2^i , the stiffness matrix of an equivalent elastic two-degree of freedom structure can be calculated. Next, by assuming a mass matrix for the wall based on tributary area, the updated first mode shape, ϕ^i can be calculated. The subsequent cycles of displacements are then imposed based on the updated first mode shape.

3.4.2 In-Plane Walls

The in-plane behavior of the masonry walls will be investigated before and after retrofit. To accomplish this, lateral displacements will be applied at the floor and roof levels of each in-plane wall. Initially the walls will be tested in the unreinforced state into the inelastic range to assess damage progression, critical members, and to validate current analytical tools (see Section 4.2). Following damage, selected critical piers in Walls 1, 2, and B will be strengthened with FRP overlays (see Section 3.3) and the walls will be retested in order to assess the effectiveness of the retrofit as well as any changes in damage progression or pier failure modes. These walls will be subjected to several cycles of damage, retrofit, and reloading in order to allow several retrofit schemes to be investigated and to validate current analysis tools (see Section 4.3). For the case of Wall A, once it has been loaded into the inelastic range to assess URM behavior, the wall will be post-tensioned with 20 psi, 40 psi, and 60 psi of additional vertical stress and retested. This series of tests is aimed at investigating the effect of different levels of post-tensioning stress on in-plane behavior. Preliminary analysis results suggest that at the high levels of vertical stress, the pier failure modes will be altered from rocking to diagonal tension. If this is observed, the piers will be retrofitted with FRP to suppress the diagonal tension failure (see Section 3.3).

The entire in-plane test will be conducted in displacement control. A modified stiffness control scheme will be employed to approximate the seismic forces on the structure. The concept of this control scheme is described in Fig. 3.31. Based on the results of the preliminary analysis and past experimental research it can be assumed that the first vibration mode controls the response of low-rise URM buildings (see Section

test step, the out-of-plane stiffness of Wall 1 can be calculated. A similar procedure will be utilized to obtain the out-of-plane elastic stiffness of Wall 2. Again, small displacements will be imposed in an attempt to ensure no damage occurs.

3.4.1.6 Test Step 1- 6

Following the portion of the testing program designed to investigate the behavior of a diaphragm composed of 1x6 straight sheathing, a 3/8" plywood overlay will be nailed to the top of the roof diaphragm. Uniformly distributed connections will be provided to connect the roof diaphragm with each of the masonry walls. This test setup is shown conceptually in Fig. 3.30.

Lateral cyclic displacements will be imposed at the center of the diaphragm in each direction. The stiffness of the retrofitted roof diaphragm will be obtained by measuring the combined stiffness of the system in each direct and subtracting out the stiffness of the out-of-plane walls (determined from the previous test steps).

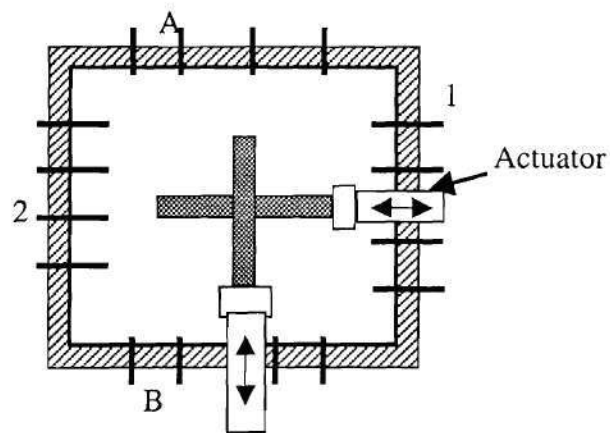


Figure 3.30. Testing of the retrofitted diaphragm

3.4.1.4 Test Step 1- 4

This test step is aimed at determining the stiffness of the entire diaphragm perpendicular to the joists. To accomplish this, uniformly distributed connections are provided between the roof diaphragm and Walls A and B. Furthermore, a 6 in. wide strip of the diaphragm will be removed adjacent to Walls 1 and 2 to allow the diaphragm to be tested independently. This test step is shown conceptually in Fig. 3.29.

Cyclic lateral displacements will be applied at the center of the entire diaphragm perpendicular to the joists. As a result, the stiffness of the entire diaphragm perpendicular to the joists can be measured. Again, small displacements will be imposed in an attempt to ensure no damage occurs.

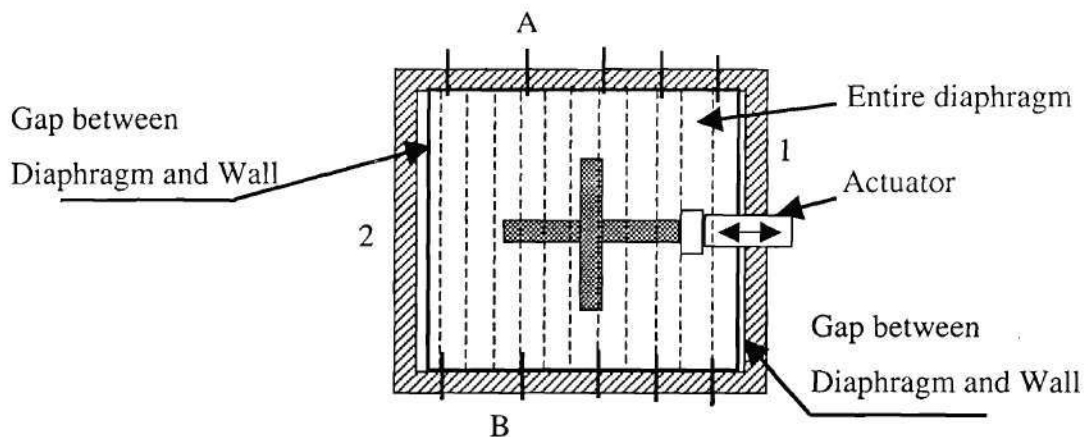


Figure 3.29. Testing of the entire diaphragm perpendicular to the joists

3.4.1.5 Test Step 1-5

Following Test Step 1-4 the portion of the diaphragm that was removed adjacent to Wall 1 will be replaced. In addition, connections will be provided between Wall 1 and the roof diaphragm. Cyclic displacements will then be imposed at the center of the diaphragm, parallel to Walls A and B, in order to measure the combined stiffness of Wall 1 and the diaphragm. Since the stiffness of the diaphragm is known from the previous

3.4.1.3 Test Step 1-3

Following Test Steps 1 and 2, the remaining half of the roof diaphragm will be constructed. Uniformly distributed connections will be provided to connect the roof diaphragm with all the four masonry walls. This test set up is conceptually shown in Fig. 3.28.

Lateral cyclical displacement will be applied parallel to Walls 1 and 2 at the center of the entire diaphragm. As a result the combined stiffness of the diaphragm and the out-of-plane walls A and B can be determined. The stiffness of the entire roof diaphragm parallel to the joists can then be calculated if the stiffness of Wall B is assumed to be equal to that of Wall A (recall the stiffness of Wall A is known from the first two test steps). This assumption is reasonable since Walls A and B have the same configuration. In addition, the number of connections between the roof diaphragm and Walls 1 and 2 will be changed to investigate its effect on the stiffness of the entire diaphragm. Again, small displacements will be imposed in an attempt to ensure no damage occurs.

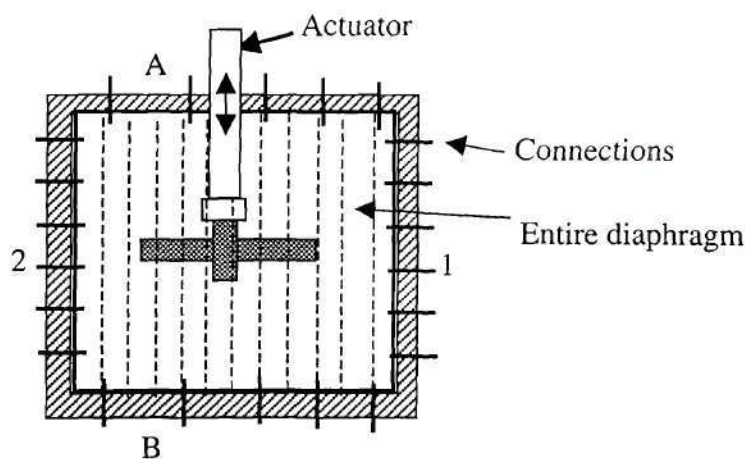


Figure 3.28. Testing of the entire diaphragm parallel to the joists

then displaced in the opposite direction and the combined stiffness of the diaphragm and Wall A is measured. This allows the stiffness of Wall A to be calculated. It should be noted that the displacements imposed during this test step will be relatively small to ensure that both Wall A and the diaphragm remain in the elastic range. Furthermore, it is expected that several configurations of the connections to Walls 1 and 2 will be employed to investigate possible difference.

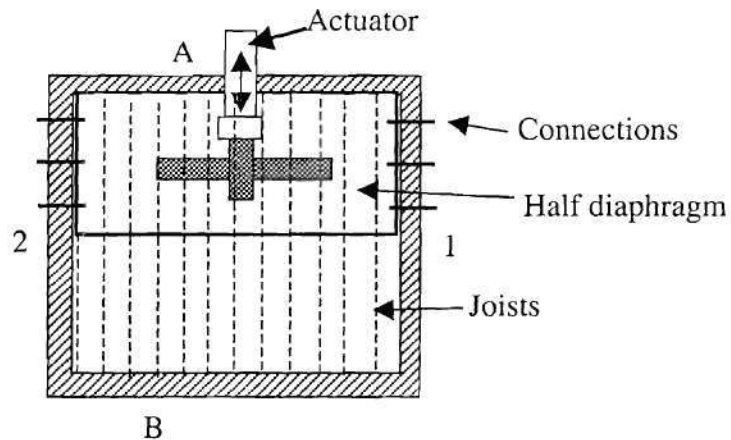


Figure 3.27. Testing of half the roof diaphragm parallel to the joists

3.4.1.2 Test Step 1-2

This test step is very similar to Test Step 1 except that uniformly distributed connections are supplied between the joists and Wall A. Cyclic lateral displacements will be applied parallel to Walls 1 and 2 in order to assess the effect of joist connections on the out-of-plane behavior of Wall A and the behavior of the diaphragm. Again, small displacements will be imposed to prevent damage to the structure.

Table 3.10. Summary of the diaphragm and out-of-plane wall test steps

Test step	Brief description of test step
1-1	Test of half the diaphragm (24ft x 12 ft) parallel to the direction of the joists
1-2	Test of the half diaphragm (24ft x 12 ft) connected with out-of-plane wall A
1-3	Test of the entire diaphragm perpendicular to the direction of the joists including diaphragm connections.
1-4	Test of the entire diaphragm parallel to the direction of the joists
1-5	Test of the entire diaphragm parallel to the direction of the joists, including diaphragm connections.
1-6	Test of the entire diaphragm (24ft x 24 ft) after the addition of plywood blocking.

3.4.1.1 Test Step 1-1

In this test step half of the roof diaphragm is to be tested parallel to the joists. In order to permit this, only half of the diaphragm was constructed. Although the joists for the entire roof diaphragm were placed during construction, no nails were supplied between the stud wall and joists so as to allow half of the diaphragm to be tested independently. To transfer the load to the in-plane walls and eventually to the foundation, anchors will be supplied along Walls 1 and 2. This test step is conceptually shown in Fig. 3.27.

During this test step the lateral force is applied at the center of the diaphragm parallel to Walls 1 and 2. At first the diaphragm is displaced away from Wall A to allow the stiffness of just the diaphragm to be determined. That is, Wall A will only offer frictional restraint in this direction, which should be relatively small. The diaphragm is

3.4 Test Sequence

The test sequence of the ST-11 building is divided into two separate test cases, which are: 1) the testing of the roof diaphragm and the out-of-plane walls and 2) the testing of the in-plane walls before and after retrofit. The loading sequence and a discussion of each of these test cases are presented in the following sections.

3.4.1 Diaphragm and Out-of-plane Walls Tests

The objectives of this test sequence are as follows:

1. Measure the elastic stiffness of half of the total diaphragm (24ft x 12 ft) along the direction of the joists, and compare with the test results of specimen MAE2 obtained from project ST-8.
2. Investigate the orthotropic elastic behavior of the entire diaphragm (24ft x 24ft), including the elastic stiffness parallel and perpendicular to the joists.
3. Investigate the effect of supplying diaphragm-to-wall connections on the behavior of the diaphragm and out-of-plane wall.
4. Investigate the effect of the addition of a plywood overlay to the top of the diaphragm on the behavior of the diaphragm and out-of-plane wall.
5. Measure the out-of-plane elastic stiffness of all four masonry walls in the ST-11 test structure.

To fulfill the above goals, this test case is subdivided into a series of test steps which are present in Table 3.10. The following sections outline each of these test steps in detail.

Table 3.8 Summary of prism test results

Prism configuration	Mean prism strength (psi)	Standard deviation	Coefficient of variation
All solid	1457.70	364.47	0.25
3 solid, 2 cored	947.59	79.34	0.08
2 solid, 3 cored	989.62	98.93	0.10
All cored	592.81	51.84	0.09

From the table it is apparent that the longitudinal core greatly effects prism strength. In addition to the large strength difference, the failure modes for the solid and cored prisms were different. The solid prisms failed due to a vertical crack through the width of the prism while the cored prisms failed due to a vertical longitudinal crack along the length of the prism. Based on these results, the two types of bricks were separated and used for different stories of the test structure as described in Section 3.2.7.

3.3.3 Brick Compressive Tests

Compressive test on both the solid and cored bricks were conducted based on ASTM C67-00, Standard Test Methods for Sampling and Testing Brick and Structural Clay Tile. In all, ten bricks were tested (5 solid and 5 cored). A summary of the results is presented in Table 3.9.

Table 3.9. Summary of brick compression results

Brick type	Mean compression strength (psi)	Standard deviation	Coefficient of variation
Solid	6030.75	1414.79	0.23
Cored	5285.82	1655.60	0.31

specimens. By comparing the tests result it is seen that the direct shear test gives shear strength between 42% and 56% of those given by ASTM E519-00. It should be mentioned that a larger amount of scatter was expected in the direct shear test results due to a decrease in shear area. As a result, the 0.5: 2: 9 mortar was chosen because the apparent ASTM E519-00 shear strength would be between 108 psi and 143 psi. Since this strength is approximately the same as the Type N shear specimens, the likelihood of cracking in the bricks is small. Furthermore, the 0.25: 2: 9 mortar was eliminated from consideration because of difficult in handling the specimens and exceptionally large scatter in the data (i.e. coefficient of variation of 0.77).

3.3.2 Prism Tests

Compression tests were conducted according to ASTM C1314-00, Standard Test Method for Compressive Strength of Masonry Prisms. These tests had two purposes: 1) assess the effect of the longitudinal core (contained in half of the donated bricks) on compression strength (see Fig. 3.17) and 2) determine the compression strength of masonry. To accomplish these objectives three five-brick prisms were tested for each of four configurations: all solid bricks, all cored bricks, alternating solid and cored bricks (three solid, two cored), and alternating solid and cored bricks (two solid, three cored). The test results for each of the four configurations in given in Table 3.8.

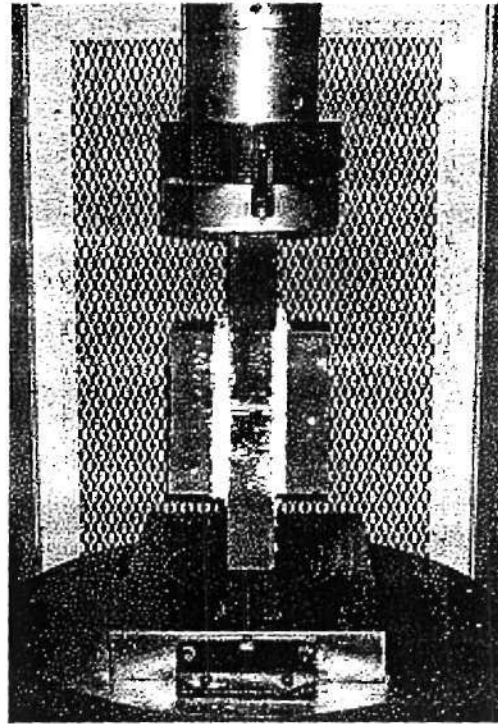


Figure 3.26 Direct shear test setup.

Table 3.7. Summary of Direct Shear Tests

Type of Brick	Mortar (portland cement:lime:sand)	Shear Strength (psi)	Standard Deviation
Cored	0.25:2:9	22	17
Solid	0.25:2:9	22	-
Cored	0.5:2:9	53	16.5
Solid	0.5:2:9	60	-
Cored	1:2:9	87	12
Solid	1:2:9	118	-

In order to compare the strengths given by the direct shear test to those obtained from the ASTM E519-00 test method, Type O mortar was used in three of the direct shear

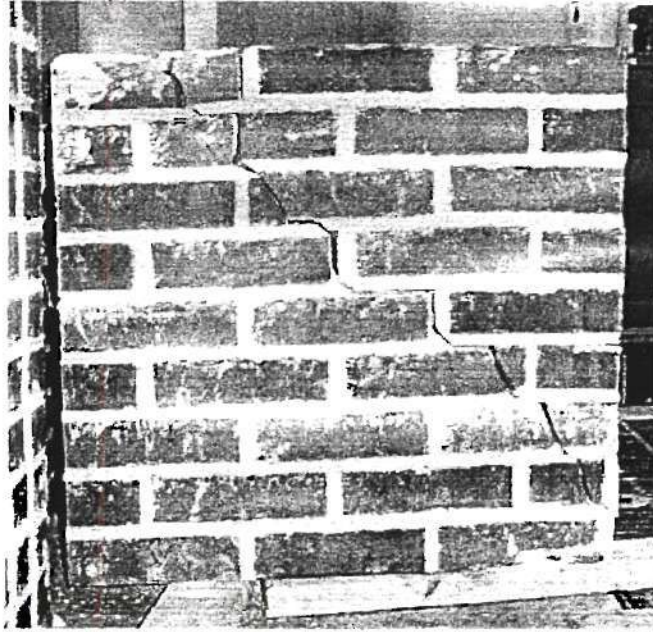


Figure 3.25. Photograph of shear failure through brick.

As a result, the third series of tests were aimed at obtaining a mortar mix that would cause a “strong brick-weak mortar” behavior. To accomplish this the amount of Portland cement was varied while keeping the amount of sand and lime constant. The three mortars that were tested were: 0.25: 2: 9, 0.5: 2: 9, and 1: 2: 9 (Portland cement: lime: sand). In all nine specimens were tested, three of each type of mortar (one solid and two cored). Due to a shortage of bricks, a direct shear test was used instead of the ASTM E519-00. Fig. 3.26 shows a photograph of the direct shear test setup. Table 3.7 gives a summary of the results.

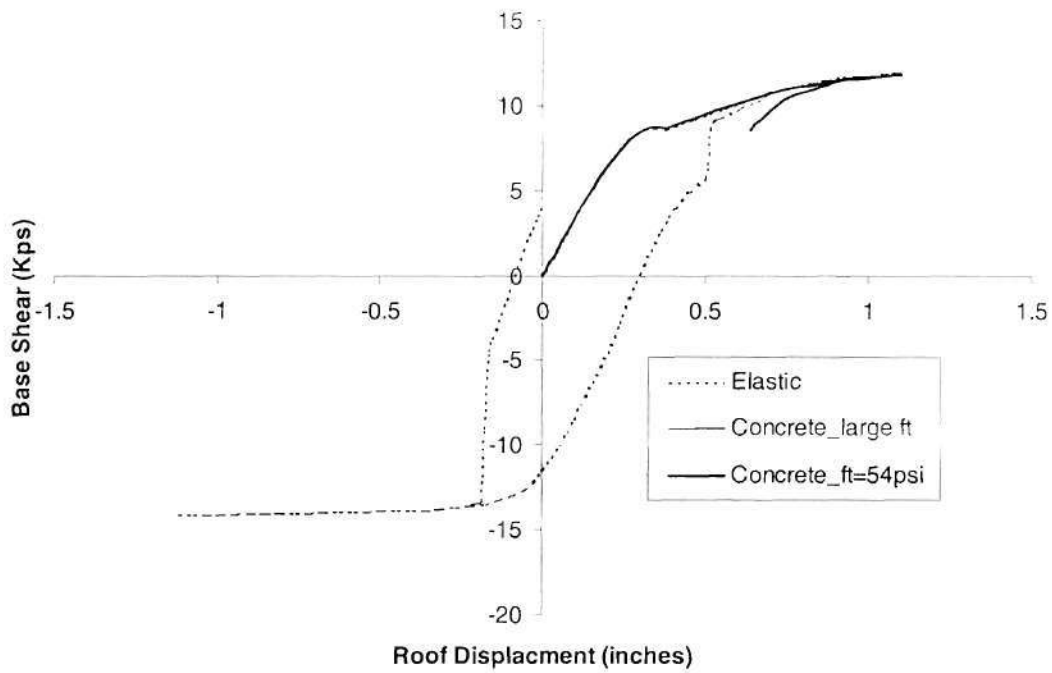


Figure 4.50. Force–displacement response of Wall 2 with different masonry properties (beginning with push to the right)

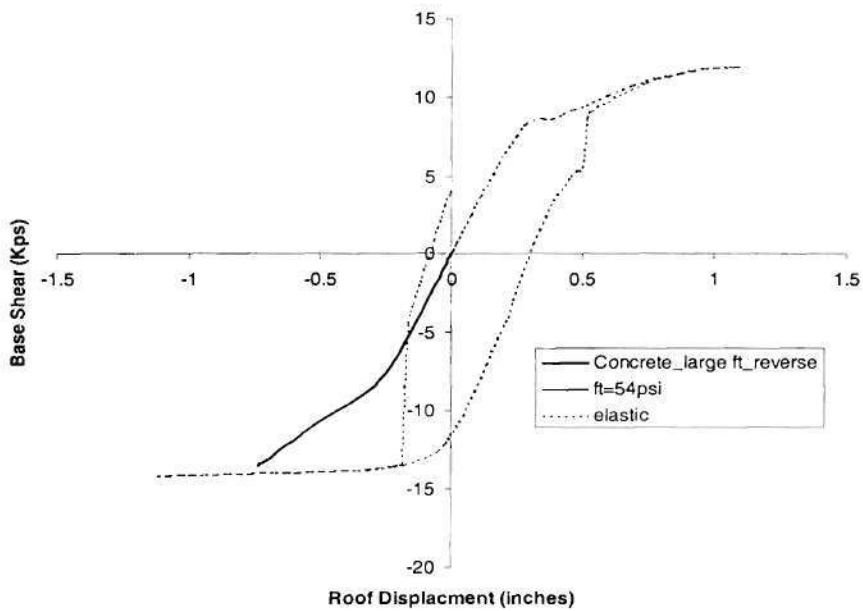


Figure 4.51. Force–displacement response of Wall 2 with different masonry properties (beginning with push to the left)

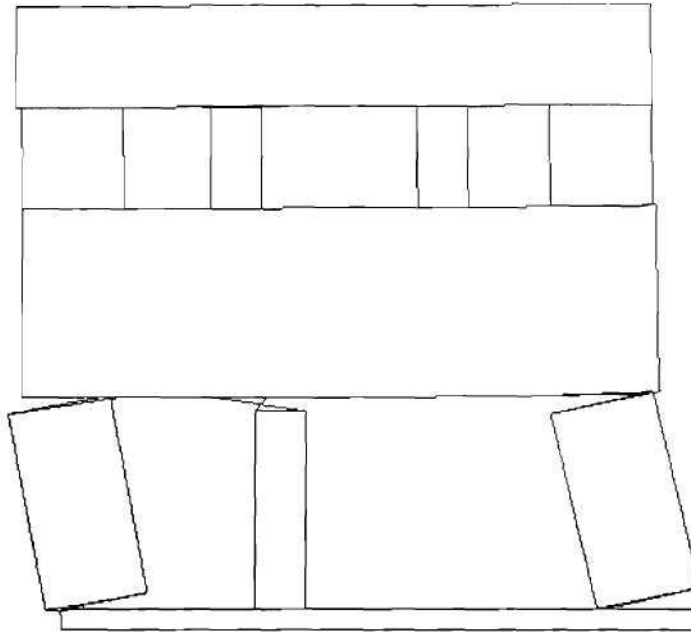


Figure 4.48. Deformed shape of Wall 2 (loaded to the left)

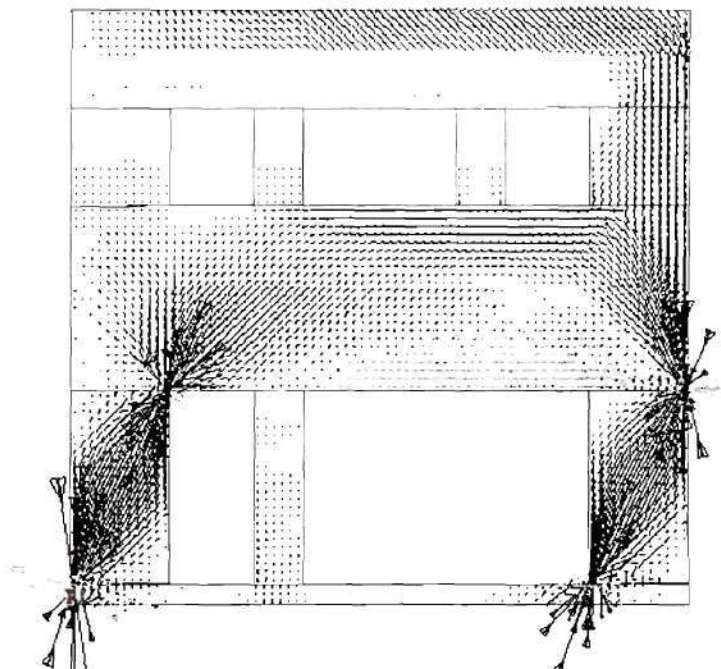


Figure 4.49. Stress contour of Wall 2 (loaded to the left)

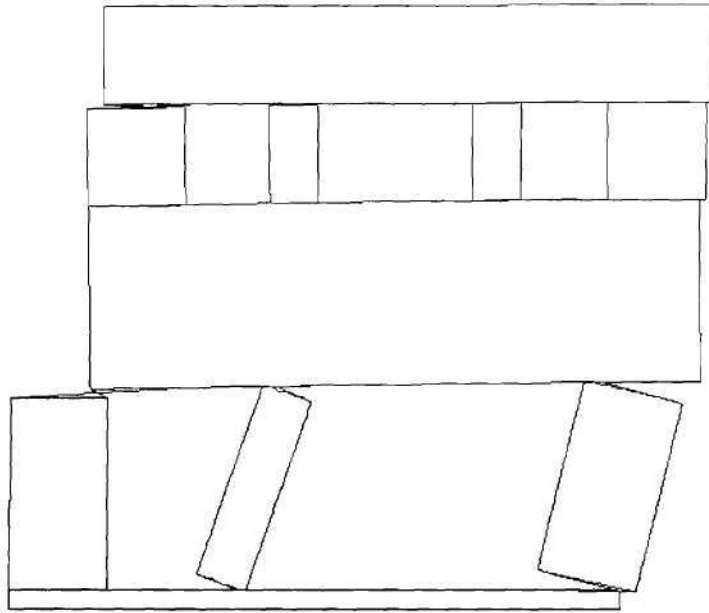


Figure 4.46. Deformed shape of Wall 2 (loaded to the right)

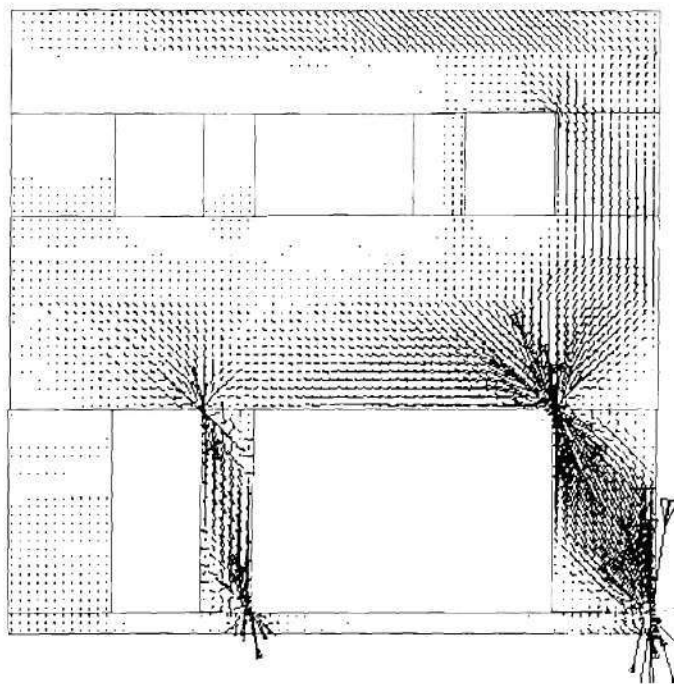


Figure 4.47. Stress contour of Wall 2 (loaded to the right)

The table shows that altering the properties of the masonry has a negligible effect on the ultimate strength of Wall 2. This suggests that diagonal tension and toe crushing failures do not govern the behavior of Wall 2. Again the ultimate strengths seem reasonable when compared with the simplified approximation. It is noted that the calculated strength are relative small compared to these values; however, this expected due to the slender nature of the piers and the rocking dominated behavior.

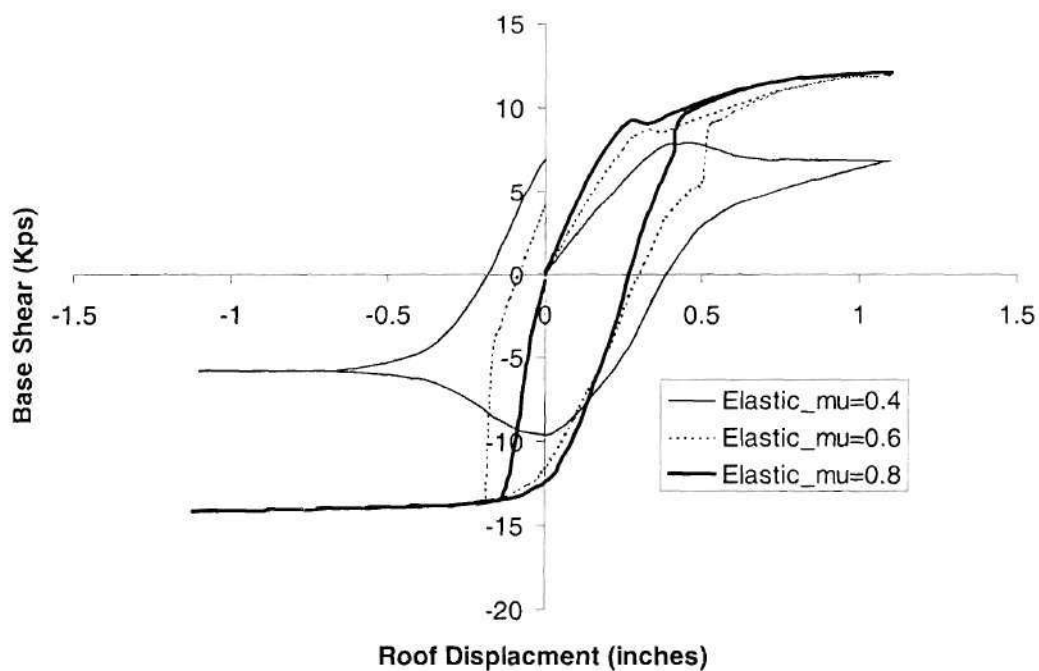


Figure 4.45. Force–displacement response of Wall 2 with different friction coefficients

4.2.4.3.2 Nonlinear FE Analysis Results of Wall 2

The analysis results of Wall 2 again show that variations of the bed-joint friction coefficient significantly affect the overall wall behavior (see Fig. 4.45). As the friction coefficient is increased area of the hysteresis loops become smaller. This means less energy is being dissipated and suggests that the behavior is gradually switching from sliding to rocking. In addition this switching of failure modes explains why the strength does not increase when the friction coefficient is increased from 0.6 to 0.8, since frictional resistance does not affect rocking.

The deformed shapes and stress contours corresponding to the different loading directions are shown in Figs. 4.46 to 4.49, which correspond to a friction coefficient of 0.6. As expected unsymmetrical behavior was observed with Piers 2-7 and 2-9 rocking when the wall is loaded towards the left, and Piers 2-8 and 2-9 rocking when the wall is loaded to right.

The hysteretic force – displacement behavior of Wall 2 (with a friction coefficient of 0.6) is shown in Figs. 4.50 and 4.51 for different masonry properties. The calculated ultimate strengths for both loading directions are listed in Table 4.27. For comparison purposes the strength estimates of Wall discussed in Section 4.2.3.7 are present as well.

Table 4.27. Calculated ultimate strength of Wall 2

Methods	Ultimate Strength when pushed to the right (kip)	Ultimate Strength when pushed to the left (kip)
Elastic	12.0	14.2
Concrete material with high tensile strength	11.8	13.5
Concrete material (tensile strength = 54psi)	11.8	13.5
Strength Estimate	20	20

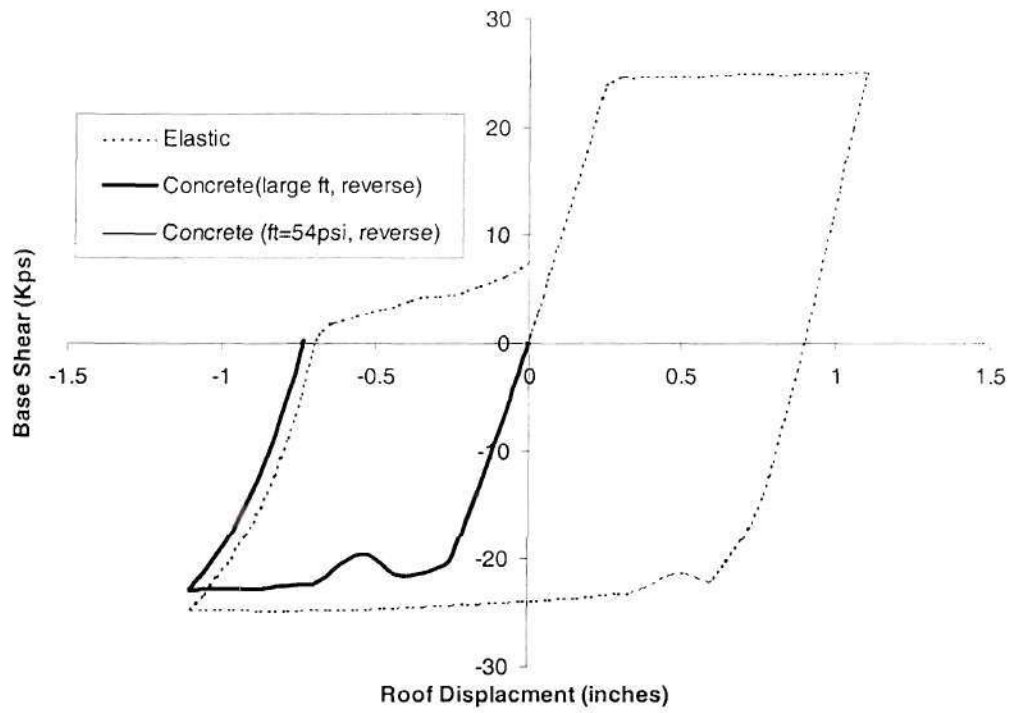


Figure 4.44. Force–displacement response of Wall 1 with different material properties (beginning with push to the left)

- Hinkley, A. T. (1996) "Tests on One-story Prestressed Brickwork Shear Walls", New Zealand Engineering, June, pp245-252.
- Hobbs, B. and Y. Daou (1988) "Post-tensioned T-Section Brickwork Retaining Walls," 8th International Brick and Block Masonry Conference, Dublin, Ireland, pp665-675.
- Huizer, A. and N. G. Shrive (1986) "Performance of a Post-tensioned, Single-Wythe, Clay Brick Masonry Wall Tested in Shear," Fourth Canadian Symposium, Fredericton, N.B., Vol. 2, pp. 609-619.
- Jabarov, M., Kozharinov, S.V., and Lunyov, A. A. (1980) "Strengthening of damaged masonry by reinforced mortar layers." Proc. 7th World Conf. on Earthquake Engrg., Vol. 4, Turkish Nat. Committee on earthquake Engrg., Ankara, Turkey. 73-80.
- Jai, J. and G. S. Springer (2000) "Reinforcing Masonry Walls with Composite Materials- Test Results", Journal of Composite Materials, Vol. 34, No. 16, pp.1369-1381.
- Jai, J. and G. S. Springer (2000) "Reinforcing Masonry Walls with Composite Materials- Model", Journal of Composite Materials, Vol. 34, No. 18, pp.1548-1581.

Hegemier, G.A, et al. (1978)., “ On the behavior of joints in concrete masonry”, Proc., North Amer. Masonry Conf., Boulder, Colo., Aug.

Hendry, A.W., and Sinha,B.P. (1969), “Shear tests on full-scale single-storey Brickwork structures subjected to Precompression”. The British Ceramic Research Association, Tech. Note 134

Hidalgo, P.A., and McNiven, H.D. (1979), “ Seismic Behavior of masonry Piers”, 1979 Earthquake Eng Res Inst Berkeley, Calif p 303-312.

Hidalgo, P.A., Mayes, R.L., McNiven, H.D. and Clough, R.W. (1978), “Cyclic Loading Tests of Masonry Single Piers, Volume 1 – Height to Width Ratio of 2”, EERC Report No. 78/27, University of California, Berkeley.

Hidalgo, P.A., Mayes, R.L., McNiven, H.D. and Clough, R.W. (1978), “Cyclic Loading Tests of Masonry Single Piers, Volume 3 – Height to Width Ratio of 0.5”, EERC Report No. 78/29, University of California, Berkeley.

Hilsdorf, H.K. (1969), “ Investigation into the failure mechanism of brick masonry loaded in axial compression”, in : Designing, engineering and constructing with masonry products, eds, F.H. Johnson, Gulf Publishing Company, Houston, Texas, USA, pp 34-41

Gulkan, Polat, Ray H., Mayes Ronald L, and Clough (1979), " Shaking table study of Single-story Masonry Houses", Volume 2: Test Structures 3 and 4", Report No. UCB/EERC-79/24.

Hamid, Ahmad A., Drysdale, Robert C.(1980), " Behavior of brick masonry under combined shear and compression loading", Proc. 2nd Canadian Masonry Symp., Ottawa, Canada, June

Hamilton III, H.R. (2000), "Hybrid FRP/steel strengthening of unreinforced Masonry structures NSF Unsolicited Proposal #1043269", University of Wyoming.

Hamilton, H. R., C. W. Dolan (2001) "Flexural Capacity of Glass FRP Strengthened Concrete Masonry Walls" Journal of Composites for Construction, Vol.5, No. 3, pp170-178.

Hamoush, S. A., M. W. McGinley, P. Mlakar, D. Scott, and K. Murray. (2000) "Out-of Plane Strengthening of Masonry Walls with Reinforced Composites" Journal of Composites for Construction, Vol. 5, No. 3, pp139-145.

Hart, G.C., Kariotis, J., and Noland, J.L. (1988), " The Whittier Narrows, California Earthquake of October 1, 1987 – Masonry Buildings Performance Survey", Earthquake Spectra, Vol, 4., N0.1, pp 181-196

- Garrity, S. W. and M. E. Phipps (1987) "A Study of the Effect of Vertical Prestress on the Horizontal Flexural Strength of Clay Brickwork" Proceedings of the Fourth North American Masonry Conference, pp28.1-28.14
- Ghobarah, A. and T. Baumer (1992) "Seismic Response and Retrofit of Industrial Brick Masonry Chimneys", Canadian Journal of Civil Engineering. Vol. 19, pp. 117-128.
- Gilstrap, J. M. and C. W. Dolan (1998) "Out-of-Plane Bending of FRP-Reinforced Masonry Walls", Composites Science and Technology, Vol. 58, pp. 1277-1284.
- Graham, K. J. and A. W. Page (1995) "The Flexural Design of Post-tensioned Hollow Clay Masonry", Seventh Canadian Masonry Symposium, McMaster University, Hamilton, Ontario, pp.763-773.
- Graham, K. J. and A. W. Page (1994) "An Experimental Study of The Flexural Behavior of Post-tensioned Hollow Clay Masonry", 10th International Brick and Block Masonry Conference, Calgary, Alberta, pp.639-648.
- Gulkan, Polat, Ray H., Mayes Ronald L, and Clough (1979), " Shaking table study of Single-story Masonry Houses", Volume 1: Test Structures 1 and 2", Report No. UCB/EERC-79/23.

Frederick P. Spalding , A. Lincoln Hyde and MAJOR Ernest F. Robinson (1926), “Masonry Structures”, press of Braunworth & CO., INC, New York.

Garrity S. W. and T. G. Garwood (1994) “The Testing of a Deep Prestressed Brickwork Diaphragm Wall to failure”, Proceedings of the British Masonry Society, No. 6, pp.244-247.

Garrity, S. W. and T. G. Garwood (1993) “Further Testing of a Prestressed Brickwork Bridge Abutment”, The Sixth North American Masonry Conference, Philadelphia, Pennsylvania, pp633-644.

Garrity, S. W. and T. G. Garwood (1991) “Prestressed Clay Brickwork Bridge Abutments”, The Masonry Society Journal, August, pp75-82.

Garrity, S. W. and T. G. Garwood (1990) “Prestressed Clay Brickwork Abutments”, Fifth North American Masonry Conference, University of Illinois, Urbana-Champaign, pp1135-1146.

Garrity S. W. and T. G. Garwood (1990) “The Construction and Testing of a Full-Scale Prestressed Clay Brickwork Diaphragm Wall Bridge Abutment”, Proceedings of the British Masonry Society, No. 4, pp.24-29.

Ehsani, M.R., Saadatmanesh, H. and Al-Saidy, A.,(1997) “Shear Behavior of URM Retrofitted with FRP Overlays,” Journal of Composites for Construction, Vol.1, No. 1, ASCE, New York, NY.

Epperson,G.S., Abrams, D.P. (1989) . “Nondestructive evaluation of masonry buildings”, Advanced construction Technology center, Report No. 89-26-03, UIUC, 208pp

Epperson,G.S., Abrams, D.P. (1992) . “Evaluating of Lateral Strength of Existing Unreinforced Brick Piers in the Laboratory”, TMS Journal, February 1992, pp 86-93

Eurocode 6, “ Design of masonry structures, Part 1-1: General rules for buildings. Rules for reinforced and unreinforced masonry”, ENV 1996-1-1: 1995, CEN, Brussels, 1995

Fisher, K., B. A. Haseltine, and W. Templeton (1989) “Structural Testing of Brickwork Retaining Walls”, 5th Canadian Masonry Symposium, Vancouver, B.C.,pp. 827-837.

Franklin, S., J. Lynch, and D. Abrams (2001) “Performance of Rehabilitated URM Shear Walls: Flexural Behavior of Piers”

- Deppe, K (1988), "The Whittier Narrows, California Earthquake of October 1, 1987 – Evaluation of strengthened and unstrengthened unreinforced Masonry in Los Angeles City", *Earthquake Spectra*, Vol, 4., N0.1, pp 157-180
- Devalapura, R. K., G. L. Krause, and M. K. Tadros (1999) "A Study on the Deflection of Prestressed Masonry Walls" *The Masonry Society Journal*, November, pp21-31.
- Devalapura, R. K., G. L. Krause, and M. K. Tadros (1996) "Development and Testing of Prestressed Clay Brick Walls" *The Masonry Society Journal*, August, pp 99-112.
- Drysdale, Robert G., and Essawy, S. (1988), "Out-of-plane Bending of concrete Block Walls", *Journal of structural Engineering*, vol. 114, N0.1, Jan, pp121-133
- Ehsani, M.R. and H. Saadatmanesh (1996) "Seismic Retrofit of URM Walls with Fiber Composites", *The Masonry Society Journal*, 14(2), 63-72.
- Ehsani, M.R. (1995) "Strengthening of Earthquake-Damaged Masonry Structures with Composite Material" *Non-metallic (FRP) Reinforcement for Concrete Structures*.pp680-687.
- Ehsani, M. R., Saadatmanesh, H., and Velazquez-Dimas, J.I. (1999). "Behavior of Retrofitted URM Walls under Simulated Earthquake Loading," *ASCE J. of Composite Construction*, 3(3), 134-142.

Countryman, D. (1955). "1954 Horizontal Plywood Diaphragm Tests", Laboratory Report 63. Douglas Fir Plywood Association.

Costley, A.C., and Abrams, D.P. (1996), "Dynamic Response of Unreinforced Masonry Buildings with Flexible Diaphragms.", NCEER-96-0001.

Curtin, W. G., and J. Howard (1998) "Lateral Loading Tests of Tall Post-tensioned Brick Diaphragm Walls" 8th International Brick and Block Masonry Conference, Dublin, Ireland, pp.665-675.

Curtin, W. G., G. Shaw, and J. Howard (1991) "Structural Testing of a Post-tensioned Brick Fin Wall," 9th International Brick and Block Masonry Conference, Berlin, Germany, pp.333-341.

Dawe, J. L. and G. G. Aridru (1992) "Post-tensioned Concrete Masonry Walls Subjected to Uniform Lateral Loading", 6th Canadian Masonry Symposium, Saskatoon, Saskatchewan, pp. 201-212.

Davidson, E.B., and Wang, L.R.L. (1985), "A study of the cyclic lateral resistance of low rise masonry wall panels", Proceedings of the Third North American Masonry Conference, Arlington, Tex., pp 48-1 to 48-15.

Chiostrini, S., Foraboschi, P., and Sorace, S., “ Problems Connected with the Arrangement of a Non-linear Finite Element Method to the Analysis of Masonry Structures”, Structural Repair & Maintenance of Historical Buildings, pp 525-534.

Chen, S-W.J., Hidalgo, P.A., Mayes, R.L., Clough, R.W., and McNiven, H.D. (1978), “ Cyclic Loading Tests of Masonry Single Piers, Volume 2 – Height to Width Ratio of 1”, EERC Report No. 78/28, University of California, Berkeley.

Clough, Ray H., Mayes Ronald L, and Gulkan, Polat (1979), “ Shaking table study of Single-story Masonry Houses”, Volume 3: Summary, Conclusions, and Recommendations”, Report No. UCB/EERC-79/25.

Colunga, Tena, Arturo (1992), “Seismic Evaluation of Unreinforced Masonry Structures with Flexible Diaphragms”, Earthquake Spectra, Vol. 8, No 2, pp305-318

Colunga, A. Tena and Abrams, D.P. (1992), “ Response of unreinforced masonry building during the Loma Prieta Earthquake”, Tenth World Conference on Earthquake Engineering, Balkema, Rotterdam. pp 79-84

Countryman, D. (1952). “Lateral Tests on Plywood Sheathed Diaphragms”, Laboratory Report 55, Douglas Fir Plywood Association.

Bruneau M. (1994), "State-of-the-art report on seismic performance of Unreinforced masonry buildings", Journal of structural Engineering. Vol 120, No. 1 , pp230-251

Bruneau M. (1995), "Performance of masonry structures during the 1994 Northridge(Los Angeles) earthquake", Canadian Journal of Civil Engineering. Vol 22, pp378-402

Calvi, G.M., Magenes, Gi., Magenes, Gu., and Pavese, A. (1992), "Experimental and numerical investigation on a brick masonry building prototype – Report 1.1 – Design of the Experimental Tests," Dipartimento di Meccanica Strutturale dell'Universita di Pavia.

Calvi, G.M., Magenes, G., Pavese, A., and Abrams, D.P. (1994), "Large-Scale Seismic Testing of an Unreinforced Brick Masonry Building," Proceedings, Fifth U.S. National Conference on Earthquake Engineering, Chicago, pp. 10.

Calvi, G.M., etc. (1995), "Experimental and numerical investigation on a brick masonry building prototype – Report 3.0 – Numerical prediction of the experiment".

Calvi, G. Michele, Gregory R. Kingsley, and Guido Magenes (1996), "Testing of Masonry Structures for Seismic Assessment", Earthquake Spectra, Volume 12, No.1, pp 145-162.

Baqi, A., N. M. Bhandari, and D. N. Trikha (1999) “Experimental Study of Prestressed Masonry Flexural Elements”, ASCE Journal of Structural Engineering, Vol. 125, No. 3, pp.245-254.

Beall, Christine, “ Masonry design and detailing, for architects, engineers, and constructors”, McGRAW-HILL, INC, third edition, 1993

Benedetti, D. and Benzoni,G.M. (1984), “ A numerical Model for seismic analysis of Masonry Buildings: Experimental Correlations”, Earthquake engineering And Structural Dynamics, Vol 12, pp817-831

Boussabah, L. and Bruneau, M.(1992), “ Review of the seismic performance of Unreinforced masonry wall”, 10 th world conference on Earthquake Engineering, Balkema, Rotterdam, pp 4537-4540

Bruneau M.(1990), “Preliminary report of structural damage from the Loma Prieta (San Francisco) earthquake of 1989 and pertinence to Canadian Structural engineering practice”, Canadian Journal of Civil Engineering. Vol 17, pp198-208.

Bruneau M. and Murat Saatcioglu (1994), “Behavior of Unreinforced Masonry Structures During the 1992 Erzincan, Turkey, Earthquake”, TMS Journal, pp 79-87.

Bruneau M. (1994), “Seismic evaluation of Unreinforced masonry buildings – a state –of-the-art report”, Canadian Journal of Civil Engineering. Vol 21, pp512-539

Abrams, D.P., and Shah, N. (1992), "Cyclic load testing of unreinforced masonry walls",
College of engineering, university of Illinois at Urbana, Advanced Construction
Technology Center Report #92-26-10

Adham, S.A., (1985b), "Out-of-plane response of masonry walls", Proceedings of the
Third North American Masonry Conference, Arlington, Tex., pp 47-1 to 47-14.

Anthoine, A., Magoneete, G., and Magenes, G. (1995), "Shear-compression testing and
analysis of brick masonry walls," Proceedings of the 10th European Conference
on Earthquake Engineering, Duma, editor, Balkema:Rotterdam, The Netherlands.

Atkinson, R.H., Amadei, B.P., S.Saeb, S. Sture (1989), "Response of Masonry Bed Joints
in Direct Shear", Journal of structural Engineering, vol 115, No 9., pp2276-2296

Ballio, G., Calvi, G.M., and Magenes, G.(1993), "Experimental and numerical
investigation on a brick masonry building prototype – Report 2.0 – Program of
scientific cooperations," Dipartimento di Meccanica Strutturale dell'Universita di
Pavia

Bariola, J., Ginocchio, J.F., and Quiun, D. (1990), "Out-of-plane response of brick
walls". Proceedings of the fifth North American Masonry Conference, Urbana-
Champaign, III, Vol.1, pp.429-439

Applied Technology Council (ATC) (1997). "NEHRP Commentary on the Guidelines for the Seismic Rehabilitation of Buildings", Publication No. 274, Federal Emergency Management Agency, Washington, D.C. (FEMA-274).

Applied Technology Council (ATC) (1999). "Evaluation of earthquake damaged concrete and masonry wall buildings, Basic procedures manual", Publication No. 306, Federal Emergency Management Agency, Washington, D.C. (FEMA-306).

Applied Technology Council (ATC) (1999). "Evaluation of earthquake damaged concrete and masonry wall buildings, Technical Resources", Publication No. 307, Federal Emergency Management Agency, Washington, D.C. (FEMA-307).

Applied Technology Council (ATC) (2000). "Prestandard and commentary for the seismic rehabilitation of buildings", Publication No. 356, Federal Emergency Management Agency, Washington, D.C. (FEMA-356).

Abrams D. P. (1988), " Dynamic and static testing of reinforced concrete masonry structures", TMS journal, pp T18-T22

Abrams D. P. (1992), " Strength and Behavior of unreinforced masonry elements", 10 th world conference on Earthquake Engineering, Balkema, Rotterdam, pp 3475-3480

Al-Hashimi and W. G. Curtin (1988) "Principal Tensile Strength and Vertical Shear Resistance of High-Strength Brickwork," 8th International Brick and Block Masonry Conference, Dublin, Ireland, pp.571-582.

Al-Manaseer, A. A., and V. V. Neis (1987) "Load Tests on Post-Tensioned Masonry Wall Panels", ACI Structural Journal, November-December, pp 467-472.

Ambrose, R. J., R. Hulse, and S. Mohajery (1998) "Cantilevered Prestressed Diaphragm Walling Subjected to Lateral Loadingm," 8th International Brick and Block Masonry Conference, Dublin, Ireland, pp.583-594.

APA – The Engineered Wood Association (APA) (1985). "Design/Construction Guide Residential and Commercial", Tacoma Washington.

APA – The Engineered Wood Association (APA) (1986). "Plywood Design Specification", Tacoma, Washington.

Applied Technology Council (ATC) (1997). "NEHRP Guidelines for the Seismic Rehabilitation of Buildings", Publication No. 273, Federal Emergency Management Agency, Washington, D.C. (FEMA-273).

6 REFERENCES

- ABK. (1981a). "Methodology for mitigation of seismic hazards in existing unreinforced masonry buildings: diaphragm testing". ABK-TR-03, Agbabian & Associates, S.B. Barnes & Associates, and Kariotis & Associates, EI Segundo, Calif.
- ABK. (1981b). "Methodology for mitigation of seismic hazards in existing unreinforced masonry buildings: wall testing, out-of-plane". ABK-TR-04, Agbabian & Associates, S.B. Barnes & Associates, and Kariotis & Associates, EI Segundo, Calif.
- ABK. (1984). "Methodology for mitigation of seismic hazards in existing unreinforced masonry buildings: the methodology". ABK-TR-08, Agbabian & Associates, S.B. Barnes & Associates, and Kariotis & Associates, EI Segundo, Calif.
- Albert, M. L., A. E. Elwi, and J. R. Cheng (2001) "Strengthening of Unreinforced Masonry Walls Using FRPs", *Journal of Composites for Construction*, Vol. 5, No. 2, pp 76-83.

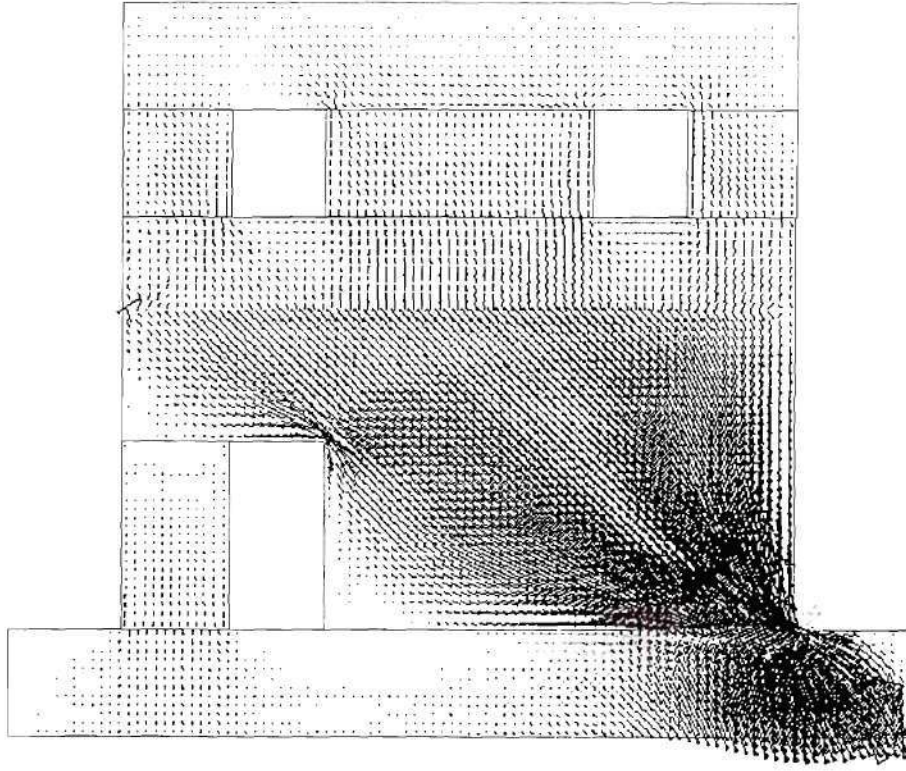


Figure 4.42. Stress contour of Wall 1 (loaded to the right)

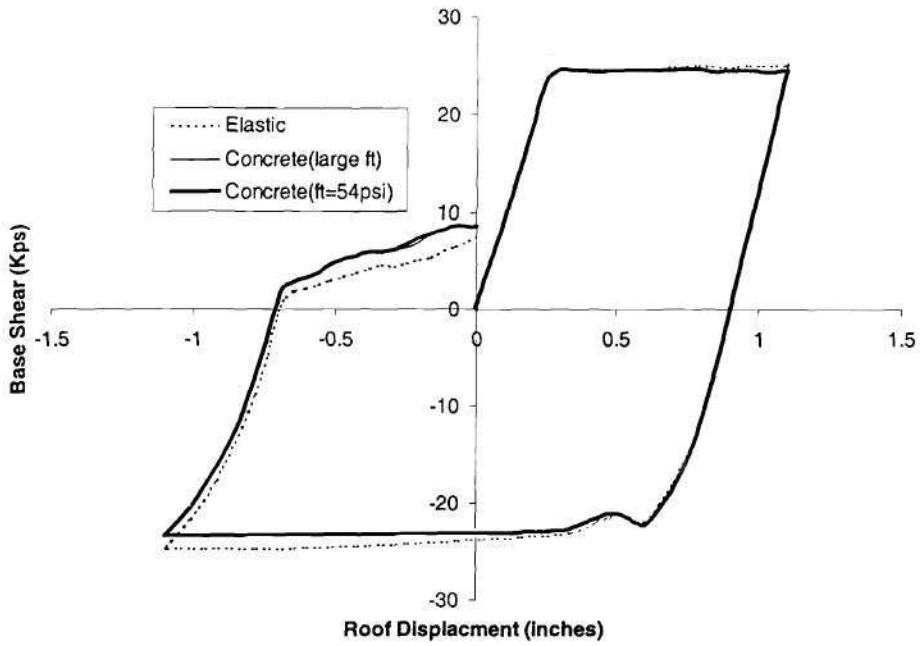


Figure 4.43. Force-displacement response of Wall 1 with different material properties (beginning with push to the right)

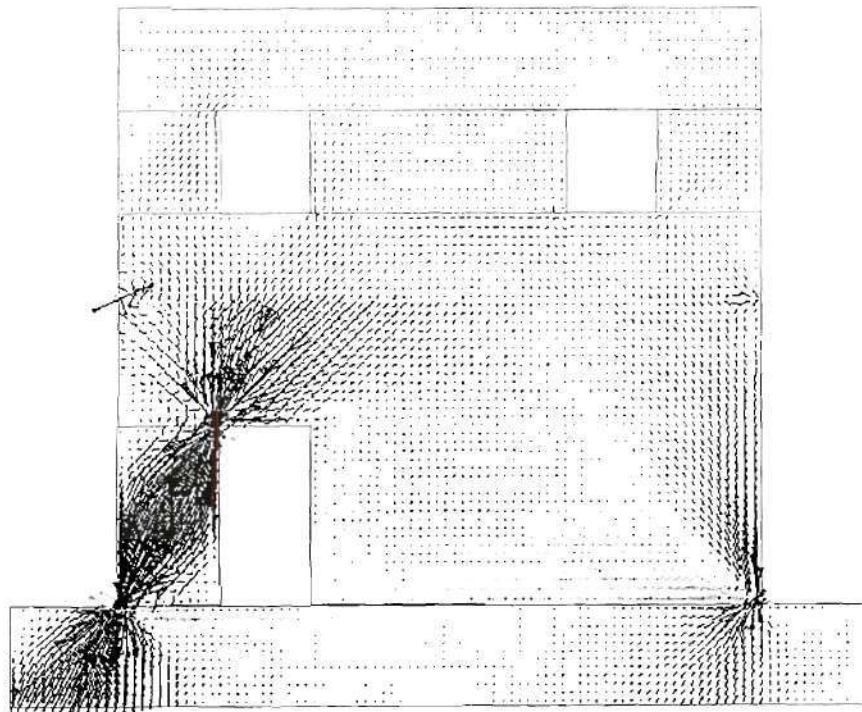


Figure 4.40. Stress contour of Wall1 (loaded to the left)

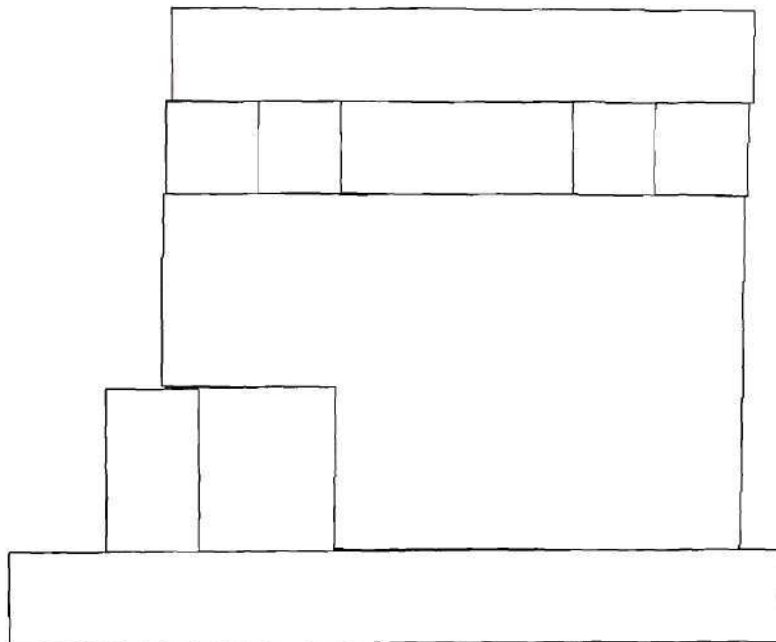


Figure 4.41. Deformed shape of Wall1 (loaded to the right)

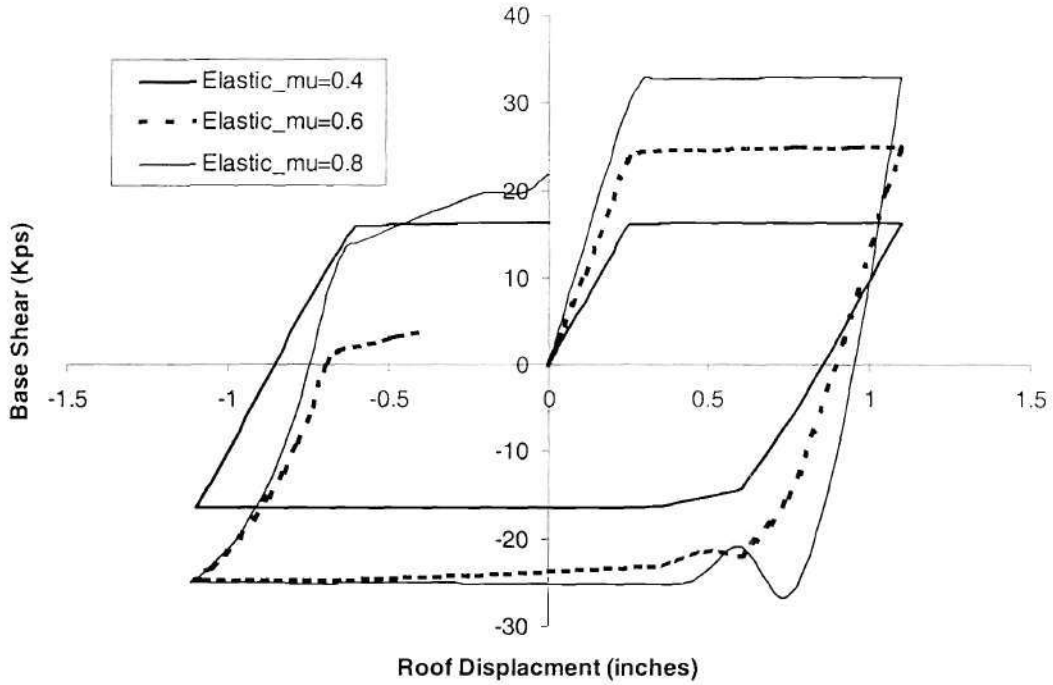


Figure 4.38. Force–displacement response of Wall 1 with different bed joint shear friction coefficients

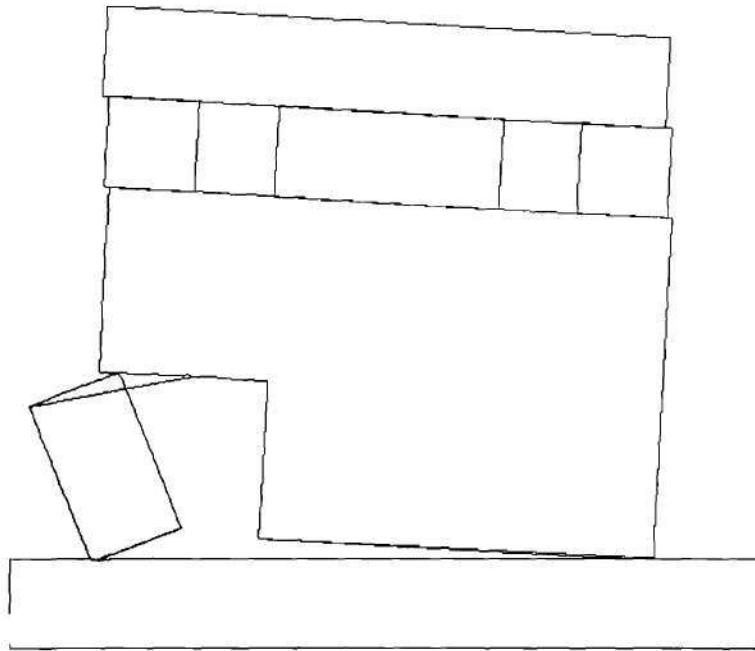


Figure 4.39. Deformed shape of Wall1 (loaded to the left)

stress concentration zones at the toe of Pier 1-7. This suggests that a toe crushing failure is possible at this location.

The hysteretic force – displacement behavior of Wall 1 with a bed joint friction coefficient of 0.6 is shown in Figs. 4.43 and 4.44 for different masonry properties. The calculated ultimate strengths in both directions are also listed in Table 4.26. For comparison purposes the strength estimates of Wall discussed in Section 4.2.3.7 are present as well.

Table 4.26. Calculated ultimate strength of Wall 1

Methods	Ultimate Strength when pushed to the right (kip)	Ultimate Strength when pushed to the left (kip)
Elastic	25.1	24.6
Concrete material with high tensile strength	24.6	22.8
Concrete material with the (tensile strength = 54psi)	24.6	22.8
Strength Estimate	25.6	25.6

The table shows that the use of concrete properties decreases the ultimate strength by a negligible amount. This suggests that neither toe crushing nor diagonal tension will dominate the behavior of Wall 1. As a result, the model that employs elastic plane stress elements supplies reasonable strength estimates for Wall 1.

4.2.4.3.1 Nonlinear FE Analysis Results of Wall 1

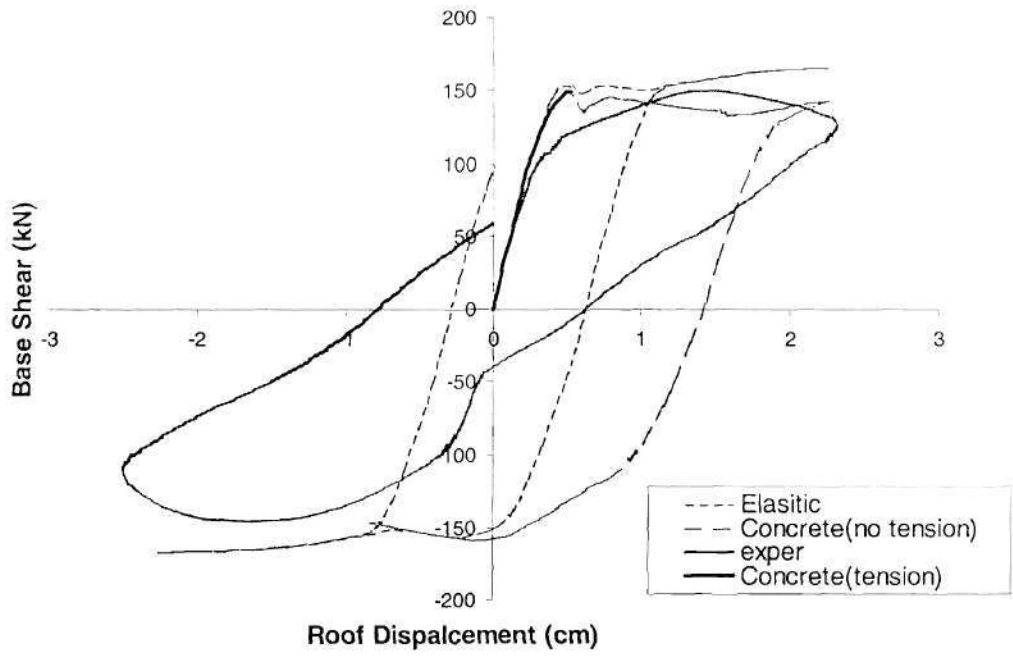
The analysis results of Wall 1 show that variations of the bed joints friction coefficient significantly affect the response of the structure (see Fig.4.38). For a friction coefficient of 0.4, the behavior of Wall 1 is dominated by sliding, which results in symmetric hysteretic behavior. Although, when the shear coefficient is increased to 0.6, the wall begins to behave asymmetrically. For loading from left to right (i.e. pier 1-6 is at the toe of the wall), sliding still dominates the behavior. However, if the wall is loaded in the opposite direction, some rocking behavior is observed. When the shear coefficient is increased to 0.8, the unsymmetrical behavior of the wall becomes more pronounced. For this case the failure modes (sliding when pushed to the right, rocking when pushed to the left) as well as ultimate strengths are different. The ultimate strength obtained for Wall 1 loaded towards the right was 33kip while the strength obtained by loading Wall 1 to the left was 27kip.

The unsymmetrical behavior of the wall with high bed joints shear frictions can also be seen from its deformation and stress contours, as shown in Fig 4.39. to 4.42, which corresponding to a friction coefficient of 0.8. When pushed to the left, pier 1-7 rocks, while the pier 1-6 is lifted up. When pushed to the right, the entire pier 1-6 slides. It can also be seen that the damage focuses on the first floor. In the case that the wall is loaded to the left, there are high stress concentration zones at the mid-height of Pier 1-7, and the spandrels above the door opening. This suggests that diagonal cracking is possible in these zones. In the case where the wall is loaded to the right, there are high

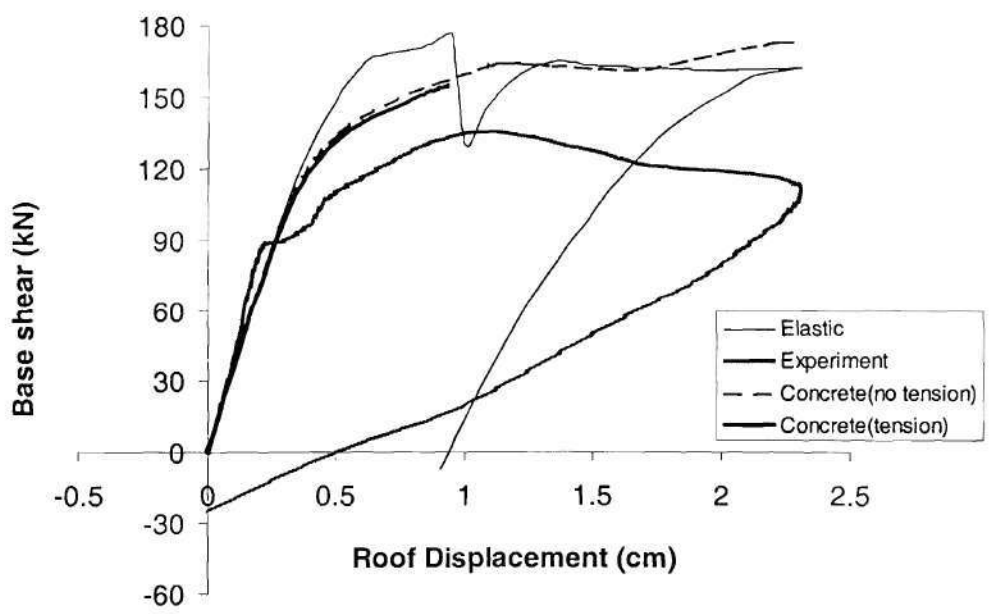
4.2.4.3 Non-linear FE Analysis of the ST-11 Test Structure

For the analysis of the ST-11 test structure, the elastic modulus of masonry was assumed to be 600 psi based on the test results of MAE center project ST-6 (reference). To investigate the possible effects of the variations in material properties, the analysis consisted of two parts. The first series of analyses were conducted using elastic plane stress elements and varying the properties of the contact elements. This series investigated the effects of different bed-joint friction coefficients on overall behavior by using 0.4, 0.6, and 0.8 for μ . In order to isolate this effect the tensile strength normal to the contact element was held constant at 20 psi. The second series of analyses were designed to investigate the effect of the nonlinear plane stress elements. For these analyses the properties of the contact element were held constant with the normal tensile strength taken as 20 psi, and the bed-joint friction coefficient taken as 0.6. Similar to the analyses of the URM structure tested at the Univ. of Pavia, two different tensile strengths were used for the 'concrete' plane stress elements. In one analysis the strength was set very high to suppress diagonal tension failures, while the other analysis employed a more realistic tensile strength of 54 psi. In both cases the compressive strength of the masonry was assumed to be 1800 psi.

To subject the walls of the ST-11 test structure to realistic gravity loads due to self-weight, the density of masonry was assumed to be 0.06944lb/in^3 . Lateral loads were applied in the form of cyclic displacements in order to allow the hysteretic behavior of the walls to be investigated. The displacement time history used for this analysis was very similar to the one shown in Fig. 4.34 except a maximum roof displacement of 1.12in was selected to give a maximum roof drift of 0.4%.

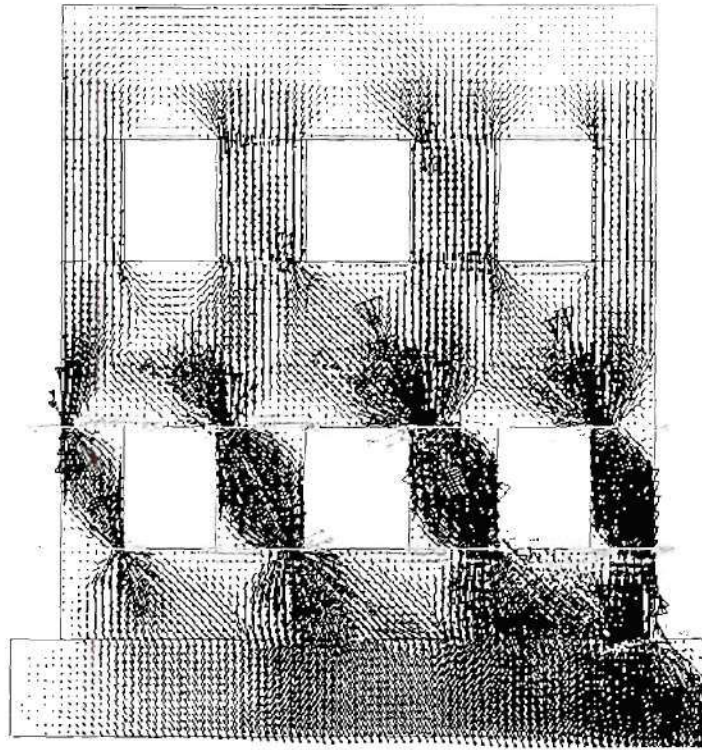


(a) Force-displacement behavior of Wall D

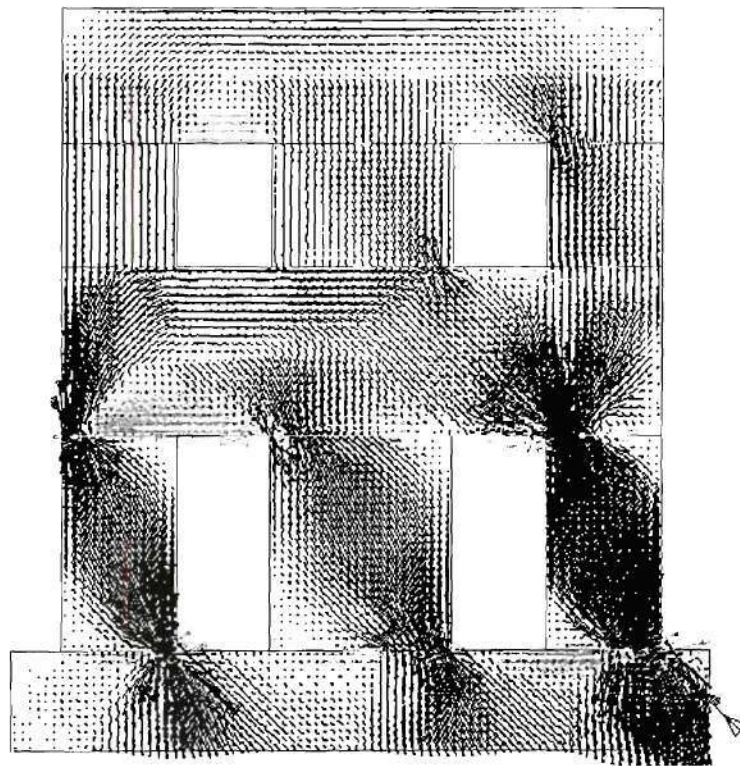


(a) Force-displacement behavior of Wall B

Figure 4.37. Force-displacement behavior of the URM masonry structure tested at Univ. of Pavia (Magenes et al , 1995)

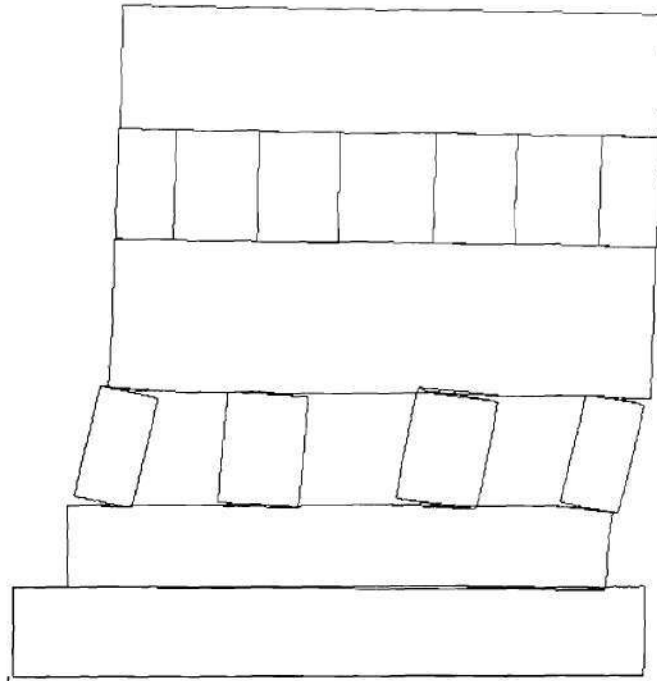


(a) Stress contour of Wall B

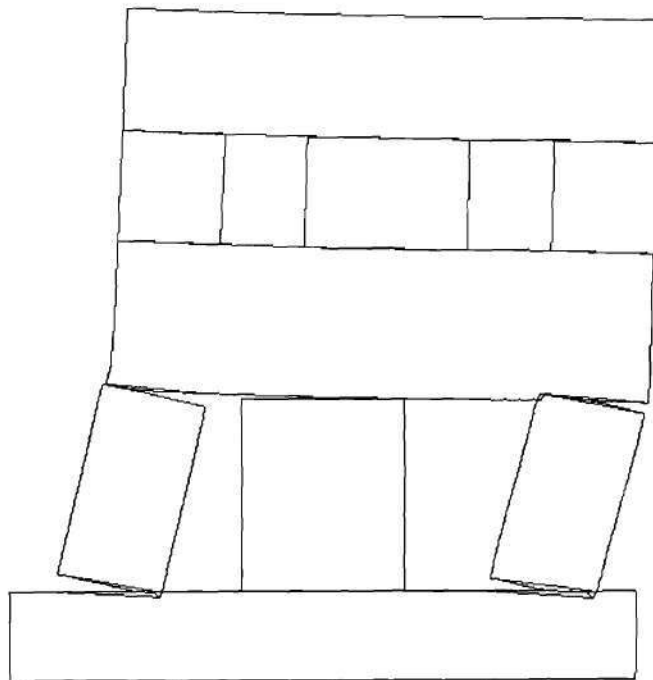


(b) Stress contour of Wall D

Figure 4.36. Stress contours of the tested walls at Univ. of Pavia



(a) Rocking and sliding of Wall B



(b) Rocking and sliding of Wall D

Fig 4.35. Failure modes of the tested wall at Univ. of Pavia

analysis is able to predict the elastic stiffness very well. However, when the experimentally determined hysteretic behavior is compared with the analysis results it is observed that the elastic plane stress-contact element analysis oversimplifies the behavior of the wall. This analysis shows that rocking and sliding, without much residual deformation or decrease in unloading elastic stiffness, dominate the behavior of the wall. In comparison, the test results showed large residual deformation and decrease in unloading elastic stiffness. The analysis employing the high tensile strength plane stress elements did result in an increase of residual deformation; however, the decrease in unloading elastic stiffness was still insignificant. A possible reason for this is that the plane stress element used was developed for the analysis of isotropic concrete materials and as a result is unable to predict the unloading behavior of orthotropic masonry. The analysis results obtained from the low tensile strength (33 psi) model was somewhat truncated in that the analysis stopped slightly past the peak point. This suggests that severe diagonal tension cracks developed and consequently caused some of the elements in the analysis model unstable. This type of diagonal cracking is consistent with experimental results.

Based on the comparison with past experimental research, it is concluded that the nonlinear FE analysis developed employing contact elements is a reasonable tool for the analysis of URM perforated walls. As a result, this method was used to analyze the four perforated walls of the ST-11 test structure and the results are presented in the following sections.

The deformed shapes of Walls B and D due to the rocking and sliding behaviors of the piers are shown in Fig 4.35. The calculated stress contours of these two walls are shown in Fig 4.36. For both walls, the two outside piers in the first floor rock first. This is most likely due their relatively large slenderness ratios, which correspond to lower rocking strengths. It can be seen from Fig. 4.36 that the damage to the walls caused by lateral forces is mainly focused on the piers and the spandrels in the first floor. Zones of high stress are present in the mid-height of the first floor piers as well as the in the spandrels above the openings. This suggests diagonal tension failures are likely in these areas. All of these behaviors are consistent with experimental observations.

The force – displacement hysteretic behavior of Walls B and D determined through this analysis is shown in Fig. 4.37. Table 4.25 gives a summary of the calculated capacities for each walls as well as the percent error compared with experimental results.

Table 4.25 Summary of nonlinear FE results for Walls B and D (Univ. of Pavia)

Plane stress element type	Wall D capacity (kip)	% error	Wall B capacity (kip)	% error
Elastic	37.5	11.2	39.6	29.8
High tensile strength	35.8	6.2	36.9	20.9
Low tensile strength	33.5	0.6	34.8	14.1

From the table it is apparent that the analysis method provides very good estimates of the ultimate strength, considering the inherent variability of masonry. Note the trend of decreasing error as the sophisticated nature of the plane stress elements increase (i.e. allow compression and tension failures). This is most likely due to the observance of these types of failures during the experiment. Furthermore, Fig. 4.37 shows that the

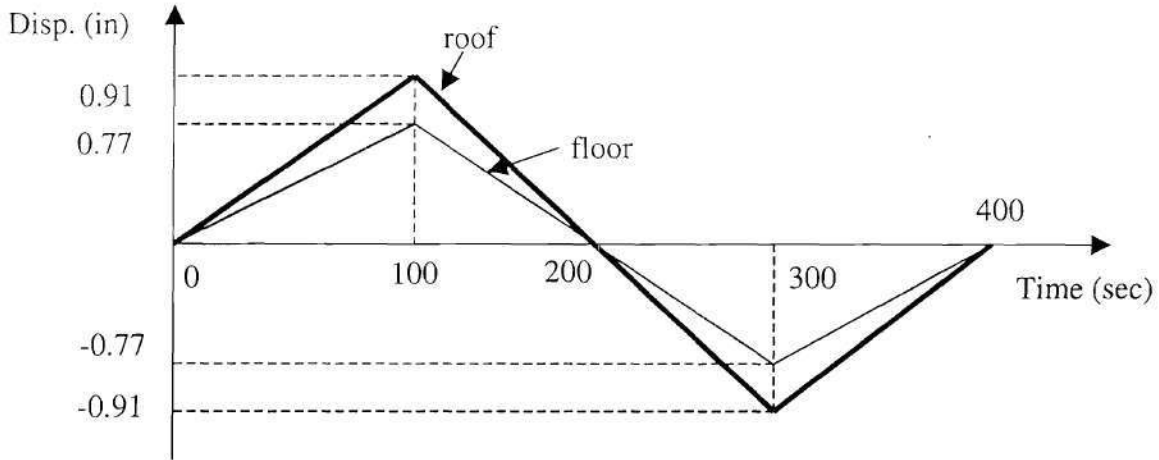


Figure 4.34. Time history for the analysis of the full-scale test in Univ. of Pavia

Three different plane stress elements were used in the analysis of both Walls B and D. The first element used was elastic with an elastic modulus of 435 ksi and a Poisson's ratio of 0.25. The second element used was the concrete element discussed previously. For this element the elastic modulus was taken as 435 ksi and the maximum compressive strength was assumed to be 900 psi (i.e. the prism strength as determined through material testing). For this material the maximum tensile strength was assumed to be very large so as to suppress any diagonal tensile cracking. The third material was identical to the second one, except that the maximum tension strength was taken as 33 psi. The first material model was used to investigate the behavior of the walls considering only rocking and sliding failure modes. The second, high tensile strength, material model was used to investigate the softening behavior of masonry as well as the possible toe-crushing failure modes. The third, low tensile strength, material model was used to investigate possible diagonal cracking in addition to the other failure modes.

are defined by a maximum compression and tension strength. As a result, these elements were capable of modeling the diagonal tension and toe crushing failure modes. It is important to mention, however, that these elements assume an isotropic material, which may cause errors since masonry is basically an orthotropic material.

4.2.4.2 Comparison of Nonlinear FE Analysis with Past Experiments

For the purpose of comparison, the nonlinear in-plane FE analysis model was used to analyze the full-scale URM building tested in the University of Pavia (Magenes et al , 1995). The dimensions of the in-plane walls of this test structure (i.e. Walls B and D) are given in Section 2.1. These walls were modeled based on the procedure outlined in the previous section. Based on the results of material tests reported for this structure the bed joint shear friction coefficient was taken as 0.57 and the maximum tensile strength of the bed joint was taken as 10.6 psi (Magenes et al , 1995).

Gravity loads were applied to each wall based on the self-weight of the wall and floors weight of 27.9 kips and 26.6 kips as specified in the test report (Magenes et al , 1995). In order to obtain the hysteretic behavior of the walls cyclic lateral displacements were imposed on the structure at each floor level. The time history of the imposed lateral displacements are shown in Fig 4.34. The displacement ratio between the floor level and the roof level was keep constant throughout loading at 0.85.

the results of past experimental research, it is clear that the potential rocking/sliding surfaces are most likely to occur at the top and bottom of the masonry piers. Therefore, the contact elements were placed at these locations (see Fig. 4.32).

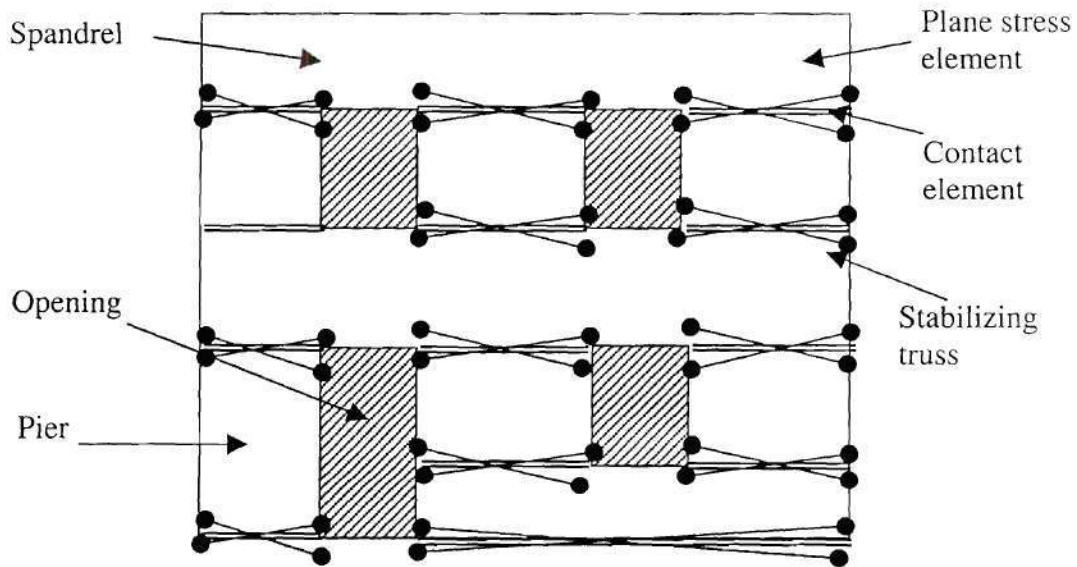


Figure 4.33. Modeling of a perforated wall with contact elements and stabilizing truss elements

During the first trial analyses it was discovered that the structure quickly became unstable due to the rigid body motion after the contact elements began to slide. To solve this problem, truss elements were added across each contact element to provide a small amount of stiffness (see Fig 4.33). The stiffness of the truss elements was set to the smallest value that enabled the structure to remain stable in an effort to minimize the error in the analysis results.

The other two potential failure modes: diagonal tension and toe crushing were described by plane stress elements developed for the analysis of concrete structures, provided by ABAQUS. These elements display a parabolic stress strain relationship and

occur prior to actual sliding (see Fig. 4.32). This modification is necessary in order to ensure the convergence of the solution; however, it also decreases the elastic stiffness of the system.

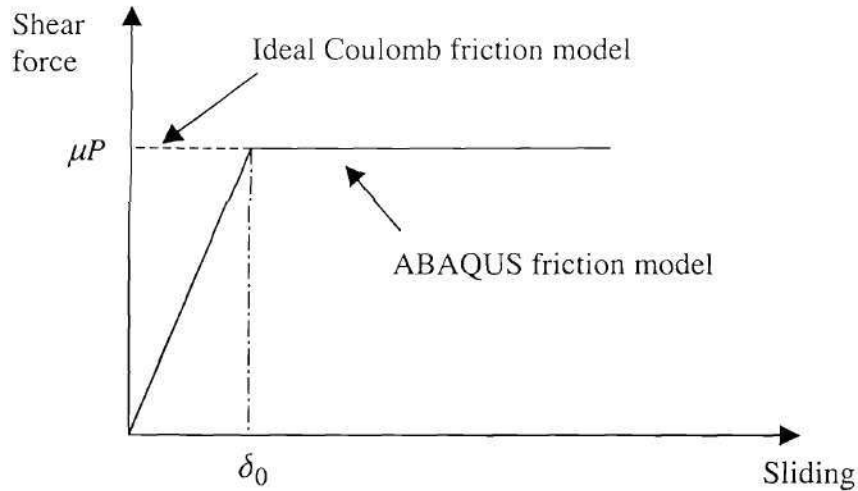


Figure 4.32. Force-Relative displacement relationship for contact elements.

It should be pointed out that the shear properties described by the Coulomb friction model are different from the actual shear properties of masonry. Essentially the Coulomb friction model ignores the initial shear strength of the bed-joint (v_{te}), thus assuming that the bed-joint is completely cracked. While strictly speaking this is incorrect, sliding typically does not develop in piers until after large flexural cracks appear. This suggests that on the onset of sliding the initial shear strength of masonry has been eliminated and only the frictional resistance of the bed-joint remains. Therefore, it appears that the Coulomb friction model can be used to reasonably approximate sliding behavior.

In order to employ the ABAQUS contact element to model rocking and sliding failures of URM piers. Potential rocking and sliding surfaces must be defined. Based on

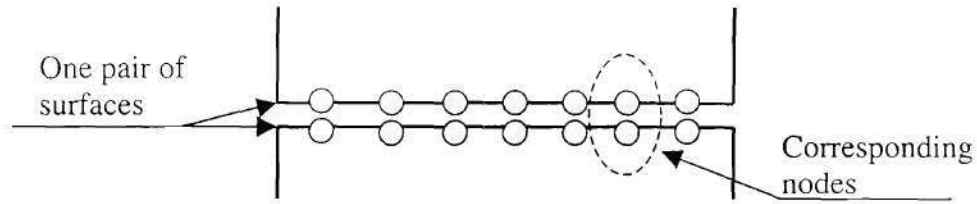


Figure 4.30. Schematic of a contact element

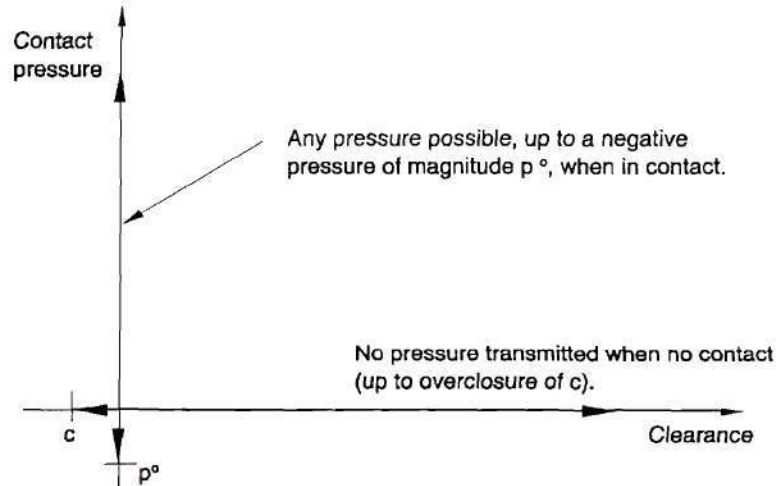


Figure 4.31. Normal forces transmitted between the pair of surfaces

(taken from ABAQUS 5.8-19 manual 23.18.37-1)

Prior to separation, the corresponding nodes can transmit shear forces as well as normal forces. Typically the Coulomb friction model is used to describe the shear properties of the contact surface. That is, the corresponding nodes transmit shear forces (or shear stresses for associated areas) up to a specified critical shear value, at which time the surfaces slide relative to one another (see Fig. 4.32). This critical shear value is defined as a fraction of the normal force or stress, which is given by the coefficient of friction μ . After sliding occurs, the transmitted shear forces remain constant μ times the normal forces. Furthermore, the ABAQUS contact element does not assume an idealized rigid-sliding behavior. Instead, the ABAQUS contact element allows an elastic slip δ_0 to

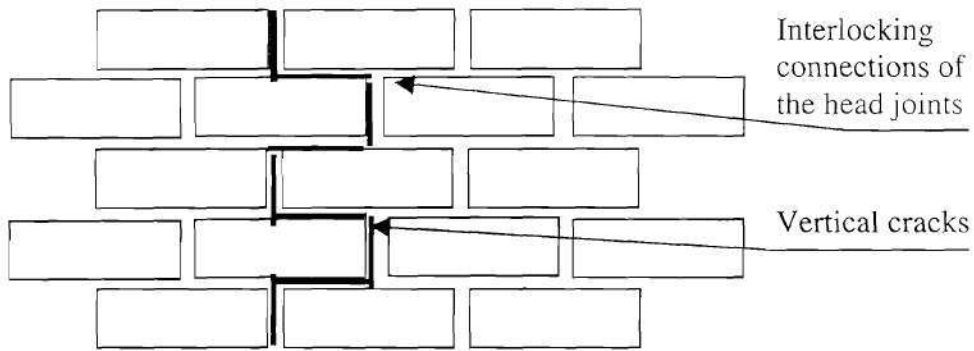


Figure 4.29. Teeth configurations of the head joints

Based on the above discussion, the possible failure modes that a realistic model must consider for each type of member are clear. In order for the model to properly address both rocking and sliding failures non-conventional elements must be employed. That is, the rigid body motion associated with rocking and sliding cannot be described by conventional FE methods since they are based on a continuous deformation assumption. A special contact element provided by ABAQUS is appropriate for this purpose. The contact element defines a pair of surfaces where potential cracking and/or sliding is likely to occur (see Fig. 4.30). Each surface is defined by a number of nodes and their associated areas. The relative movements of the corresponding nodes between the two surfaces determine the behavior of the pair of surfaces. At first, the corresponding nodes are attached to each other. They will remain attached (or in contact) until the tensile normal force between the corresponding nodes (or the tensile pressure between the associated areas) reaches a certain specified value. Once this value is reached the corresponding nodes separate and no further normal forces are transferred (see Fig. 4.31).

masonry is not an isotropic material. As a result, the possible failure modes associated with a spandrel are different from those associated with a pier. For example, the commonly observed pier failure mode of rocking is not realistic for spandrels. Although the flexural moments on a spandrel do place some head-joints in tension leading to vertical flexural cracking, the large flexural cracks associated with rocking cannot develop due to the interlocking of bricks in the vertical direction (see Fig. 4.29). Furthermore, this type of interlocking also prevents the sliding failure mechanism associated with piers. That is, in order for a spandrel to slide the bricks that cross the sliding plane would have to fail in shear. Considering the relatively high shear strength associated with the brick, the sliding failure mode is not realistic for a spandrel. In addition, the relatively small amount of compressive stress in spandrels suggests that compressive failure of masonry in spandrels is not likely to occur. Following these arguments, it can be concluded that a diagonal tension failure of the spandrels is the only realistic failure mode. As a result, only a diagonal tension type failure has to be considered for the analysis of spandrels in perforated masonry walls.

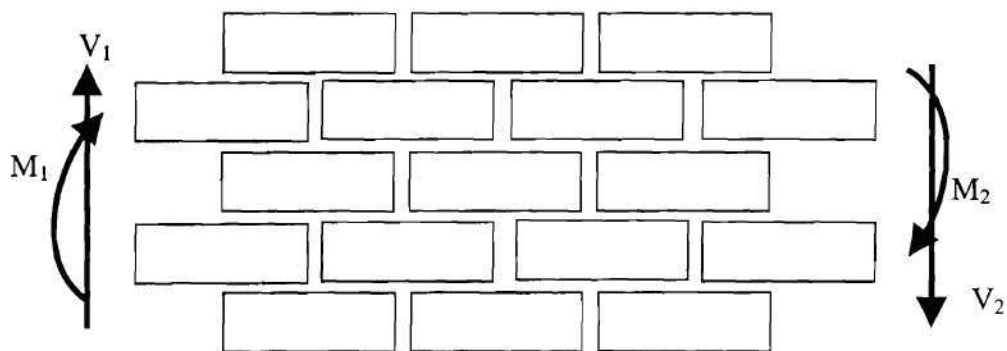


Figure 4.28. Forces on a spandrel

Kolsch, H. (1998) "Carbon Fiber Cement Matrix (CFCM) Overlay System for Masonry Strengthening" *Journal of Composites for Construction* Vol. 2, No. 2, pp 105-109.

Konig G., Walther Mann, and Atilla Otes (1988), "Experimental Investigations on the behavior of unreinforced Masonry walls under seismically induced loads and lessons Derived", proceedings of Ninth World Conference on earthquake engineering, August 2-9, Tokyo-Kyoto, Japan, Vol VIII, pp 1117-1122

Lacika, E. M. and R. G. Drysdale (1995) "Experimental Investigation of Slender Prestressed Brick Walls", Seventh Canadian Masonry Symposium, McMaster University, Hamilton, Ontario, pp.724-735.

Laursen, P. T., and J. M. Ingham (2001a) "Structural Testing of Single-Storey Post-tensioned Concrete Masonry Walls" *The Masonry Society Journal*, pp69-82.

Laursen, P., and J. Ingham (2001b) "Seismic Resistance of Prestressed Concrete Masonry Shear Walls" 2001 Structures Congress and Exposition, Washington, D.C..

Laursen, P.T., F. Seible, G.A. Hegemier, and D. Innamorato (1995) "Seismic Retrofit and Repair of Masonry Walls with Carbon Overlays", *Non-metallic (FRP) Reinforcement for Concrete Structures*, pp616-623

Jennings, Pau C. (1997), “ Enduring lessons and opportunities lost from the San Fernando Earthquake of February 9, 1971”, Earthquake Spectra, vol 3, number 1, pp 25-44

Jonhson, J. W. (1956). “Lateral Tests on Full-Scale Lumber and Plywood-Sheathed Roof Diaphragms”. The American Society of Mechanical Engineers (ASME), paper no. 56-S-16.

Jurukovski, D. and Krstevska,L., etc (1992), “ Shaking table tests of three four-storey brick masonry models: Original and strengthened by RC core and by RC jackets”, ”, Tenth World Conference on Earthquake Engineering, Balkema, Rotterdam. pp 2795-2800

Kahn, L. F. (1984). “Shotcrete strengthening of brick masonry walls.” Concrete Inst., 6(7), 34-40.

Kalita U.C., and A.W. Hendry (1970), “ An experimental and Theoretical Investigation of the stresses and Deflections in Model Cross-wall structures”, Proceedings of the second International Brick Masonry Conference held in Stoke-on-Trent, England, April, pp 209-214

Kariotis,J. C., Johnson, A.W., and Ewing, R.D. (1985). “Predictions of stability of unreinforced masonry shaken by earthquake”, Proceedings of the Third North American Masonry Conference, Arlington, Tex., pp 49-1 to 49-11

5 CONCLUSIONS

As a background study, an extensive review of the literature on both URM research as well as research conducted on retrofitting methods was presented. A detailed description of the experimental program was outlined, including a description of the test specimen, proposed retrofitting methods, loading sequence, and instrumentation plan. The first series of tests is expected to be completed by mid-March 2002, with the entire testing program scheduled for completion by early summer 2002. An extensive series of preliminary analyses was conducted in order to gain insight into the behavior of the test structure. This series was composed of four analyses methods chosen to provide estimates of specific characteristics of the test structure. Results include predictions of elastic stiffness, natural periods, damage progression, failure modes, and force-displacement behavior for the test structure in a unreinforced state as well as after retrofit. The accuracy of each analysis methods will be assessed based on the results of the experimental program.

The accuracy of the analysis methods presented will be assessed based on the results of the experimental program.

4.4 Conclusion

Four different analyses methods were employed to obtain insight into the behavior of the ST-11 test structure. Based on the results of these analyses the following conclusions are made:

- Elastic analysis of URM structures can provide insight into the significance of three-dimensional effects such as flange effects and torsional behavior, as well as some basic structural characters such as elastic natural frequencies and vibration modes. However, little information on the seismic behavior of URM structures can be obtained since this behavior is dominated by nonlinearities.
- When the three-dimensional effects of a structure are insignificant, as determined from a 3D elastic FE analysis, both of the nonlinear analysis methods developed are appropriate to determine the behavior of perforated in-plane walls. This conclusion is based upon the good correlation observed between both nonlinear methods and past experimental results.
- Considering the inherent variability of URM structures, the nonlinear pushover analysis is very similar to the nonlinear FE analysis from an accuracy standpoint; however, the nonlinear pushover analysis is superior from an efficiency point of view. Furthermore, the nonlinear pushover analysis is easily adapted to the analysis of retrofitted structures where as the nonlinear FE analysis is not.
- Both of the nonlinear methods developed are only applicable to URM perforated walls that contain well-defined pier and spandrel components.

Table 4.32. Predicted failure modes for FRP retrofitted piers

Pier	URM	Retrofit 1	Retrofit 2
AB-7	Rocking => Sliding	Diagonal tension	Tension Failure of Flexural FRP/ Rocking
AB-10	Rocking	Tension Failure of Flexural FRP/ Rocking	Tension Failure of Flexural FRP/ Rocking
1-6	Rocking	Diagonal tension	Tension Failure of Flexural FRP/ Rocking
1-7	Rocking => Sliding	Tension Failure of Flexural FRP/ Rocking	Tension Failure of Flexural FRP/ Rocking
2-7	Rocking	Diagonal tension	Tension Failure of Flexural FRP/ Rocking
2-9	Rocking => Sliding	Diagonal tension	Toe Crushing

Figs. 4.65 through 4.67 illustrate that, based on the current analysis procedure, the selected retrofit of URM piers with FRP overlays results in large increases in overall strength. However, the results also show that neither of the FRP retrofits resulted in an increased displacement capacity for any of the ST-11 walls, and in some cases a decreased displacement capacity was observed. This is expected due to the brittle nature of FRP and the ductile behavior of the walls prior to retrofit. That is, if the governing failure mode prior to retrofit is ductile, (i.e. rocking or sliding) the retrofitted structure can display a decreased displacement capacity if the failure modes resulting from the retrofit are brittle. This switching of failure modes is observed for the retrofitted piers in Wall 2 (see Table 4.32). Although, if the FRP retrofit can delay a brittle failure mode and force a ductile failure mode, large increases in displacement capacity can be expected (Luarsen et al., 1995).

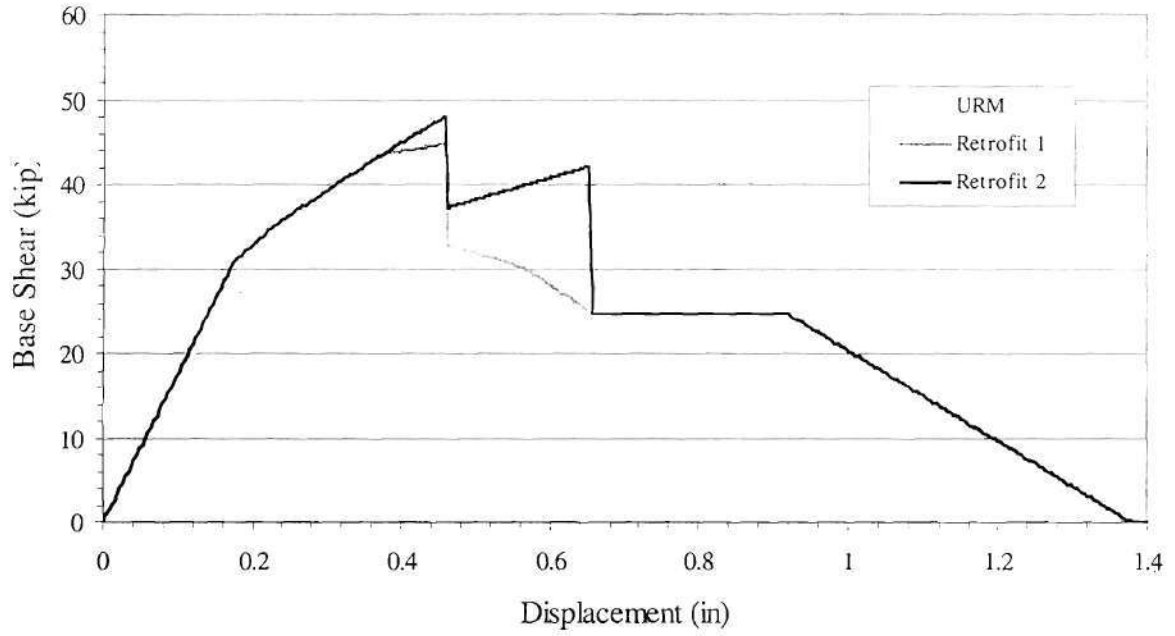


Figure 4.66. Force-displacement curves for Wall 1 in an unreinforced state and after retrofit schemes 1 and 2

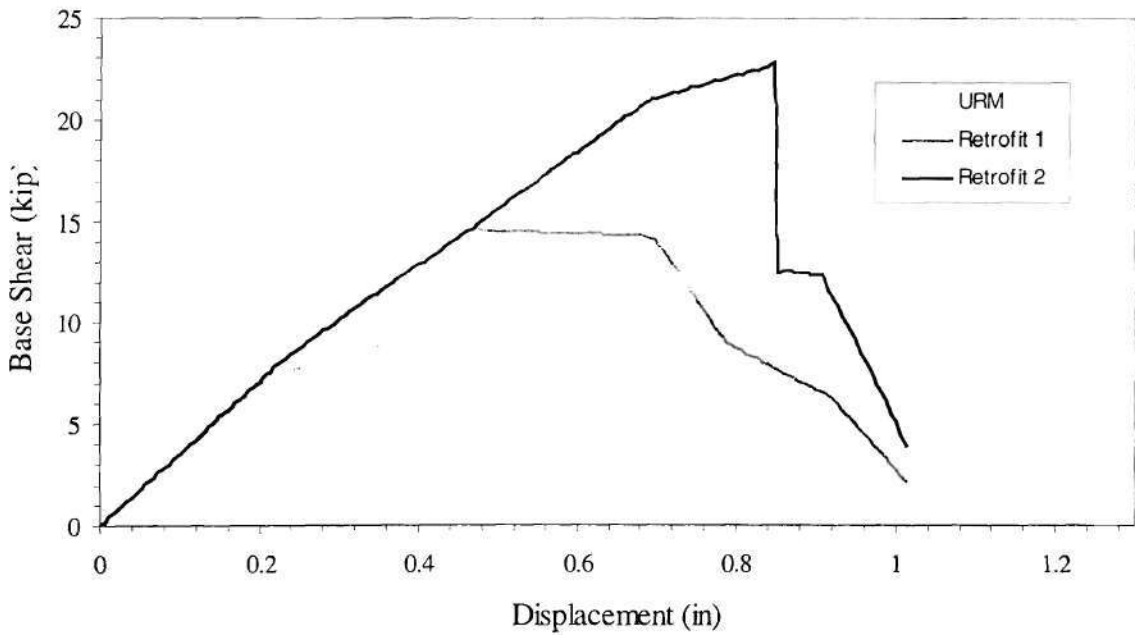


Figure 4.67. Force-displacement curves for Wall 2 in an unreinforced state and after retrofit schemes 1 and 2

Table 4.31. Properties of FRP used in analysis

	Applied Thickness (in)	E (ksi)	σ_{ult} (ksi)
27 oz Unidirectional Glass FRP	0.054in	1365	69

Figs. 4.65 through 4.67 show the force-displacement curves obtained for each wall of the ST-11 test structure after both retrofit schemes as well as in an unreinforced state, for comparison. In order to consolidate the results, only the curves obtained from loading the walls from left to right are presented. To illustrate the effectiveness of the retrofit in altering the failure modes of the strengthened piers, Table 4.32 gives the failure modes for the retrofitted piers for each analysis conducted.

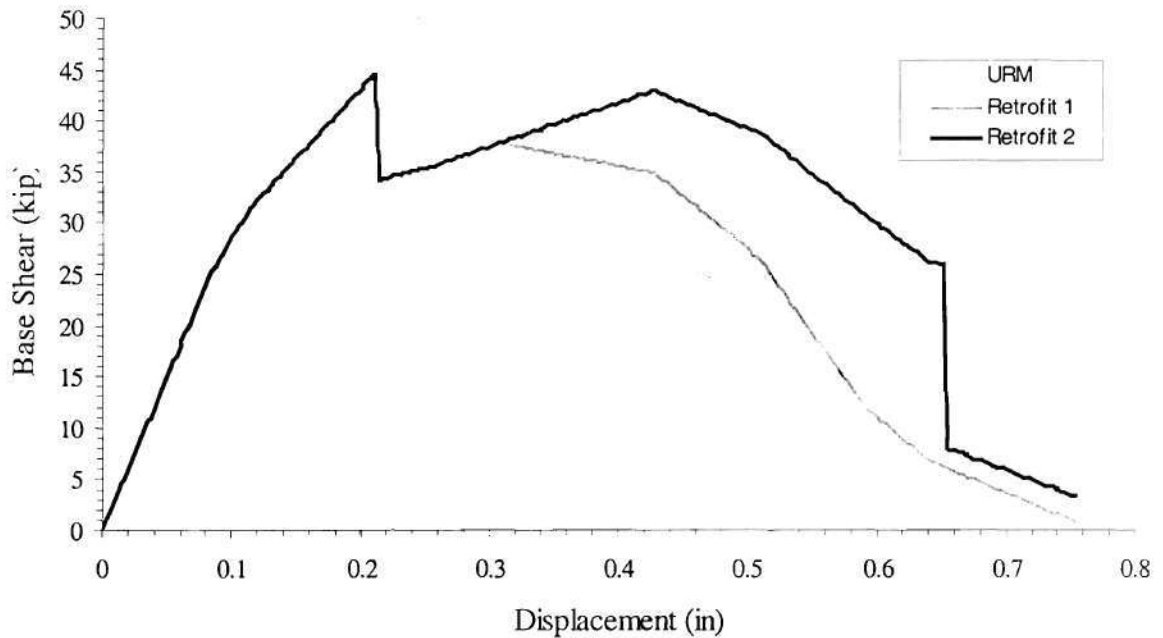


Figure 4.65. Force-displacement curves for Wall AB in an unreinforced state and after retrofit schemes 1 and 2

Table 4.30. Force-drift relationships for URM pier retrofitted with FRP overlays

Failure Mode	V_1	V_2	Drift d (%)	Drift e (%)	Drift x (%)	c
Tension Failure of Flexural FRP	V_r	V_{ff}	0.4(H/L)	0.8(H/L)	1.2(H/L)	$0.9V_r$
Shear Failure of Bed-joint FRP	V_{bjs1}	V_{bjf}	0.4	0.8	1.2	V_{bjs2}
Tension Failure of Diagonal Tension FRP	V_{dtf}	-	0.3	-	0.4	$0.5*V_{dt}$
Compressive Failure of Masonry	V_{tcf}	-	0.3	-	0.4	$0.5*V_{tc}$

4.3.2.2 Analysis Results on FRP Retrofitted ST-11 Test Structure

In order to gain insight into the effectiveness of selective FRP retrofit, each wall of the ST-11 test structure was analyzed for two different retrofit schemes. The philosophy of each retrofit scheme was to strengthen the pier beyond the governing failure mode. Since all of the failures were dominated by rocking, the first retrofit in each case employed 4 in. wide strips of flexural FRP. Due to the observation of some diagonal tension failures after the rocking strength had been increased, the second scheme employed 8in wide strips of diagonal tension FRP in addition to the flexural FRP. To investigate selective retrofit, two piers in each wall were retrofit. To maximize the effectiveness of the FRP, the outside piers on the first floor were chosen for retrofit since these piers typically damage first due to the effects of overturning moment.

Based on the preliminary results of an extensive experimental investigation currently underway at the US Construction Engineering Research Lab (CERL), a 27 oz unidirectional glass fabric with an epoxy matrix was chosen for retrofit (Sweeney, 2002). The properties of this FRP, determined through testing at CERL, are given in Table 4.31.

the URM pier. This type of retrofit should be avoided, as it does not increase the behavior of URM.

The generalized force-displacement curve used for the analysis of FRP retrofit piers are shown in Fig. 4.62. Notice that the curve shown displays a decreased positive stiffness after “yield”. This is due to the masonry cracking and the FRP strips becoming stressed. Also from the figure it is apparent that these curves display a sharp drop in strength. This represents the shear force that causes failure of the FRP strips. After this point, these curves revert back to those shown in Fig. 4.14 for URM piers. Table 4.30 gives the force-drift relationships for each of the failure modes considered. For simplicity, the allowable drifts were assumed to be the same as the allowable drifts for a URM pier. This assumption is made as a first attempt at the analysis, future work will focus of the determination of more reasonable drift limits in order to account for the decreased displacement capacity associated with an increase in FRP stiffness.

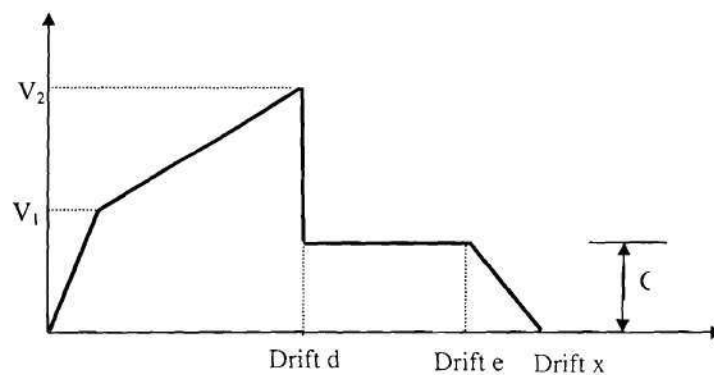


Figure 4.64. Generalized force-drift relationships for URM piers retrofit with FRP overlays.

The other type of shear failure considered is diagonal tension. An expression for shear capacity associated with this failure mode is obtained by assuming the pier is cracked along the diagonal, this assumption follows from the same logic given in the previous paragraph. The shear capacity of the retrofit pier is obtained by considering the diagonal tension FRP as a tension tie, as shown in Fig. 4.63.

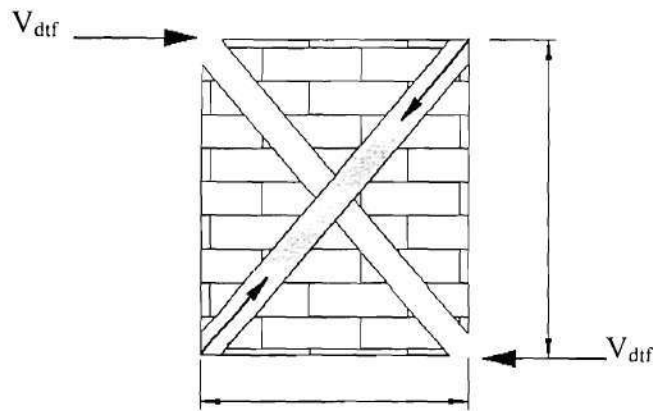


Figure 4.63. Model used to Obtain Diagonal Tension Strength of FRP Retrofit Pier

From statics the following expression is obtained:

$$V_{df} = \sigma_{df} A_{df} \left(\left(\frac{h}{L} \right)^2 + 1 \right)^{\frac{1}{2}} \quad (4.28)$$

where, σ_{df} and A_{df} are the tensile strength and area of the diagonal tension FRP, respectively.

It should be noted that the above expressions assume that the bond between the masonry and FRP is sufficient to develop the tensile or shear capacity of the FRP. If this is not the case, the strength of the FRP should be limited to the bond strength. Furthermore, if insufficient FRP is employed to mitigate certain failure modes the expressions presented may predict a lower capacity than those given in Section 4.2.3.1 for unreinforced masonry. In this case, the capacity should be based on the capacity of

Utilizing strain compatibility and equilibrium, the depth of the stress block can be written as:

$$\alpha = \frac{-f_a L t_m}{2 f_m' t_m} + \sqrt{\left(\frac{f_a L t_m}{2 f_m' t_m}\right)^2 + \frac{0.003 A_{ff} E_{ff} (L - \frac{w_{ff}}{2})}{f_m' t_m}} \quad (4.25)$$

where, E_{ff} is the modulus of elasticity of the flexural FRP. Using the above solution, the following expression is obtained for the shear capacity associated with the compressive failure of the masonry:

$$V_{icf} = \frac{2\alpha}{h} \left(L - \frac{w_{ff}}{2} - \frac{a}{2} \right) (0.85 f_m' a t_m) \quad (4.26)$$

To obtain an expression for shear capacity due to the failure of bed-joint FRP, the entire bed joint was assumed to be cracked. This assumption is reasonable when one considers the area and stiffness of the FRP compared with that of the masonry. That is, the FRP is not “activated” until the masonry has cracked. However, the resistance due to friction is additive to the strength of the bed-joint FRP. The following expression is obtained by setting the shear strength of the FRP equal to the maximum shear force along the bed-joint (note, a parabolic shear stress distribution is assumed along the bed-joint).

$$V_{bjf} = \left(\frac{2}{3}\right) L t_{bjf} \tau_{bjf} + L t_m f_a \mu \quad (4.27)$$

where, t_{bjf} is the thickness of the bed-joint FRP and τ_{bjf} is the shear strength of the bed-joint FRP. In addition, when flexural FRP is provided without bed-joint FRP, the shear resistance of the vertical FRP strips should be accounted for in Eqn 4.27.

$$V_{ff} = \frac{2\alpha}{h} \left(L - w_{ff} - \frac{d_m}{3} \right) (A_{ff} \sigma_{ff} - f_{aT} Lt_m) \quad (4.24)$$

where, σ_{ff} is the tensile strength of flexural FRP and f_{aT} is the tensile vertical stress. It should be mentioned that since elastic properties are used for masonry, equations 4.23 and 4.24 assume the pier is under reinforced, which is the case when Eqn 4.24 would govern the strength (i.e. tension failure of FRP).

To determine an expression for the shear capacity associated with the compressive failure of the masonry (i.e. cases where the pier is over reinforced) a similar procedure was used; however, to model the masonry at compressive failure the equivalent stress block analogy was employed (see Fig. 4.62). It is important to note that the presence of vertical stress was included for the determination of the shear force associated with the compressive failure of masonry because, following a previous assumption, the masonry resists all vertical stress.

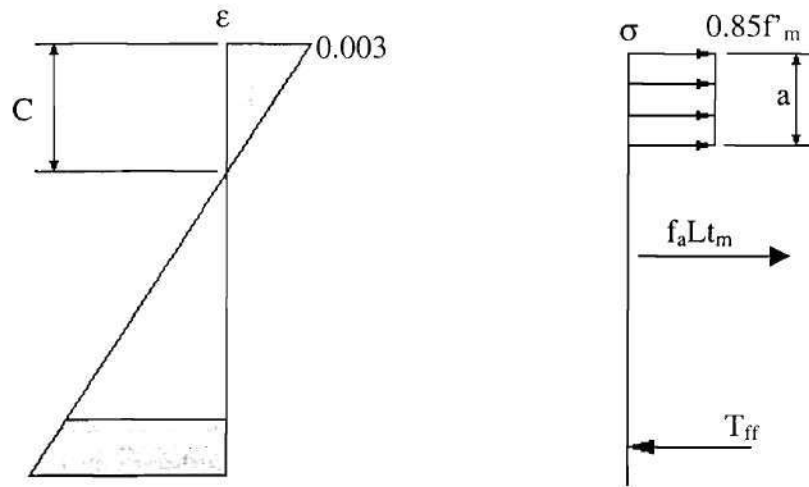


Figure 4.62. Strain and Stress Diagram used to calculate shear capacity associated with the compressive failure of masonry.

equilibrium the following expression for the distance from the compressive edge of masonry to the elastic neutral axis (d_m) was determined.

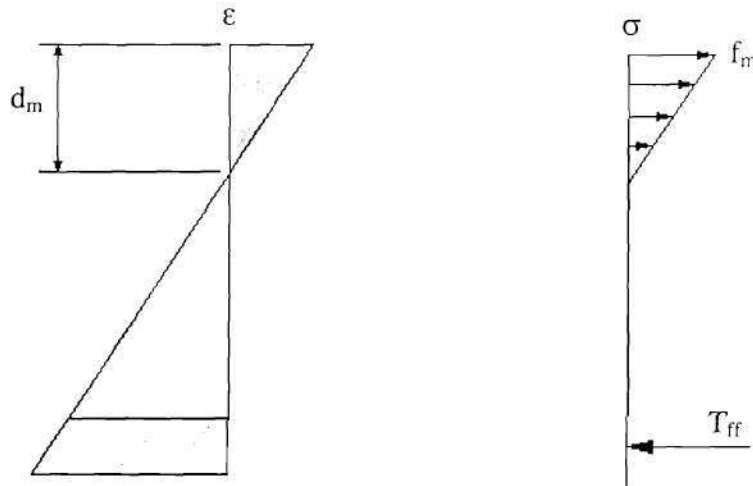


Figure 4.61. Strain and Stress Diagram for FRP Retrofit URM Pier in Flexure

$$d_m = \left(\frac{A_{ff} n}{t_m} \right) \left(\sqrt{1 + 2 \left(L - \frac{w_{ff}}{2} \right) \left(\frac{t_m}{A_{ff} n} \right)} - 1 \right) \quad (4.23)$$

where, A_{ff} is the area of the flexural FRP, w_{ff} is the width of flexural FRP, and n is the ratio of FRP elastic modulus to the elastic modulus of masonry. To obtain an expression for moment capacity associated with the tension failure of flexural FRP, the maximum stress in the FRP was set equal to the tension strength and the moment was calculated. In order to take axial load into account, it was assumed that tensile vertical stress (possibly due to overturning moment) would be resisted by the flexural FRP. As a result, the capacity of the FRP to resist bending is reduced if the overall vertical stress is tensile. The shear capacity associated with the tension failure of flexural FRP can be written as:

strip. For example, if the governing failure mode was diagonal tension, which is considered brittle, one may choose to only employ diagonal tension FRP in order to force a more ductile failure mode such as rocking or sliding (Laursen et al., 1995). The failure modes of FRP retrofit piers that were considered for the derivation of strength expressions were: tension failure of flexural FRP, compressive failure of masonry (toe-crushing), tension failure of diagonal tension FRP, and shear failure of bed-joint FRP.

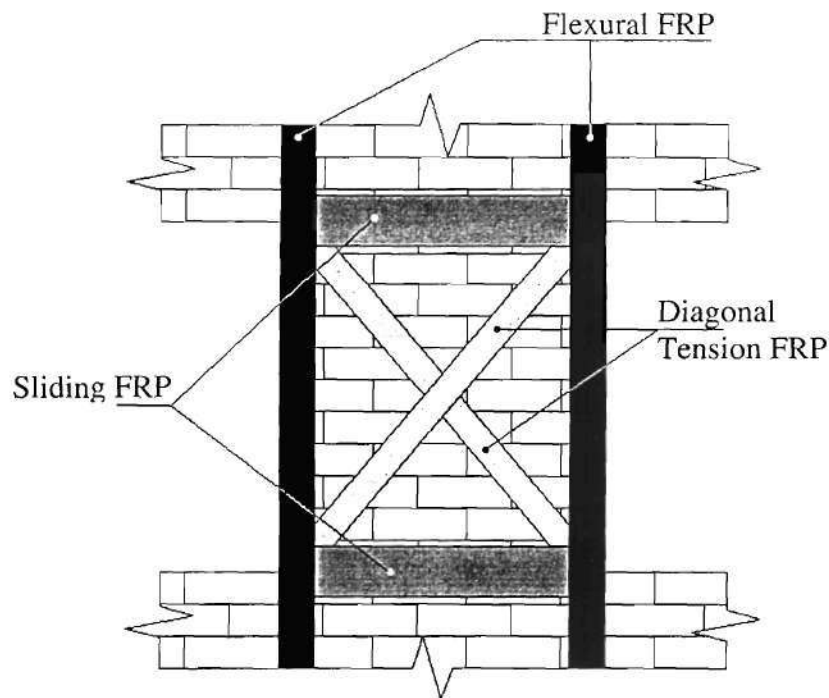


Figure 4.60. URM Retrofit with FRP Strips

In order to determine the capacity associated with the tension failure of flexural FRP, the pier was considered to be a column under flexure. The corresponding strain and stress diagrams are shown in Figure 4.61. Notice that the presence of vertical stress is ignored in the figure. This is reasonable because the flexural FRP was applied after the vertical stress and, as a result, is stress-free. By using strain compatibility and

From Fig. 4.59 it is apparent that post-tensioning is very effective at increasing the strength of URM wall; however, based on analysis results post-tensioning does not increase the displacement capacity of the wall. In fact, for high levels of vertical stress the displacement capacity decreases. This can be explained using the data from Table 4.29. Notice at the 60psi level of post-tensioning stress, some of the piers failure modes were altered from a ductile rocking mode to a more brittle diagonal tension mode. Since this type of failure mode is not desirable, either the post-tensioning stress should be limited to avoid such a failure or some diagonal tension reinforcement should be supplied (i.e. either horizontal post-tensioning or FRP).

4.3.2 FRP Retrofit

Two approaches exist for retrofitting URM with FRP overlays. The first employs sheets of FRP that are bonded over the entire area of the pier. The second involves the use of FRP strips bonded in specific locations to strengthen the pier. Past studies suggest that the use of FRP strips are superior from both an economic and behavioral standpoint and as a result, only this type of FRP retrofit will be considered (Triantafillou, 1998).

4.3.2.1 FRP Retrofitted URM Pier Damage Model

Fig. 4.60 shows a URM pier retrofit with FRP strips. The locations of the strips were determined in order to mitigate the failure modes for URM piers discussed in Section 4.2.3.1. The retrofit provides vertical strips located on the outside to increase the in-plane flexural strength (i.e. rocking), diagonal FRP strips to increase the diagonal tension strength, and horizontal FRP strips to increase the bed-joint shear strength. It should be mentioned that the retrofit of a URM pier need not include each type of FRP

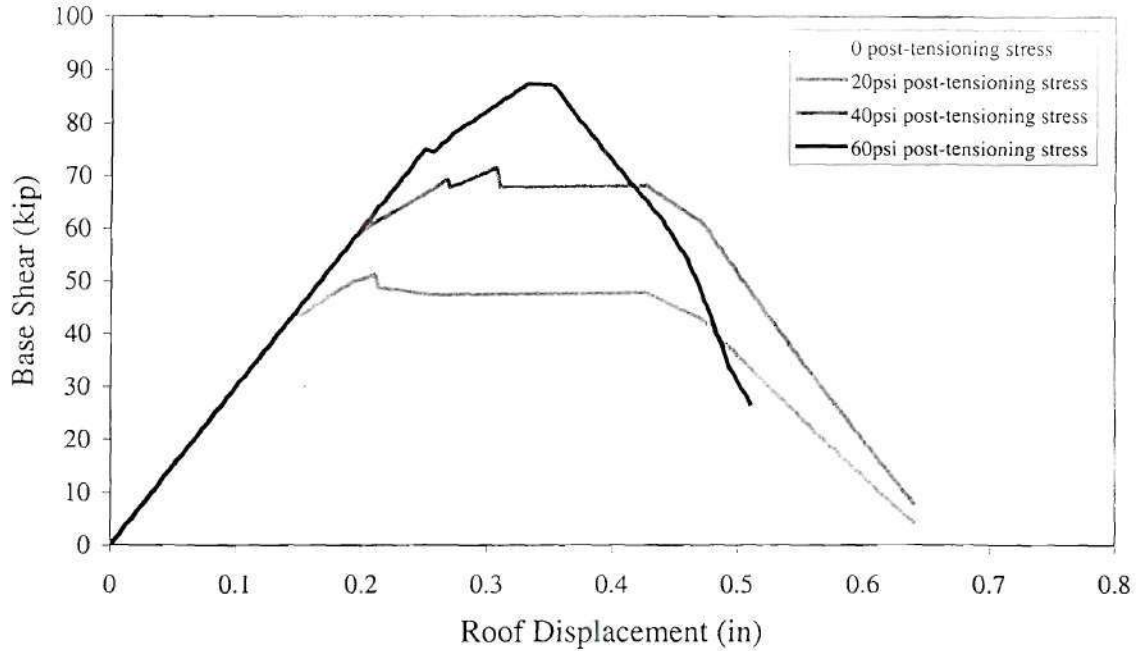


Figure 4.59. Force-displacement curves for Wall AB retrofit with different levels of post-tensioning stress

Table 4.29. Failure modes of Wall AB piers with different levels of post-tensioning stress.

Pier	URM	20psi	40psi	60psi
AB-2	Rocking	Rocking	No failure	No failure
AB-3	Rocking	No failure	No failure	No failure
AB-4	Rocking	No failure	No failure	No failure
AB-5	Rocking	No failure	No failure	No failure
AB-7	Rocking => Sliding	Rocking => Sliding	Rocking => Sliding	Rocking => Sliding
AB-8	Rocking => Sliding	Rocking => Sliding	Rocking => Sliding	Rocking => Sliding
AB-9	Rocking => Sliding	Rocking => Sliding	Rocking => Sliding	Diagonal Tension
AB-10	Rocking	Rocking	Rocking	Diagonal Tension

4.3 Analysis of Retrofit Test Structure

As mentioned previously, both post-tensioning and the use of FRP overlays will be investigated as retrofit techniques for URM walls. In order to analyze the ST-11 test structure in the retrofit state, the pushover analysis program, described in Section 4.2.3, is employed. However, modifications are made to the pier damage model to account for the specific type of retrofit. The following sections present the damage models for retrofitted piers as well as the results of the pushover analysis conducted on the ST-11 test structure.

4.3.1 Post-Tensioning

The damage model for post-tensioned URM piers used in the analysis is the same as used for URM piers outlined in Section 4.2.3.1. Since the ST-11 test structure will be retrofit with post-tensioning tendons unbonded over the two-story height, the tendons can be assumed to remain elastic throughout the experiment. As a result, the retrofit piers are modeled as URM piers with an increase in vertical stress. It should be noted that this is consistent with the recommendations given in FEMA 273 for the analysis of post-tensioned masonry with unbonded tendons.

In order to obtain insight into the effects of different levels of post-tensioning, Wall AB was analyzed with 20 psi, 40 psi, and 60 psi of post-tensioning stress. Since the post-tensioning retrofit will only be investigated for Wall AB, the other walls of the ST-11 test structure were not analyzed in the post-tensioned state. Fig. 4.59 shows the force-displacement curves obtained for the three different levels of post-tensioning stress and for the URM structure loaded from left to right.

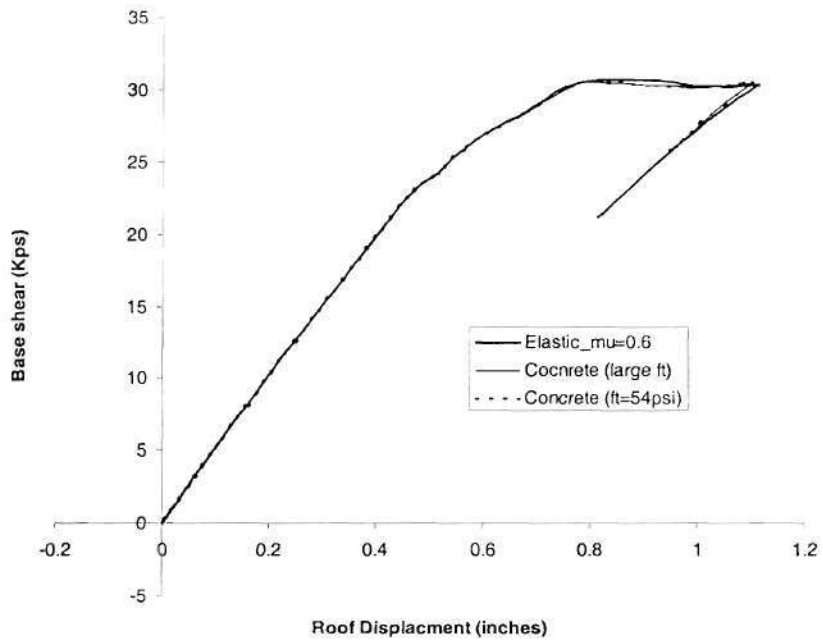


Figure 4.57. Force–displacement response of Wall AB with different masonry properties (beginning with push to the right)

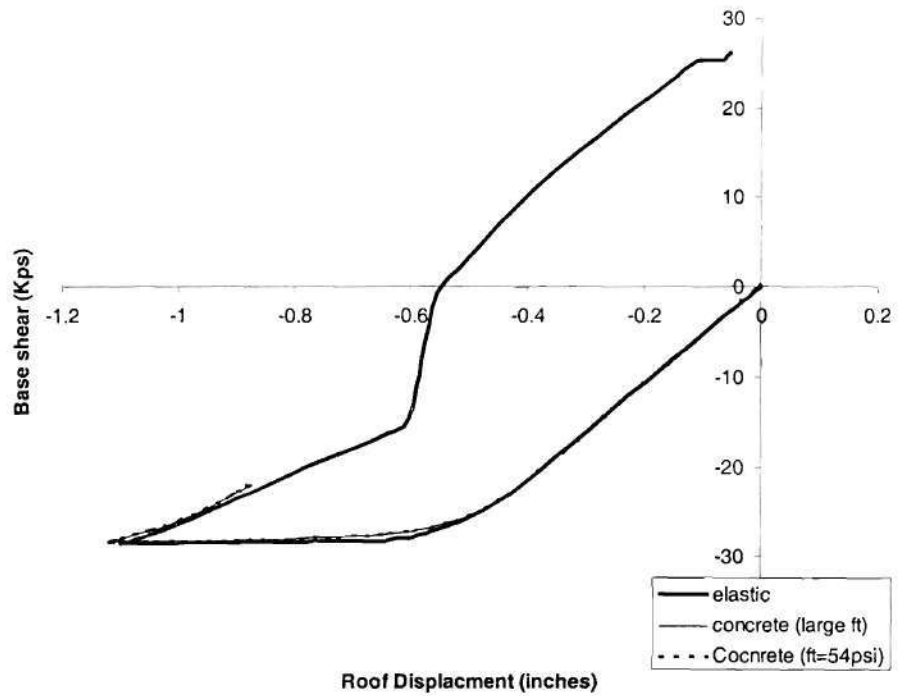


Figure 4.58. Force–displacement response of Wall AB with different masonry properties (beginning with push to the left)

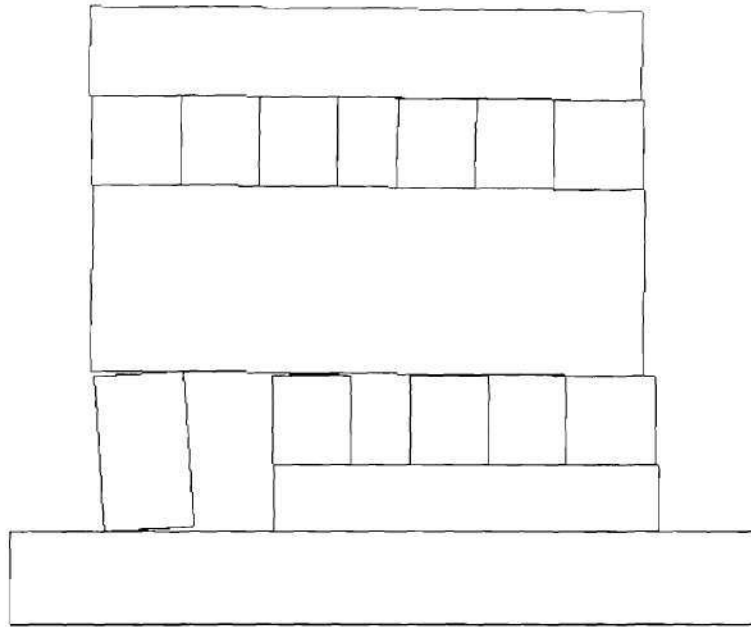


Figure 4.55. Deformed shape of Wall AB (loaded to the left)

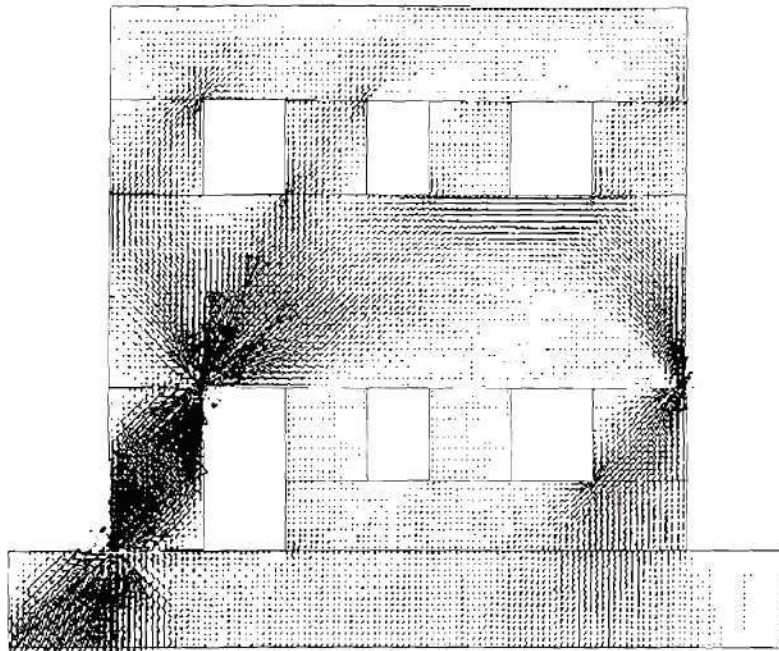


Figure 4.56. Stress contours of Wall AB (loaded to the left)

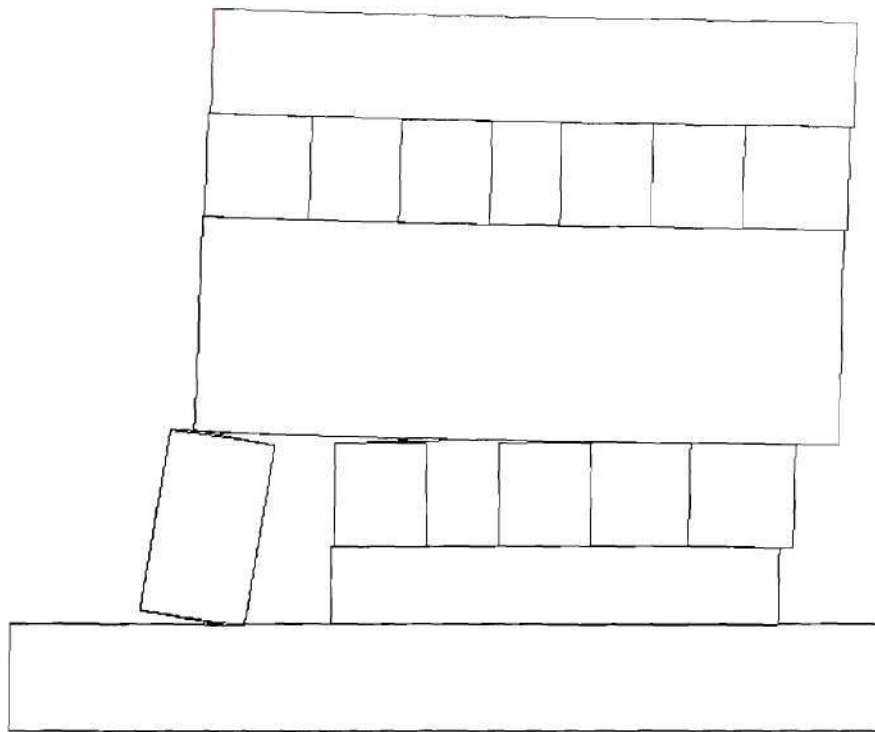


Figure 4.53. Deformed shape of Wall AB (loaded to the right)

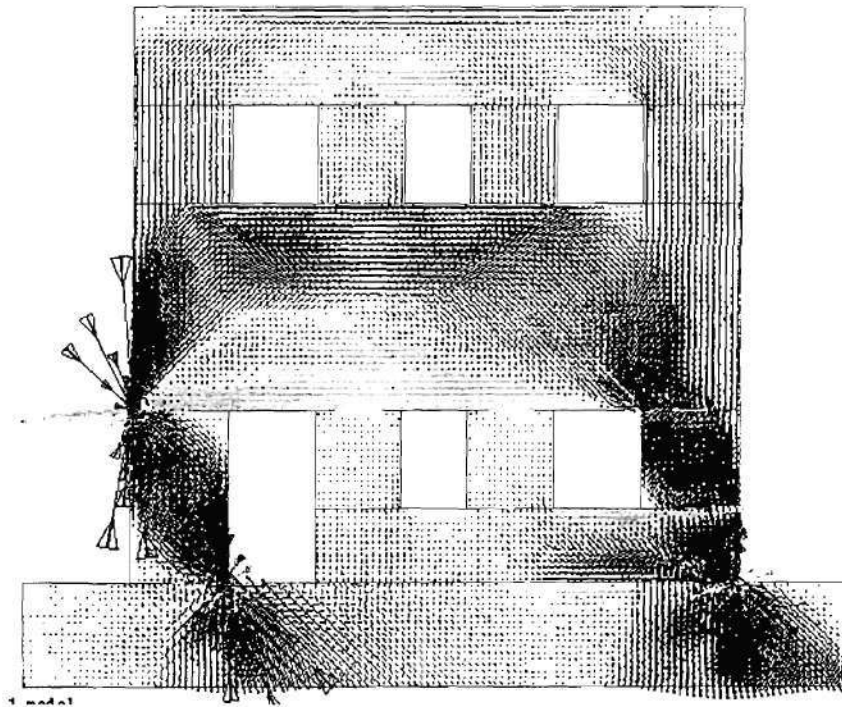


Figure 4.54. Stress contours of Wall AB (loaded to the right)

The table shows that the concrete properties give very similar results as those obtained from modeling masonry as an elastic material. This suggests that toe crushing and diagonal tension are not likely failure modes.

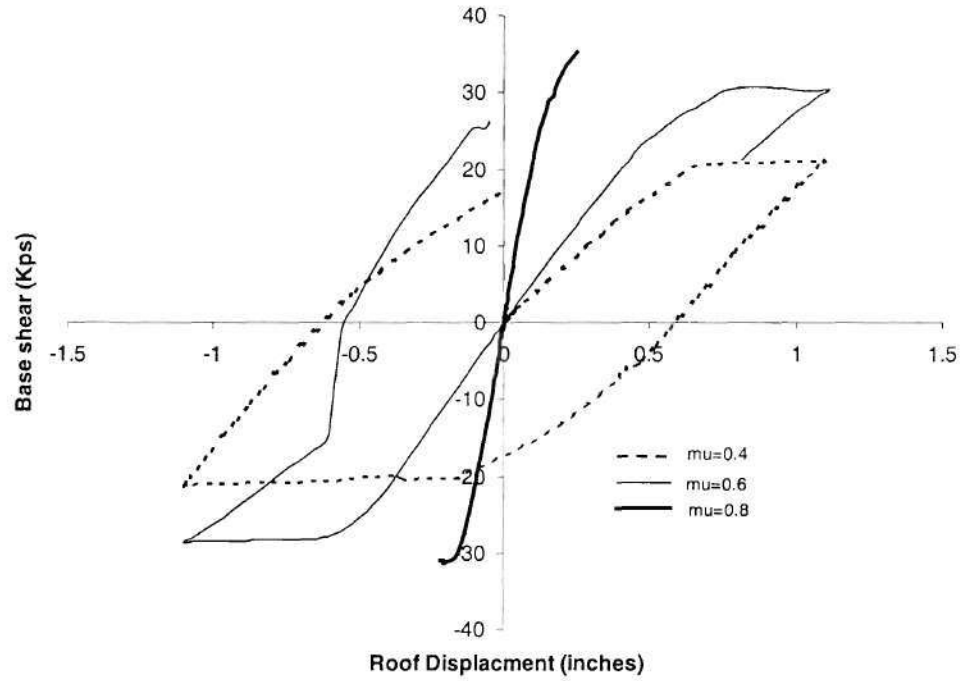


Figure 4.52. Force–displacement response of Wall AB with different friction coefficients

4.2.4.3.3 Nonlinear FE Analysis Results of Walls A and B

The same material properties and analysis strategies as those employed for the analysis of Walls 1 and 2 were also used to analyze Walls AB. Note, since the flange effects are not considered in this analysis, Wall A is identical to Wall B. The analysis shows again that increasing the friction coefficient suppresses sliding behavior and causes more rocking behavior (see Fig. 4.50). However, the dominating failure mode for Wall AB remains sliding. This can be seen from the direct dependence of strength on friction coefficient shown in Fig. 4.52. The deformed shapes and stress contours of Wall AB, shown in Figs. 4.53 through 4.56, also suggests sliding dominated behavior. These figures correspond to a friction coefficient of 0.6. The figures show that the door pier in the first floor rocks, while the window piers slide. This behavior is independent of loading direction. From the stress contours it is apparent that high stress concentrations are present in the two outside piers, and relatively low stress in the two central piers, which indicates that the two outside piers may damage before the central piers.

The force – displacement hysteretic behavior of Wall AB for different masonry properties is shown in Figs. 4.58 and 4.59 for a friction coefficient of 0.6. The calculated ultimate strengths in both directions are also listed in Table 4.28.

Table 4.28. Calculated ultimate strength of Walls AB

Methods	Ultimate Strength when pushed to the right (kip)	Ultimate Strength when pushed to the left (kip)
Elastic	30.8	28.6
Concrete material with high tensile strength	30.6	28.3
Concrete material (tensile strength = 54psi)	30.5	28.3
Simplify method results	33.0	33.0

as the measurement of local deformation is concerned, only the piers in the first floor rather than those in the second floor will be instrumented, because most of the damages of the buildings will focus on the first floor under lateral forces. For measuring the deformation of those piers, two short-range LVDTs will be placed at the center portion of the piers, where the shear stresses and the axial stresses are supposed to be relatively uniform. Therefore, the two LVDTs will measure the vertical deformation and shear deformation of the piers. At the same time, 1 inch masonry strain gages will be put at the four corners of each pier, where the local strains are large due to the stress concentration effect and the flexural moment effect. Those strain gages can be used to monitor the local large compressive deformation and the possible flexural cracking. If available, LVDTs will also be placed there to monitor the rocking behavior of the piers. The preliminary analysis shows some spandrels may also have severe damage during the test, such as the spandrel above the door opening in Wall 1. LVDTs will also be put in those areas to monitor the possible crack propagation.

Table B.5 Summary of instrumentation

Load Case	LVDT in load Cell	3 inches LVDT	1-2 inches LVDT	0.2 inches LVDT	1 inch Strain gage	Steel strain gage	Total channel
LC1, Roof diaphragm	1	6	4	0	0	6	17
LC2, Out-of-plane wall	1	7	4	0	0	8	20
LC3a, In-plane wall A/B	4	4	4+4	8+8+12	4+16+4+16	8	92
LC3b, In-plane wall 1/2	4	4	4+4	12+4+10	3+7+5+8	8	73
Maximum Number	4	7	8	28	63	30	92

Note:

- ξ In the loading case of testing the roof diaphragm, the deformations of both the wood diaphragm and the masonry walls that support the diaphragm will be measured. Meanwhile, the strains developed at the anchors that connect the diaphragm with the masonry walls will also be measured.
- ξ In the loading case of testing the out-of-plane stiffness of masonry wall, the deformations of both the in-plane walls and the out-of-plane walls will be measured. In the meantime, the deformation of the roof diaphragm, through which the external force is applied, will also be measured. The strains developed at the anchors connecting the diaphragm with the masonry walls will be measured too.
- ξ In the loading case of testing the in-plane behavior of masonry walls, both the global in-plane and out-of-plane deformations of the structure, and the local deformations of the piers and the spandrels will be measured. As far

Table B. 4 (Cont'd)






Items	Figure	Instrumentation	Number
Instruments for the global deformation of the structure		<p>LVDTs in actuator, used to measure deformation of actuators</p>	4
Floor level and roof level		<p>2 inches or 3 inches LVDTs, used to measure in-plane displacement of structure in roof level</p>	4
		<p>1 inches or 2 inches LVDTs, used to measure in-plane displacement of structure in floor level</p>	4
Elevation view		<p>0.5 inches or 1 inches LVDTs, used to measure out-of-plane displacement of structure</p>	4
		<p>Strain gages attached to the rebar connected with actuators to monitor the loss of prestressing during loading</p>	

Table B. 4 (Cont'd)


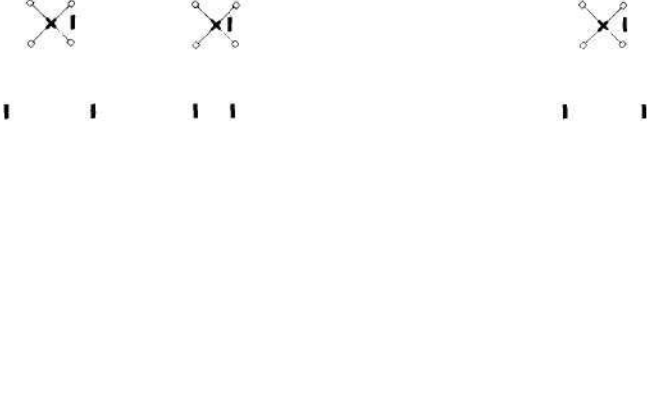
No.	Figure	Instrument type	Number
Instrum ntations used for wall piers in wall 2		0.2 inches LVDTs, used to measure vertical strain and shear strain in pier3	10
		1 inches strain gages attached at the mid height of the pier, used to measure vertical strain in piers	5
		1 inches strain gages attached at each corner of the piers, used to measure local strain at the toe during loading	8

Table B. 4 Loading Case 4: in-plane wall test of wall 1 and 2





Items	Figure	Instrumentation	Number
Instrumentations used for wall piers in wall 1		0.2 inches LVDTs, used to measure vertical strain and shear strain in piers	12
		0.2 inches LVDTs, used to measure vertical strain and shear strain in spandrel	4
		1 inch strain gages attached at the mid height of the pier, used to measure vertical strain in piers	3
		1 inch strain gages attached at each corner of the pier, used to measure local strain at the toe during loading	7

Table B.3 (Cont'd)

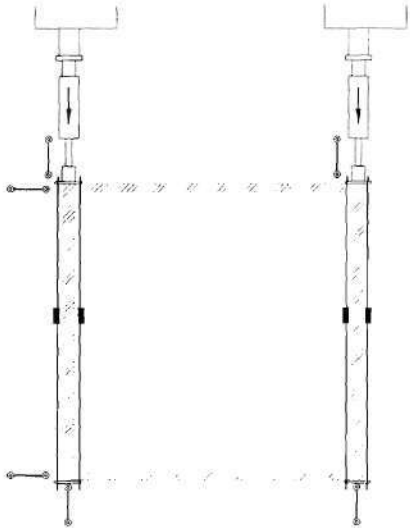
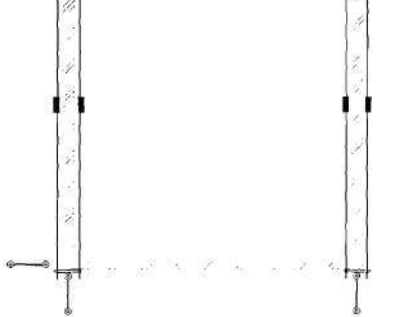
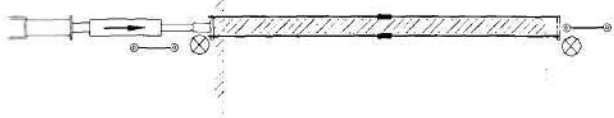


Items	Figure	Instrumentation	Number
Instruments for the global deformation of the structure		<p>LVDTs in actuator, used to measure deformation of actuators</p>	4
Floor level and roof level		<p>2 inches or 3 inches LVDTs, used to measure in-plane displacement of structure in roof level</p>	4
Elevation view		<p>1 inches or 2 inches LVDTs, used to measure in-plane displacement of structure in floor level</p>	4
Elevation view		<p>0.5 inches or 1 inches LVDTs, used to measure out-of-plane displacement of structure</p>	4
		<p>Strain gages attached to the rebar connected with actuators to monitor the loss of prestressing during loading</p>	8

Table B.3 (Cont'd)

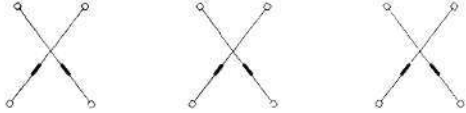

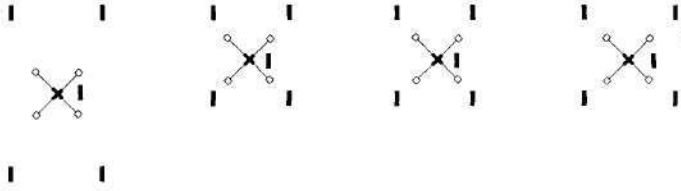
Items	Figure	Instrumentation	Number
Instrumentations used for wall piers in wall B		0.2 inches LVDTs, used to measure vertical strain and shear strain in piers	8
		0.2 inches LVDTs, used to measure axial strain and shear strain in spandrel	12
	 <p style="text-align: center;">Wall B</p>	1 inches strain gages attached at the mid height of the pier, used to measure vertical strain in piers	4
		1 inches strain gages attached at each corner of the pier, used to measure local strain at the toe during loading	16

Table B.3 Loading case 3: Test of the in--plane behavior of the masonry walls A/B

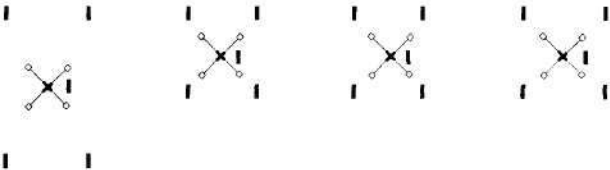
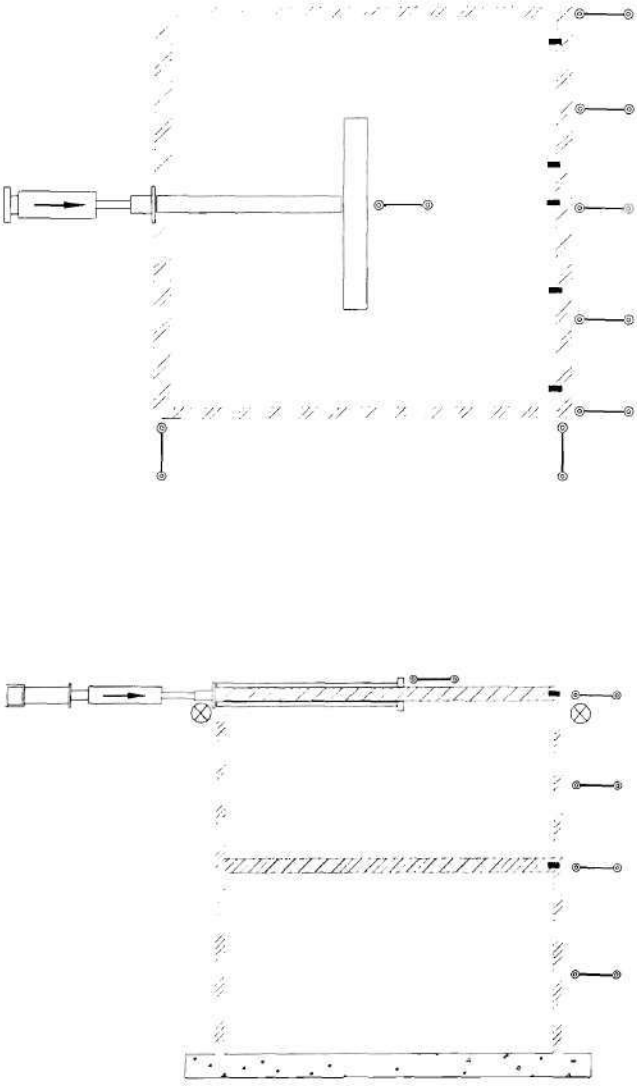
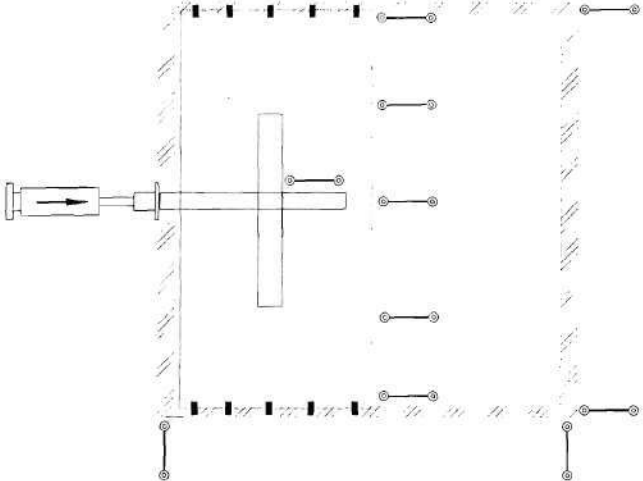
Items	Figure	Instrumentation	Number
Instrumentations used for wall piers in wall A	 <p style="text-align: center;">Wall A</p>	0.2 inches LVDTs, used to measure vertical strain and shear strain in piers	8
		1 inch strain gages attached at the mid height of the pier, used to measure vertical strain in piers	4
		1 inch strain gages attached at each corner of the pier, used to measure local strain at the toe during loading	16

Table B.2 Loading Case 2: Test of the out-of-plane behavior of masonry walls

Items	Figure	Instrumentation	Number
<p>Floor level and roof level</p>		<p>LVDTs in actuator, used to measure the deformation of the actuator</p>	1
		<p>3 inches LVDTs, used to measure the displacement of the out-of-plane wall</p>	6
		<p>1 inch LVDTs, used to measure the displacement of the in-plane walls</p>	4
		<p>3 inches LVDT, used to measure the displacement of the center of the roof diaphragm</p>	1
<p>Elevation view</p>	<p>Note: this loading case is applied to all four walls. The instrumentations set ups are similar for all the four walls</p>	<p>Strain gages, used to measure the strain in anchors</p>	8

APPENDIX B: INSTRUMENTATION

Table B.1 Loading Case 1: Test of the roof diaphragm

Items	Figure	Instrumentation	Num.
roof level diaphragm		LVDTs in actuator , used to measure the displacement of the actuator	1
		3 inches LVDTs , used to measure the deformation of diaphragm	5
		1 inch LVDTs , used to measure the displacement of masonry walls	4
		3 inches LVDTs , used to measure the deformation of diaphragm at loading beam	1
		Strain gages , used to measure the strains in the anchors	6

Zhang, Xudong, Shivas S. Singh, Desmond K. Bull and Nigel Cooke (2001), "Out-of-plane Performance of Reinforced Masonry walls with openings", Journal of structural Engineering, Vol.127, N01, Pp 51-57

Zagajeski, S., Halvorsen, G. T., GangaRao, H. V.S., Luttrell, L. D., Jewell, R. B., Corda, D., N. and Roberts, J. D. (1984). "Theoretical and Experimental Studies on Timber Diaphragms Subject to Earthquake Loads", Department of Civil Engineering, West Virginia University, Morgantown, West Virginia.

Y.K. Wen and C.L. Wu (2001), " Uniform Hazard ground motions for Mid-America Cities", Earthquake Spectra, volume 17, No 2, pp359-384

Tumialan, J. G., F. Micelli, and A. Nanni (2001) "Strengthening of Masonry Structures with FRP Composites", 2001 Structures Congress and Exposition, Washington, D.C.

Uang, C.M. and Bertero, V.V. (1990), " Evaluation of seismic energy in structures", Earthquake Engineering and Structural Dynamics, Vol. 19 (No. 1), pp 77-90

Velazquez-Dimas, J. I., M. R. Ehsani, and H. Saadatmanesh, (2000a) "Out-of-Plane Behavior of Brick Masonry Walls Strengthened with Fiber Composites," ACI Structural Journal, May-June 2000, pp. 377-387.

Velazquez-Dimas, J. I., M. R. Ehsani, and H. Saadatmanesh, (2000b) "Seismic retrofit of URM walls with fiber composites". 12th World Conference on Earthquake Engineering,

Xiao, Xiaoshong (1995), " The mechanical properties of masonry structure and numerical simulation", ph.D. thesis, Tongji university, Shanghai, China. (In Chinese)

R. Zarnic, and V. Bosiljkov (1999), " Diagonal Tests of Unreinforced Clay Brick Masonry", Eight North American Masonry Conference Proceedings, June 6-9, Austin, Texas, USA

Tomazevic, M., and Polona Weiss (1994), "Seismic Behavior of plain- and reinforced-masonry buildings ", Journal of Structural Engineering, Vol.120, N0.2, pp 325-337

Tomazevic, M.,, Marjana Lutman, and Ljubo Petkovic (1996), "Seismic behavior of masonry walls: experimental simulation", Journal of structural Engineering, Vol. 122, No.9.

Tomazevic, M.,, Claudio Modena, Tomaz Velechovsky, and Polona Weiss (1990), "The influence of structural Layout and Reinforcement on the seismic Behavior of Masonry Buildings: An Experimental Study", TMS Journal, August , pp 26-50

Tomazevic, M. (1987), "Dynamic Modeling of Masonry Buildings: Storey Mechanism Model As a simple Aternative", Earthquake Engineering And Structural Dynamic, Vol.15, 731-749.

Triantafillou, T. C. (1998) "Strengthening of Masonry Structures Using Epoxy-Bonded FRP Laminates", Journal of Composites for Construction, Vol. 2, No. 2, pp96-103.

Terceelj,Stane and Sheppard, Peter, and Turnsek, “ The Influence of Frequency on the shear strength and ductility of masonry walls in Dynamic Loading Tests.

Timoshenko, Stephen P. (1959), “Theory of plates and shells”, second edition, McGRAW-Hill Book Company.

Tissell, J. R. (1967). ”1966 Horizontal Plywood Diaphragm Tests”, Laboratory Report 106, American Plywood Association.

Tissell, J. R. and Elliott, P. E. (1997). “Report 138 – Plywood Diaphragms”, APA – The Engineered Wood Association (APA), Tacoma, Washington.

Tomazevic (1999), “Earthquake-Resistant Design of Masonry Buildings”, Imperial college Press.

Tomazevic, M., Marjana Lutman, and Polona Weiss (1996), "Seismic upgrading of old Brick-Masonry Urbaan Houses: Tying of walls with steel Ties", Earthquake Spectra, Vol 12, No.3.

Tomazevic, M., Marjana Lutman, and Polona Weiss (1993), "The Seismic Resistance of Historical Urban Buildings and the Interventions in their floor systems: An experimental Study", TMS Journal, August, pp 77-86

Shah, N., and Abrams, D.P. (1992), Cyclic load testing of unreinforced masonry walls, Advanced construction Technology Center, UIUC.

Sheppard, P. and Terceli. (1980) "The effect of repair and and strengthening methods for masonry walls." Proc. 7th World Conf. on Earthquake Engrg., Vol. 6, Turkish Nat. Committee on earthquake Engrg., Ankara, Turkey. 255-264.

Sinha ,B.P., and A.W. Hendry (1970), " Model and Full-scale Tests on a Five-Storey Cross-wall Structure Under lateral loading", Proceedings of the second International Brick Masonry Conference held in Stoke-on-Trent, England, pp 201-208

Sinha ,B.P. (1978), "A simplified ultimate load analysis of laterally loaded orthotropic brickwork panels of low tensile strength", Structural Engineer Part B, V56B, No.4, p 81-84

Sinha, B.P., (1978), A simplified ultimate load analysis of laterally loaded model orthotropic brickwork panels of low tensile strength, the structural Engineer, 56B:81-84

R.C. Smith, T.L. Honkala, C.K. Andres (1979), " Masonry Materials, Design. Construction", Reston Publishing Company, Inc, Virginia.

Reitherman, R. (1985), "The Borah Peak, Idaho Earthquake of October 28, 1983 – Performance of Unreinforced masonry buildings in Mackay, Idaho". *Earthquake Spectra*, 2(1), pp205-224

Rodriguez, R, A. A. Hamid, and J. Larralde (1998) "Flexural Behavior of Post-tensioned Concrete Masonry Walls Subjected to Out-of-Plane Loads," *ACI Structural Journal*, Vol. 95, No. 1, pp. 61-70.

Roko, K. E., T. E. Boothby, and C. E. Bakis (2001) "Strain Transfer Analysis of Masonry Prisms Reinforced with Bonded Carbon Fiber Reinforced Polymer Sheets", " *The Masonry Society Journal*, September, pp. 57-68.

Roberto Morales and Alberto Delgado (1992), "Feasibility of Construction of two-storey adobe buildings in Peru", *Tenth World Conference on Earthquake Engineering*, Balkema, Rotterdam, pp 3545-3550

Rots, J. G (1997), "Structural masonry: an experimental/numerical basis for practical design rules", Rotterdam ; Brookfield, VT : A.A. Balkema.

Sayed-Ahmed, E. Y., S. L. Lissel, G. Tadros, and N. G. Shrive (1999) "Carbon Fibre Reinforced Polymer (CFRP) Post-tensioned masonry diaphragm Walls: Prestressing, Behavior, and Design Recommendations," *Canadian Journal of Civil Engineering*, Vol. 226, pp. 324-244.

Pomonis A., R.J.S.Spence & A.W.Coburn, C.Taylor (1992), " Shaking table tests on strong motion damagingness upon unreinforced masonry", Tenth World Conference on Earthquake Engineering, Balkema, Rotterdam. pp 3533-3538.

Prawel, S.P., and Lee,H.H.. (1990a), "The performance of upgraded brick masonry piers subjected to out-of-plane motion". Proceedings of the fourth National Conference on Erathquake Engineering, Palm Springs, Calif., vol 3, pp.273-281

Prawel, S.P., and Lee,H.H.., (1990b), "The performance of upgraded brick masonry piers subjected to out-of-plane motion". Proceedings of the fifth North American Masonry Conference, Urbana-Champaign, III, Vol.1, pp.411-427

Prawl, S.P., Reinhorn, A. M., and Kunnath, S. K. (1986). "Seismic strengthening of structural masonry walls with external coatings." Proc., 3rd U.S. Conf. on Earthquake Engrg., Vol. 2, Earthquake Engrg. Res. Inst. (EERI), El Cerrito, Calif., 1323-1333.

Priestly, M.J.N, (1985). "Seismic behavior of unreinforced masonry walls". Bulletin of the New Zealand National Society for earthquake Engineering, 18(2): 191-205; 19(1):65-75

Paquette, J., M. Bruneau, and A. Filiatrault (2001) "Out-of-Plane Seismic Evaluation and Retrofit of Turn-of-the-Century North American Masonry Walls" ASCE Journal of Structural Engineering Vol. 27, No. 5, pp 561-569.

Paquette J. and Michel Bruneau (1999), "seismic resistance of full scale single story brick masonry building specimen", 8th North American Masonry Conference, June 6-9, 1999, Austin, Texas, USA, pp 227-234

Pauley, T and Priestley, M.J.N. (1992), "Seismic Design of Reinforced Concrete and Masonry Buildings", J. Wiley, New York

Paulson, and D.P. Abrams (1990), "Correlation between static and dynamic response of model masonry structures", Earthquake Spectra, vol 6, no 3, 1990, pp573-591

Paquette J. and Michel Bruneau (2000), "Pseudo- dynamic testing of Unreinforced Masonry Buildings With Flexible Diaphragm", 12th World Conference of Earthquake Engineering, 2000

Peralta, D. F. J. M. Bracci, and Mary Beth D. Hueste (2000), " MAEC project ST8 - Seismic performance of rehabilitated floor and roof diaphragms", Texas A&M University.

Phipps, M. E. and S. Al-Safi (2001) "Post-tensioned Prestressed Masonry Columns," 2001 Structures Congress and Exposition, Washington, D.C.

Montague, T. I. And M. E. Phipps (1985) "Prestressed Concrete Blockwork Diaphragm Walls," North American Masonry Conference, pp.79.1-79.15.

Moore, T.A., Kobzeff, J.H., Diri, J., and Arnold,C. (1988), " The Whittier Narrows, California Earthquake of October 1, 1987 – Preliminary Evaluation of the Performance of Strengthened Unreinforced Masonry Buildings", Earthquake Spectra, Vol, 4., N0.1, pp 197-211

Nakaki, D.K., and Hart,G.C. (1992)., "A proposed seismic design approach for masonry shear walls incorporating foundation uplift". The masonry Society Journal, 11(1), pp 29-36

NRC. (1990), "National building code of Canada", 1990. Associate Committee on the national building code. National research Council of Canada, Ottawa, Ont.

Page, A. W. (2001) "Prestressed Masonry-Recent Australian Research and Code Provisions," 2001 Structures Congress and Exposition, Washington, D.C.

Page, A. W. and A. Huizer (1998) "Racking Tests on Reinforced and Prestressed Hollow Clay Masonry Walls", 8th International Brick and Block Masonry Conference, Dublin, Ireland, pp 538-547.

Merguro, K. and M. Hakuno. (1989), Fracture analysis of concrete structures by the modified distinct element method, *struct. Eng./Earth. Eng.*, vol. 6, No.2, pp 283s-284s. Japan Societ of Civil Engineers.

Mid America Earthquake Center project: “SE-1: Inventories of essential facilities in Mid-America”, on-coming

Mid America Earthquake Center project: “ST-4: Response modification applications of essential facilities”, on-coming

Mid America Earthquake Center project: “ST-5: MDOF response of low-rising buildings”, on-coming

Mid America Earthquake Center project: “ST-6: Performance of rehabilitated URM components”, on-coming

Mid America Earthquake Center project: “ST-9: Performance objectives for essential facilities”, on-coming

Mid America Earthquake Center project: “ST-22: Performance of rehabilitated unreinforced masonry building systems”, on-coming

Mayes, R.L., Mostaghel, N.M., Clough, R.W., and Dickey, W.L.(1974), “ Cyclic Tests on Masonry Piers”, Bulletin of the New Zealand national Society for earthquake engineering, vol.7., No.3 , pp 105-114

Mayes, R.L., Omote, Y. and Clough, R.W. (1976), “Cyclic shear Tests of Masonry Piers, Volume I – Test Results”, EERC Report No. 76-8, University of California, Berkeley

Mayes, R.L., Omote, Y. and Clough, R.W. (1976), “Cyclic shear Tests of Masonry Piers, Volume II – Analysis of Test Results”, EERC Report No. 76-16, University of California, Berkeley

McDowell,E.L. McKee,K.E. and Sevin,E. (1956). “Ariching action theory of masonry walls”, Journal of Structural Division, ASCE, ST2, Mar., 915/1 – 915/18

Meli, R. (1973), “Behavior of masonry walls under lateral loads.”, Proc., 5th World Congress on Earthquake Engrg., pp 853-862

Mendola,L.L.: Papia, M., Zingone,G. (1995), “ Stability of Masonry Walls Subjected to Seismic Transverse Forces”, Journal of Structural Engineer, ASCE, Vol. 121 (11), pp 1581-1587

Mann, W. & H. Muller (1988). "Interpretation of experimental results with enlarged failure criterion considering the stresses in the head joints". In: Untersuchungen zum Verhalten von Mauerwerksbauten unter Erdbeneinwirkung. Darmstadt: Technische Hochschule (in German)

Manzouri, T., Shing,P.B., Amadei,B. (1996), "Analysis of masonry structures with elastic/viscoplastic models, 1996", Worldwide Advances in Structural Concrete and Masonry, Proceedings of the Committee on Concrete and Masonry Symposium, ASCE Structures Cogress XIV, Chicago, Illinois.

Marshall, O. S., S. C. Sweeney, and J. C. Trovillion (2000) "Performance Testing of Fiber-Reinforced Polymer Composite Overlays for Seismic Rehabilitation of Unreinforced Masonry Walls", U. S. Construction Engineering Research Laboratory, ERCE/CERL TR-00-18.

Martini, Kirk (1998), " Finite Element Studies in the two-way out-of-plane failure of unreinforced masonry", 6th U.S. National Conference of Earthquake Engineering.

Martini, Kirk (1997), " Finite Element Studies in the out-of-plane failure of unreinforced masonry", Proceedings of the international conference on computing in civil and Building Engineering, vol.1, C.K. Choi, ed., Korea.

- Lee, H. H. and S. P. Prawel (1991). "The seismic renovation and repair potential of ferrocement coatings applied to old brick masonry walls." Proc. 6th Canadian Conf. on Earthquake Engrg.
- Lissel, S. L., E. Y. Sayed-Ahmed, and N. G. Shrive (1999) "Prestressed Masonry-the Last Ten Years", 8th North American Masonry Conference, Austin, TX, pp. 599-610.
- Lissel, S. L., D. Tilleman, E. Y. Sayed-Ahmed, and N. G. Shrive (1998) "Carbon Fibre Reinforced Plastic (CFRP) Prestressed Masonry," 8th Canadian Masonry Symposium, Jasper, Alberta, pp.610-621.
- Lourenco, P.B. (1996), " Computational Strategies for masonry structures", Delft University Press, Netherlands.
- Magenes, G., and Calvi, G.M. (1992), "Cyclic behavior of brick masonry walls", Tenth World Conference on Earthquake Engineering, Balkema, Rotterdam. pp 3517-3522
- Magenes, G., and Calvi, G.M. (1995), "Shaking table tests on brick masonry walls," Proceedings of the 10th European Conference on Earthquake Engineering, Duma, editor, Balkema:Rotterdam, The Netherlands.